DOWNDRAFT GASIFICATION OF BIOMASS

JIMMY BAXTER MILLIGAN

Doctor of Philosophy

THE UNIVERSITY OF ASTON IN BIRMINGHAM

February 1994

The University of Aston in Birmingham

DOWNDRAFT GASIFICATION OF BIOMASS

JIMMY BAXTER MILLIGAN

Doctor of Philosophy
1994

SUMMARY

The objectives of this research were to investigate the parameters affecting the gasification process within downdraft gasifiers using biomass feedstocks. In addition to investigations with an open-core gasifier, a novel open-topped throated gasifier was designed and used.

A sampling system was designed and installed to determine the water, tar and particulate content of the raw product gas. This permitted evaluation of the effects of process parameters and reactor design on tar and particulate production, although a large variation was found for the particulate measurements due to the capture of large particles.

For both gasifiers, the gasification process was studied in order to identify and compare the mechanisms controlling the position and shape of the reaction zones. The stability of the reaction zone was found to be governed by the superficial gas velocity within the reactor. A superficial gas velocity below 0.2 Nms^{-1} resulted in a rising reaction zone in both gasifiers.

Turndown is achieved when the rate of char production by flaming pyrolysis equals the rate of char gasification over a range of throughputs. A turndown ratio of 2:1 was achieved for the hybrid-throated gasifier, compared to 1.3:1 for the open-core. It is hypothesized that pyrolysis is a surface area phenomena, and that in the hybrid gasifier the pyrolysis front can expand to form a dome-shape. The rate of char gasification is believed to increase as the depth of the gasification zone increases.

Vibration of the open-core reactor bed decreased the bed pressure drop, reduced the voidage, aided solids flow and gave a minor improvement in the product gas energy content. Insulation improved the performance of both reactors by reducing heat losses resulting in a reduced air to feed ratio requirement.

The hybrid gasifier gave a higher energy conversion efficiency, a higher product gas heating value, and a lower tar content than the open-core gasifier due to efficient gas mixing in a high temperature tar cracking region below the throat and reduced heat losses.

A two stage model of downdraft gasification developed as a design aid gives a pyrolysis zone depth similar to the experimental results. However the depth of the gasification zone does not compare well with experimental observations due to insufficient pore size distribution and kinetic data. The product gas composition is satisfactorily calculated by an equilibrium model.

Key words: Gasification, downdraft, biomass, open-core, hybrid-throated

ACKNOWLEDGEMENTS

I wish to thank Prof. B. J. Tighe and Dr E. L. Smith (Departmental Heads), and the Department of Chemical Engineering and Applied Chemistry for providing the facilities for this project; the Science and Engineering Research Council for their financial support and Dr. A. V. Bridgwater for supervising this project.

I also wish to thank the following:

Dr. Geraint Evans, my predecessor, for his help, advice and assistance during the first couple of years of this project.

Dr. Eric Smith for his help and advice with the modelling of the gasification process.

The departmental technical staff for their help and assistance during the construction and operation of the gasification system: Neville Roberts (retired) and Steve Ludlow, departmental superintendents; Lynn Wright in the departmental stores; Dave Walton and Paul Tack, the departmental laboratory technicians; Mike Lea and Dave Bleby, the departmental electrical technicians; Ian Murkett and Maurice Santaro, the departmental workshop technicians; and Fiona Newell for assistance in data collection.

My family and friends, who have given their support during my time at Aston, in particular Nicky Shelton.

I am especially thankful to Tina Crutchfield, my fiancee, for her considerable support throughout the course of this project.

CONTENTS

FIGURES

Chapter 7

Chapter 8

Chapter 9

Appendices

TABLES

Appendices

1. RESEARCH OBJECTIVES

1.1 Introduction

Biomass refers to energy crops, forestry and agricultural wastes, and domestic and industrial wastes which includes municipal solid waste (MSW), refuse derived fuel (RDF) and sewage sludge. Compared with fossil fuels, biomass has the advantage of being a renewable, CO_2 neutral energy resource with a low pollutant content. The direct utilization of biomass energy is usually difficult due to its low energy content, high moisture content, low bulk density and variability in size and shape which causes problems in feed handling. There is also the need to collect and transport the biomass to the point of use. The conversion of biomass into solid, liquid and/or gaseous fuels increases the energy content and allows easier transport of the energy.

Gasification is the thermochemical conversion of organic material to a fuel gas by partial oxidation at high temperatures. The product gas may be used for heat, power, electricity generation or as synthesis gas for conversion to methanol, gasoline and chemicals. Gasification is a well established technology which reached a peak during the World War II when up to a million downdraft gasifiers were used for motive power (Hos, 1987). In downdraft gasification the feed and the oxidant, usually air, move in a downwards direction. The conventional downdraft gasifier has a constriction or throat through which gasification products must pass and a lid or sealed feeding system. Open-core or stratified gasifiers consist of an open-topped tube without a throat with no the need for a sealed feeder.

A open-core downdraft gasifier constructed from transparent quartz glass has been used by previous workers (Reyes, 1988; Earp, 1988; Evans, 1992) to observe the gasification process and allow measurements of the reaction zone and of individual individual particles during gasification. This has enabled studies on the processes occurring within the reaction zone and the effects of a variety of process parameters to be carried out.

1.2 Research Objectives

This research aims to provide information on the parameters influencing the product gas quality in terms of energy content, and tar and particulate content. Previous work has not included the determination of the water content of the gas and the measurement of tar and solids loading of the gas has been unsatisfactory. These are important measurements relating to gas quality, for example, a gas lower in tars and dust requires less cleaning before it can be accepted in an engine. Efficient tar cracking within a gasifier is desirable since this minimizes the requirements of the downstream

cleaning system. The use of hybrid-throated gasifier and the agitation of the reactor bed within the open-core gasifier are investigated. The principle objectives of this research are listed below.

1) The design and use of a sampling system to enable measurement of the tar and solid particulate loading in the product gas and the water content of the raw product gas. The effects of various parameters on the production of tars and solid particulates can then be evaluated, and accurate mass and energy balances produced.

2) The design of a hybrid-throated gasifier that combines advantages of the conventional throated gasifier with those of the open-core gasifier. Investigate the affect of the throat on gasifier control and performance. Observe the gasification process within the hybrid-throated reactor, both qualitatively and quantitatively, and to compare the observations with the open-core system. The phenomena of turndown, that is the ability to control the output of the gasifier on requirement, using the hybrid-throated gasifier will be investigated and compared to the open-core system.

3) Investigate the use of a stirrer or agitator within the open-core gasifier to reduce the frequency of void formation within the bed and to maintain a level reaction zone. In previous work the formation of a void restricted the flow of material into the reaction zone and caused the zone to slope which is a problem ito the control of the reactor. The effect of the stirrer on the removal of char and ash fines from the gasifier will also be investigated as a means of maintaining a low pressure drop across the reactor.

4) To further investigate the effects of various process parameters on the performance and operation of the open-core gasifier, using the sampling system to obtain tar, solids and water content of the product gas. These include the use of insulation, feed size and type and the mode of operation.

5) Model the downdraft gasification process in order to evaluate the conditions required for optimum performance and to aid the design of a gasifier.

2. GASIFICATION THEORY AND LITERATURE REVIEW

2.1 Introduction

The chemical and thermal processes of biomass gasification in downdraft gasifiers are described in this chapter. Gasification is the thermochemical conversion of organic material to a fuel gas by partial oxidation at high temperatures. Using air as the gasification agent gives a product gas that is a mixture of CO, CO_2, H_2, 40-60% N_2 and hydrocarbon gases with contaminants such as char particles, tars and oils. The gas has a low heating value typically about 5 $MJNm^{-3}$ (Beenackers, 1984). The product gas can be burned to generate heat for boilers, kilns and furnaces, where the burning of the gaseous fuel involves simpler equipment, and greater control. The burning of the product gas results in reduced particulate and pollutant emission compared to the direct combustion of the biomass. The gas can also be used in an internal combustion engine or gas turbine for shaft power or for electricity generation; however, gas cleaning equipment is usually necessary if the gas is to be used in these applications. In order to prevent excessive engine wear particulates must be removed down to 10-50 $mgNm^{-3}$ for use in the internal combustion engine and reduced down to 2-20 $mgNm^{-3}$ for a gas turbine (Brown, 1987). Tars should also be reduced to a similar level to prevent excessive tar deposition and fouling of the equipment.

The fraction of nitrogen in the product gas can be decreased using oxygen or oxygen enriched air to give a higher heating value gas of 10-15 $MJNm^{-3}$ (Bridgwater, 1991) suitable for pipeline distribution and as synthesis gas for conversion to methanol, ammonia and other chemicals (Hos, 1987).

Gasification is a well established technology with the first commercial gasifiers produced over 150 years ago. The history of the development of gasification is reviewed by Kaupp (1983). There are several types of gasifier design of which only moving packed bed downdraft gasifiers are considered in this thesis. Other gasifier types have been extensively reviewed (e.g. Kaupp, 1984; Beenackers, 1984; Bridgwater, 1991; Bridgwater, 1993). In a downdraft gasifier the feed and the oxidant move in a downwards (co-current) direction. The primary advantage of this type of gasifier is that all the decomposition products of pyrolysis (see Section 2.2.2) pass through the hottest region of the gasifier. This results in the cracking (thermal degradation) of tars to non-condensable gases and water to give a product gas with a low tar content. This is discussed in greater detail in Section 2.6.1.

Conventional downdraft gasifiers have a region of reduced cross-sectional area or throat below the oxidant inlet. The throat aids tar cracking by increasing turbulence of

the gases within a high temperature region of the gasifier (discussed in greater detail in Section 2.6.1). The conventional throated downdraft gasifier, also sometimes known as the Imbert type gasifier, is shown in Figure 2.1. Up to one million of these units were in use during World War II for motive power (Hos, 1987). The throated gasifier is discussed further in Section 2.6.

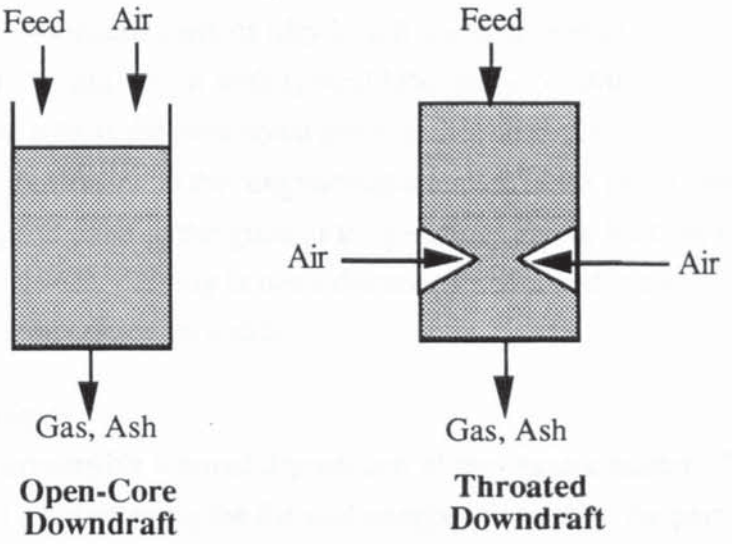

Figure 2.1 Throated and Open-Core Downdraft Gasifiers

A second variety of downdraft gasifier is the "open-core" developed by Reed and Graboski for the Solar Energy Research Institute (SERI) in 1980 as a simple derivative of throated gasifier (Reed, 1988). The gasifier type is described as "stratified" since distinct zonation of the three step process (drying, pyrolysis and gasification) occurs along the length of the reactor (Reed, 1983). This is discussed in greater detail in Section 2.5.

2.2 Chemistry of Gasification

Gasification is a series of complex concurrent and consecutive chemical and thermal processes which are not completely understood. The process is energetically self-sustaining (autothermal) as no thermal input is required. The principle stages in gasification are drying, pyrolysis, oxidation and gasification; however, the process differs in the open-core and throated gasifiers and this is examined in greater detail in Section 2.5.

2.2.1 Drying

The feed descends a downdraft gasifier as a result of the consumption of the feed in reaction zones below. Due to heat transfer from the hotter zones below drying takes place. The rate of drying is dependant upon the surface area of the feed, the temperature difference between the feed and its external environment, the velocity and relative humidity of the external medium, and the internal diffusivity of moisture

within the feed (Buekens, 1985). Water in woody biomass occurs as free moisture within pores and as bound water which is held on the cell walls by chemisorption. Water is transported within wood by capillary action within the pores, by diffusion across cell walls and by vapour diffusion where a vapour pressure gradient exists. Transport by capillary action applies to wood above the fibre saturation point, i.e. with a substantial amount of free water. Since the fibre saturation point for most woods lie between 20-30% moisture content (dry basis) water transport by capillary action is minor for wood at equilibrium with typical laboratory conditions. The microscopic structure of wood affects the directional permeability according to its orientation to the grain. The rate of diffusion in the longitudinal direction is 5-8 times faster than the rate of diffusion perpendicular to the grain at temperatures above 50°C in the hygroscopic range (Kollman, 1968). Drying is not a discreet process and it also occurs alongside pyrolysis as the temperature increases.

2.2.2 Pyrolysis

Pyrolysis is the irreversible thermal degradation of the organic matter. This takes place in the downdraft gasifier using the thermal energy released by the partial oxidation of the pyrolysis products (Section 2.2.3). The heat transfer mechanism is discussed in Section 2.5.2. The release of volatiles begins at about 250°C (Shafizadeh, 1982; Kaupp, 1983) until, under the conditions in a downdraft gasifier, 80 to 95% of the original mass is converted to a complex liquid fraction comprising of water, tars and oils and a gaseous phase including CO, CO_2, H_2 and hydrocarbons, leaving 5 to 20% highly reactive charcoal (Reed, 1983). The pyrolysis reaction within a downdraft gasifier can be considered as fast pyrolysis, since it occurs at heating rates of about 10 Wcm^{-2} (Deglise, 1987) and at temperatures of about 500°C (Diebold, 1989).

The product distribution and composition of the non-condensable products of pyrolysis primarily depends upon the composition of the feed (Bilbao, 1992; Deglise, 1987). In addition, the primary product distribution of pyrolysis is also a function of heating rate, product residence time, particle size and temperature (Buekens, 1985; Deglise, 1987; Hellgren, 1991). Graham found that the char yield decreased with temperature from 18% at 500°C to 3% at 800°C (1988), and later found the decrease in char yield extended to 900°C with a 7% yield at 650°C to 1% at 900°C (1993). Hellgren (1991), however, found that the char yield decreased from 20% at 800°C to a minimum of 10% at 1000°C before increasing to 20% at 1400°C. He explained this by the reaction of tars within the particle to form secondary char and gas. However, within a downdraft gasifier the final temperature of pyrolysis is considered to be about 500°C, well below the temperatures at which Hellgren found an increase in char yield. Graham (1993) showed that liquid yields decreased from 62% at 650°C to 20% at

900°C indicating that thermal cracking is increased with temperature, although the extent of tar cracking is unknown since water was included in the quoted liquid yields.

Larger particle sizes also increase the char yield (Raman, 1981; Chan, 1985b; Maniatis, 1988). As the particle size is increased the volatiles have a longer residence time within the particle enabling carbon deposition to take place (Shamsuddin, 1992). Evans (1992) claimed that this also occurs within the pyrolysis step of gasification. However, since he used a different material for the two different particle sizes, his claim is not substantiated. A major problem is recognized in determining the effect of particle size on product yields for the pyrolysis of coal, as larger particles tend to heat-up more slowly (Howard, 1981) and lower heating rates also increase the char yield (see below). This may also apply to some of the studies on biomass that have been undertaken and the findings on the effect of particle size on product yields mentioned above should be looked upon with caution.

Chan (1985a) measured the effect of increasing the external heat flux from 8 to 25 Wcm^{-2} on 0.5 cm long wood particles and found that char yields decreased from 24% to 20%, tar yields decreased from 62% to 55% and the gas yield increased from 14% to 25% (approximate values). Reed (1988) estimated the heat transfer to particles during flaming pyrolysis (see Section 2.5.2) under a variety of conditions to be between 2 and 15 Wcm^{-2}, so the effects described by Chan can be considered to apply to the pyrolysis process in a downdraft gasifier.

The structure of the material undergoing pyrolysis is also important in product formation as this affects the thermal conductivity and, therefore, the heating rate of the biomass. The thermal conductivity of wood ranges between 0.025 $Wm^{-1}K^{-1}$ across the grain to 0.35 $Wm^{-1}K^{-1}$ along the grain (Kollman, 1968). In addition, the structure of wood affects the outflow of the volatiles from a pyrolysing particle (Walawender, 1988a). Chan (1985a) found that the initial mass flow rate of volatiles from wood during pyrolysis is affected by the orientation of the grain to the heat flux. Particles with the grain perpendicular to the heat flux offer greater resistance to the outflow of material compared with heating occurring parallel to the grain. However, Roberts (1970) concluded that the restraints on the movement of pyrolysis products imposed by the physical structure of wood largely disappeared above temperatures of 300-320°C, and therefore structural effects would be unimportant in the conditions occurring within a downdraft gasifier. Below 300-320°C Roberts (1970) suggests that the pyrolysis products are forced into the virgin wood contributing to an autocatalytic effect. Since, in a downdraft gasifier, the particle passes through this temperature range, there would be a narrow reaction front within the particle at which the pyrolysis

products may penetrate into the unreacted material enhancing heat transfer to give rise to autocatalysis.

The heat of reaction for the pyrolysis of wood oscillates about 0 $kJkg^{-1}$ between endothermic and exothermic values (Kaupp, 1983). Espenäs (1994) found that the reaction is endothermic (+474 $kJkg^{-1}$) up to 270-300°C and thereafter becomes exothermic (-109 $kJkg^{-1}$). The heat required to remove moisture from the feed results in a peak in endothermicity between 100-200°C (Deglisse, 1987; Espenäs, 1994). Carbon dioxide was found to be the main permanent gas evolved during the endothermic period whilst hydrocarbons became dominant during the exothermic period by Espenäs (1994). This is consistent with the generally agreed view that hemicellulose decomposition occurs prior to cellulose and lignin decomposition (Deglise, 1987). The overall heat of reaction for the pyrolysis of wood vary considerably in the literature, and may depend upon the degree of char production (Antal, 1982) with fast pyrolysis giving low char yields being endothermic whilst slow pyrolysis being exothermic. Energy is also required in heating the wood to the pyrolysis temperature and to raise the volatile components to the temperature at the surface of the particle.

The kinetics of pyrolysis of pine wood has been studied by Becker (1984), who describes three stages for the reaction. The first stage is generally short and only becomes evident at temperatures above 150°C but has a higher reaction rate than the second period up to at least 400°C. In general, the second period is considerably longer than the first. The final period the reaction rate is so slow that it can be neglected for practical purposes (Becker, 1984). Each period can be described by first order kinetics, which is generally accepted in the literature (Roberts, 1970; Milne, 1979). The rate and route of the pyrolysis reactions for cellulose is extremely sensitive to catalytic and autocatalytic effects (Roberts, 1970), and this can also be considered to apply to wood. Simmons (1985) found a close agreement between the rate coefficient for cellulose and for the second period of pyrolysis indicating that decomposition of the wood constituents are taking place separately. The first period of pyrolysis may relate to the decomposition of hemicellulose. The mechanisms of pyrolysis reactions are beyond the scope of this thesis but are discussed in detail by Antal (1982; 1985) and Shafizadeh (1982; 1985).

The application of the pyrolysis studies mentioned above can only give an indication of the pyrolysis process in a downdraft gasifier since the experimental conditions are not identical with those in a downdraft gasifier. There is great difficulty in the measurement of heating rates and pyrolysis temperature within actual gasification

systems due to the imprecise nature of both measuring techniques and the position of the pyrolysis process.

2.2.3 Oxidation

The volatile products of pyrolysis are partially oxidized in highly exothermic reactions (e.g. Equations 2.1 and 2.2) which result in a rapid rise in temperature up to 1200-1600°C (Groeneveld, 1980). The heat generated is used to drive the drying and pyrolysis of the feed and the gasification reactions. The oxidation reactions of the volatiles are very rapid and the oxygen is consumed before it can diffuse to the surface of the char. No combustion of the solid char can, therefore, take place.

$$H_2 + 0.5\,O_2 = H_2O \qquad \Delta H_{298K} = -241.8\ kJmol^{-1} \qquad (2.1)$$

$$CO + 0.5\,O_2 = CO_2 \qquad \Delta H_{298K} = -285.0\ kJmol^{-1} \qquad (2.2)$$

Oxidation of the condensable organic fraction to form lower molecular weight products is important in reducing the amount of tar produced by a gasifier. The pyrolysis and oxidation processes within a downdraft gasifier are typically described together as flaming pyrolysis. Flaming pyrolysis is discussed in more detail in Section 2.5.2. The products CO_2, CO, H_2, H_2O, hydrocarbon gases, residual tars and char then pass on into the gasification zone below.

2.2.4 Gasification

In the gasification zone the char is converted into product gas by reaction with the hot gases from the zones above. The gases are reduced to form a greater proportion of H_2 and CO. The temperatures of the gases entering the zone is about 1000-1200°C. A knowledge of the thermodynamics and kinetics of the gasification reactions are important in understanding the behaviour of the reaction zone and these are discussed further in Sections 2.3 and 2.4 respectively. The gasification reactions of the liquid products of pyrolysis are complex and not widely discussed in the literature. Reyes suggested that they may be gasified via thermal cracking or by direct reaction with the gasifying agent and other pyrolysis products (1989). Charcoal conversion will be reduced by the entrainment of small charcoal particles into the gas stream. Reed (1983) gives between 2 to 5% of the char mass being carried out of a gasifier.

2.3 Gasification Reaction Thermodynamics

The generally accepted fundamental chemical reactions regarding gasification were first described by Gumz (1950) and are presented in Table 2.1.

Table 2.1 Gasification Reactions

Heterogeneous Gas-Solid Reactions

Boudouard Reaction

$$C + CO_2 = 2\,CO \qquad \Delta H_{298K} = 172.5\ kJmol^{-1} \qquad (2.3)$$

Water Gas Reaction

$$C + H_2O = H_2 + CO \qquad \Delta H_{298K} = 131.3\ kJmol^{-1} \qquad (2.4)$$

Methane Formation

$$C + 2\,H_2 = CH_4 \qquad \Delta H_{298K} = -74.9\ kJmol^{-1} \qquad (2.5)$$

Homogeneous Gas-Gas Reactions

Water Gas Shift Reaction

$$CO + H_2O = CO_2 + H_2 \qquad \Delta H_{298K} = -41.2\ kJmol^{-1} \qquad (2.6)$$

Reforming

$$CH_4 + H_2O = CO + 3\,H_2 \qquad \Delta H_{298K} = 201.9\ kJmol^{-1} \qquad (2.7)$$

Methanation

$$2\,CO + 2\,H_2 = CH_4 + CO_2 \qquad \Delta H_{298K} = -247.3\ kJmol^{-1} \qquad (2.8)$$

$$CO_2 + 4\,H_2 = CH_4 + 2\,H_2O \qquad \Delta H_{298K} = 164.7\ kJmol^{-1} \qquad (2.9)$$

The Boudouard and water gas reactions are endothermic and energy contained in the hot gases and char from the partial-oxidation zone above is required to drive the reactions. As char conversion proceeds the temperature progressively decreases, thereby reducing the kinetic rate of the reactions until they become insignificant below about 700°C (see Section 2.4). The extent of char reduction is, therefore, dependant upon the amount of energy entering the gasification zone (Chern, 1989).

The water gas shift equilibrium Equation (2.6) is obtainable by combining reactions 2.3 and 2.4. The most important gasification reactions are 2.3, 2.4 and 2.6, since they involve the maim species. The remaining reactions in Table 2.1 take place to a minor extent due to kinetic limitations. Reactions 2.3, 2.4 and 2.6 are sufficient to describe the gasification process (Chern, 1985). The equilibrium constants for these reactions are expressed;

$$K_{p1} = \frac{P_{CO}}{P_{CO2}} \qquad (2.10)$$

$$K_{p2} = \frac{P_{CO}.P_{H2}}{P_{H2O}} \qquad (2.11)$$

$$K_{p3} = \frac{P_{CH4}}{P_{H2}} \qquad (2.12)$$

$$K_{p4} = \frac{P_{CO2}.P_{H2}}{P_{CO}.P_{H2O}} = K_{p1}.K_{p2} \qquad (2.13)$$

The equilibrium constants may be calculated from the standard reaction Gibbs free energy using;

$$\Delta_r G^\circ = - RT \ln K_p \qquad (2.14)$$

where T is temperature and R is the gas constant. The use of chemical equilibria are frequently used in the prediction of product gas composition (e.g. Gumz, 1950) and their application to modelling is discussed in Chapter 9.

2.4 Kinetics of Heterogeneous Gasification Reactions

2.4.1 Introduction

Thermodynamics can predict the product gas composition at a particular temperature; however, the kinetics of the gasification reactions are important in deciding to what degree thermodynamic equilibrium is reached.

The reaction rate of H_2O and CO_2 with char (Equations 2.3 and 2.4) can either be limited by mass transfer rates or by the kinetic rate of reaction depending upon the reaction temperature, gas flow rates, and particle size. The reaction process is shown in Figure 2.2. At low temperatures chemical reactivities are rate limiting whilst mass transfer resistance becomes significant at high temperatures. The temperature at which mass transfer limitation begins is given as 900 °C by Reed (1988). Since the reactions are endothermic and there is often heat loss, the temperature decreases with depth in a downdraft gasifier. Thus, in the upper, hotter region of the gasification zone mass transfer limitations are important, whilst in lower regions chemical reaction kinetics become rate determining. Mass transfer is discussed further in Section 2.4.3.

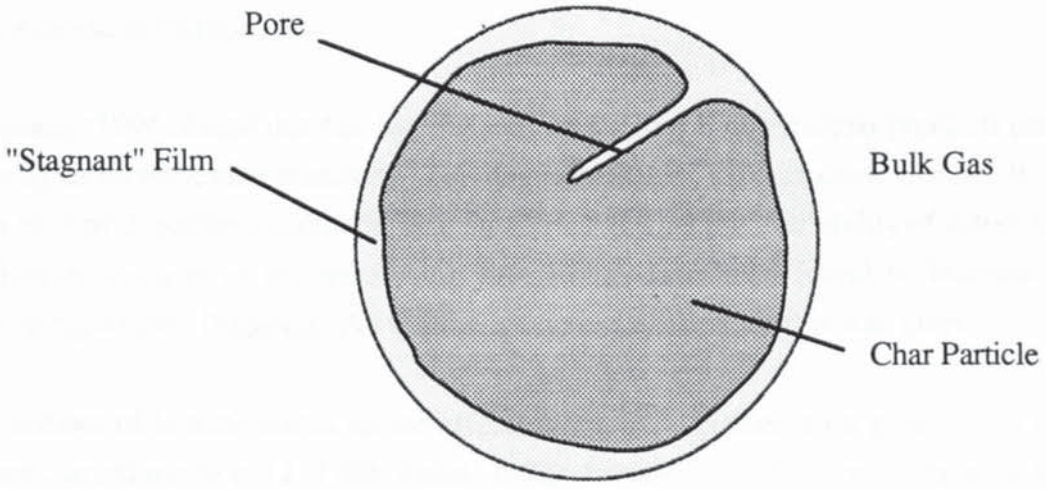

Figure 2.2 Reaction Process

2.4.2 Char Reactivity

The reactivity of a char is dependant upon its chemical composition, physical structure, the amount and distribution of active sites and catalytic elements, and the thermal history of the char. Charcoal retains the highly directional pore structure of the wood from which it was produced (Hillis, 1985). As a result, the permeability of char to gaseous reactants along the longitudinal direction is high whilst along the transverse direction the char is virtually impervious (Standish, 1988). The pores follow a bi-modal size distribution with macropores of about 20 μm in diameter, and micropores of about 2 μm (Standish, 1988). Gasification takes place at active sites on the char surface. Thermal annealing (graphite formation) occurs at temperatures between 700-1100°C (Graboski, 1979). During annealing the surface is reorganized resulting in the loss of active sites, and is also said to cause a reduction in the porosity thereby reducing the accessibility of remaining active sites to reactive gases (Graboski, 1979). Nandi (1985) found that an increase in reactivity for 'in situ' (freshly prepared) chars compared to stabilized chars (held at temperature for 30 minutes in a nitrogen atmosphere) was not accompanied by a change in surface area, indicating that thermal annealing primarily affects the number of active sites.

Reactivity alters with the degree of char conversion, known as carbon burnoff, in a complex manner. The structure changes as a result of; decomposition of the carbonaceous substance; increases in surface area due to pore formation (Kasaoka, 1983; Delikournos, 1993); and decreases in surface area due to pore expansion (Graboski, 1979; Kasaoka, 1983). Together with increases in the exposed active site surface area and increases in local concentration of catalytic minerals as the ash accumulates (Kasaoka, 1983), this leads to a complicated overall effect. Some chars show little change in reactivity with burnoff, whilst others show either increased or decreased reactivity (Graboski, 1979). For biomass chars burnoff has been found to increase the rate of gasification (Richard, 1985), which is suggested to be a result of an increase in surface area.

Espenäs (1994) found that fast heating and rapid removal of pyrolysis products during pyrolysis increase char reactivity. This suggests that tar vapours cause deactivation of the char by deposition within the char structure reducing the availability of active sites. Moisture content of the pyrolysing sample has also been found to increase the reactivity of char (Espenäs, 1994) although no explanation for this was given.

A number of investigations on the effects of catalytic elements on gasification have been carried out (e.g. Li, 1990; Rolin, 1983); however, gasification using additional catalysts is beyond the scope of this research. The indigenous calcium, potassium and

sodium content of biomass chars are known to catalyse the gasification reactions (Kannan, 1990). The ratio of the concentration of these elements to carbon concentration may increase with conversion to give an increasing rate of reaction.

2.4.3 Mass Transfer Limitations

Gas film diffusion of the reactant gas is not expected to be rate limiting at operating temperatures of gasifiers (Buekens, 1985). Calculations of external mass transfer rates are presented in Chapter 9. The lack of mass transfer data on biomass chars makes the evaluation of internal diffusion resistance difficult (Buekens, 1985). Internal diffusion resistance depends upon particle size and the effective diffusivity of gaseous reactants. Buekens (1985) suggests that for gasification at 900°C diffusion resistance becomes noticeable for particle diameters above 5 mm and limiting for particles over 10 cm in diameter. Edrich (1985) measured gasification rates of 5 mm Ponderosa pine char particles and powder with CO_2 and found that the macropore structure of chars did not affect reactivity up to 1135°C, but could not rule out mass transfer limitations in the microporous structure. Nandi (1985) argues that the larger pores act as 'feeder channels' to molecular size pores, and at high temperatures (over 815°C) restrict the diffusion of reactants to the molecular size pores.

2.4.4 Chemical Reaction Kinetics

Equation 2.15 shows a typical kinetic expressions for the gasification of char with CO_2 (DeGroot, 1984);

$$\text{Rate} = \frac{-d[X]}{dt} = kW_o(pCO_2)^n \qquad (2.15)$$

where char conversion, X, is given by;

$$X = 1 - \frac{\text{Weight of char}}{\text{Initial weight of char}} \qquad (2.16)$$

W_o is the initial weight of char, pCO_2 is the partial pressure of CO_2, n is the order with respect to CO_2 and k is the reaction rate constant in the usual Arrhenius equation;

$$k = Ae^{-Ea/RT} \qquad (2.17)$$

The activation energy (E_a) obtained by DeGroot for Douglas Fir char gasification was 221 $kJmol^{-1}$, which is comparable to activation energies obtained for various wood chars in the literature (see Table 2.2).

Table 2.2 Activation Energies of Gasification for Biomass Chars Reported in the Literature

Char, reactant	Activation energy, $kJmol^{-1}$	Reference
Douglas Fir, CO_2	221	DeGroot, 1985
Cottonwood, CO_2	196	DeGroot, 1985
Deal, $CO_2 + H_2O$	217	Groeneveld, 1980a
Rubberwood, CO_2	210	Standish, 1988
Beech, CO_2	166	van den Aarsen, 1985
Poplar, H_2O	156	Hawley, 1983

The order of the reaction with respect to CO_2 was found to be 0.6 by DeGroot (1984), and is similar to orders of 0.71 for rubberwood char (Standish, 1988), and 0.7 for deal wood particles (Groeneveld, 1980a). Groeneveld took into account the chemical reaction rate and the effective diffusivity of reactant gases as a function of the local char conversion. The reaction rate was expressed as;

$$\frac{-d[X]}{dt} = kC^n{}_A C_s \qquad (2.18)$$

where C_A is the concentration of reactant gas within a porous particle calculated using the effective diffusivity and C_s is the concentration of the solid reactant. The effective diffusivity was calculated as a function of porosity and molecular diffusivity.

The Langmuir-Hinshelwood mechanism is applicable to the CO_2 gasification reaction (Radovic, 1991) and is supported by evidence using radioactive CO (Graboski, 1979);

$$C_f \text{ (free active site)} + CO_2 \leftrightarrow C(O) + CO \qquad (2.19)$$

$$C(O) \rightarrow CO + C_f \qquad (2.20)$$

Standish and Tanjung (1988) found that conversion rates were faster at low CO_2 concentrations than at high (over 60%) CO_2 concentrations. They explained this by CO poisoning at high concentrations as the surface sites become saturated. However, the CO_2 content within an air blown gasifier are unlikely to rise above 60% so product inhibition is not significant. A similar mechanism has been proposed by Graboski (1979) for steam gasification (Equations 2.19-20), although no evidence is provided to support this mechanism.

$$C_f \text{ (free active site)} + H_2O \leftrightarrow C(O) + H_2 \qquad (2.21)$$

$$C(O) \rightarrow CO + C_f \qquad (2.22)$$

Standish and Tanjung (1988) also investigated the effect of initial particle size (D_0), and the change of particle size with conversion. The initial gasification rate varied with initial particle size as a function of $D_0^{0.81}$, although time for complete conversion (τ) varied with $D_0^{1.01}$. Particle density did not alter significantly until a decrease at about 75 % conversion. Particle size was represented by;

$$D/D_0 = (1-X)^{1/3} \tag{2.23}$$

These results are consistent with the Shrinking Core Model (SCM) controlled by gas film diffusion and chemical reaction rates. The SCM gives;

$$\therefore \tau = \rho_B \frac{D}{bk_s C_A} \tag{2.24}$$

where ρ_B is the bulk density, and k_s is the surface reaction rate.

The results give support to gasification occurring at particle external surface until 75% conversion when reaction in the pores also plays a part (Standish, 1988). Groeneveld (1980) claims that conversion occurs throughout the volume of the particle contradicting the above results. It would be expected, however, that under restricted internal mass transfer (i.e. at high temperature, see Section 2.4.3) gasification would mainly occur in the outer portions of the particle resulting in a decrease in particle size, whereas at lower temperatures the kinetic rate of reaction becomes limiting and the char particle is converted throughout its volume. As the temperature in a downdraft gasifier decreases towards the grate, gasification may at some point change from occurring predominantly at the external surface to occurring predominantly at the internal surface, and this is investigated in Chapter 9.

Moilanen (1994) gasified wood chars in 15% steam after pyrolysis at 950°C and obtained an activation energy of 196 $kJmol^{-1}$ from the rate expression;

$$\text{Rate} = \frac{1}{W}\frac{dW}{dt} = -\frac{d\ln W}{dt} = \frac{A\, k_D\, k_C}{k_D + k_C} \tag{2.25}$$

rewritten as;

$$\frac{d\ \ln D}{d(1/T)} = \frac{E_d k_D + E_a k_C}{k_D + k_C} \tag{2.26}$$

where k_D describes mass transfer rate = a T^m for which the apparent activation energy E_d = mT and k_C is chemical reaction rate = b exp ($-E_a/RT$) and constants A, m, a and b determined experimentally.

Steam gasification reaction rates increase as conversion continues, with a significant increase at about 75% conversion (Moilanen, 1994, Espenäs, 1994). In agreement

with Standish, (1988) increasing porosity has been suggested along with increasing catalyst to carbon ratio and increasing number of active sites as the cause of increasing reactivity (Moilanen, 1994).

Transient (unsteady-state) kinetics has been used to determine the site reactivity (or turnover frequency) and the number of active sites participating in the reaction (Radovic, 1991). The rate of desorption of the reactive intermediate on the surface of the char, C(O), (see Equation 2.20) is equal to the rate of reaction irrespective of the rate determining step. In steady state;

$$\frac{d[C(O)]}{dt} = \text{rate C(O) Production - rate C(O) Consumption} = 0 \quad (2.27)$$

Interrupting the steady state with an abrupt change of atmosphere from CO_2 to an inert gas allows the rate constant k to be obtained since

$$\frac{d[C(O)]}{dt}_{transient} = \text{- rate C(O) Consumption} = -k[C(O)]_{transient} \quad (2.28)$$

with

$$[C(O)]_{transient} = [C(O)]_{steady\ state} \exp(-kt) \quad (2.29)$$

Reactivity was found to have a linear relationship with the reactive surface area for coal chars by the authors (Radovic, 1991) which has been verified by other workers (Adschiri, 1991). No work on transient kinetics for wood chars was found in the literature. The use of this technique may provide a quantitative understanding of variations char reactivity with conversion.

The reaction rate of biomass char gasification is an important consideration in the design of downdraft gasifiers. Ideally, the reactor volume (or height) needed to obtain complete conversion for a specified throughput is required. Smith (1987) estimated that the gasification time of pine-wood char was 8 minutes at 900°C increasing to 518 minutes at 700°C. However, the reaction temperature within the gasification zone decreases with distance from the end of the oxidation zone due to the endothermic reactions and heat losses, reducing the gasification rate. The gasification rate may also be limited by external and internal mass transfer resistance as well as the chemical kinetics. Simulation models of downdraft gasifiers need to account for the reduction in temperature with conversion and mass transfer limitations. Modelling of downdraft gasifiers is discussed in Chapter 9.

2.5 Open-Core Downdraft Gasifiers

The open-core downdraft gasifier consists of an open topped tube through which the feed and oxidant enter and travel down towards a reaction zone supported by a grate (Earp, 1988; Reyes-Nuñez, 1989; Reed, 1983). Reed (1983), Earp (1988) and Evans (1992) all describe the open-core gasification process as a series of stratified zones shown in a general form in Figure 2.3. There are, however, certain differences in the descriptions of the zonation within the gasifier given by these workers which are discussed in the following sections.

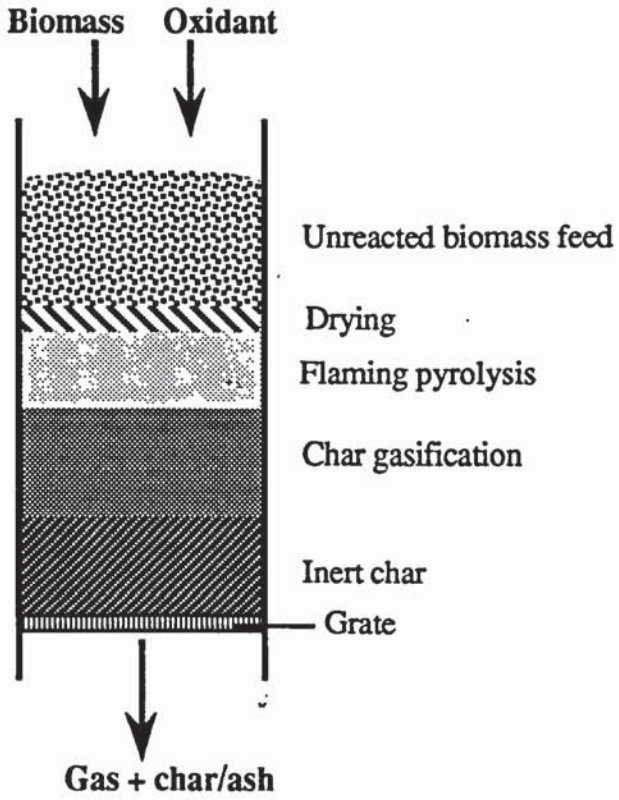

Figure 2.3 Zonation Within the Open-Core Gasifier

2.5.1 Unreacted Feed Zone

Oxidant and feed enter through the open top of the reactor forming a non reactive reservoir which is responsible for the distribution of feed and oxidant to the reaction zones below. The feed descends the reactor as a result of the consumption of material in the reaction zones, but remains unaltered until it nears the flaming pyrolysis zone. Back radiation from this zone then causes a sharp rise in temperature of the areas exposed, which results in a loss of moisture through evaporation, although very little visual change occurs (Reed, 1988). Chern (1989) suggests that the particle is completely dry at about 100°C before the particle enters the flaming pyrolysis zone. The drying process may, however, continue into the flaming pyrolysis zone (Section 2.5.2) with moisture evaporation occurring with pyrolysis at high heating rates.

Fuels with poor flow characteristics such as flat woodchips, sawdust and rice hulls form bridges within the feed zone (Reed, 1988a). Bridges prevent continuous feed flow to the reaction zone and may cause channelling of gases within the reaction zone. This may cause the formation of "cold spots" within the reaction zone thereby reducing gasification efficiency and tar cracking. The prevention of bridging may be achieved by stirring, shaking or agitating the bed and is discussed in Section 2.5.7.

2.5.2 Flaming Pyrolysis Zone

Flaming pyrolysis is the term first used by Reed to describe the process following the unreacted feed zone (Reed, 1983). Pyrolysis is observed as a charring front that progresses upwards through a particle in a wave-like manner. Soon after the onset of pyrolysis, flaming occurs as the result of the reaction of volatiles with oxygen from the air. The temperature within the particle rises slowly due to the poor thermal conductivity of wood. This results in a thermal wave passing through the particle with pyrolysis occurring wherever the temperature rises above about 250°C (Chern, 1989). Reed (1985) has calculated the biomass pyrolysis velocity to be 0.9 cm min^{-1} for an uninsulated gasifier and 3.6 cm min^{-1} for an insulated gasifier. Using the results obtained by Evans (1992) a pyrolysis velocity of 1.7-1.9 cm min^{-1} is calculated for the Aston open-core gasifier.

There is disagreement in the literature upon the propagation mechanism for flaming pyrolysis in an open-core gasifier. For propagation, heat must flow upwards to the incoming biomass against the downward flow of air and flaming gases. Reed (1985) has indicated that flames can propagate upwards into a combustible mixture of pyrolysis vapours and air, but it is unlikely that pyrolysis vapours can be transported against the downward flow of air. Convective heat transfer to incoming particles would, therefore, not be expected and this was found by Earp (1988) and Evans (1992) with flames propagating downwards away from the incoming biomass. Both Earp and Evans propose the propagation mechanism for flaming pyrolysis to be radiative heat transfer. Reed (1985) has also described radiation from hot charcoal to be an effective heat transfer mechanism to incoming biomass, but he does not say whether this is more important than heat transfer by flames propagating upwards into the biomass. Evans provides evidence for radiative heat transfer using particles extracted from just above the flaming pyrolysis zone which exhibited "thermal shadows", where only the exposed surface showed charring (see Figure 2.4). The surface remaining in contact with a neighbouring particle was unaffected indicating that conduction is insignificant in the initial stages of flaming pyrolysis. Both Earp and Evans neglect to say whether radiative heat from the solid or from the burning gases is the most important; however, since the emissivity of gases is small due to the short path lengths it can be concluded that radiation from the solid is the major mechanism.

Conduction and radiation from the reactor walls would also make a minor heat contribution to the incoming biomass. The amount of heat transfer by these mechanisms would depend upon the thermal properties of the material of construction and the amount of heat lost to the surroundings.

Figure 2.4 Thermal Shadows (from Evans, 1992)

After the commencement of flaming pyrolysis, heat transfer within the zone becomes more complicated and is poorly understood. Evolving pyrolysis vapours form a boundary layer between the surface of the particle and the oxidizing gases. Heat can be supplied from the flame via conduction across the boundary layer and by radiation. Reed (1988) has estimated the heat flux to be 1.1 Wcm^{-2} across a 3.5 mm boundary layer during flaming combustion. This compares to a value of 2.16 Wcm^{-2} required for flaming pyrolysis calculated by Reed (1988) using his modified Huff Equation (see 2.5.2). As previously stated the contribution of radiative heat from gases is relatively minor. A pyrolysing particle will continue to receive radiation from the surfaces of surrounding particles; however, once the surface temperature of the particle undergoing flaming pyrolysis matches that of its neighbours there will be no net heat flow by radiation. Surface temperature measurements on flaming particles conducted by Reed (1988) are in the range 450-700°C. As an estimation of the possible radiative heat flux, the amount of radiation received by a particle with a surface temperature at the lower end of this range from a parallel surface at 700°C is calculated using Equation 2.30;

$$\text{Radiative heat transfer} = \varepsilon\sigma(T_2^4 - T_1^4) \qquad (2.30)$$

where ε is the emissivity of charcoal (taken to equal 1), σ is the Stefan-Boltzman constant (5.67×10^{-12} $Wcm^{-2}K^{-4}$), and T_2 and T_1 are the surface temperatures of the neighbouring particles. This gives a value of 3.53 Wcm^{-2}, which is again comparable to the heat transfer rate required for flaming pyrolysis estimated by Reed (see above). In addition, there would be convection, radiation and conduction from the flames of surrounding particles, and radiation and conduction from the reactor walls.

Within the particle heat is transferred mainly by conduction. Heat is also carried by the pyrolysis vapours, but since these would flow out of the particle following the open channels created by pyrolysis, the amount of heat carried towards unreacted material can be considered negligible. The flow of volatiles from the particle would also have a cooling effect at the particle surface.

Evans (1992) suggests that the rate of radiative heat transfer to particles at the reaction zone front controls the rate of pyrolysis. He found that the temperature at the base of the flaming pyrolysis zone was approximately constant at about 1020°C during standard operation giving an approximately constant rate of pyrolysis.

Reed (1983) put forward a generalized equation (2.29) for flaming pyrolysis of a typical biomass feed to a typical flaming pyrolysis product gas (with nitrogen omitted and no hydrocarbon products) as shown (Equation 2.31);

$$CH_{1.4}O_{0.6} + 0.4\ O_2 \rightarrow 0.2\ C + 0.45\ CO + 0.35\ CO_2 + 0.45\ H_2 + 0.25\ H_2O \quad (2.31)$$

Stoichiometric combustion is given in Equation 2.32.

$$CH_{1.4}O_{0.6} + 1.05\ O_2 \rightarrow CO_2 + 0.7\ H_2O \quad (2.32)$$

The ratio of added oxygen needed for flaming pyrolysis to that required for complete oxidation is the air factor (or equivalence ratio), which, for the values presented in the equations, is 0.38. The calculated air factor is higher than that shown by Figure 2.7 (see Section 2.5.6) for ideal gasification, which indicates that the reaction given in Equation 2.31 is for non-ideal conditions. The combustion of some of the pyrolysis gases with oxygen from the air within the zone provides energy for the gasification process.

Volumes of gas released are in the order of 1000 times the volume of biomass (Reed, 1983). Reed suggests that the evolved gases form a boundary layer around the biomass particle which act as a "temperature buffer", since higher temperatures increase the thickness of the boundary layer as volatile production increases thus reducing the heat transfer to the particle. Conversely, if the temperature is low the rate of pyrolysis is reduced resulting in a thinner boundary layer and heat is more easily passed to the particle. Together with the endothermic pyrolysis reactions, this buffering boundary layer is said to limit the particle's surface temperature to between approximately 800 and 900°C and prevent the reaction of pyrolysis gases with solid char until flaming pyrolysis is complete (Reed, 1983).

The end of the flaming pyrolysis zone is distinguished by the termination of volatiles evolution from the particle and hence flaming, although flames extend below the bottom of the flaming pyrolysis zone. The time taken for flaming pyrolysis increases with increasing particle size (Reed, 1983; Evans, 1992) as shown in Table 2.3. Evans also observed the flaming pyrolysis time for 6.35-12.7 mm particles in an insulated reactor to be 37.2 seconds, which indicates that flaming pyrolysis rates are faster in higher temperature environments. Reed (1983) determined the effect of moisture content on the time for flaming pyrolysis of 11 mm diameter dowells, 25 mm long by measuring the time taken for the centre of the particle to reach the bed temperature. At 30% moisture content the particles took 180 seconds to reach the bed temperature as opposed to 48 seconds for particles at 5% moisture content. The increase in flaming pyrolysis time is due to the increased heat required to evaporate moisture from the particle.

Table 2.3 Observed and Calculated Flaming Pyrolysis Times for Different Sized Particles (Evans, 1992)

Reed (1983) modified an empirical relationship developed by Huff (1985) to predict flaming pyrolysis times from input variables of particle shape, size, moisture content, specific density, temperature and oxygen fraction of the oxidizing gas. Evans (1992) used this relationship to compare predicted flaming pyrolysis times with those observed, presented in Table 2.3. There is a good agreement between predicted and observed pyrolysis times only for the feed size 6.75-12.7 mm. At smaller feed sizes the modified Huff equation under-estimates the flaming pyrolysis time, whilst for larger sized particles the calculation over-estimates the time required.

The rate of pyrolysis is controlled by the rate of internal heat transfer within the biomass particle (Buekens, 1985). Mathematical models of pyrolysis have been used to calculate the time required for complete devolatilization. Groeneveld (1980) calculated the Fourier heat penetration times using Equation 2.33.

$$\text{Time, seconds} = \frac{F_0 D^2}{\alpha} \qquad (2.33)$$

where α is the thermal diffusivity (2×10^{-7} m^2s^{-1}), and D is the particle diameter, and F_o is the Fourier number. Groeneveld assumed a Fourier number of 0.1 for all particle sizes, and does not consider the effect of external temperature, nor does he give the temperature at which pyrolysis occurs. Calculated heat penetration times using Equation 2.33 are presented in Figure 2.5. Pyrolysis modelling is discussed further in Section 9.4.

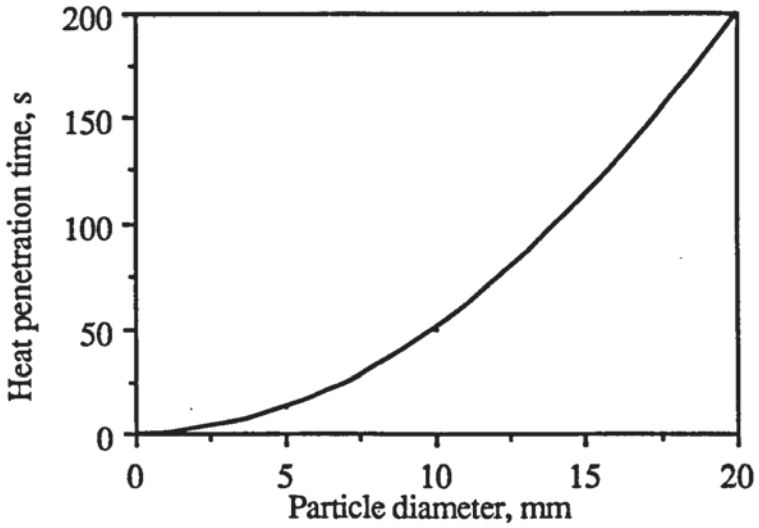

Figure 2.5 Fourier Heat Penetration Times for Pyrolysis

2.5.3 Reaction Zone Voids

Earp (1988) reported a void zone filled with flaming pyrolysis gases of between 1 to 2 particle diameters in depth directly below the flaming pyrolysis zone. He claims that particles drop directly from the flaming pyrolysis zone to the top of the char bed (i.e. the char gasification zone) through the void zone. Evans reported occasional void formation due to the bridging of particles within the flaming pyrolysis and unreacted feed zones. Voids were reported to be more prominent using irregularly shaped wood chips, no voids being observed with uniform spherical feed. The voids disappeared when the bridge above collapsed causing pyrolysing particles to fall on to the gasification char bed. Evans (1992) suggests the particles that arrive in this way more rapidly complete pyrolysis since temperatures in the top of the gasification zone were measured to be approximately 1000°C. This may lead to increased tar levels in the product gas as the residence time of the pyrolysis vapours at tar cracking temperatures are reduced. The form and effect of voids within the reaction zone is investigated in this research. Neither Chern (1989) nor Reed (Reed, 1983; Reed, 1985) mention voids within the gasifier. At the end of the flaming pyrolysis zone the particles enter the char gasification zone.

2.5.4 Gasification Zone

In the gasification zone the endothermic gasification reactions discussed in Section 2.3, take place causing the temperature of the zone to decrease from 1000-1100°C to about 700°C. At stable operation a char particle will be completely consumed within the gasification zone since there is no increase in the height of char bed within the gasifier by definition. Evans states that the particles at the base of this zone will be the smallest within the gasifier and ash may collect at the interface between the gasification zone and the following inert char zone. For low ash feeds such as woodchips it is likely, however, that as conversion proceeds the integrity of the char structure reduces and the char particle breaks up to form a dust containing the ash. A significant proportion of the ash will, therefore, be entrained into the gas stream and carried out of the gasifier. For high ash feeds (> 5-10%, e.g. straw, rice husks, MSW) the accumulation of ash at the end of the gasification zone would cause problems due to an increasing pressure drop across the reactor, or if temperatures are significantly high, ash slagging may occur. The use of an ash removal system is essential when operating with high ash feeds (Kaupp, 1983). The use of stirrers is discussed in Section 2.5.7.

The time for conversion is expected to be a function of original particle size and the temperatures within the gasifier. The kinetics of the gasification reactions have previously been discussed (Section 2.4). Earp (1988) observed the time for complete conversion including the flaming pyrolysis for particle sizes 4.75-6.35 mm to be 36 seconds. Evans' observations of the gasification of 15 mm spherical wood particles varied from 72 to 359 seconds and an average gasification time of 200 seconds for an average conversion of 87% (1992). He related the time for conversion to the relative rates of particle movement downwards through the bed. Particles moving slowly through the gasification zone were converted in the shortest time since the particle resided in a high temperature region where gasification proceeds more rapidly.

Reaction times of the order of 130 seconds have been calculated by Reed (1983) using an adiabatic kinetic model for 90% completion of reaction of char (no particle size given) with pure carbon dioxide at 1200 K. At 800°C 90% conversion is predicted in 100 seconds; however, doubling the time would only give an additional 2% conversion (Reed, 1984). Reed (1988) states that to get significantly higher carbon conversion after the bed temperature has fallen below 800°C would require a large increase in bed length. However, Reed does not indicate whether particle volume reduction with conversion is included in his models. Reed suggests that about 3% of each particle remains as carbon dust after gasification (Reed, 1985). The carbon dust

and remaining small char particles may be entrained into the gas stream to be carried out of the gasifier, or be deposited in the inert char zone (see below).

2.5.5 Inert Char Zone

The product gases pass through a char zone which is considered to be inert since the rate of gasification becomes insignificant at the temperature of the zone (below about 700°C). Reed suggests that the inert char zone may help reduce the tar content of the product gas by cracking the tars to lower molecular weight material. Tar cracking is said to occur above 800°C by Reed (1988a), but he also suggests that tar cracking is inefficient due to the short residence time available. Earp (1988) suggests that a temperature of 850°C is required for tar cracking but provides no evidence to support this. Kaupp (1983) investigated the tar cracking properties of rice husk char beds and found that the presence of a carbon surface improves the tar cracking efficiency between 680°C and 920°C (see Figure 2.6). Figure 2.6 also shows that tar conversion was found to be a linear function of temperature within the range investigated.

Figure 2.6 Tar Conversion Efficiency of Rice Hull Char Beds Compared to an Empty Tube (After Kaupp, 1983)

Kaupp suggests, however, that efficient tar cracking of greater than 95% conversion can only be expected at temperatures greater than 1000°C. Similarly, Parikh (1986) states that temperatures below 1000-1100 °C are inadequate for elimination of tar from the product gas. Since gasification occurs at temperatures in excess of 700°C the "inert" char zone will not crack tars to any great extent by definition (tar cracking in throated downdrafts is discussed in Section 2.6.1). The inert char zone may adsorb a limited amount of tar from the gas stream thereby providing a beneficial effect.

Small char particles and dust from the gasification zone enter the inert char zone. Since the height of the inert char bed is approximately constant during stable operation (see Section 2.5.6) this may lead to densification of the bed. In addition, existing char particles within the inert char zone may undergo attrition by particles carried in the gas stream or break-up as the result of stirring (see Section 2.5.7) to form dust. The increase in the amount of smaller particles with time may lead to a high pressure drop developing across the reactor which may cause problems in controlling the air flow into the reactor. Dust deposited in the inert char zone or formed by attrition and break-up within the zone may be carried out in the product gas after entrainment. The gas temperature leaving the the gasifier at the grate will further decrease due to heat loss and will depend upon the extent of insulation and the height of the char bed (Evans,1992).

2.5.6 The Operation of Open-Core Gasifiers

A wood-fed open-core gasifier can be operated in three modes (Earp, 1990);

1) Gasification dominant, where the rate of char consumption is greater than the rate of char deposition by pyrolysis. This results in movement of the reaction zone towards the grate.
2) Pyrolysis dominant, where pyrolysis occurs at a faster rate than that of gasification resulting in char accumulation and an increase in the char bed height (unless char is removed from the gasifier).
3) Stable reaction zone, where the rate of char deposition by pyrolysis equals the rate of char depletion by gasification and the reaction zone is stationary relative to the grate. This is the optimum mode of operation since the gasifier can be run for long periods with a relatively constant output compared to operation in the gasification and pyrolysis dominant modes.

Stable mode operation at the carbon boundary is the thermodynamic optimum for gasification (Double, 1989) giving the maximum output of chemical energy as product gas. Because of their fixed geometry it is likely that open-core gasifiers can only operate continually with a stable reaction zone at a fixed set of operating parameters for a given feedstock. For open-core gasifiers there is said to be only one air to fuel ratio which will permit a stable reaction zone (Earp, 1988). At this air factor the gasification process will be at its most efficient (Earp, 1988); however, a small change in any operating parameter may cause the zone to drift in either direction (Reed, 1985). For example, a decrease in the air flow rate into the gasifier, which may be caused by increasing pressure drop within the reactor, would result in the zone rising away from the grate.

For optimum performance, gasification with air occurs at an equivalence ratio (i.e. the ratio of the air supplied to the air required for complete stoichiometric combustion) of about 0.25 for a gasifier with no heat loss (Reed, 1988). Equivalence ratios of less than about 0.2 are indicative of pyrolysis and net char generation, and an equivalence ratio of 1 indicates that stoichiometric combustion is taking place. Figure 2.7 shows the effect of equivalence ratio on the composition of the product gas, with an increase in the proportions of combustion products as the equivalence ratio increases (Desrosiers, 1979).

Figure 2.7 Equilibrium Composition for Adiabatic Air/Biomass Reaction (Modified after Desrosiers, 1979)

Ideal gasification is not achieved due to heat losses from the gasifier leading to an increase in the equivalence ratio and corresponding change in the equilibrium composition of the gas. The equilibrium composition may not be reached due to kinetic effects discussed in Section 2.4.

In the pyrolysis dominant mode the reaction zone will rise until it reaches the top of the bed and will become top stabilized (Reed, 1985) and the gasifier is controlled by the feed rate. Using oxygen increases the rate of pyrolysis over the rate of gasification and the reaction zone will become top stabilized (Reed, 1988). With a stable reaction zone the rate of char production by pyrolysis equals the rate of char gasification and the position of the reaction zone will remain approximately constant relative to the

grate. Evans (1992) explains movement of the reaction zone as a result of the quantity of air entering the gasifier. An increase in the amount of air into the gasifier is said to increase the degree of oxidation of the pyrolysis products leading to higher concentrations of the gaseous reactants (carbon dioxide and water) and heat energy (Evans, 1992). Evans claimed that there is an increase in the rate of pyrolysis due to increased radiative heat transfer to the pyrolysis zone, indicated by an increase in specific capacity. However, this is said to be offset by the greater increase in gasification rates due to the additional heat generated by oxidation (Evans, 1992) resulting in a downward movement of the reaction zone. Evans supports his argument with the observation that temperatures at the top of the gasification zone (1045°C) are higher during char consumption (gasification) dominant operation than in stable zone operation (1018°C). The equivalence ratio for gasification dominant operation was 0.435 compared to 0.391 for stable operation in Evans's experiments.

Reed (1985; 1988) explains reaction zone stability in terms of flame front velocity. He claims that if the oxidant flow is too high, the flame propagation to incoming particles is not fast enough to maintain a stable position and the reaction zone moves towards the grate (Reed, 1988). This explanation is applicable only if the mechanism for propagation of the pyrolysis reaction is by the burning pyrolysis gases. The heat transfer mechanism for pyrolysis was discussed in Section 2.5.2.

In the Kansas State University gasifier (Walawender, 1985) secondary air is provided through an 'airgitator' (see Sections 2.5.7 and 2.7.2). This would aid stabilization since the gasification zone tends to move towards the oxidant inlet (Reed, 1988). The stability of the zone is therefore expected to be less sensitive to air input rate variations.

The SynGas gasifier operated with almost no unreacted feed in the gasifier with the fire stabilized on top of the bed (Graboski, 1987). The bed height was kept constant for a given air rate (which is altered to meet demand) by adjustment of the feed rate. In addition, char was extracted from the gasifier (Graboski, 1987). The rate of char extraction was reported to remain approximately constant as the wood flow rate was increased (Graboski, 1987), which suggested greater carbon conversion at higher throughputs to the investigators. This would suggest that the gasifier is operating in pyrolysis dominant mode with char removal, and that as the air and feed rate are increased pyrolysis becomes less dominating. Char removal is also used to maintain a stable reaction zone in char producing gasifiers (Wallace, 1991).

2.5.7 Stirring of the Bed

Bridging of the feed and channelling of air through the unreacted feed bed due to poor feed flow may result in poor oxidant distribution across the reaction zone thereby reducing the gasification efficiency. Stirring of the feed bed may, therefore, be necessary to distribute the feed across the cross-section of the gasifier. Channelling within the char bed can also occur as a result of blockages in parts of the bed caused by the accumulation of fines and ash slagging (Hos, 1987). The char dust and ash fines accumulate in the lower parts of the gasifier and reduce the gas flow as a result of increasing the pressure drop across the bed (the pressure drop across the unreacted feed bed is usually small compared to that within the char bed). Removal of fines from the bed is therefore important for continuous operation of the gasifier. In small scale moving beds the removal of fines is usually achieved using intermittently operated shaking grates (Hos, 1987). Other gasifiers have more complicated systems to remove fines which may also maintain regular bed movement over the entire cross-section of the gasifier and may serve as an air distributor (e.g. Walawender, 1985).

Graboski and Brogan (1987) tried a number of agitator configurations in order to remove voids generated below the feed zone by the consumption of material which would periodically collapse creating a rush of gas. Stirrers were found to be of no significant benefit as fines were not sufficiently removed and voids were not eliminated. Generally the presence of a stirrer was found to be harmful since the wood charcoal was very friable and tended to grind to dust by the stirrer. However, the grate was rotated at 3-4 rpm which is faster than that recommended by Hos (1987) who states that a speed of rotation greater than about 1 revolution an hour leads to densification of the bed.

Reed (1988) used a stirrer consisting of a rod with 8 radial rakes connected to the grate. Bars were inserted into the bed from the walls to prevent the bed moving as a single unit. High rotation rates of up to 122 revolution per hour were found to increase the amount of char removed from the gasifier dramatically decreasing the cold gas energy conversion efficiency. Reduction of stirring rates to 5-10 revolutions per hour improved char conversion, increased the bed temperature and decreased the amount of tar produced.

The Kansas State University gasifier (Walawender, 1985) uses an 'airgitator', a hollow shaft which provides secondary air through tuyeres, levels the feed bed and mixes the bed material throughout the gasifier. The airgitator is connected to the grate and rotates at between 0 and 21 revolutions per hour (Walawender, 1988). The influence of grate rotation on the performance of the gasifier has been investigated in

detail by Walawender (1987; 1988). Higher rotation rates were found to decrease the pressure drop in the bed and increase the feed rate and char yield. Increasing the rotation speed up to four revolutions per hour resulted in a sharp decrease in the air/feed ratio and a sharp increase in gas heating value. Further increases in rotation speed had little effect. A maximum in the cold gas efficiency of 70% was observed at a rotation speed of 4 revolutions per hour, after which the increase in char output reduced the cold gas conversion efficiency.

A low stirrer rotation speed (4-5 revolutions per hour) is therefore desirable in reducing the pressure drop across the char bed by the removal of fines, and to remove blockages which may occur and which may cause channelling of the gases through the char bed thereby reducing char conversion. Fast rotation speeds are to be avoided since they result in char break-up and reduce the conversion efficiency as a greater proportion of char exits the gasifier. The design of an agitator for the Aston Gasifier considering these conclusions is discussed in Section 3.11.

2.5.8 Effect of Feed Characteristics

The open-core gasifier is believed to be able to operate with a wider range of feedstocks and feed sizes than the conventional throated gasifier, since there is no resistance to material flow imposed by the reactor. For example, sugar-cane leaves (Rajvanshi, 1994), carrot fibre (Reines, 1984) and rice husk (Kaupp, 1983; Manurung, 1985) have been successfully gasified in open-core gasifiers. The feed limitations of throated gasifiers are discussed in Section 2.6.4. Evans (1992) claims that the ideal characteristic particle size (defined in Section 4.3.7) for the Aston open-core gasifier is 6.4 mm. For this feed size the required air to feed ratio for stable operation is at a minimum. Below this size Evans states that the pressure drop becomes problematic, giving rise to irregular flow of material through the reactor. Above 6.4 mm Evans suggests the increase in the air requirement needed for stable operation is due to an the increase in char yield associated with larger particles (see Section 2.2.2), although no reasons as to why this should be were given. Reed (1988) attempted to gasify 3.2 x 3.2 x 5-10 cm compressed waste wood blocks; however, the run was not successful due to overheating and melting of the grate. The depth of bed available was said to be too short for satisfactory gasification (Reed, 1988) resulting in higher temperatures at the grate. Larger particle sizes require a greater depth of bed for complete pyrolysis and gasification. The height of reactor needed can, therefore, be considered as a function of the particle size. Evans (1992) has observed the depth of the flaming pyrolysis zone to be equal to 1.2 characteristic particle diameters (D_p), and the depth of the char gasification zone, defined as the distance between the end of the flaming pyrolysis zone to the end of the glowing char,

to be 4.8 D_p. However, Evans also infers from temperature profile data that gasification takes place at a depth of 9.5 D_p. Earp (1988) reported a gasification zone depth of 1 Dp, but does not give the start and end points of the char gasification zone.

2.5.9 Gasifier Performance and Product Gas Quality

The quality of the product gas depends upon its energy, tar and solids content. The performance of selected open-core gasifiers found in the literature are presented in Table 2.4. The product gas from the Aston open-core gasifier used in previous research (Evans, 1992) has a higher nitrogen content and a lower H_2, CO, and CH_4 content than the product gas from the other gasifiers listed and this results in a lower energy content of 4.49 $MJNm^{-3}$ compared to values in the range 5.8-6.1 $MJNm^{-3}$ for other wood fed gasifiers.

The Solar Energy Research Institute (SERI) gasifier was similar in design to the Aston open-core gasifier. The energy conversion efficiency of 96% calculated by Reed (1988) is unrealistically high and indicates an error in the gas flow rate measurement. The SynGas gasifier (Graboski, 1987) used a propane burner and char removal in order to aid the maintenance of a stable reaction zone. The amount of propane used made up about 5% of the total energy input to the gasifier. The propane may have lowered the air to feed ratio required, and may also have improved the cracking of tars, resulting in a higher product gas energy content and conversion efficiency. The amount of tar produced is not reported.

The Kansas State University gasifier (Walawender, 1987) may be considered as a partial hybrid (see Section 2.7.2) since secondary air is injected into the reactive bed, although the proportion of air delivered in this way is not stated. The gasifier is calculated to have a turndown ratio of at least 3.8 from the data given by Walawender (1987). The tar content of the product gas is comparatively low, which may also be the result of secondary air injection since oxidation of the tars would occur.

The University of California, Davis (UCD) gasifier was used to gasify rice hulls. The differences in the gas composition between the UCD and the other gas compositions listed can, therefore, be attributed to differences in the feed composition and structure, and the feed flow characteristics. The particulate level in the gas is very low since it was measured after a cyclone.

The Forestry Research Institute of Malaysia used a throated gasifier in which the throat was removed to give a hybrid gasifier and is discussed in Section 2.7.2.

Table 2.4 Selected Open-Core Gasifier Performance Data

Name	Aston	KSU	SERI	SynGas	UCD	FRIM
Type	Open-core insulated	Open-core + secondary air	Open-core	Open-core + propane	Open-core	Open-core/hybrid air injection
Reference	Evans, 1992	Walawender, 1987	Reed, 1988	Graboski, 1987	Kaupp, 1983	Hoi 1990
Grate diameter, mm	75	600	nr	1370	162	550
Feedstock	Wood	Wood	Pine chips	Wood chips	Rice hulls	Rubberwood
Size, mm	6.35-12.7	0-12.7	25x25x1	nr	nr	10x10x10
Moisture, %wb	9.42	9.99	2.8	10	12.4	10
Gasifier Performance						
Spec. capacity, $kgm^{-2}h^{-1}$	321	200	nr	360	135	nr
Air/feed ratio	2.48	1.4	3.02	2.00[e]	1.4	nr
Energy efficiency[a], %	63.5	72.0	96	79.7	58	nr
Gas HHV, $MJNm^{-3}$	4.49	6.08	5.8	6.10[c]	5.0	6.81[c]
Dry gas composition, % vol.						
H_2	13.25	15.13	17	17.8	9.6	10.0
CO	17.41	19.64	19	21.2	17.6	15.5
CO_2	12.36	14.64	14	10.9	13.1	11.0
CH_4	1.50	3.09	2	2.9	5.1[b]	9.0
N_2	55.48	46.36	48	45.8	54.6	53.5
C_2+		1.13		1.4		
Raw gas water content	nr	0.26 kg/kg DAF	66 gNm^{-3}	11.4% vol.	15.4% vol.	nr
Char yield, % daf	nr	10.8	2.6	5.1	2 $mgNm^{-3}$ [d]	nr
Tar content	1.05% daf	336 $mgNm^{-3}$	585 ppm	-		nr

Notes: nr, not reported; a, cold gas; b, total hydrocarbons; c, calculated from reported gas composition; d, particulate load in gas; e, calculated

2.6 Throated Downdraft Gasifiers

The more conventional downdraft gasifier ("Imbert type") design has a constriction through which material must pass. The constriction may be in the form of a choke plate (e.g. Crane, 1979) or conventional throat (see Figure 2.8).

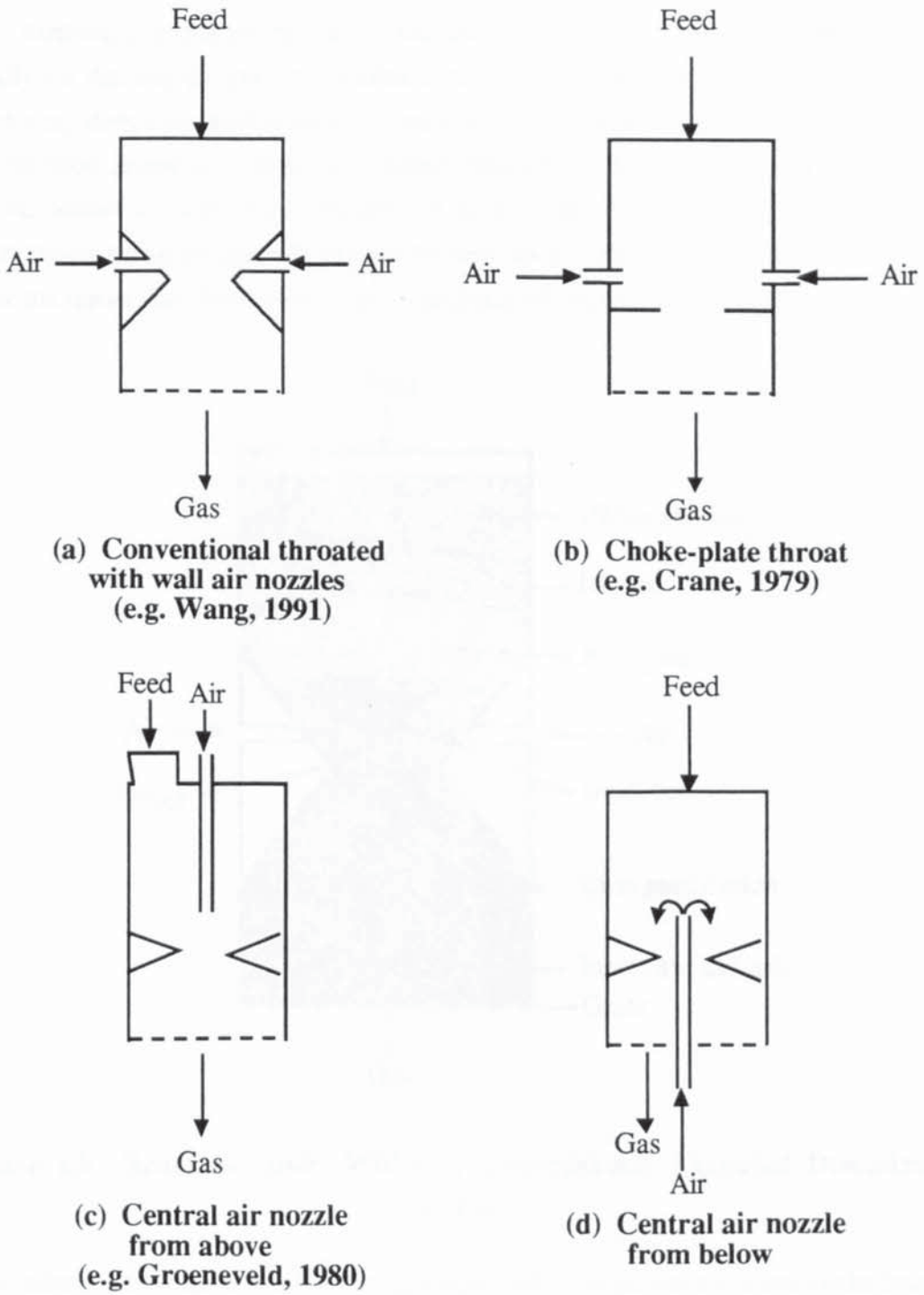

(a) Conventional throated with wall air nozzles (e.g. Wang, 1991)

(b) Choke-plate throat (e.g. Crane, 1979)

(c) Central air nozzle from above (e.g. Groeneveld, 1980)

(d) Central air nozzle from below

Figure 2.8 Throated Gasifier Designs

Discontinuous batch feeding using a gasifier with a lid, or a sealed continuous feeding system is required to prevent the ingress of air with the fuel, although a small amount of air leakage can be tolerated (Groeneveld, 1980). Leakage at the lid adversely affects gasification in Imbert type gas generators causing an upward movement of the fire

zone (Anonymous, 1979). This is reported to result in an increase in CO_2 content and a decrease in CO and H_2, with about 20% reduction in the gas heating value (Anonymous, 1979). In addition, as the fire zone rises heat stresses may damage the upper part of the gasifier which does not usually need to be constructed from high temperature materials, and damage to seals in the feeding system may be encountered. Air is directed into the gasifier at or just above the throat. The air may be supplied radially via the wall through air nozzles or tuyeres, or vertically using a central nozzle which may direct air from above (Figure 2.8 (d)) or below the throat (Kaupp, 1984). The reaction processes within a throated gasifier are commonly drawn as simple layered zones as shown in Figure 2.9 (e.g. Vigil, 1980); however, no direct observations using transparent reactor vessels were found in the literature. A void below the throat may be expected due to bridging of material across the throat.

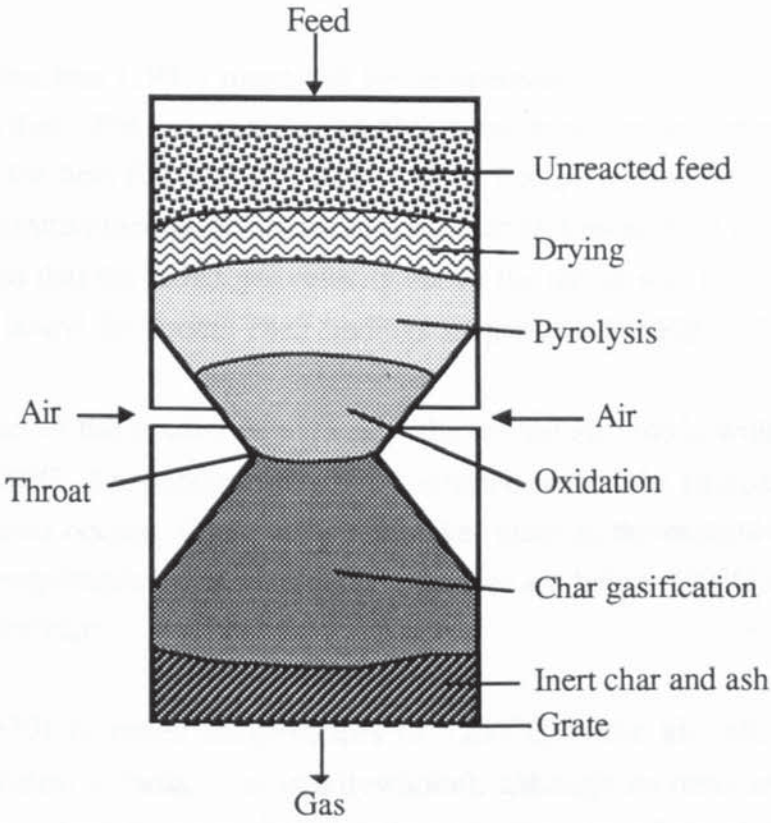

Figure 2.9 Reaction Zones Within a Conventional Throated Downdraft Gasifier

The oxidation zone is situated at the air inlets, and is sometimes known as the hearth zone. There is a sharp rise in temperature in the oxidation zone up to about 1200°C. The high temperatures attained are important in the cracking and oxidation of pyrolysis tars (see Section 2.6.1). Heat from the oxidation zone travels upwards causing pyrolysis in the zone above, which is also known as the distillation zone. Above the pyrolysis zone partial drying of the feed occurs in the drying zone (see Figure 2.9).

Below the oxidation zone the char is converted according to the reactions given in Table 2.1.

Char dust and ash are carried out of the gasifier by the product gas or pass through a grate to a collection chamber. The grate is usually shaken at intermittent intervals in order to remove fines from the char bed which would otherwise clog the bed and reduce the gas flow (Reed, 1988a). If solids removal is too rapid the reaction zone does not stabilize and may result in partially pyrolysed fuel entering the char gasification zone. The particle residence time within the hot zone and temperatures are reduced, which lead to a higher tar content in the product gas (Crane, 1977). In addition, a higher proportion of unconverted char is lost. The fines collected from below the grate may contain 10-50% ash, with char making up the balance, and represents 2-10% of the biomass input (Reed, 1988a).

Wang and Kinoshita (1991) measured the temperature field of a 90 cm diameter downdraft gasifier. They attempted to identify exothermic and endothermic zones by estimation of the heat flux and calculation of the energy released or absorbed. For example air streams entering the high temperature centres indicate an exothermic zone. It was assumed that the radial gas velocity above the throat was towards the centre, and outwards below the throat. Their findings are presented in Figure 2.10.

The hottest part of the gasifier is just below the central air nozzle with temperatures exceeding 1100°C. The exothermic region is situated around the air nozzles where the oxidation process occurs. Char gasification takes place in the endothermic region at the throat. Temperatures at the base of the gasifier are below 700°C suggesting the presence of inert char.

Williams (1979) recorded temperatures of 1260°C at the air inlets and 871°C immediately below a choke plate in a downdraft, although no measurements on the position of the air inlets to the choke plate or the diameter of the choke plate were given. Kaupp (1984) reports that the high temperatures can cause metal fatigue, melt down and cracking of the material used in the construction of the throat. Kaupp suggests that the choke plate design, shown in Figure 2.8(b), may reduce thermal stresses since no damage was observed for the UCD (University of California, Davis) gasifier after three years operation using a carbon steel choke plate.

Figure 2.10 Temperature Distribution and Reaction Zone Designation in a Downdraft Throated Gasifier (Wang, 1991)

2.6.1 Influence of Reactor Design on Tar Conversion

The tar content of the product gas can be reduced by oxidation, by thermal cracking, or by catalytic cracking. The use of catalysts in the reduction of tar from gasifiers has been reviewed by Bridgwater (1993a) and is not discussed here since it is beyond the scope of this thesis. Oxidative degradation of the tars can only take place in the oxidation zone, whilst thermal cracking requires temperatures greater than about 1000°C (see Section 2.5.5). In a throated gasifier all the products from pyrolysis must pass through the throat. Cold spots within the oxidation zone result in tars passing through uncracked. Gumz (1950) postulated that the areas between the nozzles close to the wall and at the centre of the gasifier are oxygen deficient (see Figure 2.11).

Figure 2.11 Oxidant Distribution in a Conventional Throated Gasifier (After Gumz, 1950)

However, the distribution of oxidant may not be as well defined as Gumz indicates since an air jet may impinge on a particle to give a randomly varying oxidant distribution. On average, however, there may be a non-uniform distribution. Poor

penetration by an air jet gives poor oxidant distribution which results in 'cold spots' where temperatures are not sufficiently high enough for tar cracking. Devolatilization products are said to be able to pass through these areas without oxidation, although partial thermal cracking occurs in the zone below (Gumz, 1950). Limited penetration also limits the volume of the mixing area about the point of oxidant injection (Groeneveld, 1980). Central air nozzles may possibly give a better air distribution. However, if the air is delivered from below with the tuyere passing up through the throat (see Figure 2.8d) bridging of the feed above the throat will be increased (Kaupp, 1984). There may also be a higher voidage within the char bed leading to channelling and poor tar cracking (Kaupp, 1984).

The positioning of the air injectors relative to the throat, the size of the injector nozzles, and the throat diameter all have an effect on tar conversion (Anonymous, 1979). The penetration of the feed bed by an air jet is limited by the rapid rate of oxidation with the pyrolysis products. The throat reduces the cross-sectional area of the reactor which reduces the air penetration distance required. Groeneveld (1980) found that the penetration distance of the air jet was mainly affected by particle size in cold flow modelling; however, no quantitative relationship was given. When air is supplied radially there is typically an odd number of nozzles in order that the 'jets' do not impinge upon each other (Reed, 1988a), but how this affects the performance of a gasifier is not discussed.

Using cold flow visualization and methane tracer techniques Groeneveld (1980) found that circulating flow patterns existed above the throat (see Figure 2.12). This indicates considerable mixing of gases and tars within the high temperature oxidation zone near the point of air injection. Groeneveld (1980) found that 'tar-free' (< 250 $mgNm^{-3}$) operation was possible with temperatures at the throat wall of 530°C, well below that required for tar conversion, suggesting tar transport by circulatory flows to the air inlets. Groeneveld (1980) observed that increasing the distance between the inlet nozzles and a 0.25 m throat above 0.12 m produced a sharp increase in tar production. However, he found nothing to suggest that the total air inlet flow or the air inlet velocity (which was varied as a function of the air inlet diameter) affected tar production.

Figure 2.12 Circulating Flow Patterns Within a Throated Downdraft Gasifier (Groeneveld, 1980)

Hoi (1991) compared the effect of using six air inlets compared with three air inlets and found tar production rates were higher using six nozzles. This was explained by a lower inlet velocity and implied poor penetration of the air jet. However, as previously mentioned, there are usually an odd number of nozzles to prevent hot gases from one nozzle impinging upon an opposite nozzle (Reed, 1988a) and this may be occurring in Hoi's six nozzle gasifier. How this affects tar cracking is not clear. Hoi also found that an increase in throat diameter decreased the tar output. He explained this by fuel bridging above the throat forming voids within the throat space through which tars could pass uncracked. Increasing the throat diameter would reduce the incidence of bridging and may therefore increase the tar cracking capability. Minimising heat loss to give higher temperatures throughout the gasifier also improves thermal tar cracking. Kaupp (1983) found that tar conversion was a linear function of temperature (see Section 2.5.5; Figure 2.6).

Susanto (1983) describes a downdraft gasifier which uses internal recycling of pyrolysis gases through a separate combustion chamber which produces a gas with a tar content less than 100 $mgNm^{-3}$. Thermal and catalytic tar cracking in a secondary reactor may also be used to reduce tar levels (Reed, 1988a; Bridgwater, 1993a).

2.6.2 Sizing of Gasifier

The sizing and design of throated gasifiers is mainly obtained from empirical data (Reed, 1988a). To avoid cold spots within the fire zone the reactor geometry and the gas velocity must be carefully chosen (Groeneveld, 1980). The superficial velocity (ms^{-1}) and the specific hearth load ($Nm^3h^{-1}cm^{-2}$) are both calculated from the gas production rate divided by the cross-sectional area of the narrowest part of the gasifier. For throated gasifiers a maximum hearth load of 0.9-1.0 $Nm^3h^{-1}cm^{-2}$ is reported (Anonymous, 1979; Kaupp, 1984; Reed, 1988a). The maximum hearth load is limited by the mechanical integrity of the char bed, the degree of agitation, and the time required for char conversion (Reed, 1988a). At high gas velocities entrainment of char particles could cause plugging or channelling within the char bed. Agitation of the reactor bed can increase the maximum load by reducing blockage by fines (Reed, 1988a); however, too much agitation is detrimental to the process (see Section 2.5.7). Groeneveld (1980) states that for maximum energy conversion a reactor volume of 0.5 m^3 below the air inlet per m^2 throat area would be sufficient for most wood based fuels, determined by the required residence time within the oxidation zone for complete devolatilization of wood particles. Kaupp (1984), however, points out that slight changes in the dimensions of the throat, or in the positions of the air nozzles, can have a drastic effect on the performance of a gasifier. Kaupp also states that the best configuration depends upon the feed characteristics and that the load factor must be found by trial and error. In agreement with Kaupp, Groeneveld (1983) states that the design of the throat is more or less empirical for different feed characteristics.

Scaling of the throated gasifier is said to be limited by the extent of oxidant penetration into the bed (see Section 2.6.1). The introduction of more oxidant inlet points would hinder the downward flow of feed material (Groeneveld, 1980b). Attempts to scale Imbert-type gasifiers to larger sizes have resulted in an increase in tar production, although increasing the feed size with gasifier size has shown some success (Reed, 1988a). The maximum throughput is about 0.7 tonne per hour (Bridgwater, 1993). Groeneveld (1980) presents a design for a 100 tonne per day gasifier using an annular throat; however, the design has not been built.

2.6.3 Turndown

Turndown is the ability to alter the gas production rate as demand changes and is measured by the turndown ratio which is usually given as the highest gas production rate to the lowest gas production rate. This is most important in vehicle operation where ratios of at least 8:1 are said to be required (Reed, 1988a). Kaupp (1984), however, states that a turndown of 4 to 6 is sufficient for most gasifiers for vehicle operation. The turndown ratio of World War II gasifiers is reported to vary between 3 to 18 depending upon the amount of insulation used (Reed, 1988a). However, it is

uncertain whether the values reported can be maintained for long periods or are just for 'transient' periods of short duration. Operation at high or low throughputs can adversely affect the performance of the gasifier in terms of product gas heating value and tar content (discussed below), so turndown should only apply to the production of gas of an acceptable quality for its end use.

Operating at low throughputs (or low turndown) produces a gas low in H_2 and CO, and high in tar (Kaupp, 1984). Williams (1979) found that it was difficult to maintain temperatures for optimum gasifier operation at low throughputs (feed consumption rates were in the range 8-36 kgh^{-1}), which was said to allow tars to escape thermal cracking, although the amount of tar produced was not determined (Williams, 1979). The product gas from Hoi's rubberwood gasifier (1991) produced tar content of up to 60.83 gNm^{-3} at low throughput compared with 34.74 gNm^{-3} at normal (optimum) throughput. Hoi explained the increase by the existence of cold spots within the reactor through which the tars could pass uncracked. Zerbin (1985) states that for an Imbert gasifier "a minimum of a quarter load has to be guaranteed", adding that a blower may be necessary in order to achieve this, but gives no indication of the consequences if the minimum is not maintained.

High loads are said to lead to excessive carbon outflow in the ash, decreased efficiency, increased pressure drop, and increased temperature which may lead to damage in the equipment (Kaupp, 1984). The tar content of a product gas may increase as a gasifier nears its maximum capacity due to the residence times of the tars within the pyrolysis zone becoming too short for complete degradation (Knoef, 1991). Hoi (1991) found an increase in tar production at high feed rates. This, he suggested, was due to the reaction zone 'bubble' (see below) growing in size until it becomes unstable resulting in the disintegration of the tar cracking mechanism.

The throated gasifier is said to be self adjusting by Reed (1988a) since if there is insufficient char at the throat more char is produced by pyrolysis; if there is too much char, the char rises to the air inlet and is consumed by oxidation. The oxidation zone would therefore be maintained at the throat.

Hoi (1991) attempted to explain turndown for a rubberwood gasifier with a turndown ratio of about 5 using a hypothesis he described as 'bubble theory'. Two mechanisms were proposed (Figure 2.13). In the first of these the reaction zone forms an arch or hemispherical shell around the throat. As gas demand increases the surface area of the shell increases to achieve a larger capacity. Hoi calculated that this would give a maximum turndown in capacity of 16.5. The second mechanism is based upon a

bubble around or between the air inlets. The bubble expands to increase the surface area of the reaction zone thereby increasing the specific capacity of the gasifier to meet demand. Overall capacity is said to depend upon the ratio of the reactor bed diameter to throat diameter in the first mechanism and to distance between air injectors in the second. Hoi suggests that the bubble would expand or contract in response to changes in feed properties such as shape, size and composition.

Figure 2.13 Throat and Air Inlet Centred Bubbles Giving Turndown (from Hoi, 1991)

Hoi's bubble theory only considers turndown as a function of the surface area of the flaming pyrolysis zone and does not include how turndown is achieved in the gasification zone. For a stable (stationary) reaction zone char production must equal char consumption and Hoi's theory does not recognize this. The second mechanism postulated by Hoi of an air inlet centred bubble may be considered to be the most accurate since the reaction zone would tend to travel towards the oxidant at low throughputs (see Section 2.5.6).

2.6.4 Feedstock Limitations

The constriction within throated gasifiers limits the shape of biomass fuels that can be successfully gasified due to bridging of the material above the throat. Imbert-type gasifiers require a blocky-type fuel that is generally greater than 2 cm along the smallest dimension and free of twigs, sticks and bark shreds (Reed, 1988a). Caking of certain feeds, such as rice hulls, within the pyrolysis zone can cause obstructions to the flow of material to the reaction zone (Kaupp, 1983). Reactor bed penetration by the air jets is mainly determined by the particle size of the feed (Groeneveld, 1980).

Since penetration reduces with decreasing particle size there will be a minimum size for effective oxidant distribution at the throat. Smaller feed sizes (0.5-1.3 cm) have been found to increase the amount of tar produced to 3-4% (w/w feed) compared to 1.3-2.5 cm chips with 1-2% tar (Winship, 1980; Graham, 1981). The pressure drop across the reactor bed associated with smaller particles can also limit the minimum size acceptable.

The upper particle size is limited by the physical size of the gasifier and the residence time within the pyrolysis zone for complete devolatilization. Short residence times lead to incomplete carbon conversion, too long a residence time may increase slag formation (Kaupp, 1984). The ratio of maximum fuel size to smallest cross-section of the gasifier (at the throat) should be at least 6.8:1 in order to avoid bridging (Kaupp, 1984). In addition, the size distribution range should be as small as possible since separation of the fines and course particles may lead to channelling and clinker formation (Kaupp, 1984). Large feed stock sizes can also have a high bed voidage which may result in channelling of the product gases (Manurung, 1981).

The moisture content is limited to about 20% moisture (Reed, 1988a) with difficulties reported above this level (Kaupp, 1984). High moisture contents affect the gasification process since energy is expended in evaporation of the moisture reducing the amount of heat available for gasification. A high moisture content may, therefore, effectively quench the reaction. High feed moisture contents also produce a gas with a high tar content (Graham, 1981).

Ash slags formed in the high temperature zone will flow downwards to cool and solidify in the lower zones (Kaupp, 1984). Gasifiers operating on high ash fuels require a rotating grate and temperatures below the ash melting point (Kaupp, 1984). Kaupp also stated that bridging of large particles above the throat is the main cause of slag formation since local temperatures may rise to 2000°C as a result of the increase in the local air to fuel ratio.

Unsuitable biomass fuels may be used successfully in downdraft gasifiers if mixed with a suitable amount of wood chips (e.g. L'Ecuyer, 1981), although the proportion required will have to be determined by experimentation.

2.6.5 Gasifier Performance and Product Gas Quality

The performance of selected throated gasifiers found in the literature are presented in Table 2.5. The gas compositions and gasifier performance indicators are, in general, similar to those presented in Figure 2.4 for open-core gasifiers. Direct comparisons are difficult due to differences in the feed used (composition and particle size). This is illustrated by the results obtained with the Forintek gasifier (Graham, 1981) in which a single parameter (feed size) was investigated. Table 2.5 shows that increasing the feed size from 5-13 mm to 13-25 mm range resulted in a decrease in the tar yield from 4% to 1%, and an increase in the conversion efficiency from 55% to 80%. No investigation using identical feedstocks in both an open-core and a conventional throated gasifier of similar dimensions was found in the literature. This would be necessary in order for a direct comparison of the two gasifier types to be significant.

The reported tar yield from the Forestry Research Institute of Malaysia (FRIM) gasifier of between 2 and 14% is very high, and this can be attributed to the low temperatures existing at the throat of about 800-900°C (Hoi, 1991) which is lower than the 1000°C suggested for efficient tar cracking (Kaupp, 1983; see Section 2.5.5).

In comparison, the Twente gasifier and the RIT (Royal Institute of Technology, Sweden) gasifier produce a gas with a low tar content of 250 and 610 $mgNm^{-3}$ respectively, indicating a greater tar cracking efficiency of the gasifiers, which operate at temperatures of 1070°C (Twente) and 1000°C (RIT). Higher temperatures within the gasifier, therefore, lead to a lower product gas tar content. However, the different methods used in measuring the tar content of the product gas from different gasifiers make comparisons of reported values difficult (Esplin, 1985).

The variation in the product gas heating values for the selected gasifiers presented in Table 2.5 ranges from 4.75 $MJNm^{-3}$ (for the Twente gasifier) to 6.39 $MJNm^{-3}$ (Forintek gasifier operating on 13-25 mm wood chips). The difference in heating values can, in part, be explained by the differences in the air to feed ratios of the gasifiers. The Twente gasifier was operated at a high air to feed ratio of 2.65, compared to the Forintek gasifier with an air to feed ratio of 1.39 (for the 13-25 mm feed size). The product gas from the Twente gasifier has about 30% more nitrogen than the product gas from the Forintek gasifier, which effectively dilutes the energy content of the product gas. Taken on a nitrogen free basis the energy content of the gas from the Twente gasifier is 10.5 $MJNm^{-3}$, which is similar to the nitrogen free energy content from the Forintek gasifier of 10.9 $MJNm^{-3}$. Comparisons between gasifiers should, therefore, be made with caution.

Table 2.5 Selected Throated Gasifier Performance Data

Name	FRIM	Twente	Howden EE	Forintek	Forintek	RIT
Type	Throated	Throated central nozzle	Throated central nozzle	Throated	Throated	Throated
Reference	Hoi, 1991	Groeneveld, 1980a	Groeneveld, 1985	Graham, 1981	Graham, 1981	Liinanki, 1983
Grate diameter, mm	550	500	nr	nr	nr	nr
Throat diameter, mm	202	250	nr	nr	nr	90
Feedstock	Rubberwood	Woodchips	Woodchips	Woodchips	Woodchips	Birch
Size, mm	30x30x10	10	10	5-13	13-25	50x50
Moisture, %wb	10.3	13.8	18	6.3	5.1	nr
Gasifier Performance						
Spec. capacity, $kgm^{-2}h^{-1}$	943[a]	810[a]	(32 kgh^{-1})	nr	nr	nr
Air/feed ratio	nr	2.65	1.81	1.06	1.39	1.79
Energy efficiency[b], %	60.48	67	75.1	55	80	75.6
Gas HHV, $MJNm^{-3}$	4.97	4.75[c]	5.45[c]	6.18	6.39	5.21(LHV)
Dry gas composition, % vol.						
H_2	18.4	15.0	18.6	13.9	18.0	19.0
CO	18.9	16.8	17.1	23.9	26.3	21.5
CO_2	12.3	12.6	14.4	10.2	9.2	11.0
CH_4	0.6	0.9	2.3	3.1	2.8	1.4
N_2	49.8	54.7	47.6	45.2	41.5	47.1
C_2+				1.7	1.6	
Raw gas water content	nr	10.50% vol.	nr	15% wt	4% wt	nr
Char yield, % daf		nr	nr	4%	3%	nr
Tar content	950-1450 $mgNm^{-3}$	250 $mgNm^{-3}$	nr	4% daf	1% daf	610 $mgNm^{-3}$

Notes: nr, not reported; a, by throat area; b, cold gas; c, calculated from reported gas composition

2.7 Hybrid Gasifiers

There are two species of 'hybrid' gasifiers that combine characteristics of the open-core with characteristics of the conventional throated design that are considered:

a) Open-topped (or 'topless') gasifier with a throat (Section 2.7.1).

b) Throatless gasifier with air injection (Section 2.7.2).

2.7.1 Topless Throated Hybrids

Eoff (1987) modified an open-core gasifier by placing a restriction within it, as shown in Figure 2.14. The high temperature reaction zone is separated from the reactor wall by a zone of insulating ash and char which allowed the gasifier to be constructed from mild steel (Eoff, 1987). A gasifier using 25 mm wood blocks operated at about 14 kgh^{-1} with the dimensions shown in Table 2.6 (Eoff, 1988).

Figure 2.14 Topless Throated Hybrid Gasifier (Eoff, 1988)

Table 2.6 Throughputs and Dimensions of the Topless Throated-Hybrid Gasifier (Eoff, 1988)

The reaction zone was said to be stabilized at the bottom of the feed and air inlet pipe (Eoff, 1988); however, no supporting evidence was given. The purpose of the throat was to reduce the flow volume and to maintain a high temperature to promote tar cracking. Recurring randomly spaced episodes of poor gas production were encountered, although no cause was given. The feed rates given in Table 2.3 indicate a turndown ratio of between 2 and 3 depending upon the dimensions of the construction. No details on the quality of the gas produced were found in the literature.

Eoff seems to suggest that the reaction zone lies above the throat (see Figure 2.14), stabilized at the end of the air inlet pipe, in which case the position of the throat may not be at the optimum distance away from the air inlet. Ideally the throat should be placed at the end of the flaming pyrolysis zone where the highest temperatures exist to achieve the greatest degree of tar cracking. This would suggest that the depth of the flaming pyrolysis zone is about 15 cm or about 6 particle diameters, which is greater than that found by other workers (see Section 2.5.8).

Rajvanshi (1989) found that there was a tendency for the reaction zone to travel towards the top of a 15 cm diameter open-core gasifier. To prevent this Rajvanshi introduced two side air injection nozzles through which 70-80% of the air requirement passed, the remaining 20-30% entering through the open top of the reactor, and an 8 cm diameter throat. The gasifier is therefore a partial hybrid of this type. Tar production was reported to be 0.5-1.5% (w/w feed) with char production at 3-14%. The temperature of the reaction zone was reported to be 800-1050°C which was said to be too low for proper cracking of the tars and responsible for the high char production rate, although these temperatures are usual for an air blown gasifier. Turndown for the gasifier was not reported but the average feed rate varied between 2.5 and 4.7 kgh-1 indicating a turndown of at least 1.9:1.0. The oxygen content of the gas was reported to be 4-11%, which indicates extremely poor mixing in the combustion zone. The gasifier is stabilized by the addition of a substantial addition of air at the throat,

and may be considered to represent a conventional throated gasifier with air entering the gasifier at the feeder.

2.7.2 Throatless Hybrid With Air Injection

The second hybrid species has air injected into the reaction zone of the gasifier. The Kansas State University (KSU) gasifier used secondary air supplied through tuyeres via a central shaft or 'airgitator' (Walawender, 1988), and may be considered as a partial hybrid. The proportion of air delivered by the tuyeres is not stated; however, the 'airgitator' may aid reaction zone stabilization as discussed Section 2.5.6. Performance data from the KSU gasifier was presented in Table 2.4. Hoi (1990) operated a throatless gasifier with air injected through three radial nozzles. No operating difficulties were encountered with the gasifier except when using a feed with greater than 20% moisture content which produced a gas of inconsistent quality. Table 2.4 presents product gas compositions from the gasifier using rubberwood feed with 10% moisture.

A throatless hybrid gasifier using air injection is expected to have a reaction zone that is centred upon the air inlets and would, therefore, be stationary for a range of gas production rates. However, the problem of insufficient bed penetration by the air jets would occur resulting in a gas with a high tar content due to poor cracking of the tars by oxidation and thermal degradation. The problem would be greater in this type of hybrid than that discussed previously for the conventional throated gasifier (see Section 2.6.1) since the throat reduces the distance of penetration needed to provide an even distribution of the oxidant over the cross-section of the gasifier. The throatless gasifier with air injection is, therefore, unlikely to be of much practical use since turndown would adversely affect the quality of the gas. In addition, a sealed feeding system such as that used for the conventional throated gasifier would, by definition, be required. Partial hybrids with a proportion of the oxidant delivered via air nozzles with the remainder delivered through the open top of the gasifier, as is the case in KSU gasifier (Walawender, 1988), may provide greater reaction zone stability whilst providing an even distribution of the oxidant across the cross-section of the gasifier. The position of the nozzles directed into the bed, and he proportion of air delivered through them, will be of great importance to the performance of the gasifier and may need to be adjusted as the throughput (to give turndown) changes.

2.8 Summary

Thermochemical gasification of biomass occurs in four main stages: drying, pyrolysis, oxidation and char gasification. Two main varieties of downdraft gasifiers exist. Open-core gasifiers consist of a simple open-topped tube through which the feed and an oxidant travel down towards a series of reaction zones supported on a bed of inert

char. The conventional throated gasifier possesses a throat, where the oxidant is introduced, and a sealed feeding system. The purpose of the throat is to create a high temperature zone and induce circulation of vapours within the gasifier in order to promote tar cracking. Throated gasifiers have a turndown capability allowing the changes in the rate gas production without adversely affecting gas quality. The throated gasifier has greater feedstock limitations than the open-core gasifier, and has limited scale up potentials due to the limited penetration of the oxidant into the reactor bed. Two species of hybrid downdraft gasifiers are considered; the topless throated hybrid gasifier and the throated hybrid gasifier with air injection. Examples of open-core, throated and hybrid gasifiers in the literature were presented and gasifier performance compared.

Nomenclature for Chapter 2

A	Arrhenius constant
a,b	Constants
α	Thermal diffusivity
C_A	Reactant gas concentration
C_s	Reactant solid concentration
D	Particle diameter
ε	Emissivity
E_a	Activation energy
E_d	Apparent activation energy
F_o	Fourier number
k, k_c	Reaction rate constant
k_D	Mass transfer rate
K_p	Equilibrium constant
k_s	Surface reaction rate constant
m	Constant
n	Reaction order
P_i	Partial pressure of component i
R	Gas constant ($8.314\ JK^{-1}mol^{-1}$)
ρ_B	Bulk density
σ	Stefan-Boltzman constant ($5.67 \times 10^{-12}\ Wcm^{-2}K^{-4}$)
T	Temperature (K)
t	Time
τ	Time for complete reaction
W	Weight
X	Char conversion
ΔH_r	Reaction enthalpy
$\Delta_r G$	Gibbs free energy

3. EQUIPMENT

3.1 Introduction

The original Aston gasifier designed by Earp (1988) consisted of a quartz glass reactor vessel, heat exchanger, wet gas scrubber and a vacuum pump. The gas processing system was totally redesigned by Evans (1992). The first year of this research was spent working with Evans. This experience was useful in identifying the various problems and inadequacies of the system. Important modifications were made to solve these problems, to improve safety and operation of the system, and to extend the quality and range of results. The gasifier system used by Evans is shown in Figure 3.1 (dotted lines) along with the modifications made in this research shown as solid lines. This chapter gives a description of the gasification system used by Evans, discusses problems encountered with the equipment during this research, and describes the measures taken to improve the system.

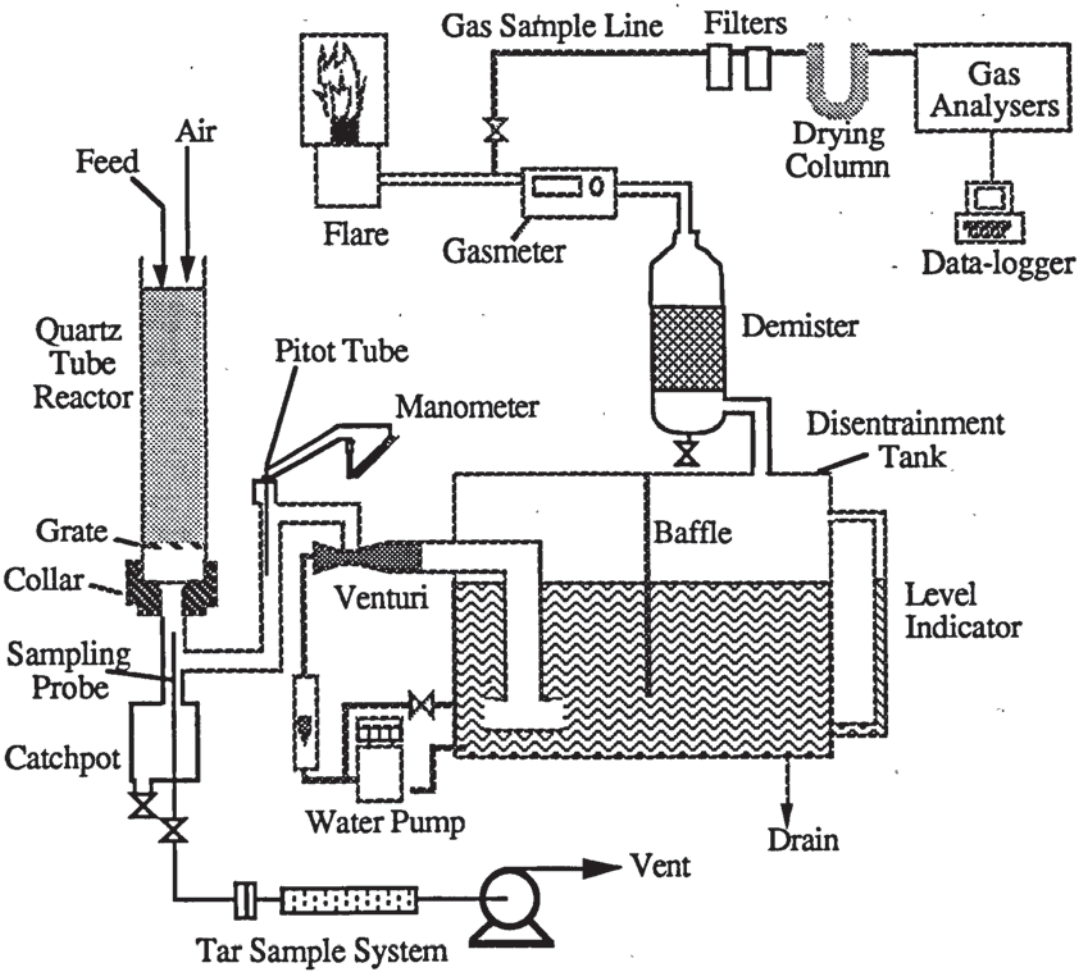

Figure 3.1 Gasification System

3.2 Feeding

Evans (1992) used an automatic screw feeder for wood chips passing a 6.35 mm sieve. Larger sized wood chips were fed into the gasifier in batches by hand because the feeder screw size limitations would mean that the particles would block the screw and this may result in damage to the feeder. Evans reported that manual batch feeding was easier to record and allowed greater control of the depth of unreacted material within the reactor.

Since it was decided to use a 6.35 to 12.7 mm feed size as the base case feed for this research (see Chapter 4) the screw feeder was removed and the batch method of feeding used. Batches were weighed to 0.01 g and fed through the open top of the reactor to a pre-determined level at 2-5 minute intervals.

3.3 Reactor and Reactor Collar

An open topped quartz tube 0.5 m in length and of 75 mm internal diameter was used as the reactor vessel. The bed is supported within the reactor by a stainless steel grate with sixty-two 5 mm diameter perforations designed by Earp (1988). The reactor was supported by a collar designed by Earp which was tapered to receive the reactor using 3 mm 'Kaowool' high strength paper as a seal, which can be used up to temperatures of 1260°C (Morganite, undated). The full design procedure for the reactor and reactor collar is given by Earp (1988). To assess the effect of heat loss the reactor can be insulated using the method described by Evans (1992). Insulation was provided by a 38 mm thick Kaowool sleeve with a 20 mm vertical strip for observation and measurement of the gasification process. The insulation was attached to the reactor using metal straps Evans calculated that the heat loss from an insulated gasifier using the insulation would be about 20 % of the heat loss from the uninsulated gasifier. The effects of using insulation are discussed in Chapter 7.

3.3.1 Reactor Sealing

During this research it was found that sealing the reactor to reactor collar using Kaowool paper seal was sometimes inadequate since an inward leakage of air at the seal was indicated by a high level of nitrogen reaching the gas analysers. An improved method of sealing was therefore sought. Bright (1984) found that the use of a refractory cement cracked during operation; however, the use of 'Pyruma' fire cement which can withstand temperatures in excess of 1250°C in addition to the Kaowool paper was found to be successful. The fire cement was applied in two layers as shown in Figure 3.2. The first application was allowed to dry overnight prior to the second application before operation of the gasifier. Cracking of the cement was observed but the seal was not broken during gasifier operation. The reactor was

occasionally difficult to remove after a run but it was found that wetting the cement aided removal.

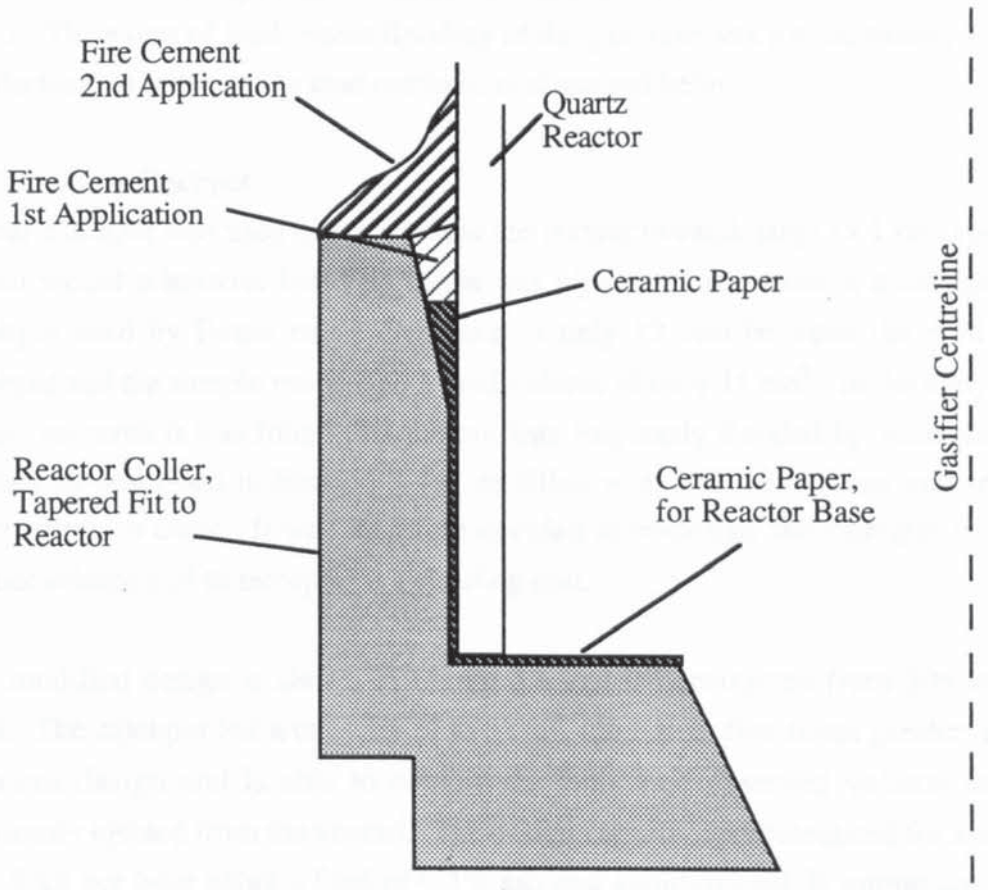

Figure 3.2 Reactor to Collar Seal

3.4 Gas Processing System

The collar connects to a venturi ejector via 25.4 mm stainless steel piping connected by Ermeto compression fittings. A catchpot fitted directly below the reactor captures char from the gas stream prior to the venturi.

3.4.1 Venturi Ejector

A venturi ejector provides the driving force pulling air into the reactor and the product gas through the processing system. The venturi also performs gas cooling and cleaning. Full details of the design procedure are given by Evans (1992). A major problem was experienced with this piece of equipment when the flow rate of water through the venturi was reduced unless this was done slowly. The high pressure difference between the disentrainment tank and the gas pipe forced water through the gas inlet to the venturi and into the gas pipe. Flooding of the char catchpot, sample probe and, in severe cases, the reactor vessel occurred. The problem was alleviated in this project by reducing the pressure drop between the tank and the burner by reducing the length of piping to the burner, partial removal of knitmesh in the burner and

ensuring the piping was free from blockages and accumulation of tarry deposits. In addition shut-down was carried out by slowly reducing the water flow rate through the venturi such that a large pressure difference between the tank and the venturi did not occur. The event of inadvertent flooding of the gas pipe was a contributory factor in the decision to redesign the char catchpot as discussed below.

3.4.2 Char Catchpot

A char catchpot was used directly below the reactor to catch large (> 1 mm) particles which would otherwise build up in the gas pipe and may cause a blockage. The catchpot used by Evans had a clearance of only 12 mm between the wall of the catchpot and the sample probe, and a total volume of only 71 cm^3. In the early stages of this research it was found that the pot was frequently flooded by water from the venturi as described in Section 3.4.1, or filled with char after a run and required dismantling to clear. It was therefore decided to re-design the catchpot to have a greater volume and to incorporate a cleaning port.

The modified design is shown in Figure 3.3 and is constructed from 306 stainless steel. The catchpot has a capacity of 496 cm^3, more than five times greater than the previous design and is able to contain the estimated observed volume of water previously ejected from the venturi. The design capacity was calculated for a feedrate of 1.5 kg per hour using a feed of 0.5% ash and assuming solids output containing 50% char and a specific density of 0.36 gcm^{-3} (Perry, 1986). The catchpot volume allows 7 hours of continuous operation if the catchpot collected all of the solids output from the gasifier. A drain fitted to the catchpot allowed removal of the water without disassembly of the piping should flooding occur. The drain valve also allowed access for the removal of solids accumulated in the catchpot after a run thereby enabling a series of runs to be made without disassembly of the pipe work. The catchpot deposits were blown out of the catchpot using a compressed air line and collected in a plastic bag. A water/acetone mix was used to clear deposits that may be adhering to the walls of the catchpot.

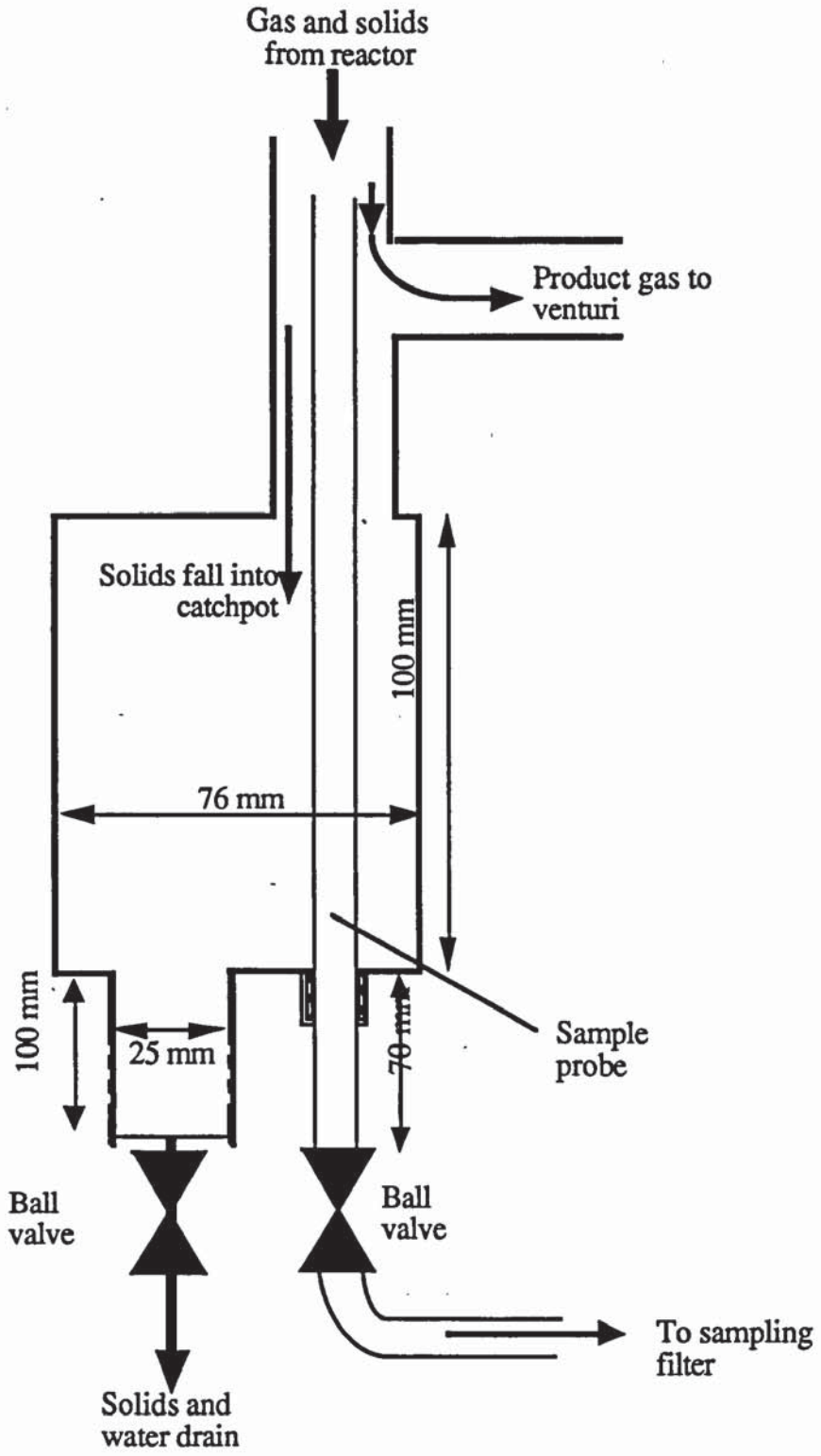

Figure 3.3 Char Catchpot

3.4.3 Disentrainment tank

Disentrainment of the gas from the scrubbing water takes place in a baffled water tank. Access to the tank is via a lid sealed using a non-setting putty and toggle clamps. Full details of the design of the disentrainment tank are given by Evans (1992). The tank has a pressure release system for safety reasons consisting of a water manometer to give protection up to 3.31 psig (Evans, 1992).

3.4.4 Demister

The gas leaving the tank is saturated with water vapour and carries water droplets. A demister is placed directly after the tank in order to remove some of this water before passing through downstream instruments. The demister element is made from KnitMesh, an interlocking fabric of metallic asymmetric loops (KnitMesh, 1988).

Entrained droplets are separated from a vapour stream by the principle of impingement. While vapour takes open pathways through the mesh the greater inertia of droplets projects them in a straight line to impinge on the mesh. The liquid flows down the wires of the mesh to collect at the base of the element where droplets grow to a sufficient size for gravity to exceed the combined effect of surface tension and velocity and fall away. In order for the demister to operate effectively the velocity of the gas stream should be between a maximum and minimum value. Below the minimum velocity entrained droplets follow streamlines around the mesh and do not impinge on the wires and at velocities greater than the maximum re-entrainment of the droplets occurs (KnitMesh, 1988). The calculation of the velocity limits required for efficient separation is the principle of the demister design. The design calculations are given in Appendix B1.

During the course of this research it was found that errors made by Evans (1992) had resulted in a demister pad element of 22 cm diameter for a flow rate of 3 Nm^3h^{-1}, compared to 2.7 cm for a maximum flow rate of 6.4 Nm^3h^{-1} (see Appendix B1). However, the entry pipe diameter to the demister was calculated to be 3 cm based upon the correct sizing calculation (Evans, 1992). The inlet to demister pad distance should be at least 300 mm (KnitMesh, 1988) but due to limited space available under the rig extraction hood there was only a distance of 35 mm. The velocity of the droplets impinging upon the demister pad are, therefore, assumed to be at the gas velocity entering the demister. Reducing the demister pad size did not improve the collection of water (see Appendix B1). This was possibly because the larger demister allows for coalescing of droplets into larger drops that are more easily caught. In addition, there was a smaller pressure drop across the 22 cm demister pad. A larger demister was not considered due to the limited space under the extraction hood and the need for periodic removal of the demister in order to gain access to the tank. The demister pad size of 22 cm was, therefore, retained throughout the course of this research. However, several important modifications were made. An elbow was introduced at the entrance to the demister to prevent re-entrainment of droplets into the gas stream (see Figure 3.4), whilst in Evans' gasifier system droplets fell back into the tank. A tap fitted to the base of the demister allows drainage at the end of a run. The disengagement height was also increased to 250 mm from 200 mm; however, this is still short of 300 mm

recommended by KnitMesh (1988). There is no further space available beneath the rig extraction hood to extend the demister. A 65 mm layer of 11 mm glass beads were placed on top of the KnitMesh to provide a surface for condensation and water drainage.

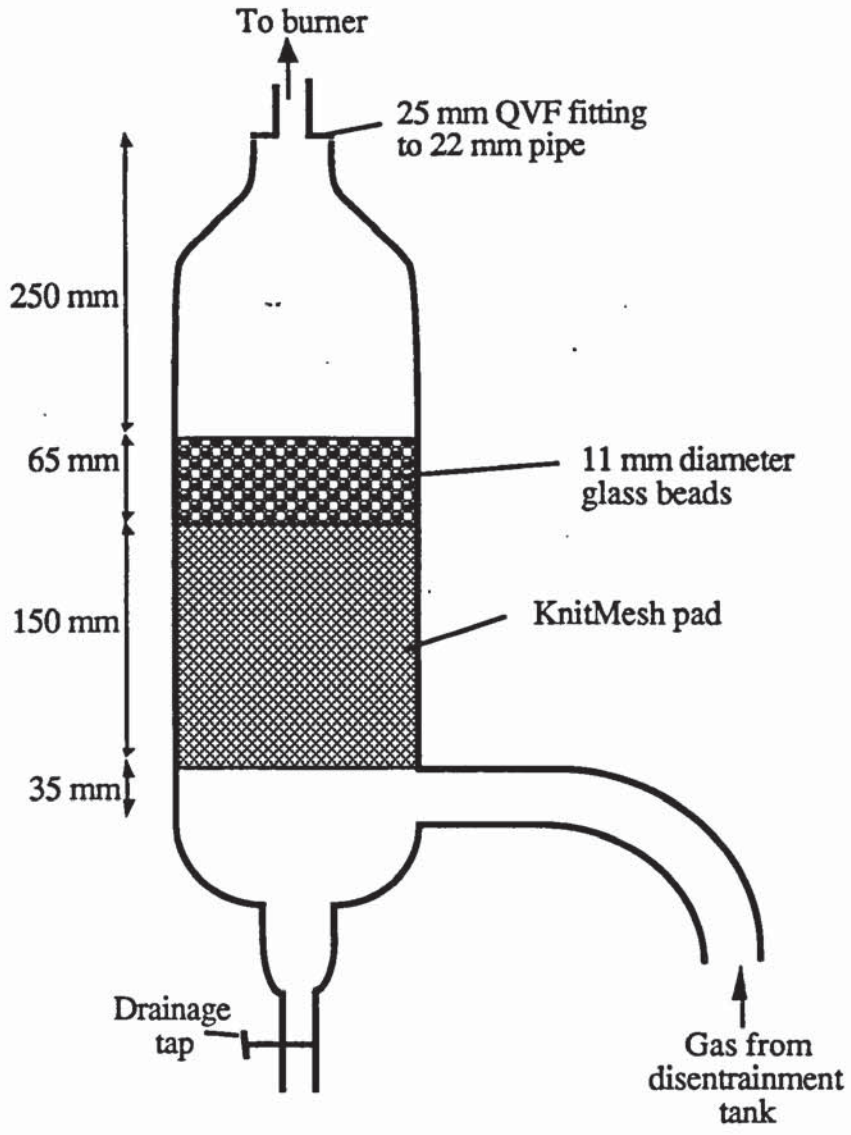

Figure 3.4 Demister

3.5 Gas Flow Rate Measurement

The measurement of the gas flow rate is extremely important in assessing the gasifier performance, without which mass and energy balances are worthless. Evans (1992) measured the gas flow was measured by: a Platon Flowbits Gapmeter type CMI for gas flowrates over the range 0.8 to 8.0 m^3h^{-1}; and a type U16 cumulative volume gasmeter from Thorn EMI.

3.5.1 Flow Metering Devices

At the start of this research difficulties were experienced in obtaining reliable results from these instruments. The U16 gasmeter gives a reading in units of 10 cubic feet

(0.28 m^3) which may give rise to a maximum error of ±10 % in volume for a 30 minute run at about 6 m^3h^{-1}, although there is a test dial that revolves every cubic foot. Using the test dial it has been found that the difference in the calculated flow rates for air and the flow rates measured by a 18K rotameter was less than 1.5 %. However, it is impractical to obtain a continuous set of readings using this method.

Evans (1992) reported that the Platon Gapmeter gave unreliable measurement of the product gas flow rate. In this research the Platon Gapmeter was found to be very erratic. The Gapmeter should generate an analogue electrical signal directly proportional to the gas flowrate (Evans, 1992); however, many calibration plots of the previous research were found not to result in a straight line, with readings at some flows having a very high standard deviation. In addition, a comparison of flow rates of air with the U16 gasmeter and 18K rotameter showed that the Platon Gapmeter read about 35% too low. During operation, however, the Platon gave flowrates 35% higher than the gasmeter. Tarry deposits were found within the Platon after a run. This was thought to have caused sticking of the float within the meter thereby given erroneous measurements. The Platon was therefore disconnected for the majority of this research.

Since reliable gas flow measurements are essential to this research an alternative technique was sought. A survey of alternatives was made with regard to the suitability to flow measurement of the product gas (see Appendix C1). It was concluded that a pitot tube, already installed into the system for gas velocity measurements required for iso-kinetic sampling (Section 3.8.2), could meter the raw gas flow with the accuracy required. No problems were encountered with blockages of the static holes of the pitot tube during its use for velocity measurement.

It was therefore decided to use the pitot static tube to measure the gas flow rate. The pitot static tube has the advantages of having no moving parts, can be used at temperatures up to 550°C (Airflow, undated) and gives the raw gas flow rate measured between the gasifier and the venturi, as opposed to a wet gas flow rate measured after the demister using the gasmeter and Platon Gapmeter. This method means that the amount of water vapour carried in the wet gas from the disentrainment tank does not have to be estimated to enable a mass balance to be carried out. The product gas flow rate is obtained by multiplying the gas velocity (corrected by calibration, see below) with the cross-sectional area of the gas pipe. A 300 mm x 4 mm pitot tube conforming to BS 1042: Section 2.1 (1983) was fitted to the gas pipe before the venturi by a stainless steel connector. The fitting included a port for a type k thermocouple for temperature measurement. The standard (BS 1042, 1983) specifies the use of pitot

tubes in calculating fluid flow. The pitot tube was positioned thirteen pipe diameters downstream of a bend and five and a half diameters upstream of a bend to avoid disturbances to the flow. The pitot tube was aligned facing the direction of the flow and the differential pressure existing between the total and static pressure points was measured using Type 4 Laboratory manometer by Airflow Developments. The manometer has a resolution of 0.25 Pa and an accuracy of 1% (Airflow, undated a).

The velocity of the gas is given by;

$$v = \alpha (1 - \varepsilon)\sqrt{2\Delta P/\rho} \qquad (3.1)$$

where v is the velocity in ms^{-1}, α is the pitot tube calibration factor, $(1 - \varepsilon)$ is the compressibility correction factor, ρ is the gas density in kgm^{-3} and ΔP is the differential pressure in Pa. Since the ratio d/D, the cross-sectional area of the pitot stem over that of the pipe, is greater than 0.02 a correction is needed to account for stem blockage which causes a velocity increase between the stem and the pipe wall. Calculations used in obtaining the values of these factors are given in Appendix C2. Validation of the velocities obtained is subject to the conditions also presented in Appendix C2. The calibration factor was obtained for each run by calibrating the pitot against the test dial of the U16 gasmeter with air.

Although the pitot tube was covered in sooty deposits at the end of a run, the pitot static holes never became blocked and there was little effect on gas flow rate measurement. Most of the deposition was thought to occur during the initial start-up period since tars are likely to remain in the vapour phase at the operating temperature of 250-300°C. The pitot tube was thoroughly cleaned after every use using acetone.

A comparison of the flows calculated from pitot tube measurements with the Platon gapmeter and the gas meter was made by running the system cold at various air flow rates achieved by varying the water flow rate through the venturi. The results are presented in Figure 3.5. The measured flows obtained using the Platon meter are consistently lower than the flows calculated from the pitot tube and the gas meter. The average flow rates obtained using the pitot tube and gasmeter are within 5%.

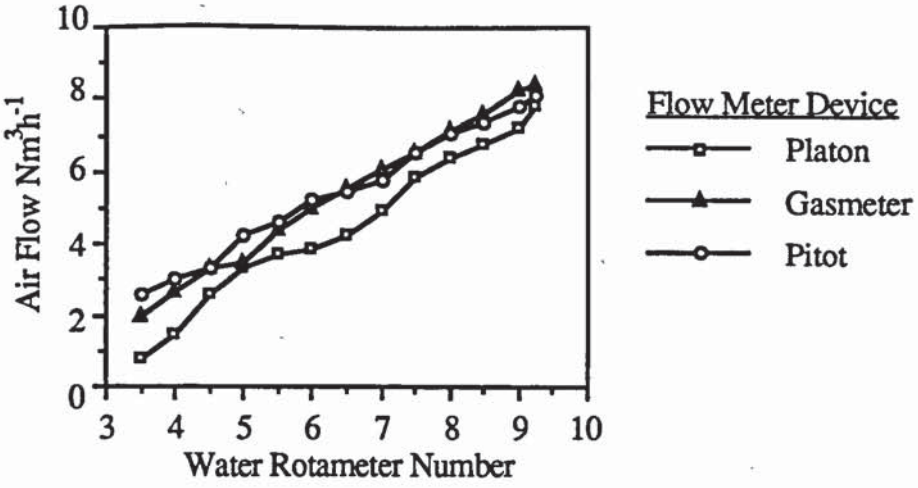

Figure 3.5 Air Flow Rates Obtained Using the Metering Devices

3.6 Gas Sampling System

The product gas was sampled via a valve after the gas meter. In the previous system a sample conditioning unit, the "hotbox", removed tars and particulates. A 2 m column of silica gel removed moisture from the gas before it passed into the gas analysers (see Section 3.7). Since experimental tests with a stable reaction zone began after a period of consistent gas composition data readings gas adsorption onto the silica gel is not important (i.e a dynamic equilibrium exists between the sample and the adsorbed gases).

3.6.1 Gas Sample Conditioning Unit Replacement

The hotbox, Perma Pure model 4112E, consisted of a high efficiency by-pass filter in which the gas sample passed through a 1 μm heated sintered filter whilst particulates are by-passed via a teflon eductor (Perma Pure, undated). A secondary filter removed condensible material. The sealing of the secondary filter housing was of doubtful quality and because of frequent gasket splitting it was decided that a new filter housing would be designed and built. The replacement secondary filter housing, shown in Figure 3.6, provided better sealing against the ingress of air. This was tested by passing the span gas used for calibration of the gas analysers through the system and measuring its composition.

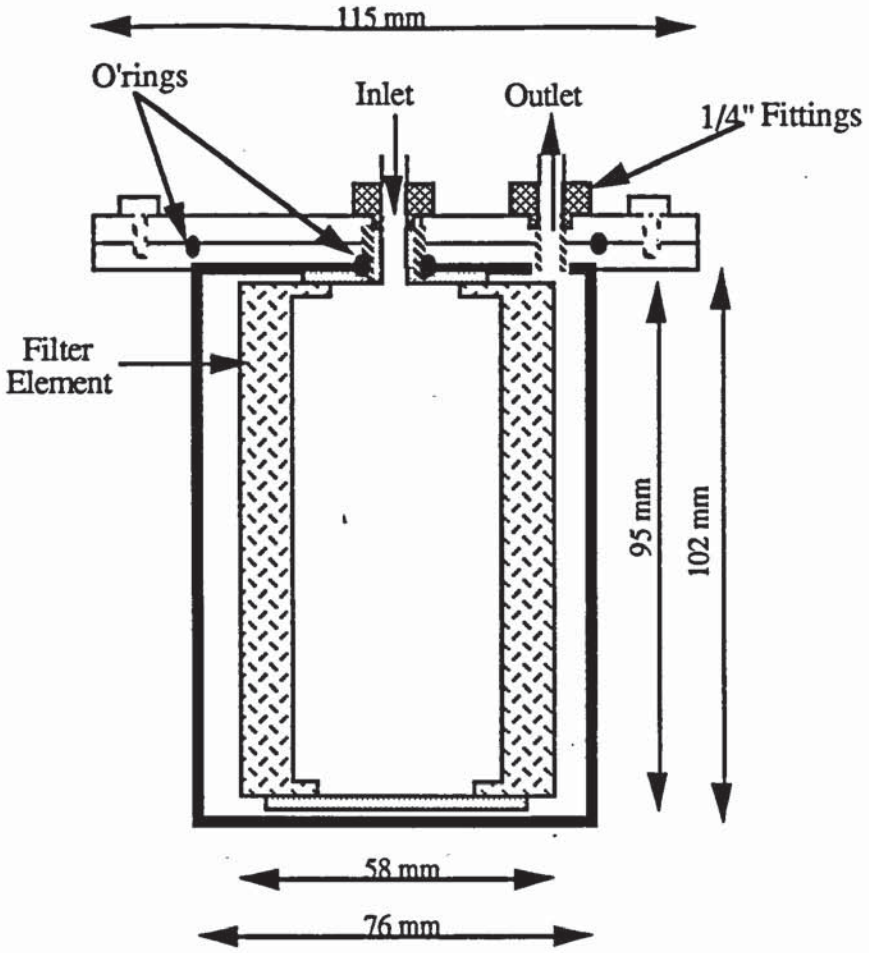

Figure 3.6 Secondary Filter Housing

At the beginning of this research a leak of air into the hotbox was suspected since there was progressively increasing nitrogen levels in the product gas composition. Using the calibration span gas running through the hotbox the heated filter unit was found to be the cause of the problem. As no leaks could be found when the unit was pressurized, it was concluded that the eductor was mis-aligned. This was believed to be due to excessive wear on the PTFE eductor block threads (refer to Figure 3.7). The eductor works according to Bernoullis principle, the high velocity of the air jet at B creating low pressure which is used to suck the sample gas into the filter. Mis-alignment of the jet at A may force air past B to mix with the product gas inside the filter at C which is then drawn through the filter towards the gas analysers (at D) by the sampling pump.

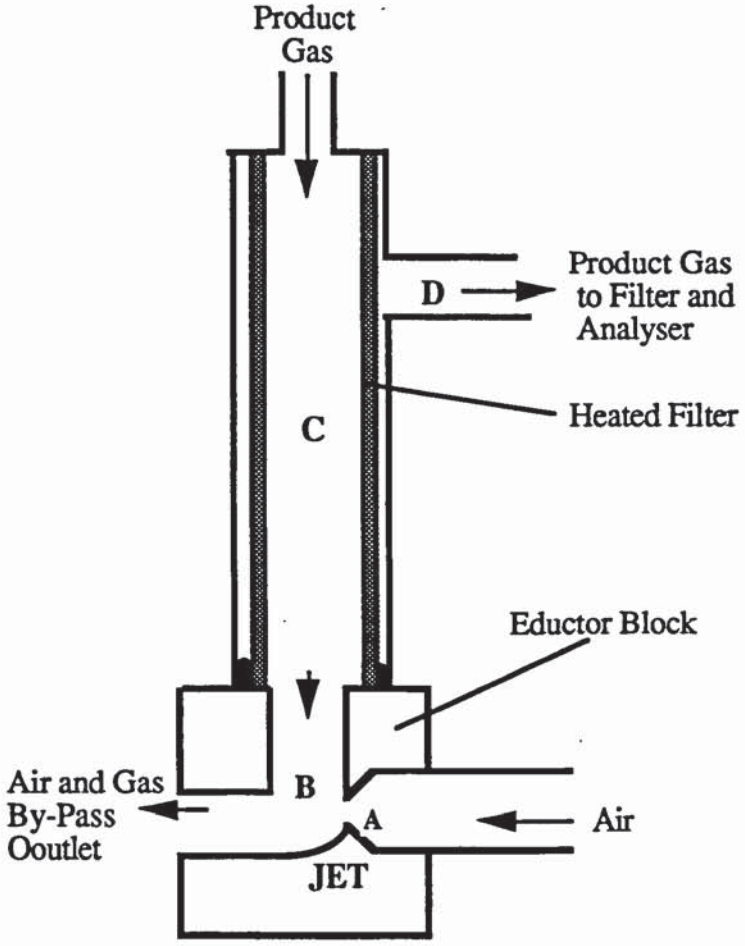

Figure 3.7 Gas Flow Within the Eductor

The supplier was consulted over the necessity of the hotbox with regard to the gas analysers, and the availability and cost of replacement parts. It was found that the hotbox was unnecessary for protection of the gas analysers from excessive pressure. Alternative systems were sought because the removal of the sintered filter of the hotbox was difficult and required considerable time in replacing and leak-proofing. It was decided to purchase a Balston A912A coalescing filter assembly (Balston, 1989). This offered high efficiency cleaning (99.99% claimed for 0.1 μm particles and droplets), whilst being simple in design and easy to use. In addition a faster delivery could be expected and the overall cost would be less than that for hotbox replacement parts. The secondary filter of the hotbox was used as a pre-filter to improve the protection to the gas analysers. The silica gel column was retained to ensure a dry gas before it entered the gas analysers.

3.7 Instrumentation

The gas composition was measured by Lira 2000 infra-red analysers for methane, carbon dioxide and carbon monoxide, and by a Hydros thermal conductivity analyser for hydrogen. Nitrogen was assumed to make up the difference.

Temperatures were measured at various points in the system using type k thermocouples; their positions are given in Appendix D. A movable thermocouple within a stainless steel sheath allowed the measurement of the temperature profile of the bed. The reactor external wall temperatures were measured using a contact thermocouple surrounded by a 6 cm square of insulation moulded to the curvature of the reactor vessel. A high temperature lubricant was used to obtain good heat transfer between the wall and the thermocouple contact disc. Temperatures were recorded by the data-logger (see below).

A pressure transducer measured the pressure after the demister and was recorded by the data-logger, and the tank pressure was recorded manually. Appendix D lists the instrumental positions using a piping and instrumentation diagram.

The data-logging system employed was the same as that used by Earp (1988) and Evans (1992). A Biodata Microlink interface converts the analogue signals from the thermocouples, pressure transducers, and gas analysers to a digital output. The signal is then transmitted to a BBC micro-computer via a IEEE 488 databus. The BBC micro-computer then converts the signal into the appropriate reading, displays the reading on the VDU and writes to a data file on floppy disc using the data-logging programs of Earp (1988). The data was then transferred into a spreadsheet (Excel 2.2) on an Apple Macintosh via a VAX mainframe computer.

3.8 Product Gas Tar and Particulate Sampling

The raw product gas from the gasifier contains particulates of tar, char and ash, the proportions of which depend on the operating conditions of the gasifier (Brown, 1987). A method of measuring the amount of each component is necessary when investigating the effects of operating conditions and feedstock characteristics on gasification.

3.8.1 Sampling System Design

The previous sampling system designed by Reyes (1989) consisted of a side-stream sample line, a heat exchanger for gas cooling, a series of wash bottles containing acetone and acetone/water mixtures, and a impinging disentrainment bottle. However since the sample was taken from a side-stream the samples may not be representative of the product gas. In order that a representative sample can be taken the velocity of the sample should equal the velocity of the bulk gas flow it was taken from, a condition termed as iso-kinetic. Only one sample per run was taken by Reyes. Since fluctuations in the tar content of the gas are expected a tar sampling system that allows a series of samples to be taken is desired.

The tar and particulate sampling system fitted included an iso-kinetic sample probe for representative sampling with a means for determining the flow (and hence the velocity) in both the product gas pipe and the sample pipe. It was decided to remove solids and tars simultaneously by filtration as opposed to solid removal in a heated filter followed by condensation of the tars due to difficulties in condensing tars. The system was capable of performing a series of samples to be taken during a single run so that the tar and particulate loading during start-up, steady-state and other operating conditions could be evaluated.

3.8.2 Iso-kinetic Sample Probe

Iso-kinetic conditions are obtained when the velocity of the sample entering the sample probe is equal to the velocity of the gas stream at the point of sampling, and is required when particle sizes exceed 10 μm (Reed, 1988a). There is a ±10% error in the measured concentration for sampling velocity to product gas velocity ratios in the range of 0.5 to 2 (Reed, 1988a). An iso-kinetic sampling probe was designed and fitted below the reactor by Evans (1992). This was modified in this research by reducing its length by 20 cm in order to reduce the surface area available for condensation of tar and water which have to be cleaned out of the pipe. Sample probe design requirements are given in BS 893: 1978. The probe nozzle has a thin walled (maximum 0.2 mm) sharp edged inlet as shown in Figure 3.8, and a diameter of 10 mm.

Figure 3.8 Design of the Sample Probe Nozzle (BS 893: 1978)

The probe was fitted in a straight length of pipe over one pipe diameter upstream of a bend and greater than two diameters downstream of a bend, or similar disturbance to flow in accordance with standard BS 3405 (1983).

3.8.3 Sampling Lines and Sampling Control

The sample line for condensates and particulates was made as short as possible to minimize time lags during sampling and reduce the amount of surface area available for condensation of material prior to the filter. Initially a purge/by-pass line was installed to aid the control of the gas through the sample line and also to purge the system of toxic gas. However after trials this was removed to further reduce the amount of piping needed and to avoid a dead space within the system which may have caused memory effects where gas from a previous sample occupying the dead space contaminates gas in following samples (Cornish, 1981). In addition, the sample turnover rate was reduced by making the system simpler. Purging of the sampling system with air was achieved by opening the filter holder with the suction pump on. The sampling system is shown in Figure 3.9.

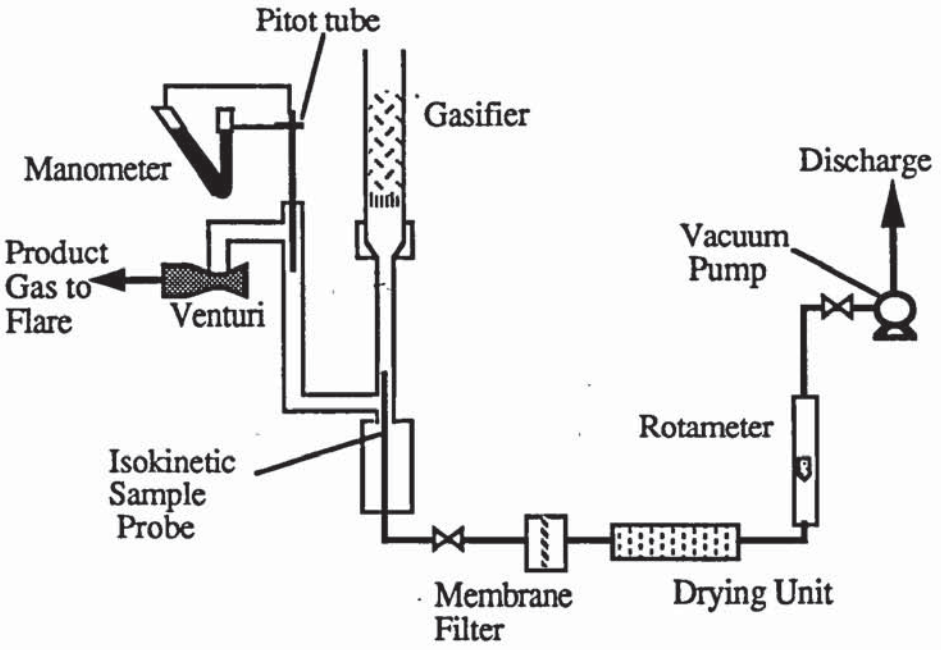

Figure 3.9 Raw Product Gas Sampling System

A sample was drawn through the line using a model 2SC50B Edwards high vacuum pump, and a rotameter meters the flow. The pitot tube (Section 3.5.1) was used to measure the velocity of the product gas. The sample flow rate was adjusted to achieve and maintain iso-kinetic conditions. Flow rate control was achieved using the control valve at the vacuum pump. The gas was vented directly into the fume hood above the gasification rig. Since the pump was left on toxic gas does not linger in the sample line, and on opening the filter housing air quickly purges the system.

3.8.4 Sample Filters

The particulates were collected on a nylon membrane filter housed in a 47 mm stainless steel in-line filter model HGS 47 purchased from Whatman (1991). The filter used had a pore size of 0.1 μm, and was claimed to retain 99.99% of material above 0.1 μm and some of the smaller particles less than 0.1 μm (Whatman, 1991). Nylon filters were chosen since these do not deteriorate under the sampling conditions and are compatible with acetone as a the washing solvent. Grade 542 Whatman hardened ashless paper filters were also used. These filters have a pore size of 2.7 μm and were used as a pre-filter to the membrane filters when required. The paper filters retain their strength even when wet and will absorb much of the moisture in the sample. In addition, a low ash content of 0.008% makes them suitable for ash determination of the captured solids (Whatman, 1980). The filters were pre-dried to constant weight at 80°C before use. The filters were carefully weighed to 0.0001 g

3.8.5 Sampling Procedure

A sample was taken by opening the sampling valve and setting the flow to the rate required and after a measured period of time the sample valve was closed. After purging with air, the pump was switched off and the sample filters removed. Start-up samples were taken by pre-setting the flow rate through the filter for iso-kinetic conditions and, with the sampling valve open, the time interval between lighting the gasifier and turning the sample valve off was measured. The filters were kept in resealable plastic bags together with any char particles collected from the filter holder. The membrane and paper filter act as a screen filter as most particles are trapped on to the surface. However, larger particles greater than about 0.5 mm tend to be loose. Care needs to be taken that these particles are weighed with the filters. After the initial weighing and drying procedure the filters were washed in acetone to remove the tar fraction. This is done by soaking the filters in clean acetone for about ten minutes and rinsing with fresh acetone. The quantitative determination of the components is given by the procedure;

1) Pre-drying (80° C)	weight = w_0
2) Usage	weight = w_1
3) Drying (80° C)	weight = w_2
4) Acetone wash, drying (50° C)	weight = w_3
5) Incineration (900° C), paper filter only	weight = w_4

The mass of water, tar, solids, and ash are given by;

$$\text{Mass of water} = w_1 - w_2 \quad (3.2)$$

$$\text{Mass of tars} = w_2 - w_3 \quad (3.3)$$

$$\text{Mass of solids} = w_3 - w_0 \quad (3.4)$$

$$\text{Mass of ash} = w_4 - (0.00008 \times w_0) \quad (3.5)$$

The washings from the sampling line and filter holder were also taken and the amounts of each component weighed and added to the above results. Tar and particulate concentrations are expressed in $mgNm^{-3}$ by dividing the total catch weight by the sample volume.

3.9 Water Content of Raw Product Gas

The amount of water in the raw product gas is an important factor that requires determination for accurate mass balances and gasifier performance data. The development of a suitable method of measuring the water content of the gas before the venturi ejector was, therefore, a prime objective. Earp (1988) suggested that a humidity probe may be used; however, this method is unsuitable since condensate water will also have to be measured. Gravimetric determination of moisture content by passing a volume of gas through a pre-weighed dryer assembly containing dessicant is given as a suitable method by Reed (1988). This method was chosen to determine the moisture content of the product gas.

The use of molecular sieve type 4A was chosen as the dessicant for a water removal unit after a comparison of several commonly used dessicants (see Appendix B2). Molecular sieve has the best capacity at low humidities (ie less than 7.5 mm Hg vapour pressure), and can provide the driest gas. A pellet size of 1.6 mm was used using a 25 cm length of tubing 2.25 cm internal diameter as a vessel to contain the volume of dessicant required. Sizing calculations are given in Appendix B2. The water content of the raw gas is expressed as a volume percentage.

3.10 Throated Reactor Design

One of the main objectives of this research was to investigate the use of a throat within a quartz reactor. This allows observation of the gasification process in the throated gasifier, and comparisons to be made with the open-core gasifier, including measurement of tar and particulate loading of the product gas and an investigation into turndown ratios. Feeding and air intake was through the open top of the reactor as for the open-core gasifier previously described, unlike traditional downdrafts which have

a sealed lid and air injection (see Section 2.6). It is therefore appropriate to use the term 'hybrid' in describing the reactor (see Section 2.7).

3.10.1 Design of Hybrid-Throated Gasifier

The throated reactor vessel had an external diameter of 75 mm and fitted into the reactor collar used by the open-core vessel (Section 3.3). The sizing of a gasifier is dependant upon the gas supply rate required. Groeneveld (1980) states that the gas velocity at the throat should be well chosen to avoid cold spots through which tars could pass uncracked. The superficial velocity (ms^{-1}) is the normalized gas production rate divided by the cross-sectional area of the narrowest part of the gasifier. For a 15 cm Imbert type gasifier a maximum superficial velocity of 2.5 ms^{-1} is reported (Anonymous, 1979; Reed, 1988), whilst for the SERI 15 cm open-core gasifier a maximum superficial velocity of 0.28 ms^{-1} is reported (Reed, 1988). Evans (1992) measured the gas production rate to be 5.16 Nm^3h^{-1} for a base case run. This gives a superficial velocity of 0.324 ms^{-1}. It was decided to begin operating with a throat size of 40 mm giving a superficial velocity of 1.14 ms^{-1} at the same gas production rate as for Evans' base case run. The throat diameter could then be reduced, if required, by placing a smaller throat on top of the existing one to give a higher superficial velocity. The height of the throat above the grate was 100 mm based upon a maximum gasification zone depth of 97.5 mm observed for the open-core reactor during runs 1 and 2. At this height the depth of inert char is minimized reducing the pressure drop across the bed. The throat is shown in Figure 3.10, with the dimensions given in Figure 3.11.

Figure 3.10 Hybrid-Throated Reactor

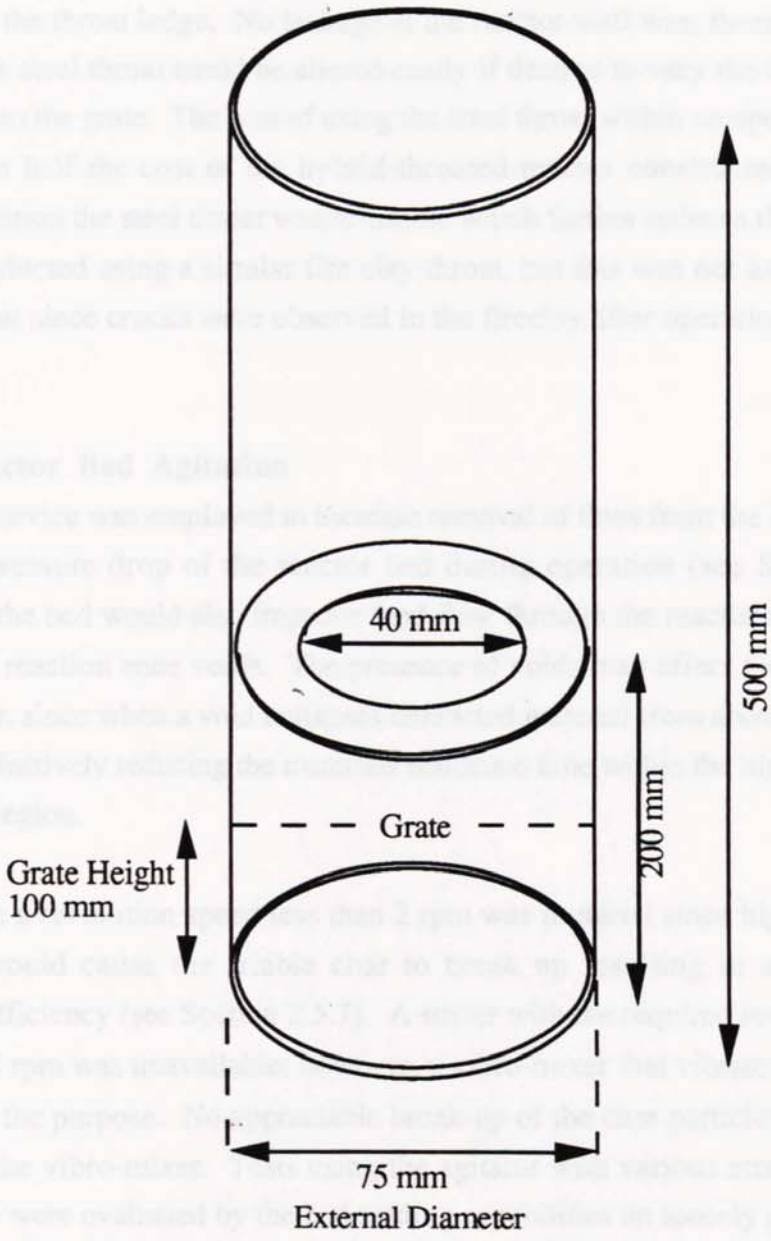

Figure 3.11 Hybrid-Throated Reactor Vessel Dimensions

During a run using the hybrid-throated reactor with insulation the reactor cracked just below the throat during start-up. It was believed that the thermal expansion in the lower part of the reactor exceeded that at the throat causing stress to the reactor.

Tests were conducted to find an alternative material for a throat placed within the standard open-core reactor. The extended grate designed by Evans was modified to obtain an aperture of 40 mm, the same as the quartz throat, which could then be placed directly on to the grate. The distance of the throat from the grate was identical to the all-quartz reactor at 100 mm. The steel throat was found to be successful (see Section 5.2; Section 8.5), and no damage was observed after use. No gas streams were

observed to pass between the throat and the reactor wall and a char/ash layer was deposited on the throat ledge. No leakage at the reactor wall was, therefore, believed to occur. The steel throat could be altered easily if desired to vary the throat size and the height from the grate. The cost of using the steel throat within an open-core reactor was less than half the cost of the hybrid-throated reactor constructed from quartz alone. In addition the steel throat was re-usable which further reduces the cost. A test was also conducted using a similar fire clay throat, but this was not as successful as the steel throat since cracks were observed in the fireclay after operation (see Section 5.2).

3.11 Reactor Bed Agitation

An agitation device was employed to increase removal of fines from the bed in order to reduce the pressure drop of the reactor bed during operation (see Section 2.5.7). Agitation of the bed would also improve feed flow through the reactor and reduce the frequency of reaction zone voids. The presence of voids may affect the performance of the gasifier, since when a void collapses unreacted material from above falls into the void space effectively reducing the materials residence time within the high temperature tar-cracking region.

A stirrer with a revolution speed less than 2 rpm was required since higher speeds of revolution would cause the friable char to break up resulting in a reduction in conversion efficiency (see Section 2.5.7). A stirrer with the required revolution speed of less than 2 rpm was unavailable; however, a vibro-mixer that vibrates at 50 Hz was available for the purpose. No appreciable break-up of the char particles was found to occur using the vibro-mixer. Tests using the agitator with various attachments were made. These were evaluated by the bed settling capabilities on loosely packed beds of wood blocks and char by measurement of bulk densities after 3 minutes use of the agitator. A piece of mesh plate connected to the base of a shaft was found to be marginally more efficient than other designs. This was then tested with radial arms extending from the shaft at intervals of about 5 cm; there was only a slight improvement found in the reactor bed. It was decided to use the shaft in contact with the grate to allow the vibrations to be passed on to the grate. This allowed the vibro-mixer to be removed if required. The vibro-mixer shaft passed through the unreacted feed bed, which improved material flow to the reaction zones (see Section 7.6).

3.12 Summary

Modifications to an existing gasification system have been made in order to resolve operational problems and to improve the quality and the range of measurements taken. The modifications include: increasing the capacity of a char catchpot to increase run

duration and to allow collection of the outflow char; the introduction of an elbow and drain to a demister to reduce re-entrainment of droplets into the product gas; the introduction of a raw gas flow metering device; the introduction of a sampling system to determine the tar and particulate content of the product gas. A hybrid-throated reactor vessel constructed from quartz glass has also been developed. In addition, the use of a vibro-mixer to improve material flow and reduce the occurance of voids within the open-core gasifer has been described.

4. FEED SELECTION, PROCESSING AND CHARACTERIZATION

4.1 Selection of Feed Types

The principal feed material consisted of softwood blocks produced in-house by the procedure given below (Section 4.2). The feed is consistent with that used by Evans (1992) and allows direct comparisons to be made with his research. The fraction sieved between 6.35-12.7 mm was chosen as the base case feed as this was the easiest to produce in the quantities required and has been found to have better flow characteristics than other size fractions (Evans, 1992). Woodchips of 4.75-6.35 mm sieved fraction were also used to investigation the effect of particle size on tar production and within a throated reactor.

The gasification process and a comparison of gasifier performance has also been investigated using sewage sludge and charcoal. The sewage sludge was obtained from Wessex Water Laboratories, as 4 mm granules. Rubberwood charcoal was supplied by the Forestry Research Institute of Malaysia. Charcoal production from the woodchips used in this research was also considered by operating the gasifier in pyrolysis dominant mode (see Section 2.5.6), but this proved to be too time consuming to produce in the quantities required.

4.2 Processing Procedure

The wood was purchased from a local builders merchant as 25 x 25 mm lengths (batch 1) or as 38 x 38 mm lengths (batch 2). Ultimate analysis of the two batches showed that they differed slightly in composition (Table 4.1) although they were both white pine. The variations may be due to differences in the original source, wood age or the processing history. It was not possible to obtain this information from the supplier. The wood was allowed to dry in the laboratory for 2-3 days since wet wood was found to be more difficult to cut using a band saw, thereby taking a longer time to process. The lengths were sliced transverse to the grain on the band saw into approximately 6 mm slabs. The slabs were then processed through a mechanical granulator until they passed a 12.7 mm sieve; occasionally a hand mill was used for this purpose for small batches or to further reduce particle size. The feed was then sieved into three fractions; 6.35-12.7 mm, 4.75-6.35 mm and particles passing through a 4.75 mm sieve (fines) that are unsuitable for use in the gasifier due to the high pressure drops encountered with them. The wood chips are then stored in the laboratory to allow the moisture content of the chips to reach equilibrium with the laboratory conditions at about 10% moisture (wet basis).

The dried sewage sludge was received as granules which were sieved to remove undersized particles below 2.1 mm. The rubberwood char was reduced to a size fraction of 4.75-12.7 mm.

4.3 Feed Characterization

The process of gasification is affected by the characteristics of the feed. The moisture content of the biomass is the main parameter affecting the composition of the product gas (Hos and Groeneveld, 1987). The particle size and size distribution will have a great influence on reaction times and the pressure drop within the reactor (Hos and Groeneveld, 1987; Reed, 1988). Density and the shape of the particles will also affect how the material flows through the reactor. The volatile matter content of the feed will affect the process of flaming pyrolysis and the ash content may cause problems due to slag formation. Hence it is important to characterize the feed according to its physical properties and chemical composition in order that comparisons may be made between different feeds.

4.3.1 Moisture Content

The moisture content was determined as the percent weight loss of a 10 g sample at 105°C to constant weight, at weighing intervals of 1 hour. At least 3 determinations were made for each run. Average moisture contents are presented in Table 4.1 below.

Table 4.1 Moisture Contents of Feed Materials Used, % Wet Basis

	Wood (Batch 1)	Wood (Batch 2)	Sewage Sludge	Rubberwood Charcoal
Average, % wb	9.04	10.51	4.50	7.47
Range, % wb	8.86-9.31	9.08-12.08	3.90-5.09	7.45-7.48

4.3.2 Ultimate and Proximate Analysis

The ultimate analysis were carried out by British Gas (for wood batch 1) and by Medac Ltd. (for remaining feeds). The results are presented in Table 4.2. Ash contents for woodchips (batch 2), sewage sludge and charcoal were obtained according to the procedure given by ASTM D 1762 (1984).

Table 4.2 Ultimate Analysis of Feed Materials Used

	Wood (Batch 1)	Wood (Batch 2)	Sewage Sludge	Rubberwood Charcoal
Dry Basis:				
Carbon	53.01	49.84	28.51	79.42
Hydrogen	6.12	6.09	3.86	2.10
Nitrogen	0.93	<0.1	2.85	0.50
Sulphur	0.01	<0.1	0.80	<0.1
Oxygen	39.86	43.54	18.32	16.97
Ash	0.07	0.48	45.66	1.01
Dry Ash -Free Basis:				
Carbon	53.04	50.08	52.47	80.23
Hydrogen	6.12	6.12	7.10	2.12
Nitrogen	0.93	0.05	5.24	0.51
Sulphur	0.01	0.00	1.47	0.00
Oxygen	39.9	43.75	33.71	17.14

The volatile matter and ash content of the feed materials were determined according to ASTM D 1762 (1984). The percentage of fixed carbon was determined by mass balance (Equation 4.1).

$$\text{Fixed carbon (\%)} = 100 - [\text{Volatile matter (\%)} + \text{Ash (\%)}] \qquad (4.1)$$

At least three determinations were carried out per sample, except for the sewage sludge where only one determination was carried out. This was to avoid unnecessary risks from the unpleasant fumes given off. The average results are presented in Table 4.3

Table 4.3 Proximate Analysis of Feed Materials Used

	Wood (1)*	Wood (2)#	Sewage Sludge#	Charcoal#
Dry Basis:				
Volatile matter	84.75	82.68	47.61	23.10
Fixed carbon	15.19	16.67	6.73	75.89
Ash content	0.07	0.48	45.66	1.01

* Carried out by British Gas.

According to ASTM D 1762 (1984)

For wood (batch 2) the standard deviation in the ash and volatile matter determinations were 0.07% and 1.18% respectively. Estimated weighing errors are ± 0.05%, indicating that in the volatile determination slight variations in the method occurred.

The volatile analysis of sewage sludge agrees with the average result achieved by Wessex Water Laboratories (1991) of 47.5 % on a different batch of granules.

4.3.3 Energy Content

The higher heating value (HHV) of the feedstocks used in this project were calculated from the ultimate analysis using the IGT equation (Graboski, 1980) given in Equation 4.2.

$$HHV = 0.341\ C + 1.323\ H + 0.068\ S - 0.0153\ Ash - 0.12\ (O + N) \quad (4.2)$$

This is reported to be the most accurate method of calculating the energy content of biomass by Graboski (1980) with an average error of 1.7%. Evans (1992) measured the heating value experimentally using a bomb calorimeter and obtained a value within 10 % of that calculated using the IGT equation for the same wood used in this research; however, his determinations showed a variance greater than 5%.

The higher heating values obtained using the IGT equation for woodchips, sewage sludge and charcoal are presented in Table 4.4.

Table 4.4 Higher Heating Values of Feed Materials Used, Dry Basis

	Wood (1)	Wood (2)	Sewage Sludge	Charcoal
HHV, $MJkg^{-1}$	21.68	19.81	11.64	27.75

4.3.4 Bulk Density

The bulk density of the feed was obtained by dividing the weight of an air dried sample by the volume it occupied in an 80 cm diameter measuring cylinder. The cylinder was tapped 100 times to achieve settling of the feed. This was repeated at least six times to obtain the average values presented in Table 4.5.

4.3.5 Specific Density

For wood the specific (apparent) density was measured according to ASTM D 2395 (1983) as weight divided by volume using whole pieces left from the band sawing procedure. The density of sewage sludge was calculated by immersion in an oil of known density and dividing the gain in weight by the change in volume. The values are presented in Table 4.5.

Table 4.5 Physical Characteristics of Feed Materials Used

	Wood (small feed)	Wood (base case)	Sewage Sludge	Rubberwood Charcoal
Sieved size fraction, mm	4.75-6.35	6.35-12.7	2.41-8.0	4.35-12.7
Bulk density, gcm^{-3}	0.278	0.277	0.559	0.160
Specific density, gcm^{-3}	0.497	0.497	1.304	0.335
Voidage, %	44.1	44.3	57.1	52.2
Dimensions, mm (see Section 4.3.7 and Figure 4.1)				
a	5.44	5.52	2.78	4.76
b	3.23	7.94	3.43	8.03
c	8.17	13.94	4.37	13.76
Characteristic size, mm				
cubic	5.08	8.36	2.77	7.89
diameter	6.31	10.37	3.44	9.79
Sphericity	0.729	0.746	0.884	0.722
Average weight, g	0.045	0.256	0.022	0.108

4.3.6 Voidage

The percent voidage is calculated in Equation (4.3) using the specific density (ρ) and the bulk density (ρ_B) of the feed. The values are presented in Table 4.5.

$$\text{Voidage} = \frac{\rho - \rho_B}{\rho} \times 100\% \qquad (4.3)$$

4.3.7 Dimensions

Woodchips are predominantly cuboid shaped (block-type feed) whilst the sewage sludge granules are predominantly spherical or ellipsoidal in appearance. The dimensions of the woodchips were measured according to Figure 4.1. The dimension "a" was measured parallel to the grain and is determined by the slab width cut by the band saw. The sewage sludge granules and charcoal particles were measured with "c" as the longest axis and "a" along the smallest axis, since grain orientation is absent in sewage sludge and could not be distinguished clearly enough for the charcoal particles. A single value for size is useful in characterization of feed. The length of one side of a cube occupying the same volume of a particle gives the cubic characteristic size, and the diameter of a sphere occupying the same volume gives the characteristic size. The values are presented in Table 4.5.

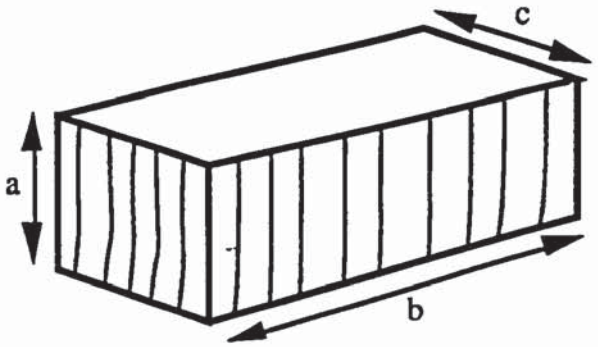

Figure 4.1 Measurement of Wood Chip Dimensions

4.3.8 Sphericity

The sphericity describes the shape as the ratio of the surface area of the feed to the surface area of a sphere occupying the same volume as the feed. The surface areas of the feed materials were calculated using the measurements of the dimensions previously discussed, assuming the wood and charcoal particles to be cuboid in shape, and the sewage sludge particles to be ellipsoidal. Spherical particles have a sphericity of 1, whereas a flat chip of 1 x 10 x 10 mm has a sphericity of 0.434, and a pin of 1 x 1 x 10 mm a sphericity of 0.537. Since flat chips and pins form bridges and voids and spheres have good flow characteristics (Evans, 1992), the sphericity gives an indication of how well material flows through the gasifier. The sphericity is also predicted to influence the time for completion of flaming pyrolysis by Reed and Markson (1983) with flat chips undergoing flaming pyrolysis faster than a cube of equal volume. Sphericities of materials used are presented in Table 4.5.

4.4 Summary

Woodchips in the size fraction 6.35-12.7 mm were chosen as the standard feed as this was the easiest to produce, showed good flow characteristics and would allow a direct comparison with previous workers. Other feed types chosen were woodchips of 4.75-6.35 mm, sewage sludge and rubberwood charcoal to enable investigations of the effect of feed size and type on the gasification process. Chemical and physical analyses were carried out in order to characterize the different feeds.

5. EXPERIMENTAL PROGRAMME

5.1 Selection of Parameters for Investigation

The parameters selected for investigation were outlined in the objectives listed in Chapter 1 and are described below for both the open-core and the hybrid throated gasifiers.

5.1.1 Definition of Base Case Conditions

To evaluate the effect of a particular process parameter under investigation a set of base case runs are needed in order that comparisons can be made. A base case test is defined as using 6.35-12.7 mm wood blocks within an uninsulated open-core gasifier during stable operation (see Section 2.5.6), since this gives a gasifier performance that is approximately constant with time. The base case uses the feed size that is in greatest supply, in order that feed shortages do not hamper the experimental programme. Tests lasting longer than 15 minutes were considered acceptable since this was thought to be long enough for any drift in the performance measurements (e.g char bed height, gas composition and gas flow rate) to become apparent and for short term fluctuations to average out (see Appendix E).

5.1.2 Open-Core Gasifier Programme

The parameters selected for investigation using the open-core gasifier are:

- The effect of different char bed heights under base case conditions.
- The effect of insulation, using 38 mm Kaowool insulation described in Section 3.3, compared to base case operation.
- The effect of feed size, using a 4.75-6.35 mm sieved fraction compared with base case feed.
- The use of sewage sludge granules and rubberwood charcoal (see Chapter 4) compared with the base case feed.
- Mode of operation, under stable, pyrolysis dominant (char production) and gasification dominant (char consumption) conditions (see Section 2.5.6) using base case feed.
- The effect of reactor bed agitation using the vibro-mixer compared to base case operation.

5.1.3 Hybrid-Throated Gasifier Programme

The parameters selected for investigation using the hybrid-throated gasifier are:

The operation and performance of the hybrid-throated gasifier compared with the base case open-core gasifier.

- The effect of insulation, using 38 mm Kaowool described in Section 3.3 compared to the uninsulated throated and the insulated open-core gasifiers.

- The effect of feed size using a 4.75-6.35 mm sieved fraction compared with base case feed.
- The use of sewage sludge granules and rubberwood charcoal (see Chapter 4).
- Investigate the turndown capability of the hybrid-throated gasifier.

5.2 Test Summaries

In order to make the most efficient use of gasifier operating time, a run may consist of several test periods with different experimental conditions. Thus several sets of results can be obtained during each run of the gasifier resulting in less time spent on gasifier cleaning, preparation and start-up. Test 1.1 refers to the first set of experimental conditions during run 1. After the completion of a test, the system is allowed to stabilize (in terms of gas composition and reaction zone position) before commencement of the next test. The interval between tests will therefore depend upon the parameter that has been changed, but is typically about 10 minutes. The system gives the benefit that start-up and shut-down time, during which data readings are inaccurate due to rapidly changing conditions, are excluded from mass and energy balances. Test numbering for throated runs begin with "T".

Standard data collected for all runs (unless otherwise stated in the test summaries which follow) consists of feed rate, gas flow rate using pitot tube, gas composition, char bed height and reaction zone depth and exit temperature of product gas from the gasifier. A successful test is defined as a test of adequate duration fulfilling its objectives. Table 5.1 lists all tests carried out in this research, and includes the specific data collected for particular tests. Greater detail is given in the test summaries in Appendix G1.

Table 5.1 Individual Test Summaries

Open-Core Tests

Test Number 1.1	Insulated open-core. Duration 41 minutes.
Feed used	Wood blocks (6.35-12.7 mm) batch 1.
Objective	Gasifier core temperature profile and insulation temperatures.
Specific data collected	Gas flow rates using gasmeter. Particle pyrolysis times.
Specific capacity	285 $kgm^{-2}h^{-1}$
Air/feed ratio	2.31
Comments	Test successful. Insulation removed for test 1.2.
Test Number 1.2	Base case open-core. Duration 43 minutes.
Feed used	Wood blocks (6.35-12.7 mm) batch 1.
Objective	Gasifier core temperature profile.
Specific data collected	Gas flow rates using gasmeter.
Specific capacity	242 $kgm^{-2}h^{-1}$
Air/feed ratio	3.26
Comments	Test successful.

Table 5.1 continued

Test Number 2.1	Insulated open-core. Duration 53 minutes.
Feed used	Wood blocks (6.35-12.7 mm) batch 1.
Objective	Tar and solids sampling.
Specific data collected	Insulation temperatures measured. Gas flow using gasmeter.
Specific capacity	241 $kgm^{-2}h^{-1}$
Air/feed ratio	2.37
Comments	Test successful. Insulation removed for test 2.2.
Test Number 2.2	Base case open-core. Duration 40 minutes
Objectives	Gasifier core temperature profile.
Feed used	Wood blocks (6.35-12.7 mm) batch 1.
Specific data collected	Gas flow using gasmeter.
Specific capacity	314 $kgm^{-2}h^{-1}$
Air/feed ratio	2.98
Comments	Test successful.
Test Number 2.3	Open-core. Duration 19 minutes.
Feed used	Wood blocks (6.35-12.7 mm) batch 1.
Objectives	Operation in rising zone mode. Tar and solids sampling.
Specific data collected	Gas flow rates using gasmeter.
Specific capacity	155 $kgm^{-2}h^{-1}$
Air/feed ratio	3.32
Comments	Test successful.
Test Number 3	Base case open-core. Duration 39 minutes.
Feed used	Wood blocks (6.35-12.7 mm) batch 2.
Objective	Tar, solids and water sampling.
Specific data collected	External reactor temperature profile.
Specific capacity	260 $kgm^{-2}h^{-1}$
Air/feed ratio	3.49
Comments	Test successful.
Test Number 4	Base case open-core. Duration 73 minutes.
Feed used	Wood blocks (6.35-12.7 mm) batch 2.
Objective	Start-up tar, solids and water sampling.
Specific data collected	External reactor temperature profile.
Specific capacity	296 $kgm^{-2}h^{-1}$
Air/feed ratio	3.58
Comments	Test successful.
Test Number 5	Base case open-core. Duration 18 minutes.
Feed used	Wood blocks (6.35-12.7 mm) batch 2.
Objective	Demonstration.
Specific data collected	Reaction zone temperatures at 7.5 and 10 cm.
Specific capacity	296 $kgm^{-2}h^{-1}$
Air/feed ratio	3.58
Comments	Run terminated due to line filter blockage by char/tar in water circulation system.

Table 5.1 continued

Test Number 6	Base case open-core. Duration 103 minutes.
Feed used	Wood blocks (6.35-12.7 mm) batch 2.
Objective	Demonstration.
Specific data collected	Reaction zone temperatures at 7.5 and 10 cm.
Specific capacity	245 $kgm^{-2}h^{-1}$
Air/feed ratio	3.65
Comments	Test successful.
Test Number 7	Insulated open-core. Duration 73 minutes
Feed used	Wood blocks (6.35-12.7 mm) batch 2.
Objectives	Tar, solids and water sampling.
Specific data collected	External temperature profile.
Specific capacity	365 $kgm^{-2}h^{-1}$
Air/feed ratio	2.63
Comments	Test successful with 3 tar and solids samples taken allowing repeatability of sampling procedure to be evaluated.
Test Number 8	Open-core. Duration 92 minutes.
Feed used	Wood blocks (4.75-6.35 mm) batch 2.
Objectives	Test using smaller feed size. Tar, solids and water sampling.
Specific data collected	Core and external temperature profile.
Specific capacity	312 $kgm^{-2}h^{-1}$
Air/feed ratio	3.03
Comments	Test successful.
Test Number 9	Open-core. Duration 97 minutes.
Feed used	Wood blocks (6.35-12.7 mm) batch 2.
Objectives	Test using vibro-mixer. Tar and solids sampling.
Specific data collected	Duration and frequency of use of vibro-mixer. External temperature profile.
Specific capacity	235 $kgm^{-2}h^{-1}$
Air/feed ratio	3.69
Comments	Low specific capacity possibly due to slowly rising char bed of 3.71 cmh^{-1}. Char bed movements erratic with a period of operation with no char bed, ie operation on the grate. Samples taken not used due to air leak into sampling system.
Test Number 10	Open-core on extended grate, agitated using vibro-mixer.. Duration approx. 28 minutes of which approx. 10 minutes with sewage sludge gasification.
Feed used	Wood blocks (6.35-12.7 mm) batch 2; dried sewage sludge granules approx. 4 mm diameter.
Objective	Use of wood blocks and sewage sludge in alternate batches.
Specific capacity	Feed rates unknown since steady state operation not achieved.
Air/feed ratio	Not determined.
Comments	Test terminated due to severe clinkering of sewage sludge within reaction zone.

Table 5.1 continued

Test Number 11	Open-core agitated using vibro-mixer. Duration 63 minutes.
Feed used	Wood blocks (6.35-12.7 mm) batch 2.
Objectives	Tar and solids sampling after demister to determine the cleaning efficiency. Char data profile measurement.
Specific data collected	External temperature profile and internal reaction temperature.
Specific capacity	277 $kgm^{-2}h^{-1}$
Air/feed ratio	2.96
Comments	Test successful. Three samples taken of the tar and solids content of gas exiting demister. Char size distribution, moisture, volatile matter and ash content profile
Test Number 12	Open-core agitated using vibro-mixer. Duration 63 minutes.
Feed used	Wood blocks (6.35-12.7 mm) batch 2.
Objective	Tar and solids sampling after demister, as in test 11.
Specific data collected	Duration and frequency of vibro-mixer usage. Catchpot char size distribution.
Specific capacity	332 $kgm^{-2}h^{-1}$
Air/feed ratio	2.91
Comments	Test successful. Three samples taken of the tar and solids content of gas exiting demister.
Test Number 13.1	Insulated open-core, agitated. Duration 31 minutes.
Feed used	Wood blocks (6.35-12.7 mm) batch 2.
Objective	Tar and solids sampling.
Specific data collected	External temperature profile. Batch gas analysis.
Specific capacity	344 $kgm^{-2}h^{-1}$
Air/feed ratio	2.42
Comments	Batch gas analysis indicated air leak into sample taken, otherwise test successful. Insulation removed for test 13.2.
Test Number 13.2	Open-core, agitated. Duration 32 minutes.
Feed used	Wood blocks (6.35-12.7 mm) batch 2.
Objectives	Tar and solids sampling.
Specific data collected	External temperature profile. Batch gas analysis.
Specific capacity	347 $kgm^{-2}h^{-1}$
Air/feed ratio	2.87
Comments	Test successful.
Test Number 14.1	Open-core. Duration 40 minutes.
Feed used	Wood blocks (6.35-12.7 mm) batch 2.
Objectives	Operation in pyrolysis mode. Tar and solids sampling.
Specific data collected	Rate of reaction zone movement.
Specific capacity	207 $kgm^{-2}h^{-1}$.
Air/feed ratio	2.68
Comments	Test successful.
Test Number 14.2	Open-core. Duration 9 minutes.
Feed used	Wood blocks (6.35-12.7 mm) batch 2.
Objectives	Operation in gasification mode. Tar and solids sampling.
Specific data collected	Rate of reaction zone movement.
Specific capacity	439 $kgm^{-2}h^{-1}$.
Air/feed ratio	2.92
Comments	The short duration of the test was due to the reaction zone reaching the grate. The test is therefore repeated in 14.4.

Table 5.1 continued

Test Number 14.3	Open-core. Duration 33 minutes.
Feed used	Wood blocks (6.35-12.7 mm) batch 2.
Objectives	Operation in pyrolysis mode.
Specific data collected	Rate of reaction zone movement.
Specific capacity	336 $kgm^{-2}h^{-1}$.
Air/feed ratio	2.88
Comments	Test successful.
Test Number 14.4	Open-core. Duration 14 minutes.
Feed used	Wood blocks (6.35-12.7 mm) batch 2.
Objectives	Operation in gasification mode. Tar and solids sampling.
Specific data collected	Rate of reaction zone movement.
Specific capacity	359 $kgm^{-2}h^{-1}$.
Air/feed ratio	2.92
Comments	Test successful, although the test was 1 minute short of the targeted duration.
Test Number 15.1	Open-core. Duration 68 minutes of which 29 minutes was in pyrolysis dominant mode (not used).
Feed used	Wood blocks (6.35-12.7 mm) batch 2.
Objectives	Operation at different char bed heights. Tar and solids sampling.
Specific data collected	None.
Specific capacity	Average = 253 $kgm^{-2}h^{-1}$.
Air/feed ratio	Average = 2.73
Comments	5 tar samples taken at different bed heights.
Test Number 15.2	Open-core. Duration 8 minutes.
Feed used	Rubberwood charcoal (4.75-12.7 mm).
Objectives	Investigate the use of charcoal in gasifier.
Specific data collected	None.
Specific capacity	327 $kgm^{-2}h^{-1}$ (approx.).
Air/feed ratio	2.91 (approx.).
Comments	Unable to stabilize reaction zone (rising).

Hybrid-Throated Tests

Test Number T1	Test aborted.
Feed used	Start-up material (Char, paper, sawdust).
Objectives	Throated commissioning run.
Specific data collected	Aborted test.
Specific capacity	Aborted test.
Air/feed ratio	Aborted test.
Comments	Test unsuccessful due to fall through of material at the throat. No grate present below throat.
Test Number T2	Test aborted.
Feed used	Wood blocks (6.35-12.7 mm) batch 2.
Objectives	Throated commissioning run.
Specific data collected	Aborted test.
Specific capacity	Aborted test.
Air/feed ratio	Aborted test.
Comments	Failed to maintain reaction zone stability. Throat inhibited flow of fuel to reaction zone.

Table 5.1 continued

Test Number T3	Throated reactor configuration. Duration 13 minutes.
Feed used	Wood blocks (6.35-12.7 mm) batch 2.
Objectives	Tar, solids and water sampling.
Specific data collected	None.
Specific capacity	261 $kgm^{-2}h^{-1}$
Air/feed ratio	3.41
Comments	Test successful.
Test Number T4.1	Throated reactor configuration. Duration 50 minutes.
Feed used	Wood blocks (6.35-12.7 mm) batch 2.
Objectives	Tar, solids and water sampling.
Specific data collected	External temperature profile.
Specific capacity	405 $kgm^{-2}h^{-1}$
Air/feed ratio	3.53
Comments	Test successful.
Test Number T4.2	Throated reactor configuration. Duration 21 minutes.
Feed used	Wood blocks (4.75-6.35 mm) batch 2.
Objectives	Investigation of using small feed size.
Specific data collected	External temperature profile.
Specific capacity	382 $kgm^{-2}h^{-1}$
Air/feed ratio	3.07
Comments	Rising reaction zone moved above grate. Increased air input rate for test T4.3.
Test Number T4.3	Throated reactor configuration. Duration 15 minutes.
Feed used	Wood blocks (4.75-6.35 mm) batch 2.
Objectives	Using small feed size.
Specific data collected	None.
Specific capacity	405 $kgm^{-2}h^{-1}$
Air/feed ratio	2.96
Comments	Test successful.
Test Number T5.1	Throated reactor configuration. Duration 19 minutes.
Feed used	Wood blocks (6.35-12.7 mm) batch 2.
Objectives	Operation at medium air input rate.
Specific data collected	Reaction temperature at 2 cm below throat.
Specific capacity	401 $kgm^{-2}h^{-1}$
Air/feed ratio	3.47
Comments	Test successful.
Test Number T5.2	Throated reactor configuration. Duration 2 minutes.
Feed used	Wood blocks (6.35-12.7 mm) batch 2.
Objectives	Operation at low air input rate.
Specific data collected	Reaction temperature at 2 cm below throat.
Specific capacity	Approx. 302 $kgm^{-2}h^{-1}$ (short test duration).
Air/feed ratio	Not determined.
Comments	Reaction zone rising above the throat.

Table 5.1 continued

Test Number T5.3	Throated reactor configuration. Duration 20 minutes.
Feed used	Wood blocks (6.35-12.7 mm) batch 2.
Objectives	Operation at medium-high air input rate. Tar, solids and water sampling.
Specific data collected	Reaction temperature at 2 cm below throat.
Specific capacity	477 $kgm^{-2}h^{-1}$.
Air/feed ratio	3.68
Comments	Test successful.
Test Number T5.4	Throated reactor configuration. Duration 4 minutes.
Feed used	Wood blocks (6.35-12.7 mm) batch 2.
Objectives	Operation at high air input rate. Tar, solids and water sampling.
Specific data collected	Reaction temperature at 2 cm below throat.
Specific capacity	Approx. 466 $kgm^{-2}h^{-1}$ (short test duration).
Air/feed ratio	Not determined.
Comments	Reaction zone fell to grate.
Test Number T6.1	Throated reactor configuration. Duration 30 minutes.
Feed used	Wood blocks (6.35-12.7 mm) batch 2.
Objectives	Operation at low air input rate. Start-up tar, solids and water sampling. Tar, solids and water sampling.
Specific data collected	Reaction temperature at 2 cm below throat.
Specific capacity	276 $kgm^{-2}h^{-1}$.
Air/feed ratio	3.72
Comments	Test successful.
Test Number T6.2	Throated reactor configuration. Duration 30 minutes.
Feed used	Wood blocks (6.35-12.7 mm) batch 2.
Objectives	Operation at medium air input rate. Tar, solids and water sampling.
Specific data collected	Reaction temperature at 2 cm below throat.
Specific capacity	333 $kgm^{-2}h^{-1}$.
Air/feed ratio	3.13
Comments	Test successful.
Test Number T6.3	Throated reactor configuration. Duration 8 minutes.
Feed used	Wood blocks (6.35-12.7 mm) batch 2.
Objectives	Operation at high air input rate.
Specific data collected	Reaction temperature at 2 cm below throat.
Specific capacity	Approx. 466 $kgm^{-2}h^{-1}$ (short test duration).
Air/feed ratio	Not determined
Comments	Char bed lost.
Test Number T6.4	Throated reactor configuration. Duration 31 minutes.
Feed used	Wood blocks (6.35-12.7 mm) batch 2.
Objectives	Operation at medium-high air input rate. Tar, solids and water sampling.
Specific data collected	Reaction temperature at 2 cm below throat. External temperature profile.
Specific capacity	464 $kgm^{-2}h^{-1}$.
Air/feed ratio	3.83
Comments	Test successful.

Table 5.1 continued

Test Number T7.1	Throated reactor configuration. Duration 22 minutes.
Feed used	Wood blocks (4.75-6.35 mm) batch 2.
Objectives	Operation using small feed size. Tar, solids and water sampling.
Specific data collected	None.
Specific capacity	497 $kgm^{-2}h^{-1}$.
Air/feed ratio	2.95
Comments	Test successful.
Test Number T7.2	Throated reactor configuration. Duration approx. 4 minutes.
Feed used	Sewage sludge granules approx. 4 mm diameter.
Objectives	Using sewage sludge as feed.
Specific data collected	None.
Specific capacity	Not determined.
Air/feed ratio	Not determined.
Comments	Test terminated due to severe clinkering within reaction zone
Test Number T8	Insulated throated. Aborted.
Objectives	Insulated. Tar, solids and water sampling.
Feed used	Wood blocks (6.35-12.7 mm) batch 2.
Specific data collected	Aborted test.
Specific capacity	Aborted test.
Air/feed ratio	Aborted test.
Comments	Test terminated due to breaking of reactor vessel at the throat.
Test Number T9	Throated reactor configuration. Duration 9 minutes.
Feed used	Wood blocks (6.35-12.7 mm) batch 2.
Objectives	Trial test using stainless steel throat.
Specific data collected	Reaction temperature at 2 cm below throat.
Specific capacity	Not determined.
Air/feed ratio	Not determined.
Comments	No visual damage to throat.
Test Number T10	Throated reactor configuration. Duration 9 minutes.
Feed used	Wood blocks (6.35-12.7 mm) batch 2.
Objectives	Trial test using fireclay throat.
Specific data collected	Reaction temperature at 2 cm below throat.
Specific capacity	Not determined.
Air/feed ratio	Not determined.
Comments	Slight cracks in the fireclay, probably unsuitable for repeat usage.
Test Number T11	Insulated throated using stainless steel throat. Duration 40 minutes. The test lasted a further twenty minutes but the data was lost due to a disc writing error.
Feed used	Wood blocks (6.35-12.7 mm) batch 2.
Objectives	Tar, solids and water sampling.
Specific data collected	Reaction temperature at 2 cm below throat. External temperature profile.
Specific capacity	376 $kgm^{-2}h^{-1}$.
Air/feed ratio	2.11
Comments	Test successful.

Table 5.1 continued

Test Number T12	Throated. Duration 3 minutes.
Feed used	Rubberwood charcoal (4.75-12.7 mm).
Objectives	Investigate use of charcoal in gasifier.
Specific data collected	None.
Specific capacity	Not determined.
Air/feed ratio	Not determined.
Comments	Unable to stabilize reaction zone (rising). Run terminated due to blockage in gasmeter (tank pressure relief manometer discharged). Emergency shut down implemented.

5.3 Summary

The experimental programme has been described together with a summary of the tests carried out. The summary includes details of the of the objectives of each test, the measurements taken and the degree of success of each test.

6. MASS AND ENERGY BALANCE

6.1 Introduction

The quality of the gasifier performance data depends upon the accuracy and completeness of the measurements obtained. Since both mass and energy are conserved in the gasification process, a measure of the accuracy and completeness of the measurements can be expressed as a percentage of total outputs to total inputs to give the mass and energy balance closures. The mass and energy balances are used to check instrumental analysis and other measurements, and may possibly be used to locate sources of material loss errors. This chapter presents the measurements and calculations used in obtaining the mass and energy balances and discusses the accuracy of the results obtained.

6.2 Mass Balance

The start and end points of a run test period were decided on the basis of the stability of the gasification reaction zone, gas composition and gas flow rate, except for investigations on unstable (falling and rising) reaction zones (see Appendix E). For unstable reaction zone investigations, the test began after a period of stable operation (of at least 5 minutes) and ended before the reaction zone reached the top of the gasifier in the case of pyrolysis dominant (rising zone) operation, and before the reaction zone reached the grate for gasification dominant investigations. The gasifier was batch fed and was filled to a pre-determined level at the start and end of each test period to allow the feed rate to be determined. The duration was calculated as the elapsed time between the start and end points. The mass balance was calculated over the duration of the test for the successful tests listed in Section 5.1. The mass inputs and outputs used in the mass balance are shown in Figure 6.1 for steady state operation using wood. In tests where the reaction zone is not steady, i.e. with a rising or falling reaction zone, the depletion or accumulation of char and wood within the reactor was calculated from the change in the volume of the char zone within the reactor and the bulk densities of the materials (see Appendix F1).

The calculations used in the mass balance are given in Appendix F1. The feed rate is measured by weighing the batch additions to the gasifier (see Appendix F1). The H_2, CO, CO_2 and CH_4 contents of the product gas are measured (see Section 3.7) and nitrogen is assumed to make up the balance. The air flowrate into the gasifier is calculated from the nitrogen content of the product gas, with the air moisture content calculated using psycometric charts (Perry, 1985). The water, tar and solids output from the gasifier was measured for several tests (see Appendix G1) and assumed for

the remaining tests. The closure for the mass balance is calculated and presented as a percentage of outputs divided by the inputs using Equation 6.1;

$$\text{Closure, \%} = \frac{(\text{Gas + Tar + Ash + Char + Water})}{(\text{DAF Feed+ Ash + Feed } H_2O + \text{Air + Air } H_2O)} \times 100\% \quad (6.1)$$

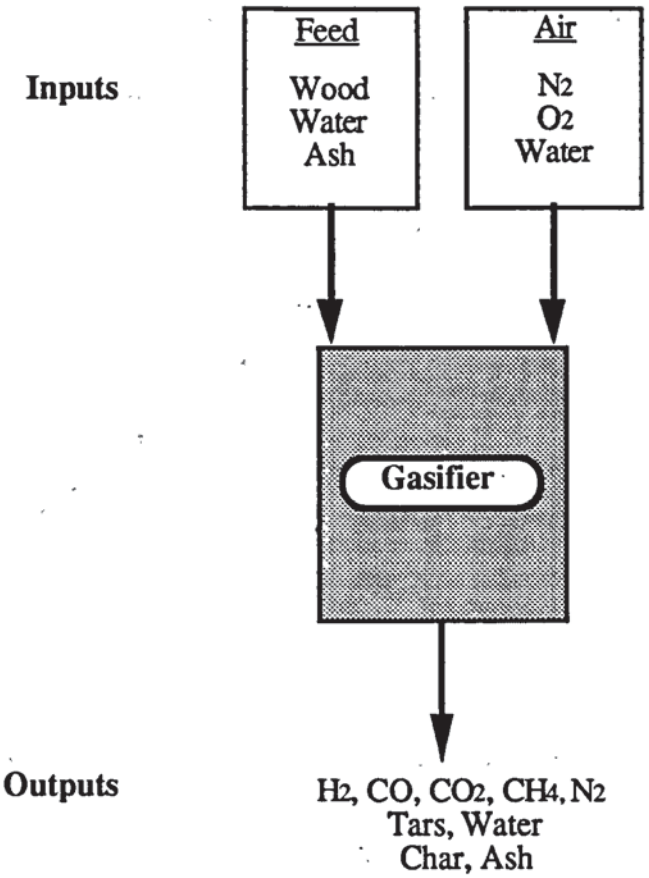

Figure 6.1 Mass Balance Flow Diagram

The elemental closures for carbon, hydrogen and oxygen are calculated using the elemental compositions of the inputs and outputs. The closure for nitrogen is always 100% since the air flow rate in is calculated from the nitrogen content of the product gas stream.

6.2.1 Mass Balance Results and Discussion

Mass and elemental balances were carried out for 31 test runs. The average closures are presented in Table 6.1. All mass balances lie within 5% of closure. This compares with 56% of Evans's runs within the same margin obtained previously with the Aston gasifier (1992) indicating an improvement in the measurement of input and output flow rates. Figure 6.2 shows that good mass balance closures were obtained over the full range of input rates and operating conditions. Mass and elemental balances for individual tests are given in Appendix G1.

Table 6.1 Mass and Elemental Balance Closures, Average Values		
	Average, %	Standard deviation
Mass	98.57	1.96
Carbon	104.53	8.25
Hydrogen	94.92	10.79
Oxygen	93.68	5.47

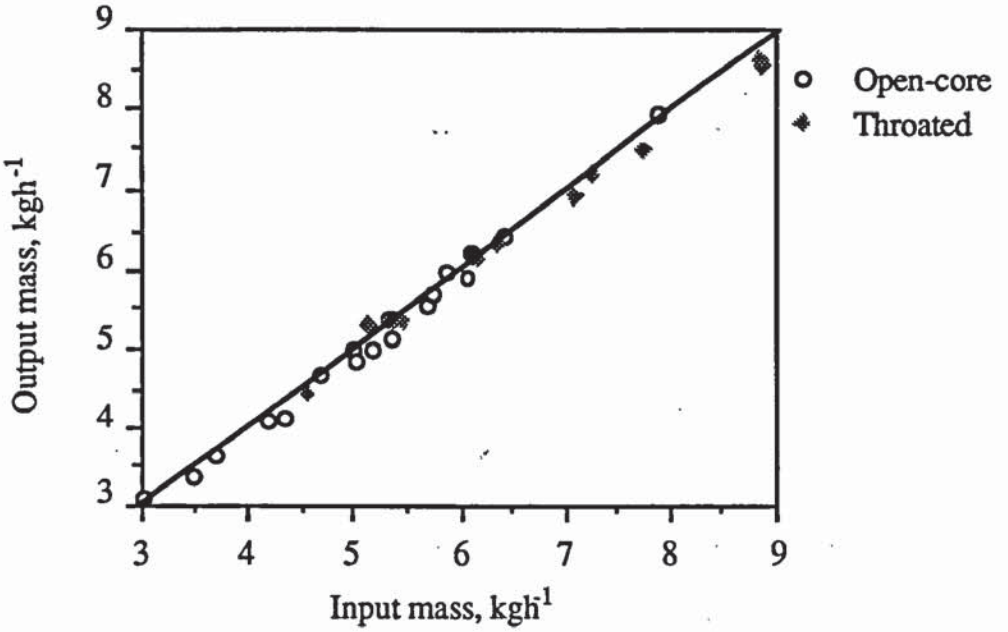

Figure 6.2 Input Mass Flow Rates Against Output Mass Flow Rates for the Test Results

Figure 6.2 also shows that the mass balance is good for both reactor types across the range of results achieved. The sample used in the ultimate analysis (see Section 4.3.2) may not be representative of the wood used in all the runs conducted since the batch was processed over a period of one year. The measured gas composition would also contain errors since C_2+ hydrocarbon gases were not measured, except for the batch gas analyses carried out, and are not included in the mass balance. These errors may explain the differences between the elemental balance closure shown in Table 6.1. However, the elemental closures are acceptable occurring within 10% of closure on average.

6.3 Energy Balance

The energy balance is performed in order to provide information on the efficiency of the conversion process. The process is the conversion of the chemical energy of the feed to chemical energy of the product gas, tars and char, and to heat energy retained as sensible heat or lost to the surroundings from the gasifier by convection and radiation. The energy flow diagram is shown in Figure 6.3. The calculations used in

obtaining the energy balance are given in Appendix F2. The quality of the energy balance depends upon the quality of the mass balance on which it is based, and upon the estimation of heat losses from the gasifier.

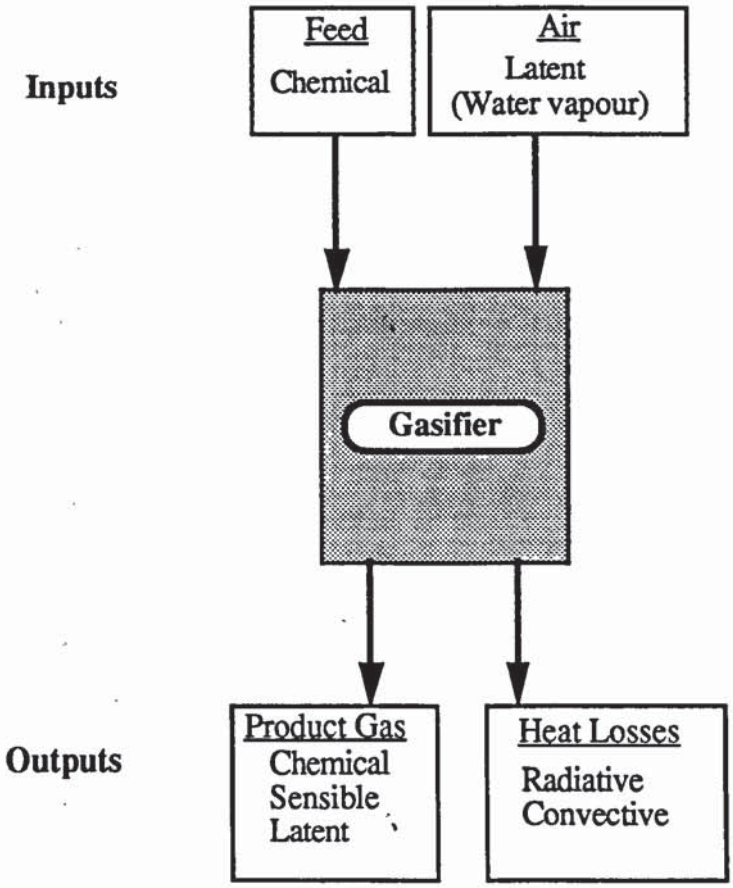

Figure 6.3 Energy Balance Flow Diagram

The method used to calculate heat losses from the gasifier is similar to that used by Reyes (1989), and Evans (1992). A full description of the calculations are given in Appendix G1, which show that accurate measurement of the outer temperature of the reactor is important. Estimated heat losses from insulated and uninsulated gasifiers are presented and discussed in Section 7.4.1.

6.3.1 Energy Balance Results and Discussion

Energy balances for the experimental tests are given in Appendix G2, with the closures given in Appendix G1. The average closure for the energy balance for 31 tests is 104.1% with a standard deviation of 10.5%. Figure 6.4 shows how the energy output varied with energy input for open-core and throated reactor configurations. It can be seen that the results have a greater scatter from closure than for the mass balance (Figure 6.2), which may be due to inaccuracies in estimating the heat loss from the gasifier (see Section 7.5.2) or due to inaccuracies in the mass balance (see Section 6.2.1).

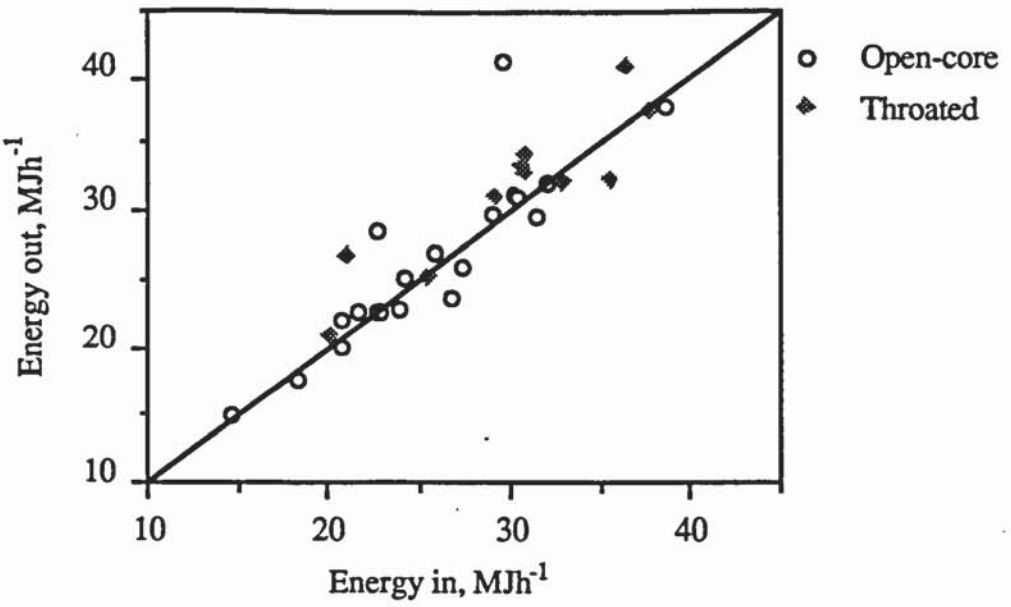

Figure 6.4 Input Energy Flow Rate Against Calculated Output Energy Flow Rate

6.4 Gasifier Performance Indicators

Gasifier performance indicators are required in order to evaluate and compare the effects of process variables investigated, and to enable comparisons with other gasifiers. The calculation of the specific capacity, volumetric yield, equivalence ratio and conversion efficiencies are described in Sections 6.4.1 to 6.4.4.

6.4.1 Specific Capacity

The specific capacity of a gasifier is used to compare gasifiers of different sizes. The DAF feed input rate is divided by the area of the grate (or of the throat for throated gasifiers).

$$\text{Specific Capacity, kgm}^{-2}\text{h}^{-1} = \frac{\text{DAF Feed}}{\text{Area of Grate}} \qquad (6.5)$$

6.4.2 Volumetric Yield

The volumetric yield gives a measure of the amount of gas produced per unit of feed and is defined here as the ratio of the normal dry gas volumetric flow rate and the DAF feed input rate to the gasifier.

$$\text{Volumetric Yield, Nm}^3\text{kg}^{-1} = \frac{\text{Gas Volume}}{\text{DAF Feed}} \qquad (6.6)$$

6.4.3 Air to Fuel Ratio and Equivalence ratio

The ratio of dry air mass flow rate to dry feed rate is the air/fuel ratio. The equivalence ratio is a measure of the degree of oxidation, given by Equation 6.7, where $[O_2:Feed]_a$ is the oxygen to feed ratio occurring and $[O2:Feed]_s$ is the oxygen to feed ratio for complete combustion. Calculation of the equivalence ratio is given in Appendix F.

$$\text{Equivalence ratio} = \frac{[O_2:Feed]_a}{[O_2:Feed]_s} \qquad (6.7)$$

6.4.4 Cold, Hot and Raw Gas Conversion Efficiencies

The measure of the conversion of energy in the feed to energy in the product gas is the cold gas efficiency of the gasifier. Similarly, the conversion to energy in the hot clean gas is the hot gas efficiency, and conversion to the hot gasification products is the raw gas efficiency. These are calculated in Equations 6.8-6.10.

Cold Gas Efficiency, η_c, %;

$$\eta_c = \frac{\text{Cold Gas Energy}}{\text{Feed Energy Input}} \times 100\% \qquad (6.8)$$

Hot Gas Efficiency, η_h, %;

$$\eta_h = \frac{\text{Hot Gas Energy}}{\text{Feed Energy Input}} \times 100\% \qquad (6.9)$$

Raw Gas Efficiency, η_r, %;

$$\eta_r = \frac{\text{Raw Gas Energy}}{\text{Feed Energy Input}} \times 100\% \qquad (6.10)$$

Since the raw gas efficiency may also be expressed as the energy input from the feed minus losses this is also calculated since it gives a measure of the efficiency assuming that 100% closure is achieved.

$$\eta_r\,(100\%\ \text{closure}) = \frac{\text{Feed Energy Input - Heat Loss}}{\text{Feed Energy Input}} \times 100\% \qquad (6.11)$$

6.5 Summary

The mass balances for the 32 tests for which a mass balance was carried out are all satisfactory and lie within 5% of closure. The elemental balance for the C, H and O are within 10% of closure on average. The average energy balance closure for the test runs was 104%. The calculation of gasifier performance indicators and energy efficiencies are given.

7. OPEN-CORE GASIFIER RESULTS AND DISCUSSION

The performance of the gasifier under base case conditions (defined in Section 5.1.1) is presented in Section 7.1. The influence of the parameters under investigation (see Chapter 5) are then compared against the base case tests (Section 7.1). Comparisons are made to previous results obtained with the Aston gasifier (Earp, 1988; Evans, 1992) and with other downdraft gasifiers.

7.1 Base Case Tests

A total of six base case tests were conducted (test numbers 1.2, 2.2, 3, 4, 5, and 6) with char bed heights in the range 3.7-22.2 cm, allowing comparison of average base case data values (thereby reducing errors) and also comparison of tests conducted at different char bed heights under different investigative conditions. The effects of char bed height on gasifier performance is reported and discussed in Section 7.3. Table 7.1 lists the average results for the base case tests carried out in this research.

Table 7.1 Open-Core Base Case Performance Data and Comparison with Previous Work (Average Values)

	This research	Standard deviation	Earp* (1988)	Evans (1992)
Number of runs	6		3	2
Duration, minutes.	52.64		9.15	58.5
Feed moisture, % wet basis	10.31	1.15	10.77	9.49
Char bed height, cm	11.36	7.19	11.25	17.23
Specific capacity, $kgm^{-2}h^{-1}$	271.38	28.79	278.40	276.39
Gas volumetric yield, Nm^3kg^{-1}	3.37	0.19	2.80	2.94
Air/feed ratio	3.38	0.24	2.73	2.81
Gasifier exit temperature, °C	417.25	55.63	nr	440.39
Dry gas composition, % vol.				
H_2	9.45	0.64	12.60	9.25
CO	15.20	0.80	15.93	14.22
CO_2	10.53	1.19	10.10	13.69
CH_4	1.04	0.14	1.30	1.01
N_2	63.78	1.45	60.10	61.82
Gas HHV, $MJNm^{-3}$	3.54	0.12	4.13	3.38
Raw gas water content, % vol.	11.93	-	nr	nr
Cold gas efficiency, %	64.47	7.17	58.70	46.69

* 4.75-6.35 mm feed. nr, not reported.

Table 7.1 shows that the results obtained during this research are similar to those previously obtained. A comparison of the Aston open-core gasifier with other gasifiers in the literature is carried out for the insulated reactor in Section 7.4.

7.2 Operation of the Open-Core Gasifier

7.2.1 Mode of Operation

The open-core gasifier can be operated in gasification dominant (char consuming, falling char bed), pyrolysis dominant (char producing, rising char bed) and stable operation regimes (see Section 2.5.6) as shown in Figure 7.1.

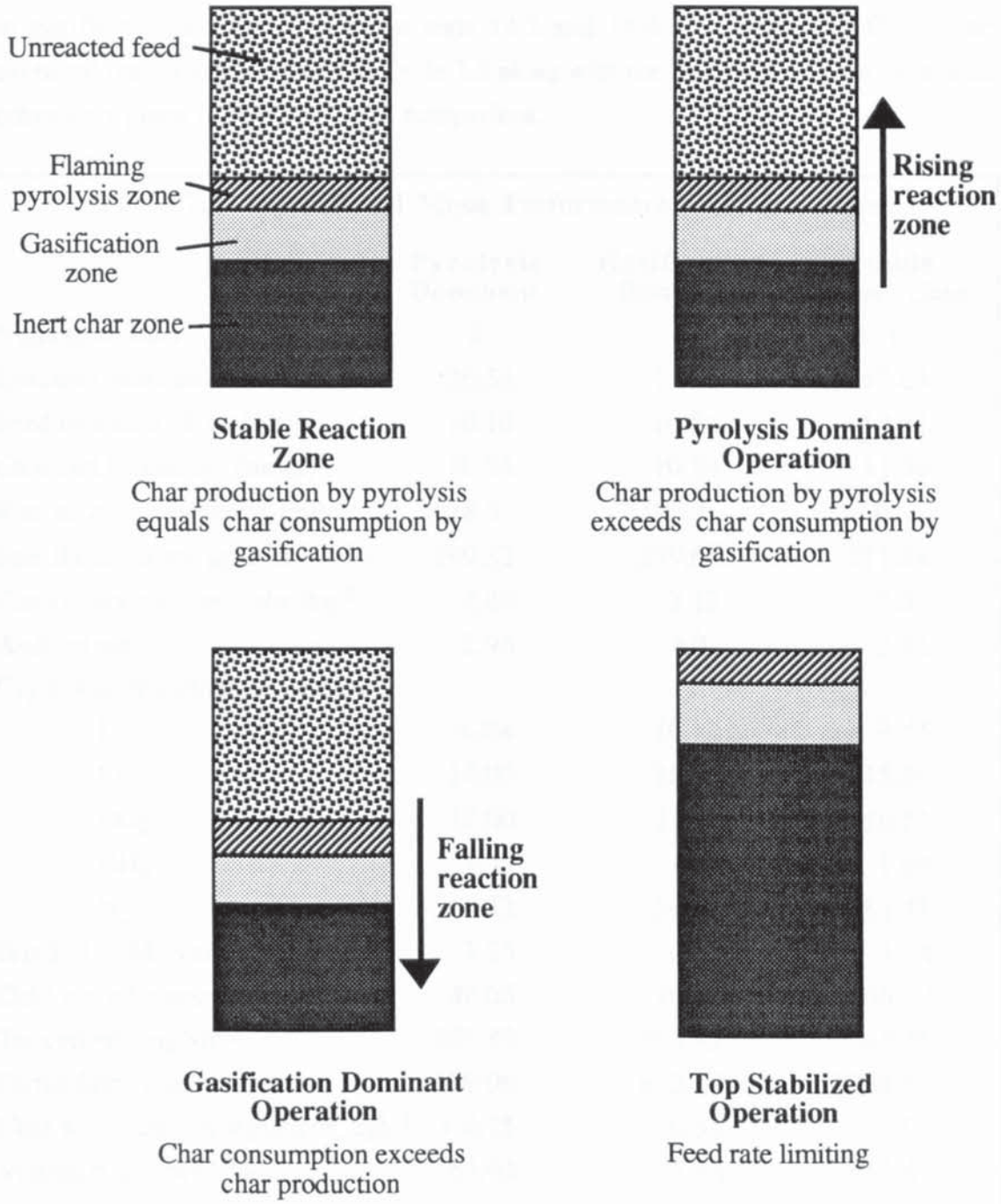

Figure 7.1 Operational Modes of the Open-Core Gasifier

The mode of operation depends upon the relative rates of pyrolysis and gasification. The gasifier can also be operated in a top stabilized mode in which the rate of feed input to the gasifier is limiting as shown in Figure 7.1 (the reaction zone may not necessarily be at the top of the reactor as depicted in Figure 7.1). No tests were conducted in top stabilized mode, which would require continuous feeding (batch feeding would result in the gasifier alternating between operating with an unreacted feed zone and operating without a feed zone). The gasifier was operated in pyrolysis dominant, gasification dominant and stable modes in order to obtain information on the mechanism for stable operation (which allows continuous operation for long periods).

The gasifier was operated in pyrolysis dominant mode in tests 2.3, 14.1 and 14.3, and in gasification dominant mode in tests 14.2 and 14.4 (see Appendix G1). The averaged results are presented in Table 7.2 along with the base case performance data previously given in Section 7.1 for comparison.

Table 7.2 Operational Mode Performance Data (Average)

	Pyrolysis Dominant	Gasification Dominant	Stable Base Case
Number of tests	3	2	6
Duration, minutes	30.59	11.51	52.64
Feed moisture, % wet basis	10.16	10.81	10.31
Char bed height, cm (mean)	10.88	10.84	11.36
Rate of zone movement, cmh^{-1}	+28.5	-105.3	0
Specific capacity, $kgm^{-2}h^{-1}$	199.32	399.05	271.38
Gas volumetric yield, Nm^3kg^{-1}	2.86	3.12	3.37
Air/feed ratio	2.96	2.92	3.38
Dry gas composition, % volume			
H_2	6.84	10.87	9.45
CO	14.00	16.32	15.20
CO_2	12.00	11.98	10.53
CH_4	1.53	1.32	1.04
N_2	65.63	59.51	63.78
Gas HHV, $MJNm^{-3}$	3.25	3.97	3.54
Cold gas efficiency, %	48.05	70.16	64.47
Tar content, $mgNm^{-3}$	657.89	269.83	665.36
Particulates, $mgNm^{-3}$	629.06	622.69	1001.62
Char accumulation/depletion[a], kgh^{-1}	+ 0.15	-0.56	0.00
System efficiency[b], %	65.93	47.65	64.47

Notes: a, char density = 120 kgm^{-3}; b, includes production or consumption of char.

For pyrolysis dominant operation a lower air to feed ratio than that needed for stable operation is claimed to be required (Earp, 1988), although it will later be shown to depend upon the superficial gas velocity. Both Earp and Evans (1992) have reported a higher air factor during pyrolysis dominant operation than when the reaction zone is stable (see Table 7.3). Both authors explain the difference between theory and practise as a result of greater heat loss in the pyrolysis dominant mode, with less energy passed on to the gasification zone, and hence less char conversion; however, this is shown to be untrue below.

Table 7.3 Experimental Air Factors Obtained for Different Operational Modes

Dominant mode	Earp (1988)[a]	Evans (1992)[b]	This research[b]
Stable	0.384	0.391	0.506
Pyrolysis	0.419	0.404	0.441
Gasification	no data	0.435	0.448

Notes: a, 4.75-6.35 mm feed; b, 6.35-12.7 mm feed.

The average energy output distribution (see Appendix G2) for each of the three modes is given in Figure 7.2 using the results of this research.

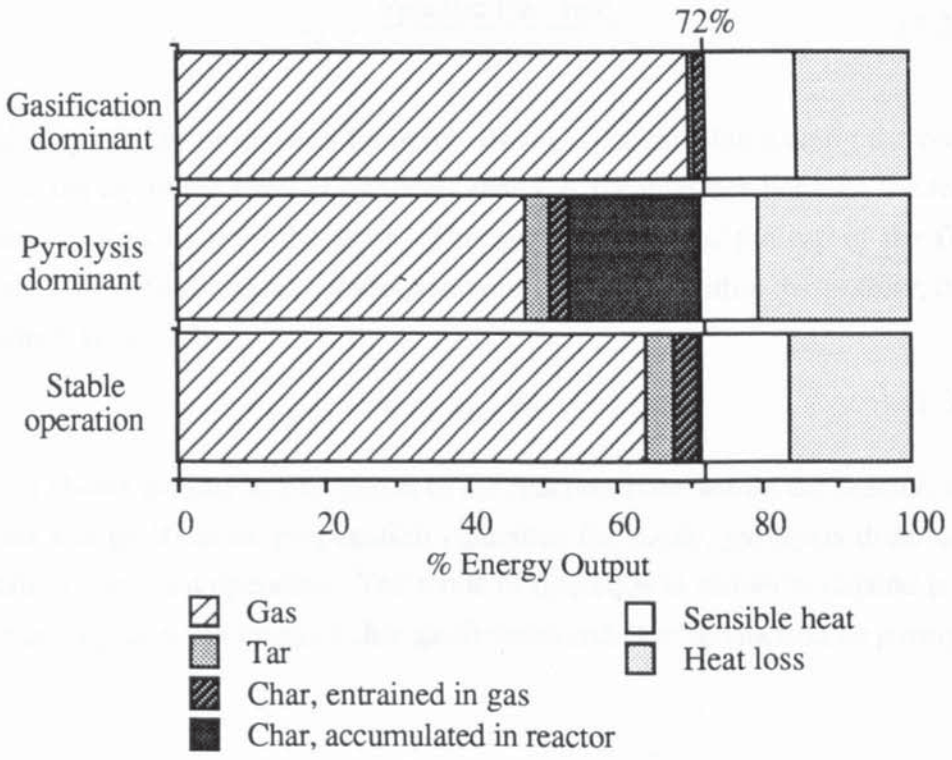

Figure 7.2 Energy Output Distribution of the Open-Core Gasifier Operating in Stable, Pyrolysis and Gasification Dominant Modes

Figure 7.2 shows that the sum of the energy lost and the sensible heat of the products is approximately constant at 28%. Furthermore, it will be shown in Section 7.3 that although heat loss increases with char bed height, the air to feed ratio actually decreases for open-core operation with a stable reaction zone. Heat loss from the reactor increasing the air demand is, therefore, an unsatisfactory explanation for the similar air requirement of the different operational modes.

The relative rates of the pyrolysis and gasification processes are important in determining reaction zone stability. Using the biomass gasification reaction velocity calculations given by Reed and Markson (1985), the rates of propagation of pyrolysis and gasification were calculated. Reed suggested that the rates of propagation are proportional to the volumetric and mass conversion rates as shown by Equation 7.1,

$$v = \frac{V}{\pi r^2} = \frac{M}{\rho_B \pi r^2} \qquad (7.1)$$

where v is the velocity of propagation, r is the radius of the reactor vessel, ρ_B is the bulk density, and V and M are the volumetric and mass conversion rates respectively. Reed assumes that there is no reduction in volume during pyrolysis and, therefore, the velocity of char consumption (v_c) is equal to the velocity of the feed bed, which was calculated from the specific feed rate (Equation 7.2).

$$v_c = \frac{\text{Specific feed rate}}{\rho_B \pi r^2} \qquad (7.2)$$

The velocity of char production by pyrolysis (v_b) was calculated using the observed motion of the top of the flaming pyrolysis zone (i.e. the interface between the feed and the char) towards or from the grate. The rate of motion of the top of the flaming pyrolysis zone defines the rate of reaction zone movement within the gasifier, denoted as v_r, which is given by;

$$v_r = v_c - v_b \qquad (7.3)$$

Table 7.4 shows the rate of movement of the reaction zone within the reactor, and the pyrolysis and gasification propagation velocities for stable, pyrolysis dominant and gasification dominant operation. The mode of operation is shown to depend upon the relative propagation velocities of char gasification and char production by pyrolysis.

Table 7.4 Biomass Gasification Reaction Velocities Using the Method of Reed and Markson (1985)

Average values	Stable	Pyrolysis dominant	Gasification dominant
Zone velocity (v_r), cmh^{-1}	0 (stationary)	+28.5 (rising)	-105.3 (falling)
Gasification velocity (v_c), cmh^{-1}	96.7	71.2	142.7
Pyrolysis velocity (v_b), cmh^{-1}	96.7	99.7	37.2
	$v_c = v_b$	$v_c < v_b$	$v_c > v_b$

Using the method of Reed and Markson (1985), Table 7.4 shows that the rate of char production by flaming pyrolysis is approximately the same for stable (96.7 cmh^{-1}) and pyrolysis dominant operation (99.7 cmh^{-1}), but is very much reduced for gasification dominant operation (37.2 cmh^{-1}). The gasification velocity increases from pyrolysis to stable to gasification dominant operation. Therefore, a rising reaction zone is a result of decreased char gasification, whilst a falling reaction zone is a result of decreased char production by pyrolysis and increased char removal by gasification. The calculation of reaction velocities using the method of Reed and Markson involves several simplifications. It is assumed that no volume reduction takes place as a result of pyrolysis, whereas in fact shrinkage is observed (see Section 7.3). The velocity of propagation may not be proportional to the volumetric mass conversion rate (see Equation 7.1) due to changes in particle size and changes in the specific and bulk densities of the char as conversion proceeds. However, the calculation of pyrolysis and gasification reaction velocities provides a useful method of estimating the relative reaction rates and, therefore, the stability of the reaction zone.

Radiative heat transfer appears to be the major mechanism involved in the initial stages of pyrolysis since the surface of the unreacted feed exposed to the zone below has been observed to char without coming into contact with flaming gases. The flames were observed to be pulled predominantly downwards, thereby confirming the observations of Earp (1988) Evans (1992). The rate of pyrolysis is, therefore, thought to be a function of the rate of radiative heat transfer. A reduction in temperature at the flaming pyrolysis front would reduce the rate of heat transfer for pyrolysis (see Equation 2.30, Section 2.5.2). No reaction zone temperature measurements were made during pyrolysis and gasification dominant tests in this work; the error involved in such measurements is likely to be high due to the rate at which temperature changes within the small distances involved (see Figure 7.4, Section 7.3.3) and because the reaction zone is continually moving when the gasifier is operated in either of the two modes. Calculation of the relative radiant heat transfer

rates to the pyrolysis front during different modes of operation is not possible without supporting temperature measurements.

The reduction in the velocity of pyrolysis propagation during gasification dominant operation (see Table 7.4) may be explained by the forced convection of heat away from the flaming pyrolysis zone as the air flow into the reactor is increased, giving a convective cooling effect. The flow of heat to the gasification zone is increased as the flames are pulled downwards further into the zone (i.e. forced convection), thereby increasing the rate of char gasification. Thus, as the air flow rate into the reactor is increased (increasing the superficial velocity of gases through the reactor) the rate of char gasification becomes increasingly dominant.

Table 7.5 shows that the lowest superficial product gas velocities (calculated from the normalized gas production rates, see Sections 2.6.2 and 3.10.1) were obtained for the gasifier operating in pyrolysis dominant mode and the highest superficial gas velocities obtained for the gasification dominant tests. The results in Table 7.5 lends support to the hypothetical heat transfer mechanism to the gasification zone described above.

Table 7.5 Superficial Product Gas Velocities for the Open-Core Gasifier During Different Modes of Operation

Pyrolysis Dominant		Stable Operation		Gasification Dominant	
Test number	Superficial gas velocity, Nms^{-1}	Test number	Superficial gas velocity, Nms^{-1}	Test number	Superficial gas velocity, Nms^{-1}
2.3	0.135	1.2	0.208	14.2	0.378
14.1	0.149	2.2	0.267	14.3	0.311
14.3	0.183	3	0.251		
		4	0.291		
		5	0.245		
		6	0.239		
Average	0.156		0.250		0.345

The maximum superficial gas velocity obtained for stable operation of 0.291 Nms^{-1} (Table 7.5) is similar to the maximum superficial gas velocity obtained by Reed (1988) of 0.28 Nms^{-1}. An average superficial gas velocity of 0.226 Nms^{-1} was calculated from the results of Evans (1992), within the range of values given in Table 7.5 for stable operation. A velocity of 0.265 Nms^{-1} was calculated for gasification dominant operation from Evans results, however, this was for a larger feed size (9.5-12.7 mm) which may affect the process. Evans' results for the pyrolysis dominant operation cannot be compared here since they were obtained for an insulated reactor. A

superficial velocity of 0.217 Nms^{-1} was calculated from Earps' results, although this was for a feed size of 4.75-6.35 mm, smaller than the feed size used here. It is concluded that for stable operation superficial gas velocities are intermediate to those obtained during pyrolysis and gasification dominant operation, and lie within the known range of 0.208 to 0.291 Nms^{-1}.

The observations and conclusions given above are compatible with the theory that the heat transfer mechanism for pyrolysis propagation is mainly by radiation given by Earp (1988). However, occasionally flames were also observed to propagate both horizontally and upwards into unreacted material (see Section 7.3). Heat transfer by these flames provides a minor contribution for pyrolysis propagation, which was suggested by Reed (1985) to be the main transfer mechanism. Heat transfer from the reactor walls by radiation and conduction are also believed to provide a minor amount of heat for pyrolysis propagation, but in a large scale gasifier these become negligible.

The open-core gasifier can be turndowned for a limited duration by operating in the pyrolysis dominant mode until the reaction zone reaches the top of the gasifier where it becomes top stabilized. However, the gasifier would then have to be operated in gasification dominant mode in order for the reaction zone to return to its initial position unless char can be removed from the reactor. The turndown of the open-core gasifier can be increased by operating in the pyrolysis dominant mode with continuous char removal from the gasifier in order to achieve a stationary reaction zone. The heating value of the gas is reduced by 9.2% (see Table 7.2) when operating in pyrolysis mode which may cause problems when used, although the result is not significant.

7.2.2 Operating Range of the Open-Core Gasifier

The operating range of the open-core gasifier, in terms of both the specific capacity and gas production rate, gives an apparent turndown ratio of 1.3:1 (see Table 7.6). Two possible hypotheses are put forward to account for apparent turndown obtained which are discussed further below. Firstly, there may be an increase in capacity as the temperature increases (e.g. as a result of operating with a higher air to feed ratio) which increases the rate of pyrolysis and gasification; secondly, there may be an increase in capacity as the area of the interface between the unreacted feed zone and the pyrolysis zone increases as a result of a sloping reaction zone.

Table 7.6 Minimum and Maximum Specific Capacities and Gas Production Rates Obtained for the Base Case Tests

	Specific Capacity, $kgm^{-2}h^{-1}$	Gas Production, $Nm^{-3}h^{-1}$
Minimum	242 (test 1.2)	3.538 (test 1.2)
Maximum	315 (test 2.2)	4.249 (test 4)
Max:Min	1.30:1	1.31:1

Temperature Hypothesis

For the base case tests the maximum specific capacity obtained was 315 $kgm^{-3}h^{-1}$. The approximate temperature of the flaming pyrolysis interface with the unreacted feed zone was measured to be 693°C; however, since temperature is rapidly increasing with depth in this region of the gasifier (see Figure 7.3) and because of the errors in the positioning of the thermocouple, the reliability of this measurement is poor. This compares with 518°C measured at the minimum specific capacity of 242 $kgm^{-3}h^{-1}$. At the higher temperature the rate of radiative heat transfer to unreacted material is greater (see Equation 2.30), thus increasing the rate of pyrolysis.

The higher temperatures may also result in less char production from pyrolysis (see Section 2.2.2) at the higher throughput. It is calculated that if the rate of gasification (char conversion) is constant then the amount of char produced by flaming pyrolysis has to be reduced by about a third in order to maintain a stable reaction zone. Higher temperatures would also reduce the time required for devolatilization of a particle thereby increasing the capacity as more particles can pass through the flaming pyrolysis zone. A model predicting the time required for pyrolysis is presented in Section 9.4. In order to increase the specific capacity by a factor of 1.3, the pyrolysis time must be reduced by 23% for a flaming pyrolysis zone of constant volume. The temperature increase required at the bottom of the flaming pyrolysis zone predicted by the model in order to achieve a 23% reduction in the flaming pyrolysis time is 365°C. This amount of temperature variation at the bottom of the flaming pyrolysis zone has not been observed during the experimental test runs, although there is considerable difficulty in the accurate measurement of temperature (see Section 7.2.1). Further investigations would be required in order to validate the temperature hypothesis, which would need an accurate method of measuring the temperature within the flaming pyrolysis zone.

Interfacial Area Hypothesis

The apparent turndown of the open-core gasifier may also be caused by a sloping reaction zone, which would increase the surface area of the flaming pyrolysis zone front. The turndown ratio would in this case be given by the cross-sectional area of

the gasifier divided by the area of the upper surface of the sloping flaming pyrolysis zone expressed in geometric terms as;

$$\text{Turndown ratio} = \frac{\pi r^2}{\pi r^2/\cos \alpha} \qquad (7.4)$$

where r is the radius of the gasifier and α is the angle of the reaction zone slope. For the apparent turndown ratio of 1.3:1 a slope angle of 40° is required. During the experimental tests, the reaction zone was occasionally observed to have a slight slope. A reaction zone slope of 43° was measured during the start-up period of a run; however, this was only maintained for 1-2 minutes and did not constitute part of a test. When a sloping reaction zone formed the reaction zone was levelled using a poker, since the angle of slope usually became greater with time leading to difficulties in operation.

Sloping reactions zones are thought to occur as a result of partial blockages in the char bed and uneven feed distribution. These lead to channelling of the reactive gases through the gasification zone and consequently reduced gasification in part of the char bed which then increases the angle of slope. In the tests conducted the reaction zone was more or less level throughout the period of operation and therefore it is thought that the apparent turndown ratio of 1.3:1 is mainly a result due to some other effect. However, an investigation of sloping reaction zones within the open-core gasifier is recommended since if the throughput can be increased in this way the induction of a sloping zone within the gasifier would allow the gas production rate to be increased which is important for practical use.

The apparent turndown is not thought to be a result of variations in the feed characteristics since the variations are small (see Chapter 4); they may, however, contribute to the overall effect. Since the tests involved a stationary reaction zone, increases in the rate of pyrolysis by either of the methods discussed must be balanced by an equal increase in the rate of gasification. Within the gasification zone throughput may be increased as a result of enhanced kinetic reaction rates due to temperature increases or as a result of an increase in the depth of the gasification zone thereby increasing the particle residence time for gasification.

7.3 Qualitative and Quantitative Analysis of the Open-Core Gasification Process

Qualitative and quantitative analysis of the gasification process within the open-core gasifier was made in order to confirm previous results (e.g. Evans, 1992) and to provide further understanding of the mechanisms involved.

7.3.1 Description of the Gasification Process

Observations of the behaviour of single particles were made during stable operation (i.e. with a stationary reaction zone). Figure 7.3 is a diagram of the observed gasification processes with approximate temperatures shown.

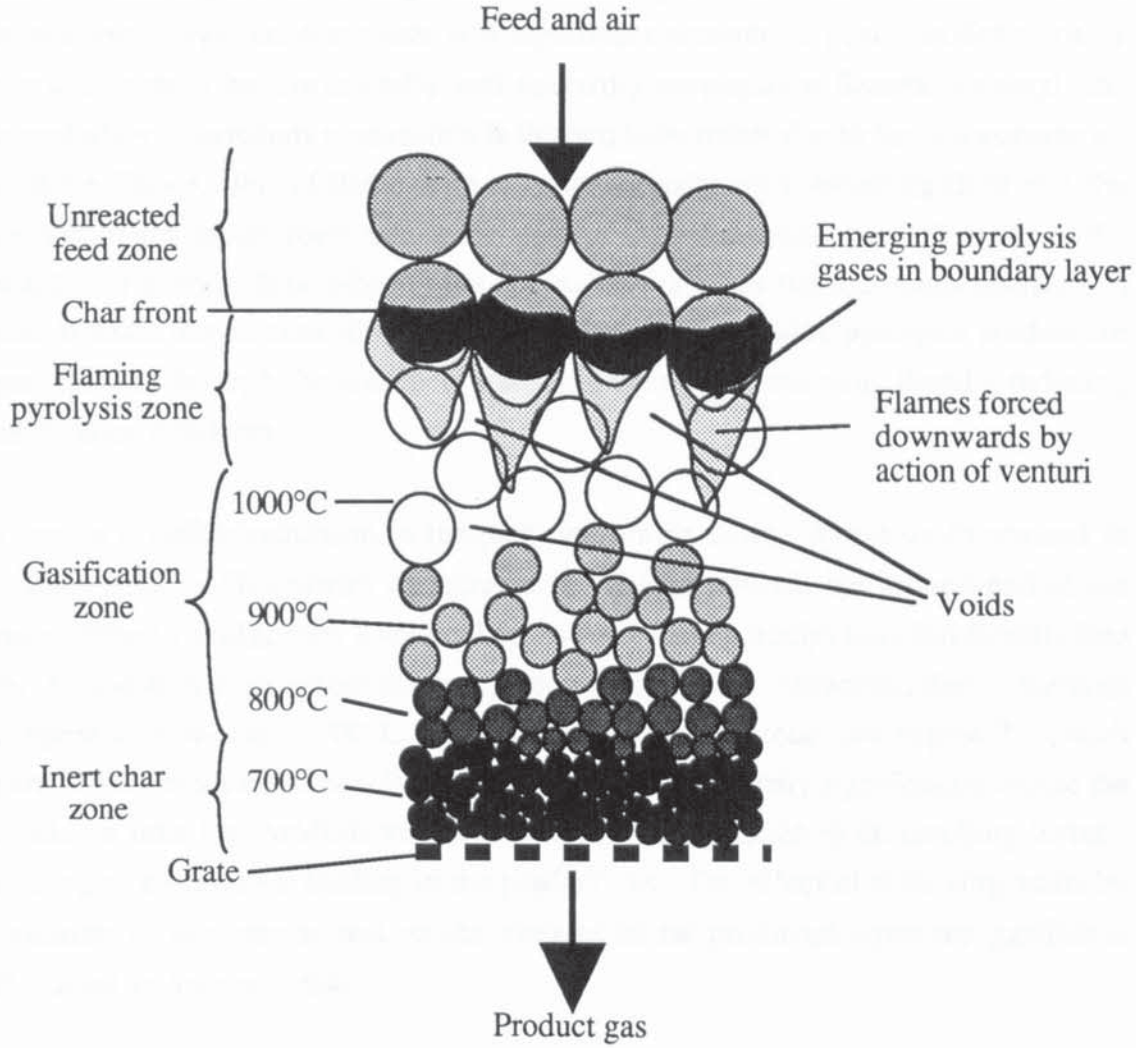

Figure 7.3 Open-Core Gasification Process

In general, Figure 7.3 agrees with the description of the gasification process discussed in Section 2.5. The feed descends the reactor as biomass is consumed in the reaction zones below. The rate of descent is approximately constant throughout the length of the unreacted feed bed, although bridges were observed to develop and collapse which caused sudden movements of the feed bed.

As a single particle reaches the top of the flaming pyrolysis zone the base of the particle begins to char. The particle is progressively charred in a wave-like manner. Directly after pyrolysis, flames can be seen evolving from the particle as the pyrolysis products are oxidized. The time delay between the beginning of charring and the start of flaming is approximately 1-2 seconds. The flames are pulled predominantly downwards, confirming the observations of Earp (1988) and Evans (1992). Occasionally, however, flickers of flame have been observed to travel both horizontally and vertically upwards which may be the result of high turbulence within the zone caused by the release of a large volume of gas from the particle. The flame is, however, prevented from contacting with the unreacted surface of the particle due to the evolution of gases from the particle, termed a "pyrolysis wind" by Reed (1988). It is possible, however, that there is a significant amount of heat transfer to other particles nearby by horizontally and upwardly propagating flames, although the contribution to pyrolysis propagation is thought to be minor due to the low occurrence of these flames. Jets of flame were also occasionally seen streaming deep into the gasification reaction zone, taking the path of least resistance through voids in the reactive char bed. This indicates the channelling of gases through voids resulting in poor oxidant distribution across the reaction zone and allowing pyrolysis products to pass directly through the zone below without completely reacting, thereby reducing gasification efficiency.

There is a visible reduction in the particle volume during pyrolysis (discussed in Section 7.3.2). This causes an increase in voidage towards the bottom end of the zone. When a bridge over a void collapses pyrolysing particles may fall directly into the gasification zone before the completion of pyrolysis. However, due to the high temperatures of about 1000°C found in the gasification zone (see Figure 7.3), such particles are expected to rapidly complete pyrolysis. This may significantly reduce the residence time for pyrolysis vapours resulting in a reduction in tar cracking thereby leading to a higher tar loading in the product gas. The effect of removing voids by agitation of the reactor bed on the amount of tar produced from the gasifier is discussed in Section 7.6.4.

It was noted that there were a number of cracks running through several particles after flaming pyrolysis, both during operation and for particles removed from the bottom of the flaming pyrolysis zone after operation. A crack may develop from a pre-existing weakness in the original wood particles, or as a result of the thermal process. It is possible that a number of particles have been divided up into smaller particles by the development of the cracks through the particle. This would result in a smaller average

particle size entering the gasification zone which may affect the rate of gasification (see Section 9.6). A particle size profile of the gasifier is discussed in Section 7.3.4.

Observations give the length of the flaming pyrolysis (FP) zone to be approximately 15 mm or 1.4 particle diameters in depth (for 6.35-12.7 mm feed), although individual flames can be longer than this. Measurements concerning the mass and volume reduction within the FP zone are discussed in Section 7.3.2. When the particle is completely charred and flaming ceases the particle exits the flaming pyrolysis zone and enters the gasification zone below.

The gasification zone appears as a bright orange zone (indicating temperatures of between 900 and 1100°C) of incandescent char, approximately 6 to 8 cm deep (or 5.8-7.7 particle diameters). Towards the end of the glowing orange zone, the colour of the char darkens through cherry red, dull red to black as the temperature decreases. A sharply defined end to the gasification zone is not distinguishable. Individual particles cannot be distinguished at the bottom of the reaction zone since gasification has either totally consumed or greatly reduced the size of the particle. The start-up char is still recognizable on removal of the reactor, indicating that gasification rates in the inert zone are negligible.

7.3.2 Flaming Pyrolysis Zone Measurements

A sample of 12 charred particles removed from the gasifier after test 13 (see Section 7.3.4) showed a decrease in average volume of 60.3% within the flaming pyrolysis (FP) zone. This compares to a volume reduction of 92.3% reported by Evans (1992) for a feed size of 4.75-6.35 mm. The difference in the reduction in volume measured in this research and that measured by Evans is appreciable, and is thought to arise due to different measurement techniques. Evans measured particle diameters from video recordings. In this research the depth, length and width of the particles extracted from the zone were measured to calculate the actual volume of the particles, although there may be errors involved in the method due to difficulties in shutting down the gasifier immediately and the selection of particles from the precise location at the end of the FP zone.

The average weight loss of the particles during flaming pyrolysis was measured to be 82.7% of the original mass of the feed. Evans (1992) calculated the reduction in mass to be 94.6% from the reduction in particle volume and an assumed char density of 0.36 gcm^{-3}. However, the assumed char density Evans used is much higher than the char densities measured in this research of between 0.09 and 0.16 gcm^{-3}, representing an error factor of over two in his calculation of mass loss during pyrolysis. Using a

char density of 0.12 gcm^{-3} gives a mass loss of 98.2% using the reduction in volume result obtained by Evans, which suggests that the char yield is much lower than the fixed carbon content of the biomass (see Section 4.3.2). The results obtained by Evans are, therefore, considered to be incorrect.

The average time for a particle to transverse the FP zone was measured to be 44.5 seconds by direct observation of individual particles during test 1.2, and 55.5 seconds for the base case tests by calculation using Equation 7.5 (assuming a length of 15 mm for the flaming pyrolysis zone, i.e. the approximate FP zone length observed; see Section 7.3.1).

$$\text{Time for FP} = \frac{\text{Length of FP Zone x Bulk density x 36}}{\text{Specific capacity}} \qquad (7.5)$$

The difference in the observed and the calculated FP times may be due to particles not being packed to the bulk density used in the calculation and errors in the measurement of the length of the zone. The time for flaming pyrolysis observed by Evans (1992) was 46.7 seconds, which is comparable to the times observed above.

7.3.3 Temperature Profile

A temperature profile of the open-core gasifier (Figure 7.4) was obtained during test 2.2 using a search thermocouple within a stainless steel sheath (see Section 3.7).

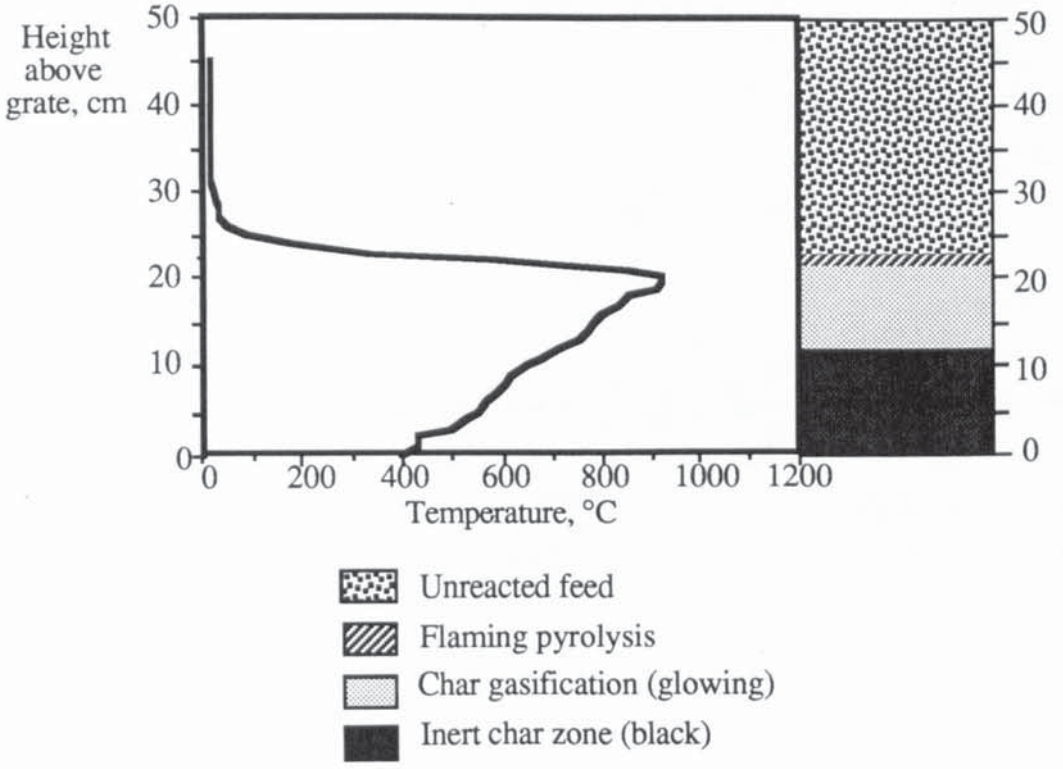

Figure 7.4 Temperature Profile of Steady State Uninsulated Open-Core Gasifier (Test 2.2)

The temperature profile shows the rapid increase in temperature that occurs at the beginning of the flaming pyrolysis zone and steady decline in temperature in the gasification zone confirming the findings of Evans (1992). The maximum temperature recorded in the gasifier was 1023°C measured just below the bottom of the flaming pyrolysis zone. The inert char zone starts when the temperature falls below about 700°C (by definition), at which the rate of gasification becomes negligible. The temperature decreases towards the grate within the inert char zone as a result of heat loss from the reactor.

7.3.4 Gasification Profiles

Particle size and the volatile matter, fixed carbon and ash composition profiles with depth were obtained from test 13 using the method described below. This information was required in order to help identify the end of the gasification zone. At this point the particle size should be at a minimum.

The gasifier was run in stable mode for over 1 hour before it was shut-down using CO_2 injection through the open top of the gasifier at 15 litres per minute. This allowed fast quenching of flaming pyrolysis by the exclusion of oxygen, thereby maintaining a snapshot of particle size distribution within the gasifier. However, due to the temperatures existing within the gasifier, feed continued to undergo pyrolysis resulting in the upward movement of charred material by about 2 cm. After the reactor had cooled it was removed from the collar with the grate in place thus retaining the char within the reactor. A piston was used to eject material out of the base of the reactor in steps of 1-3 cm. This method was preferred over using the piston from the base of the reactor or by the progressive digging out of material since it was easy to perform, involved less mixing between layers and would result in less particle break-up.

Fractions were taken in layers of 1 cm from the gasification zone rising to 3 cm from the unreacted feed zone where less variation of the material was expected. Layers were then weighed prior to sieving into 8 size fractions. The weight average size (the size at which 50% of the mass passes through a sieve) was then calculated using the data presented in Appendix H by plotting the percentage cumulative weight against size (given in Appendix H). The weight average particle size profile is presented in Figure 7.5.

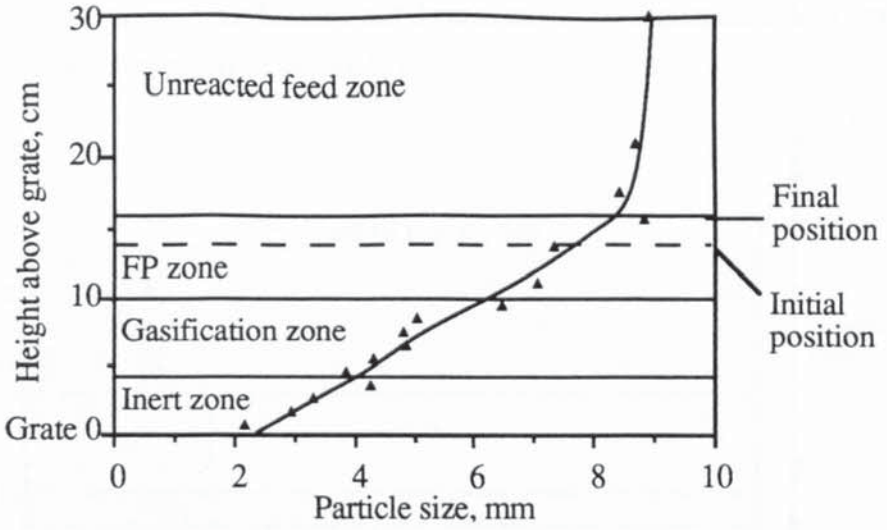

Figure 7.5 Weight Average Particle Size Profile (Test 13)

Figure 7.5 shows the boundaries of the reaction zones at the time of shut-down and the initial and final position of the pyrolysis front. The weight average particle size apparently decreases with depth at an approximate linear rate of 0.38 mm per cm. Among the factors contributing to the decrease in particle size are particle splitting (see Section 7.3.1), particle attrition, and char conversion (carbon burn-off). It was not possible to evaluate the relative contributions of these factors to the decrease in particle size using the data obtained, nor can an appropriate method be suggested, although char conversion by gasification is thought to be the dominant process. The particle size distribution affects the pressure drop across the gasifier, which may cause operational problems (see Section 7.6). The bulk density of the material (see Figure 7.6) decreases initially due to the loss of volatiles in the flaming pyrolysis zone, reaching a minimum of 0.05 gcm^{-3} prior to the inert char zone. In the inert char zone the higher density start-up char (rubberwood) has remained unconverted, resulting in an increase in bulk density towards the grate.

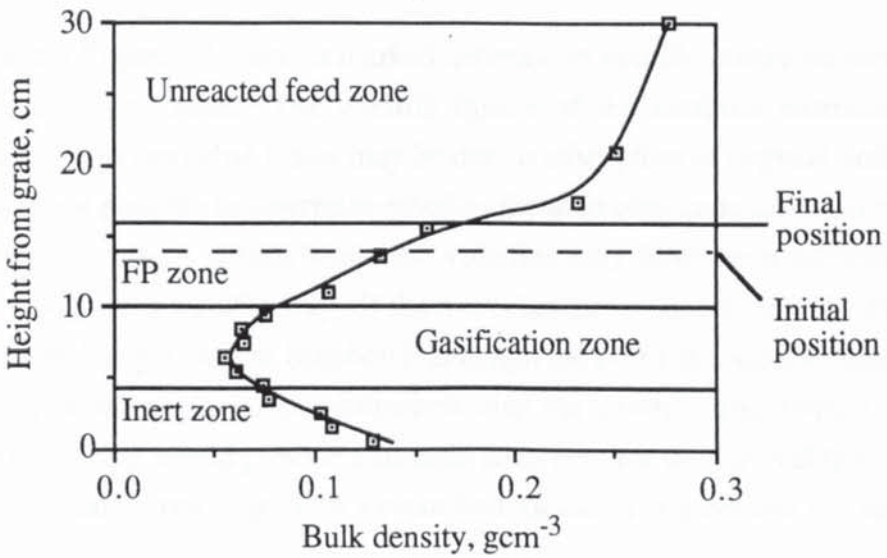

Figure 7.6 Bulk Density Profile in the Open-Core Gasifier

A proximate analysis (see Section 4.3.2) was carried out on a sample from each layer. The results are presented in Figure 7.7.

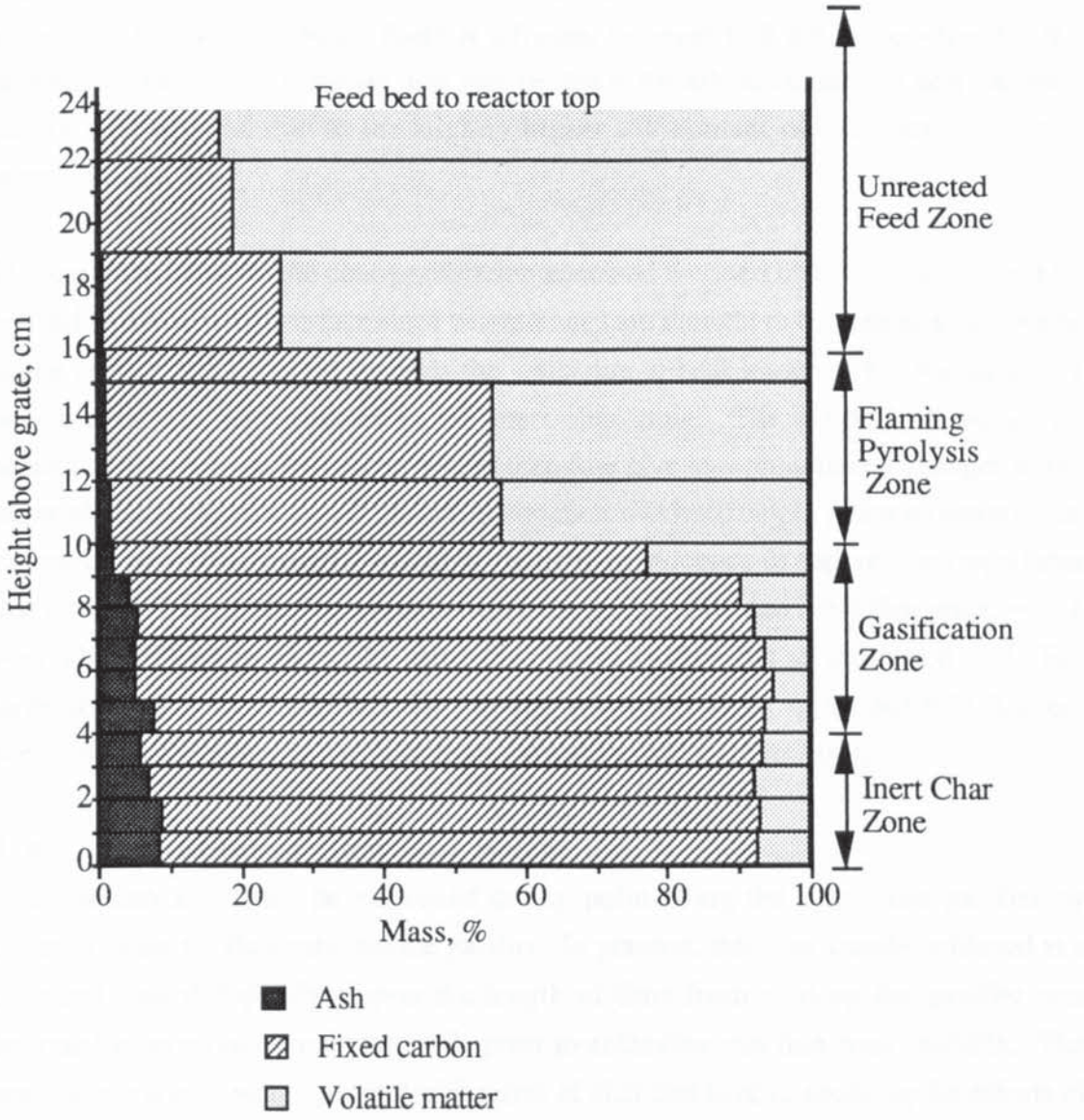

Figure 7.7 Proximate Analysis Profile in the Open-Core Gasifier

As expected Figure 7.7 shows a marked decrease in volatile matter content within the flaming pyrolysis zone. The volatile matter of the material extracted from the gasification and inert char zones may be due to adsorption of organic volatiles by the char. It is not possible to determine whether the inert char zone can adsorb tars during operation from these results since the volatiles may have been adsorbed after the gasifier had cooled significantly. If the inert char zone can actively adsorb tars then a high char bed height may be beneficial, although the char may become saturated during operation resulting in tar breakthrough into the product gas stream. However, devolatilized char would provide a suitable adsorbent for tar removal from the product gas in a secondary bed to provide a clean fuel for use in engines and gas turbines.

The ash content of the material is found to increase with depth to 8.0% within the 4-5 cm layer and this is thought to correspond to the end of the char gasification zone. This suggests that there is accumulation at the base of the gasification zone as postulated by Evans (1992). There is a further increase to 8.8% ash content for the material near the grate; however, this may be due to the ash accumulation near the grate during start-up, and due to the slightly higher ash content of the start-up char of between 1 and 8%.

The interface between the char gasification zone and the inert char zone should not be defined as a horizontal surface since temperatures are thought to be greater at the centre of the reactor and decrease towards the walls due to heat losses. This would give a concave surface with respect to the inert char zone. The method of extracting horizontal layers from the reactor would therefore give less pronounced changes in the material characteristics than if the actual zonation was horizontal. A three-dimensional survey of the reactor material would be required as evidence to support the hypothesis that a concave interface is present between the gasification and inert char zone, which would be difficult to undertake using the present reactor due to its limited size. For large scale open-core gasifiers the reaction zones would be approximately flat and horizontal as the effect of heat loss from the reactor walls are reduced.

7.4 The Effect of Char Bed Height

The reaction zone may be stabilized at any point along the open-core gasifier by controlling the air flow rate into the gasifier. In practice, this was usually achieved at a char bed height dependant upon the length of time from start-up the gasifier was operated in pyrolysis dominant mode prior to achieving reaction zone stability. The base case test runs were operated with range of char bed heights enabling the effects of char bed height to be analysed. The height of the char bed is important in the design of open-core gasifiers since a certain depth of 'inert' char may be required for optimum operation. The inert char provides a buffer zone which reduces the effects of fluctuations in the position of the reaction zone. In addition the inert char zone may condition the product gas by removing a limited amount of tar by adsorption as discussed in Section 7.3.4. A high inert char bed height would, however, cause problems related to a high pressure drop across the gasifier.

7.4.1 The Effect of Char Bed Height on Product Gas Quality

Earp (1988) and Evans (1992) found that increasing the height of the char bed had a minimal effect on gas quality, and only a slight improvement in gas heating value. However Earps' findings are taken from single runs in which the char bed was continually rising, i.e. in pyrolysis dominant operation (refer to Section 7.2.1 for effect on gasifier performance), whilst Evans' results were taken from runs using

different feed sizes (refer to Section 7.7 for effect on gasifier performance). In both cases the increasing energy content of the product gas with char bed height may be due to differences in the mode of operation and feed size and not upon the char bed height, casting doubt on the conclusions made by Earp and Evans. Figures 7.8 and 7.9 show the variation in the product gas composition for the base case feed size during stable operation obtained in this research, with char bed height as the only variable.

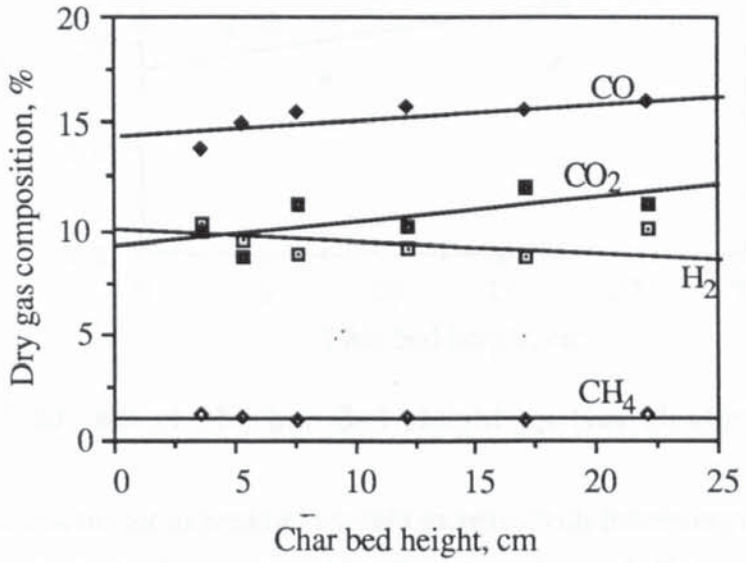

Figure 7.8 Gas Composition Variation with Char Bed Height

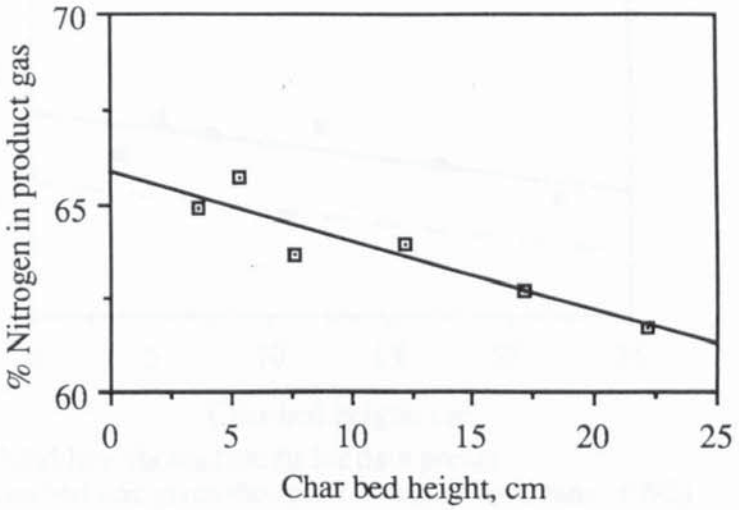

Figure 7.9 Nitrogen Content of Product Gas Against Char Bed Height

The percentage of CO and CO_2 in the product both increase with char bed height (see Figure 7.8) possibly as a result of higher char conversion, whilst the proportion of N_2 is significantly reduced at higher char bed heights (Figure 7.9) which is discussed later in this section. Figure 7.10 shows that there is a minor improvement in the product

gas heating value as the char bed height increases, which is due to the lower N_2 content of the product gas.

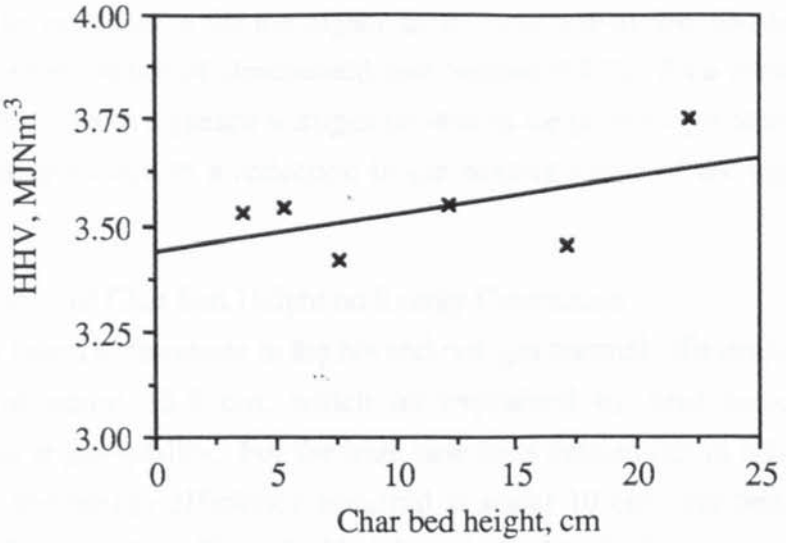

Figure 7.10 Effect of Char Bed Height on Gas Heating Value

It was expected that the air to feed ratio would increase with increasing char bed height as a result of an increasing proportion of energy being lost from the gasifier. However, this was found not to be the case as shown by Figure 7.11.

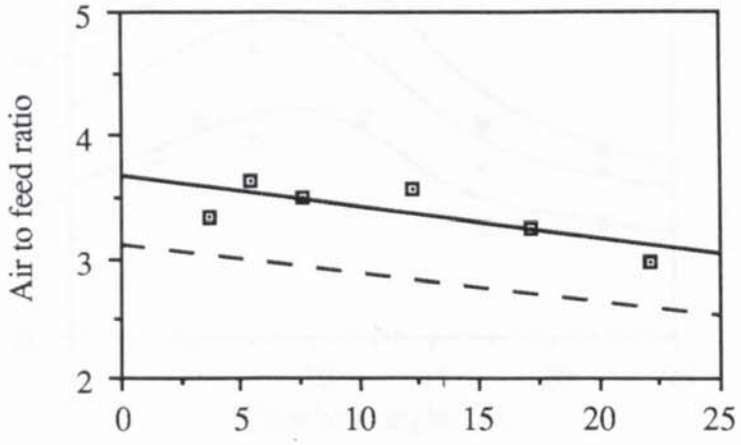

Solid line shows best fit for data points
Dashed line gives the result obtained by Evans (1992)

Figure 7.11 Air to Feed Ratio as a Function of Char Bed Height for the Open-Core Gasifier in Stable Operation

Evans (1992) also reports a reduced air requirement at increased char bed heights, shown as a dashed line in Figure 7.11, but he does not offer any explanation for this. Although not reported by Earp (1988) his data also indicates a similar result. One possibility is that for optimum operation (i.e. maximum energy conversion efficiency)

the gasification zone needs to be longer than previously thought. For stable operation at low bed heights a higher gasification rate may be required, which may be achieved by increasing the temperature within the gasifier as a result of a greater degree of oxidation. The explanation for the higher air to feed ratio at low bed heights agrees with the modeling studies of Groeneveld (see Section 9.6.7). As a result of a higher air to feed ratio, there is a greater nitrogen content in the product gas at lower char bed heights. This gives rise to a reduction in the heating value of the gas (see Figure 7.10).

7.4.2 Effect of Char Bed Height on Energy Conversion

Evans (1991) found a maximum in the hot and raw gas thermal efficiencies with a char bed height of about 13.5 cm, which he explained by heat losses offsetting improvements in gas quality. For the base case tests carried out in this research the maximum in the energy efficiency occurred at about 10 cm char bed as shown in Figure 7.12. Beyond about 20 cm bed height little further decline in energy efficiency is expected as additional heat losses are small. The maximum reflects the higher air to feed ratio at low bed heights where more energy is required to heat the additional nitrogen from the air, and the increasing heat loss for char bed heights over 10 cm.

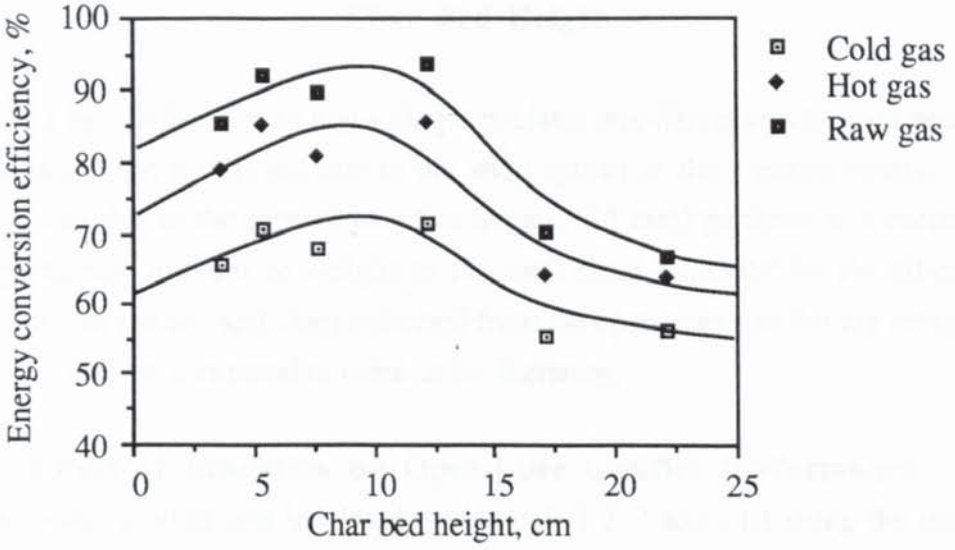

Figure 7.12 Energy Conversion Efficiencies Within the Open-Core Gasifier at Different Char Bed Heights

7.4.3 Effect of Char Bed Height on Tar and Particulate Production

The raw gas tar and particulate content were determined using the equipment and method described in Section 3.8. Figure 7.13 shows the measured tar and particulate content of the product gas at different char bed heights. A best fit line drawn through the tar data points shows that tar levels decrease with increasing char bed height, however the fit is poor with a correlation coefficient (R^2) of 0.10, and is not significant. Higher tar levels at low char bed heights may be due to the decreased bed

length available for tar cracking or for tar adsorption as postulated by Earp (1988). Greater tar cracking will lead to an increase in product gas heating value as the energy in the tars is released. However, since the difference in the quantity of tar is small, improved char conversion and reduced nitrogen content at higher bed heights is thought to be the most significant factor as previously discussed (Section 7.4.1).

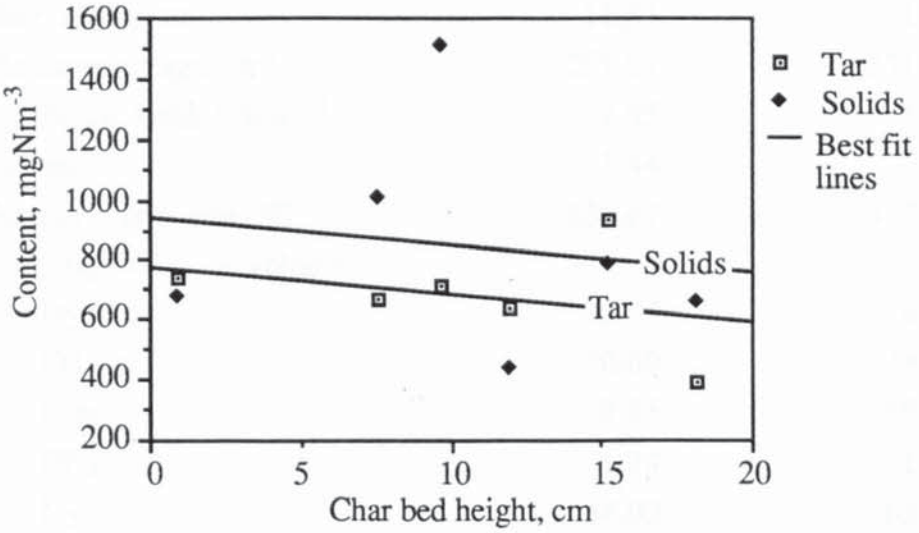

Figure 7.13 Tar and Solid Content of Product Gas as a Function of Char Bed Height

Although a best fit line shows that solid particulates also decrease with char bed height the results are not significant due to the wide spread of the measurements. This is thought to be due to the capture of a few large (>0.5 mm) particles that contribute a disproportionate amount of weight to the total mass captured by the filter. The composition of the tars and chars collected from the open-core gasifier are presented in Section 7.9 and are compared to those in the literature.

7.5 Effect of Insulation on Open-Core Gasifier Performance

The open-core gasifier was insulated in tests 1.1, 1.2, 7 and 13.1 using the insulation described in Section 3.3. In test 13.1 the vibro-mixer (Section 3.11) was also used and this result is, therefore, not included here, but is discussed in Section 7.6.5.

7.5.1 Experimental Results

The results from the insulated tests are presented in Table 7.7, along with the average base case data.

Table 7.7 Insulated Open-Core Average Gasifier Performance Data Comparison

	Insulation	Base case
Test numbers	1.1, 2.1, 7	(see Section 7.1)
Feed moisture, % wet basis	10.08	10.31
Char bed height, cm	11.85	11.36
Specific capacity, $kgm^{-2}h^{-1}$	297.07	271.38
Gas volumetric yield, Nm^3kg^{-1}	2.85	3.37
Air/feed ratio	2.44	3.38
Gasifier exit temperature, °C	633.67	417.25
Dry gas composition, % volume		
H_2	13.75	9.45
CO	20.60	15.20
CO_2	9.83	10.53
CH_4	1.74	1.04
N_2	54.09	63.78
Raw gas water content, % vol.	6.55	11.93
Gas HHV, $MJNm^{-3}$	5.04	3.54
Cold gas efficiency, %	69.72	64.47
Superficial gas velocity, Nms^{-1}	0.235	0.250

The results show a significant improvement in product gas heating value and in the cold gas conversion efficiency. The reduction in heat loss (see Table 7.9 later) increases the temperature of the gasification zone and thereby improves both the conversion to CO and H_2 and the kinetics (Section 2.4) of the char conversion reactions.

Specific capacities range from 241 to 365 $kgm^{-2}h^{-1}$ (with an average of 297 $kgm^{-2}h^{-1}$) for the insulated tests and from 242 to 315 $kgm^{-2}h^{-1}$ (average of 271 $kgm^{-2}h^{-1}$) for the uninsulated gasifier (Appendix G1). The similarity in the specific capacities suggest that there is little increase in the rates of pyrolysis and gasification as a result of higher temperatures within the gasifier (shown later), indicating that the temperature hypothesis for turndown given in Section 7.2.2 is invalid. The superficial product gas velocities within the insulated open-core gasifier are in the range of 0.189 to 0.308 Nms^{-1}, with an average of 0.235 Nms^{-1}. The velocity values are similar to those obtained using the uninsulated reactor (Table 7.5), and suggests that the superficial velocity required for a stable reaction zone is not greatly influenced by heat loss from the reactor. However, operation in the gasification and pyrolysis dominant modes using the insulated gasifier would be required in order evaluate the effect of heat loss

on reaction zone stability. This is recommended for further investigation in Section 11.3.1.

Table 7.8 presents observed and calculated (using Equation 7.5) average flaming pyrolysis times which show that the time required is reduced by about 2 seconds when insulation is applied. The results obtained by Evans are included for comparison, and show a larger difference between the insulated and uninsulated pyrolysis times. The calculated pyrolysis time should be more accurate as it is obtained from the specific capacity and therefore is an average of all particles passing through the FP zone.

Table 7.8 Average Flaming Pyrolysis Times of 6.35-12.7 mm Particles in Insulated and Uninsulated Gasifiers

Time in seconds for complete pyrolysis

	Observed	Calculated	Observed (Evans, 1992)
Insulated	42.6	52.0	37.2
Uninsulated	44.5	55.5	46.7

The turndown ratio (the ratio of the maximum and minimum gas production rates) obtained using the insulated open-core gasifier is 1.32:1, which is almost identical to the turndown ratio of 1.31:1 obtained with the uninsulated open-core gasifier (see Table 7.6). However, since only three insulated tests were conducted the turndown ratio achieved is of low statitistical significance, and the actual maximum turndown ratio may be greater than 1.32:1. Further investigations are required in order to confirm this finding.

7.5.2 Heat Loss Calculation Methods and Results

Evans (1992) calculated heat loss from the core temperature measured using a thermocouple which could be moved up and down in a close fitting stainless steel sheath. Temperatures were measured at 1 cm intervals near the central axis of the gasifier. This method was used for tests 1.1, 1.2 and 2.2 of this research. The temperature measurements using this method were expected to be higher than those actually occurring at the surface of the reactor since a constant radial temperature distribution was thought to be unlikely. Evans found that this method over-estimated the heat lost by up to 40% of the feed energy input from an uninsulated reactor in 80 % of his experiments when compared to heat losses calculated by difference in the energy balance.

For most of this research a contact thermocouple was used (Section 3.7) which gave a direct measurement of the external surface temperature of the gasifier and thus a

potentially more accurate measure of heat loss. The gasifier was divided along its length into sections and the average of three temperature measurements using the contact thermocouple used in the calculation of heat losses by convection and radiation from each section of the gasifier as described in Appendix F. The temperatures for insulated runs were measured by Evans using thermocouples embedded within the insulation, with the whole reactor assumed to be insulated. In this research heat losses were calculated for both the insulated reactor area and for the un-insulated observation strip area at the measured temperatures.

Figure 7.14 shows how heat loss calculated from core and external temperature measurements compare to heat loss calculated by closing the energy balance for this research.

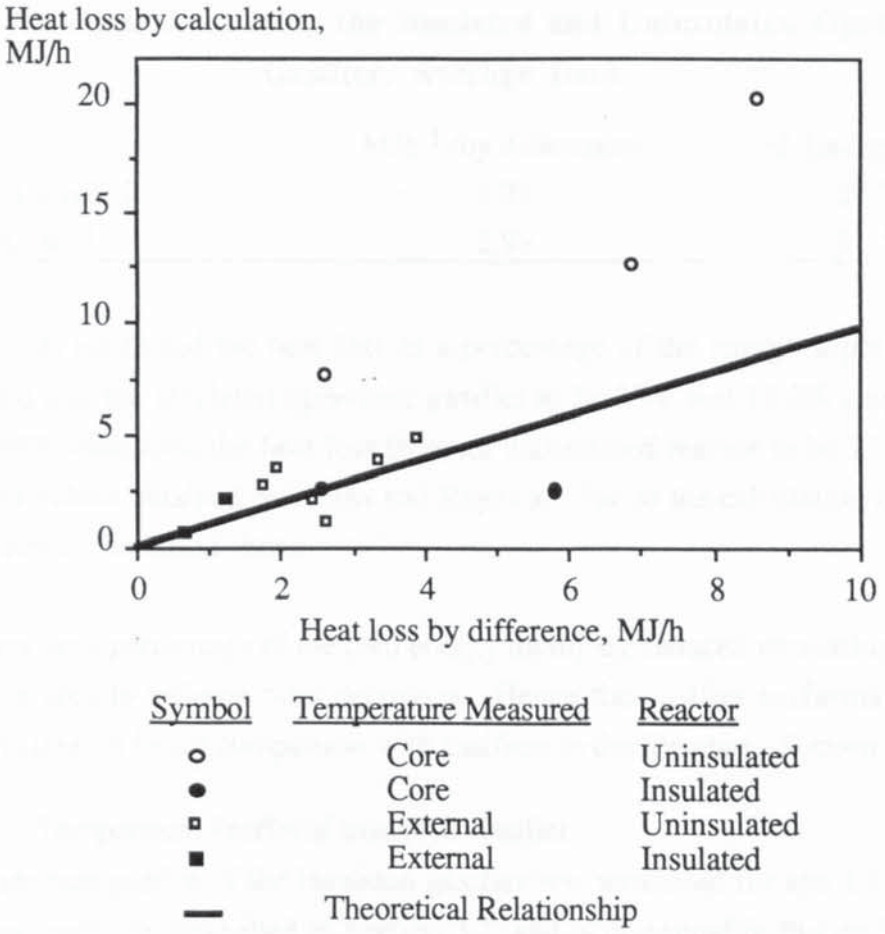

Figure 7.14 Comparison of Heat Loss Calculated from Measured Reactor Temperatures with the Heat Loss by Difference in Energy Balance (Includes Data from Open-Core and Hybrid-Throated Tests)

It can be seen that using core temperatures over-estimates the heat loss from the uninsulated gasifier by an average of 130%. This confirms the findings of Evans (1992). He also under-estimated the heat loss from an insulated gasifier by an average of 43% which can be attributed to his treatment of the gasifier as being totally insulated and neglect of the observation strip. About 10% of the external surface of the gasifier is uninsulated in order to allow observation of the reaction zone, which has been considered in the heat loss calculation in this research (see Appendix F). The two results presented in Figure 7.14 for insulated gasifier heat loss calculated from core temperatures are not significantly different to heat loss calculated by difference. The heat loss using external temperatures show a much closer agreement with the theoretical heat loss calculated by difference. Table 7.9 shows that insulation reduces the amount of heat loss by about 59% on average.

Table 7.9 Heat Loss from the Insulated and Uninsulated Open-Core Gasifier, Average Data

	MJh^{-1} (by difference)	% Energy loss
Uninsulated	7.21	27.97
Insulated	2.98	11.56

Evans (1992) estimated the heat loss as a percentage of the energy input from the uninsulated and the insulated open-core gasifier to be 39% and 16.6% respectively. Reyes (1988) estimated the heat loss from an uninsulated reactor to be 23.8-38.1%. The higher values obtained by Evans and Reyes are due to the calculation using core temperatures as discussed above.

Heat losses (as a percentage of the feed energy input) are reduced on scaling-up since the surface area to volume ratio decreases. Hence the gasifier performance using insulation allows a better comparison with gasifiers in the literature (Section 7.5.5).

7.5.3 Temperature Profile of Insulated Gasifier

The temperature profile of the insulated gasifier was measured for test 1.1 using the search thermocouple described in Section 3.7, and is presented in Figure 7.15. The reduction of heat loss when using insulation results in higher temperatures throughout the reactor bed (Figure 7.15) compared to the uninsulated gasifier (Figure 7.4). The high temperatures measured in the unreacted feed bed for the insulated gasifier are believed to be errors since pyrolysis, which begins at 250-350°C, was not observed. Conductance of heat from the lower reaction zones along the thermocouple sheath are believed to give rise to the erroneously high temperatures measured in the feed bed.

The maximum temperature measured using the search thermocouple was 1128°C compared to 1023°C recorded for the uninsulated gasifier. The temperature within the gasifier decreases towards the grate after the start of the gasification zone as a result of heat loss and the endothermic char gasification reactions (see Table 2.1). The temperature decrease is most pronounced within the first half of the gasification zone, which may be explained by a higher rate of char conversion. The temperature also decreases quickly close to the grate due to heat losses through the base of the reactor.

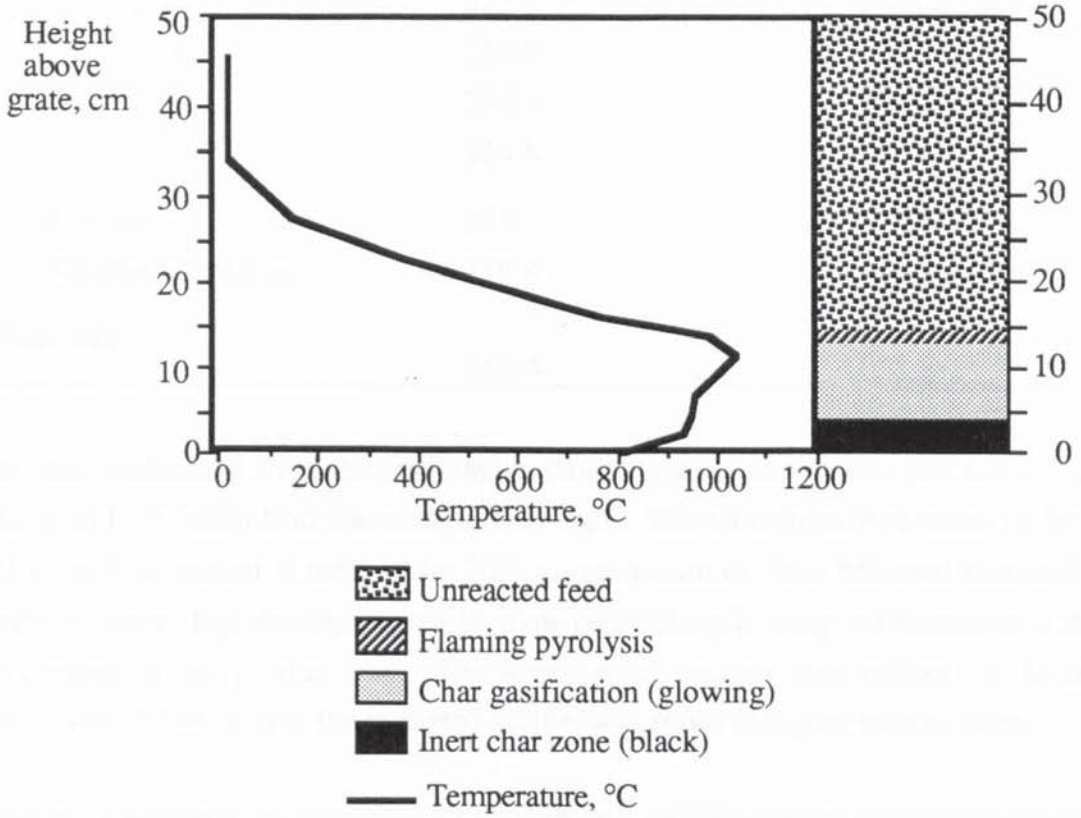

Figure 7.15 Temperature Profile from Insulated Open-Core Gasifier Test 1.1

As heat losses increase, the amount of oxidation required to maintain a stable reaction zone also increases. This results in a higher air to feed ratio ratio for the uninsulated gasifier compared to the insulated reactor (see Table 7.7). At higher air to feed ratios the product gas contains a higher fraction of nitrogen and consequently has a lower heating value.

7.5.4 Effect of Insulation on Tar and Particulate Content of the Product Gas

In Section 2.6.1 it was stated that the tar content of the product gas is reduced by thermal cracking in the gasifier. At lower temperatures there is poorer cracking of pyrolytic tars. Increasing the temperature within the gasifier is achieved by reducing the heat loss using insulation. The tar level of the product gas from the insulated gasifier is therefore expected to be lower than that from the uninsulated gasifier.

The tar and solids loading of the product gas from the insulated gasifier were measured in test 2.1 and test 7 (three samples obtained), and are presented in Table 7.10.

Table 7.10 Tar and Particulate Content of the Product Gas from Insulated and Uninsulated Gasifiers

Test (sample)	Tar $mgNm^{-3}$	Solids $mgNm^{-3}$
Insulated		
2.1	522.8	245.0
7 (1)	210.0	420.1
7 (2)	270.1	282.2
7 (3)	339.8	258.5
Average	335.7	301.4
Standard deviation	117.4	69.8
Uninsulated		
3	665.4	1001.6

The results obtained from the insulated gasifier are consistent with each other, and significantly different from the uninsulated results. The tar content is reduced by 50% and the solids content is reduced by 70% using insulation. It is believed that in the insulated reactor higher temperatures promote tar cracking leading to a reduction in the tar content of the product gas. The lower solids output may reflect the better conversion of fines within the insulated gasifier as a result of higher temperatures.

For test 7 the average tar content is 273.3 $mgNm^{-3}$, and the average particulate content of 320.3 $mgNm^{-3}$. The repeatability of the sampling measurement is within 19.4% of the average for tar and within 22.3% for particulates.

7.5.5 Comparison with Open-Core Gasifiers in the Literature

The results presented in Tables 7.8 and 7.10 are compared to the selected gasifiers presented in Table 2.4. The results obtained with the Aston gasifier are similar to the previous work (Evans, 1992), which was operated at a similar air to feed ratio of 2.48 compared to 2.44 in this research. The product gas energy content is slightly higher at 5.04 $MJNm^{-3}$ compared to 4.49 $MJNm^{-3}$ reported by Evans. The difference is attributed to the higher CO/CO_2 ratio of 2.1 obtained in this research compared to a ratio of 1.5 obtained by Evans since the higher temperatures obtained during this research (maximum of 1128°C) improved the conversion to CO, compared to the lower temperatures (maximum of 1040°C) measured by Evans. Evans also operated the insulated gasifier with a char bed height of 19 cm, higher than the average char bed height of 12 cm for this research; thus heat losses from Evans' reactor may have been

higher. The energy conversion efficiency obtained with the insulated gasifier is consequently higher by 6% for this research compared to that obtained by Evans.

Comparison with the other gasifiers listed in Table 2.4 is more difficult due to the variation in feeds used, air to feed ratios and gasifier dimensions as discussed in Sections 2.5.9 and 2.6.5. The gas heating value obtained is within the range of values given in Table 2.4, although it is lower than that produced by the KSU, SERI and SynGas gasifiers. The lower gas heating value can be attributed to the higher nitrogen content in the product gas from the Aston gasifier. The product gas from the Aston gasifier is also lower in CO_2 in comparison with the other gasifiers, which may be due to higher char conversion due to higher reactor temperatures as discussed above. Temperatures are only reported for the KSU gasifier, in which the maximum temperature was 899°C (Walawender, 1987), much lower than the maximum temperature measured within the Aston gasifier (see Section 7.5.3). The water content of the raw product gas from the Aston insulated gasifier was measured to be 6.6% by volume, however only one measurement was achieved. The measured water content is less than that reported for the SynGas and UCD gasifier (see Table 2.4) which both give a water content of over 11%; hence the water content obtained in this research may be unreliable. The raw gas water content measured for the uninsulated gasifier was 11.9% (see Table 7.1), which is similar to that measured for the SynGas gasifier (with a water content of 11.4% by volume).

The tar content of the product gas from the insulated Aston gasifier (see Table 7.10) is lower than that reported by Reed (1988) for the SERI gasifier, and is the same as that reported for the KSU gasifier (see Table 2.4). Tar cracking within the Aston gasifier will be improved by the higher reactor temperature. In the KSU gasifier the injection of secondary air and the use of a stirrer may aid tar cracking to achieve a similar tar level. However, differences in the method of tar content measurement makes direct comparisons difficult as mentioned in Section 2.5.5.

In summary, the results obtained with the insulated open-core gasifier are generally similar to that reported for various gasifiers in the literature, with differences due to variations in the feeds used, reactor temperatures and air to feed ratios.

7.6 Investigation of the Effects of Agitating the Reactor Bed

The reactor bed was agitated using the vibro-mixer described in Section 3.11. The objectives of agitating the bed were to:

- reduce the reactor bed pressure drop by the removal of fines
- improve the flow of the feed material to the reaction zone
- reduce the occurrence of voids within the reaction zone. This may effect the tar production from the gasifier since the residence time in the tar cracking zone is reduced for material falling into the void space.

The vibro-mixer was used in four tests (Table 7.11) and in test 13.1 using insulation (see Section 7.6.5). In test 9 the agitator was initially operated for a period of about 3-4 minutes when the pressure drop across the reactor increased beyond an arbitrary value of 2 kPa. In later tests (11, 12 and 13.2) the vibro-mixer was used for 10-30 seconds at intervals of 2-5 minutes.

7.6.1 Qualitative Observations

The vibro-mixer was observed to cause a rapid settling of the material within the gasifier as soon as it was switched on. Operation of the vibro-mixer for three seconds (after a period of 1-2 minutes in which the vibro-mixer was not operating) caused unreacted feed particles within the reactor to drop by 3-5 cm from 30 cm above the grate. The top of the flaming pyrolysis zone was also observed to fall by up to 1.5 cm. The height of the inert char zone was less affected and changes were not beyond the usual fluctuations observed during normal operation. The operation of the vibro-mixer was effective at improving feed flow and reducing the occurrence of large voids both in the feed zone and within the reaction zones. Experimental tests were conducted to evaluate the effect of using the agitator on gasifier performance and product gas quality (see Section 7.6.2 below).

7.6.2 Comparison with Base Case Performance

The performance of the gasifier using agitation is presented in Table 7.11.

Table 7.11 Open-Core Gasifier with Bed Agitation Performance Data Comparison (Average Values)

	Agitated	Base Case
Test numbers	9, 11, 12, 13.2	(see Section 7.1)
Feed moisture, % wet basis	10.28	10.31
Char bed height, cm	6.05	11.36
Specific capacity, $kgm^{-2}h^{-1}$	297.65	271.38
Gas volumetric yield, Nm^3kg^{-1}	3.18	3.37
Air/feed ratio	3.11	3.38
Gasifier exit temperature, °C	495.75	417.25
Dry gas composition, % volume		
H_2	9.80	9.45
CO	13.63	15.20
CO_2	12.02	10.53
CH_4	1.59	1.04
N_2	61.97	63.78
Gas HHV, $MJNm^{-3}$	3.73	3.54
Cold gas efficiency, %	66.88	64.47
Superficial gas velocity, Nms^{-1}	0.260	0.250

Table 7.11 shows that there is a lower CO and N_2 content and a higher H_2, CO_2 and CH_4 content in the product gas from the agitated gasifier. The product gas heating value and the cold gas energy conversion efficiency are both improved significantly. A 10% increase in specific capacity is observed with the use of agitation, which is possibly due to the reduction of reaction zone voids. A large void, whether it is in the flaming pyrolysis zone or in the gasification zone, would reduce the effective reactor volume for reaction. Agitation reduces the size of voids by improving the flow of solids into spaces to increase the packing. The reduction in voidage may improve the conversion efficiency since more particles occupy the hottest part of the gasifier. The distribution of oxidant may also be improved since the air to feed ratio is reduced with the use of agitation. In the gasifier without agitation the bridges and voids in the unreacted feed and flaming pyrolysis zones could cause channelling of the gases resulting in an increase in the air to feed ratio required in order to maintain a stable reaction zone. Agitation did not significantly affect the superficial gas velocity in the gasifier.

The product gas composition for test 13.2 was also determined by gas chromatography (GC) and the results are presented in Table 7.12 along with the on-line analysis.

Table 7.12 Gas Composition of Test 13.2

	On-Line Analysers	Gas Sample (GC)
H_2	11.36	9.73
CO	15.19	14.96
CO_2	12.72	12.12
CH_4	1.50	1.26
N_2	59.23 (balance)	59.29
O_2		2.99*
C_2-C_4 gases		0.95
Total	100.00	101.29

* indicates a possible air leak into the sampling system

The composition of the gas sample as measured by GC is close to the composition measured by the on-line analysers (see Table 7.12). The lower amount of H_2 in the gas sample is probably due to leakage of the gas from the sample cylinder between sampling and analysis. An oxygen content of 2.99% in the sample was indicated by the analysis. This is within the range of 1.1-3.5% previously obtained by Reyes (1989) from the Aston gasifier using the same method which was attributed to an air leak into the system. Oxygen is rapidly consumed in the flaming pyrolysis zone and is therefore unlikely to be present in the product gas.

7.6.3 Gasifier Pressure Drop

Figure 7.16 shows the wet feed rate and dry gas production rate for test 9, and Figure 7.17 shows the pressure drop across the gasifier during the same test. The variation in gas flow rate reflects the adjustments made in order to maintain a stable reaction zone at between 5 and 10 cm from the grate (see Figure 7.17).

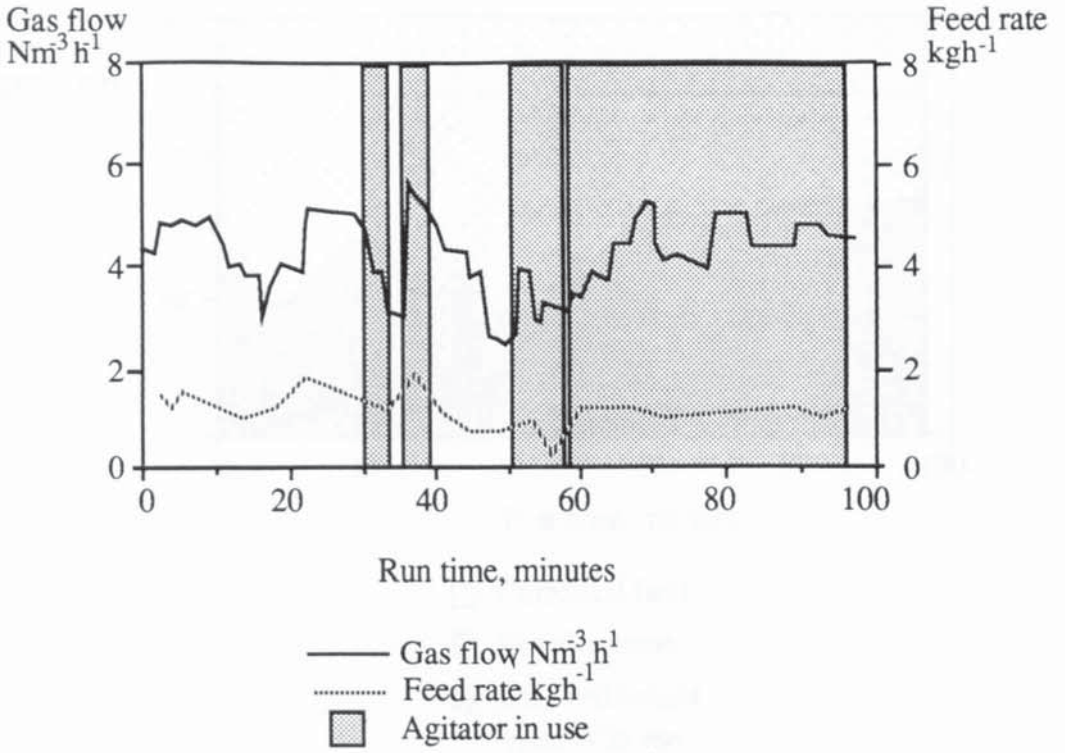

Figure 7.16 Dry Gas Flow and Wet Feed Rate During Test 9

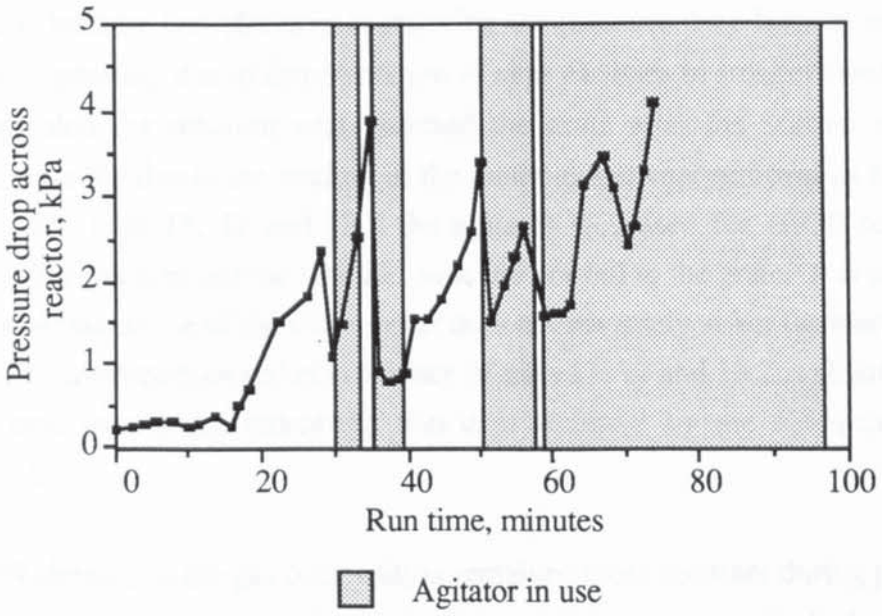

Figure 7.17 Pressure Drop Across Gasifier During Test 9

After the first period of agitator operation the pressure drop across the gasifier was reduced by about 1 kPa, and after the second period of operation the pressure drop was reduced by nearly 3 kPa to 0.85 kPa. Figure 7.18 shows that after the second period of operation the char bed height had fallen to the grate. This suggests that the rate of char consumption by gasification was increased relative to the rate of char production by pyrolysis; however, this may be due to fragmentation of the char by the action of the vibro-mixer followed by entrainment into the product gas stream.

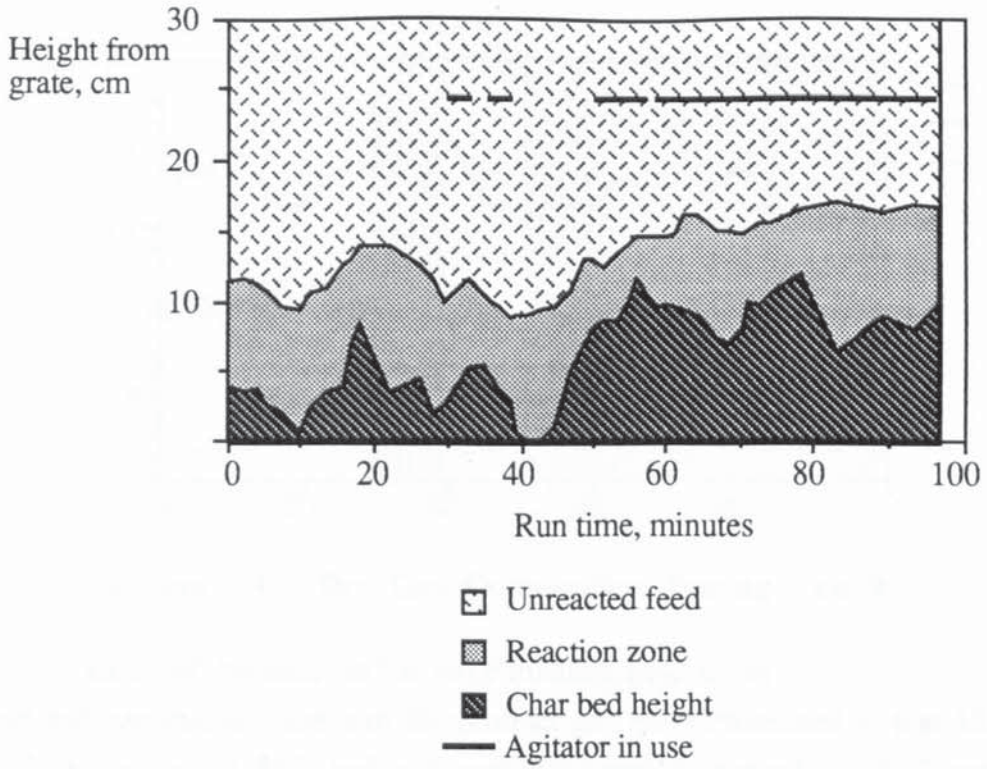

Figure 7.18 Zonation Within the Gasifier During Test 9

The agitator became less effective at reducing the pressure drop later in test 9 (see Figure 7.17), possibly due to fragmentation of char particles to smaller sizes. Figure 7.18 shows that the reaction zone reached the grate after the second period of operation, possibly due to the settling of the material and char removal as a result of agitation. For tests 11, 12 and 13.2 the agitator was used for 10-30 seconds at intervals of 2-5 minutes and the reaction zone did not fall to the grate. It is concluded that semi-continuous use of the vibro-mixer does not adversely affect the reaction zone position. The average conversion efficiency of tests 11, 12 and 13.2 is slightly higher than the base case tests, indicating that char removal by the vibro-mixer was insignificant.

Figure 7.19 shows that the gas composition remained more constant during periods of agitation, compared to the period prior to the use of the agitator which shows larger fluctuations. The fluctuations in the composition are believed to be due to changes in the char bed height (see Figure 7.18). In the period prior to the use of the agitator, the position of the reaction zone is affected by the formation and collapse of large voids within the zone. It is believed that the removal of these voids by agitation of the reactor bed reduces fluctuations in the position of the reaction zone and hence the gas composition.

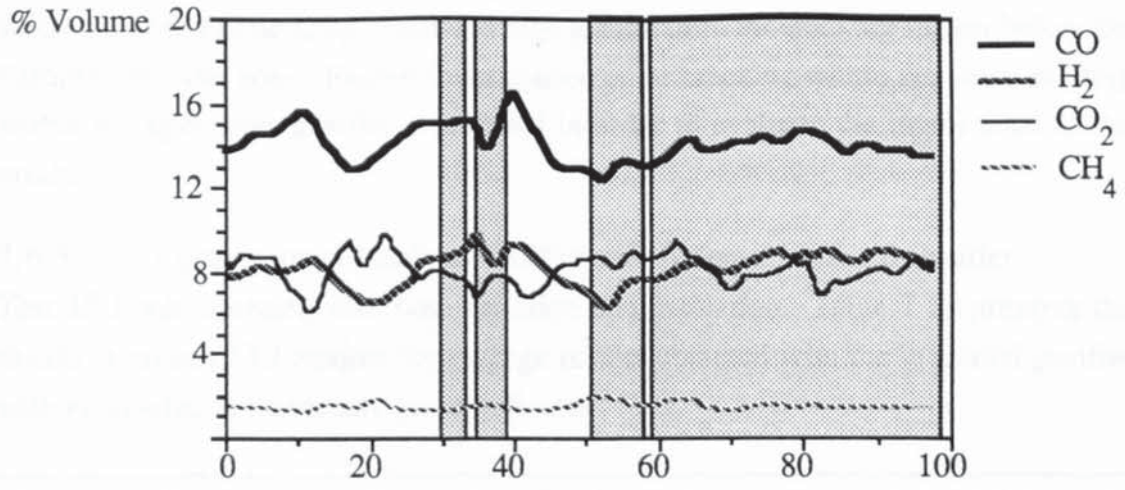

Figure 7.19 Dry Gas Composition During Test 9

7.6.4 Effect of Agitation on Tar and Particulate Production

The tar and particulate content of the product gas was determined in test 13.2. A particulate content of 843 $mgNm^{-3}$ was measured compared to 1002 $mgNm^{-3}$ measured for test 3 without agitation. A higher solids output for the base case test was not expected since the agitator was predicted to increase the rate of char removal by entrainment in the product gas from the gasifier, although the result is not significant since only one sample was obtained. The amount of char collected by the catchpot could not be used as a comparison since this depends upon the length of operation, the amount of fines in the start-up material, the amount of operation time spent at the grate during start-up, and char bed height.

The tar content of the product gas from the agitated gasifier was determined to be 823 $mgNm^{-3}$, higher than the 665 $mgNm^{-3}$ measured for test 3 without agitation, although again the result is not significant since only one sample was obtained during the test. The higher tar content was unexpected since it was thought that the removal of voids from the reaction zone would result in a more even temperature distribution with less cold spots where the tars could pass through uncracked. A higher tar loading was similarly observed for the insulated reactor (see Section 7.6.5). A possible explanation is that the voids are 'hot spots' within the reactor. The larger voids may be at higher temperatures than their surrounding volume since endothermic char gasification reactions locally reduces the temperature. The product gas carrying tar vapours may, therefore, channel through the higher temperature voids resulting in a greater degree of tar cracking. Agitation of the bed would remove the hotter voids, which may then result in an increase in tar passing through the reaction zone uncracked. The position of the voids is also significant, since they are usually found immediately below the flaming pyrolysis zone in the hottest part of the bed where most

thermal cracking of the tars is likely to occur. It is concluded that the presence of the voids may be beneficial by creating a high temperature tar cracking region below the flaming pyrolysis zone. Further investigation of tar cracking within the voids existing within the open-core gasifier is required in order to evaluate the importance of the voids.

7.6.5 Comparison of Insulated Gasifier with Agitated Insulated Gasifier

Test 13.1 was operated with both agitation and insulation. Table 7.13 presents the results from test 13.1 against the average results obtained with the insulated gasifier without insulation previously given in Section 7.5.1.

Table 7.13 Insulated Open-Core Gasifier Performance Data With and Without Agitation

	Agitated	**Not Agitated**
Test numbers	13.1	(see Section 7.5.1)
Feed moisture, % wet basis	10.20	10.08
Char bed height, cm	4.28	11.85
Specific capacity, $kgm^{-2}h^{-1}$	344.15	297.07
Gas volumetric yield, Nm^3kg^{-1}	2.93	2.85
Air/feed ratio	2.42	2.44
Gasifier exit temperature, °C	689	634
Dry gas composition, % volume		
H_2	15.65	13.75
CO	18.13	20.60
CO_2	12.25	9.83
CH_4	1.86	1.74
N_2	52.11	54.09
Gas HHV, $MJNm^{-3}$	5.03	5.04
Cold gas efficiency, %	73.85	69.72
Tar content, $mgNm^{-3}$	629.1	335.7
Particulate content, $mgNm^{-3}$	691.3	301.4

As with the uninsulated gasifier, agitation increases the H_2, CO_2 and CH_4 content of the product gas. The specific capacity is increased and there is an improvement in the conversion efficiency when agitation is used, as was found with the uninsulated gasifier. The explanation for the differences in these results is the same as for the uninsulated reactor, discussed previously in Section 7.6.2. The tar and particulate content of the product gas was found to be higher with agitation than without. It was expected that the solid particulate content would increase as the agitator would cause

char break-up, and this is indicated by the results in Table 7.13. An explanation for the increase in tar levels has already been given in Section 7.6.4.

7.7 Feed Size

Previous investigations on the effect of feed size on the performance of the open-core gasifier were discussed in Section 2.5.8. In this section the effects of using a smaller feed size (4.75-6.35 mm) compared to the base case feed (6.35-12.7 mm) are reported and discussed. Only one test using the smaller feed size was conducted due to the limited quantities of the feed available in this size range. The duration of the test was 92 minutes and no operational problems occurred. The results are presented in Table 7.14, and compared to a base case test with a similar char bed height.

Table 7.14 Gasifier Performance Data for Different Feed Sizes

Feed size range, mm	**4.75-6.35**	**6.35-12.7**
Test number	8	6
Feed moisture, % wet basis	10.79	11.16
Char bed height, cm	5.77	5.39
Specific capacity, $kgm^{-2}h^{-1}$	312.39	245.14
Gas volumetric yield, Nm^3kg^{-1}	3.17	3.53
Air/feed ratio	3.03	3.65
Maximum bed temperature, °C	1009	1134
Dry gas composition, % volume		
H_2	9.84	9.59
CO	17.89	14.93
CO_2	10.01	8.71
CH_4	1.40	1.09
N_2	60.86	65.68
Gas HHV, $MJNm^{-3}$	4.07	3.54
Cold gas efficiency, %	72.48	70.77
Superficial gas velocity, Nms^{-1}	0.273	0.239
Tar content, $mgNm^{-3}$	455.22	665.36*
Particulate content, $mgNm^{-3}$	486.89	1001.62*

Note: * Test 3 measurement (no samples taken for test 6).

The higher specific capacity of the smaller feed size is due to the shorter time required for devolatilization within the flaming pyrolysis zone (Groeneveld, 1980; see also Section 9.4) and for complete gasification in the zone below, allowing a greater throughput of particles. The total depth of the reaction zone for the 4.75-6.35 mm particles was 5.5 cm compared to 7.5-9.5 cm for the base case feed (Section 7.3). In

terms of characteristic particle diameters (dp; Section 4.3.7) the reaction zone is 8.7 dp for the 4.75-6.35 mm feed which is within the range of between 7.2 to 9.1 dp for the base case feed.

The results in Table 7.14 show that the heating value of the product gas using the smaller feed size is higher than that obtained using the base case feed. The base case feed size required a higher air to fuel ratio which led to a higher nitrogen content in the product gas thereby explaining the difference in heating value. The higher air to feed ratio for the base case feed may be required in order to raise the temperatures within the gasifier, as shown in Table 7.14, to increase the rate of gasification to maintain a stable reaction zone. Table 7.14 shows that there is a higher superficial gas velocity within the gasifier using the 4.75-6.35 mm feedstock compared to test 6; however, it is still within the range of 0.208-0.291 Nms^{-1} obtained for the 6.35-12.7 mm feed. Further test data, including tests under pyrolysis and gasification dominant conditions, are required to assess the operating range of the gasifier for different feed sizes.

7.8 Feed Type

The gasification of sewage sludge granules and rubberwood charcoal was attempted as discussed below.

7.8.1 Operation of Open-Core Gasifier on Sewage Sludge Granules

An investigation was conducted to see if the sewage sludge could be gasified in the gasifier. Test 10 used the open-core reactor with the extended grate designed by Evans (1992) in order that the reactions could be viewed through a clean section of the reactor. The vibro-mixer was also used. The gasifier was lit in the normal way using charcoal and paper. Wood was used to raise the reactor to normal operating temperatures and a stable zone was obtained with a char bed depth of about 2 cm. A 170 g batch of sewage sludge was then added to the gasifier, followed by 100 g of wood (6.35-12.7 mm feed size). A further 150 g of sewage sludge was added before the run was terminated for reasons discussed below.

On entering the reaction zone there was little change in the visible appearance of the sewage sludge, a slight darkening in colour only. No flaming of the evolving vapours occurred, although later in the run white smoke was seen to evolve from the particles in top stabilized mode. No distinct flaming pyrolysis zone could be observed. In the gasification zone a slight decrease in size was observed, but no measurements were made as the test was carried out for initial qualitative assessment. Approximately 2-3 cm below the reaction front incandescent material was observed in what was believed to be the gasification zone. During the gasification of the second batch of sewage sludge, the glow intensified and it was noticed that the particles had fused together. A

sludge, the glow intensified and it was noticed that the particles had fused together. A large void formed below the glowing fused material. The void would not collapse, and was resistant to forceful poking. The reactor was operated in top-stabilized mode (see Section 7.2.1) for 5.9 minutes before shut-down. After operation a large clinker was removed from the gasifier (see Figure 7.20).

Figure 7.20 Clinker of Sewage Sludge Removed from Reactor After Test 10

The high ash content of the sewage sludge used (45.7% by weight) resulted in fusion of the material to form a large clinker which prevented the flow of further material to the reaction zone. The clinker contained some material that had not fully reacted (see Figure 7.20), thus clinker formation reduces conversion. Sewage sludge cannot, therefore, be successfully used within the Aston open-core gasifier.

Evans (1992) also used dried sewage sludge in the open-core gasifier and, although the duration of the run was 40 minutes, the feedstock was said to be unsuitable for gasification in the Aston gasifier. An energy conversion efficiency of 43% to cold gas is reported with a product gas heating value of 1.58 $MJNm^{-3}$. The ash content of the dried sewage sludge used by Evans was 31.8% by weight. The ash was reported to accumulate in the gasifier increasing the pressure drop across the gasifier. Evans attempted to overcome the rising bed and increasing pressure drop by progressively

Evans (1992) suggests the possibility of using sewage sludge mixed with wood to make it more acceptable to the system. However, due to the differences in the physical characteristics of the feeds (see Table 4.5) separation is likely to occur within the reactor which may lead to blockages as the sewage sludge ash fuses together. It is concluded that sewage sludge used in this research is unsuitable for gasification within moving bed downdraft systems; however, gasification using a fluidized bed may be possible.

7.8.2 Operation of Open-Core Gasifier on Rubberwood Charcoal

The use of rubberwood charcoal within the open-core reactor was investigated in test 15.2. A stable reaction zone was obtained using the base case wood feed with a product gas similar to that obtained with the base case tests (see Section 7.1). Rubberwood charcoal was then added to the gasifier. A glowing front was observed to progress through a charcoal particle in a wave-like manner. Violet flames were observed extending 4-6 cm downwards into the reaction zone. The reaction zone (the region of glowing char) was about twice the depth of that observed using wood, at about 15 cm deep. Particles exiting the zone could be observed. Very little change in the particle size could be distinguished; however, a light grey ash could be seen on the surface of particles.

The reaction zone steadily moved upwards towards the top of the gasifier. Attempts to control the height of the reaction zone above the grate by increasing the air flow rate failed. The test was terminated when the reaction zone reached the top of the reactor. The char has a low volatile matter content and a high fixed carbon content compared to the wood feed used (see Table 4.3). Therefore, less volatiles are given off during pyrolysis whilst there is a correspondingly large amount of char entering the gasification zone. The oxidation of the pyrolysis vapours is believed to be insufficient to achieve the high temperatures needed to increase the rate of char consumption by gasification to match the mass flow of char into the gasification zone. Thus, the reaction zone rises to the top of reactor, and a stable reaction zone (with an unreacted feed zone above it) cannot be achieved. The gasification of the char within the open-core gasifier may, however, be successfully operated in a top stabilized mode, although this has not been attempted in this research (see Section 7.2.1).

7.9 Tar and Char Product Analysis

Tar and char collected from the Aston gasification system was analysed by Medac in order to obtain the elemental compositions required for the mass balance (Chapter 6). The analyses are compared with those given in the literature. Any differences in the compositions may be due to differences in the operation of the gasifier systems and of differences in the tar and char collection and analysis methods.

7.9.1 Tar Analysis

The tars were collected from the gasification system by dissolving the tars in acetone and filtering through a 2 μm filter paper to remove solid particulates. The acetone was then allowed to evaporate to leave the tar product. Three samples from the open-core gasifier were analysed (Table 7.15). Sample 1 is the tar collected from the raw gas sampling system after run 13, sample 2 contained tars from the whole system (raw gas sampling system, hot product gas piping and disentrainment tank) after runs 1-6, and sample 3 was from the disentrainment tank alone after run 13. The tar collected from the raw gas sampling system after tests T6.1, T6.2 and T6.4 using the hybrid-throated gasifier is included in Table 7.15 for comparison.

Table 7.15 Tar Compositions from Biomass Gasification Systems

	Ultimate Analysis, % dry ash free				Ash, % dry
This Research	C	H	O	N	
Aston OC, sample 1	81.4	7.3	11.2*	0.2	nd
Aston OC, sample 2	77.1	6.8	15.7*	0.4	nd
Aston OC, sample 3	87.9	6.0	6.1*	0.1	nd
Aston, hybrid-throated	80.2	7.1	12.5*	0.2	nd
Other Downdraft					
Aston OC (Reyes, 1988)	72.2	9.6	17.5	nd	nd
T (Brown, 1987)	68.6	5.9	25.5	nd	2.0
T (Hoi, 1992)	74.8	8.6	16.6	nd	nd
T (Esplin, 1986)	66.5	10.3	23.2	-	0.5
Other Comparative Analyses					
FB, 480°C (Brown, 1987)	53.0	6.2	40.7	nd	0.6
FB, 880°C (Brown, 1987)	85.4	5.8	8.8	nd	1.6
1°oil (avg.) (Reed, 1988)	56.1	5.8	38.1	nd	nd
2°tar (avg.) (Reed, 1988)	82.3	5.5	12.2	nd	nd

Notation: OC = Open-core; T = throated; FB = fluidized bed; nd = not determined; *by difference.

The analyses show that the composition of the tar from the open-core gasifier is higher in carbon and lower in oxygen than for tars previously obtained from the Aston gasifier by Reyes (1988), and others in the literature. The tar from the hybrid-throated gasifier is very similar to that from the open-core gasifier collected from the same place (sample 1, from the raw gas sampling system).

The tar composition, as well as the amount produced, depend upon the operating conditions of the gasifier and principally on the thermal history within the gasifier (Brown, 1986). Higher temperatures and longer residence time increase the proportions of aromatic deoxygenated tar (Brown, 1986). This is seen for the tars produced from a fluidized bed gasifier where the carbon content increases and the oxygen content decreases at higher temperatures (see Table 7.15). The composition for primary pyrolysis oil and tar produced by secondary reactions are also shown in Table 7.15. The tar produced by secondary reactions has a higher carbon content and a lower oxygen content than the primary pyrolysis oil. As the tars from the Aston gasification system during this research were found to have a high carbon content and low oxygen content this may, therefore, suggest a higher operating temperature than the other gasifiers listed in Table 7.15. However, the difference in the analyses may also be due to the different methods of collection.

Detailed analysis of the compounds in gasification tars are beyond the scope of this thesis, but listings of compounds found in the tar product are given by Pakdel (1991) and Knoef (1987).

7.9.2 Char Analysis

The char samples analysed from the open-core gasifier were collected from the catchpot below the gasifier, from the bottom (0-5 cm from the grate) and from the top of the gasifier (5-10 cm) after open-core run 8. Char samples were dried at 105°C to constant weight to remove moisture prior to analysis. The ultimate analysis are presented in Table 7.15.

Table 7.16 Analysis of Chars from Downdraft Biomass Gasifiers

Test 8

Reactor	Position	Ultimate Analysis, % dry ash free				Ash, % dry
		C	H	O*	N	
Open-core	Catchpot	95.4	1.5	2.7	0.4	48.6
Open-core	0-5 cm	94.0	0.8	5.0	0.1	7.4
Open-core	5-10 cm	91.7	0.8	7.0	0.5	2.0

Chars from Downdraft Gasifiers in the Literature

Reactor	Reference	Ultimate Analysis, % dry ash free				Ash, % dry
		C	H	O	N	
Throated	Esplin (1986)	95.1	0.3	4.4	0.2	5.0
Throated	Hoi (1992)	96.3	1.2	2.5	0.1	7.4
Open-core	Chee (1988)	92.4	0.8	6.2	0.6	20.2

* calculated by difference

The char compositions in the literature are similar to those obtained from the open-core gasifier. As mentioned in Section 2.2.2, the yield of char from the pyrolysis reaction is strongly affected by the final temperature at which it is formed. In addition, the composition of the char alters as the temperature increases as shown in Table 7.17.

Table 7.17 Compositions of Char Formed by Pyrolysis at Different Temperatures (Buekens, 1985)

The trend of increasing carbon content and decreasing oxygen content with increasing temperature is comparable to the chars collected from the open-core gasifier. The char collected from 5-10 cm bed height includes char that has just been formed by pyrolysis and has not passed through the hottest region of the gasifier, whilst those from 0-5 cm have passed through this region and has a composition that is between those formed at 500°C and 1000°C given in Table 7.17. This suggests that remaining the oxygen and hydrogen in the char can react to form gaseous products at the temperatures within the gasification zone. The ash content also increases towards the grate (see Section 7.3.4). The average ash content of the solids collected in the catchpot was 51.8% for runs 1, 2, 3, 7 and 8, and was 39.4% after run 9 in which the agitator was in use.

The results suggest that there is lower char conversion when using the agitator, which might be due to increased char removal from the reactor (see Section 7.6.4).

7.9.3 Start-Up Tar and Particulate Content

The tar and particulate content of the out flow gas during the start-up period of a run was measured in order to evaluate the amount of tar produced during this period. The start-up period typically lasts about 20 minutes (the time taken for the gasifier exit temperature and gas compositions to stabilize). Initial start-up tar production from a gasifier is expected to be high since the temperatures during this period are not sufficiently high enough for tar cracking (see Section 2.5.5). In addition, a suitable char bed height will have to be produced by operating the gasifier in pyrolysis dominant mode (Section 7.2.1) which may result in higher tar levels as there is less oxidation of pyrolysis vapours. Tars produced during the start-up period will condense in downstream gas lines and equipment which may then become blocked and require cleaning.

Start-up tar and particulate levels were measured for run 4 using the open-core gasifier and for run T6 using the hybrid-throated gasifier, which is included here since the effect of the throat is not thought to be significant during the start-up period as the char bed lies below the throat on start-up (see Section 8.1.2). Both samples involved uninsulated reactors and the base case feed size (6.35-12.7 mm wood). Sampling began directly after the gasifier was lit. The measurements are presented in Table 7.18.

Table 7.18 Start-Up Tar and Particulate Levels

Run Number	Sample Time, mins.	Tar, $mgNm^{-3}$	Particulates, $mgNm^{-3}$
4 (open-core)	10	1850	1948
T6 (hybrid-throated)	8	1594	921
Average	9	1722	1435

The average tar content of the gas during the start-up period is about 160% greater than that measured for the open-core gasifier during stable operation (Section 7.1) and about 400% greater than the average tar content of the product gas from the hybrid-throated gasifier (Section 8.4). The values presented in Table 7.18 are, in addition, likely to be less than the actual tar contents of the gas due to condensation of the tars on to cold gas pipes. The particulate content of the gas during the start-up period is also higher than during stable operation by up to about 40% for the open-core gasifier and 110% for the hybrid-throated gasifier. The higher particulate out flow may be due to the entrainment of dust particles from the start-up char.

Because of the higher tar and particulate output during the start-up period of the gasifier it may be necessary to use a by-pass system or filter to prevent fouling of downstream equipment until the gasifier has reached normal operating temperature.

7.10 Scrubbing Efficiency of the Venturi Ejector

The gas processing system consists of the water ejector venturi, disentrainment tank and demister. The venturi ejector was installed as a gas mover, and not specifically as a gas scrubber (see Section 3.4.1); however, it was expected to remove a significant amount of particulate material from the product gas. The tar and solid particulate content of the product gas was measured after the demister during tests 11 and 12 using the same equipment as for the raw gas sampling (see Section 3.8.3), except with a static sampling point instead of an iso-kinetic sample probe. Static sampling was used since it was expected that few particles would exceed 10 μm size which require iso-kinetic sampling (Reed, 1988a). Since these tests both used the agitator, they are compared to the tar and particulate sample obtained during test 13.2. The results are presented in Table 7.19.

Table 7.19 Product Gas Tar and Particulate Content After the Demister

Test	Tar $mgNm^{-3}$			Solids $mgNm^{-3}$		
11 (3 samples)	68.3	139.7	82.6	45.5	163.1	31.1
12 (3 samples)	63.7	67.8	43.9	84.6	104.6	90.5
Average		77.7			86.5	
Raw gas tar and particulate content						
13.2		823.1			843.6	

The removal efficiency of the venturi ejector to demister assembly is 90.6% for tars and 89.7% for solid particulates. Liquid ejectors are not often used for particulate collection, but efficient removal of 1-2 μm mist particles can be achieved (Perry, 1985). The removal efficiency is dependant upon the liquid to gas volumetric flow ratio and the liquid pressure at the ejector (Harris, 1966). Using the graphs provided by Harris (1966) the removal efficiency of 1 μm particles by the Aston gasifier venturi ejector is estimated to be 50-80% under normal operating conditions. Vapours are simultaneously removed from the gas stream (Harris, 1966). Venturi injector scrubbers can remove 95% of particles over 1 μm (Brown, 1986). The efficiency of tar removal was found to vary from 51 to 98.5% for a venturi injector scrubber by Chowdhury (1992), with the efficiency dependant upon the dimensionless Weber number and the ratio of gas volumetric flow to liquid volumetric flow.

Although the particulate content of the product gas is reduced by 90%, there is still too much for use in an internal combustion engine which requires less than 10-50 mgm^{-3} in order to prevent excessive engine wear (Brown, 1986). Further gas cleaning (e.g. by filtration) would be required in order to provide a gas of sufficient quality for engine use. Liinanki (1985) suggests that the maximum tar level acceptable for use within in a internal combustion engine is about 1000 mgm^{-3}; thus the product gas from the Aston gasifier may be used directly on the basis of its tar content.

7.11 Summary

The open-core gasifier has been used to investigate the gasification process under various operational parameters The operation of the gasifier was investigated under stable, pyrolysis and gasification dominant modes. It was concluded that the mode of operation depends upon the relative rates of pyrolysis and gasification, with the rate of of pyrolysis controlled by radiative heat transfer. The superficial gas velocity was found to be a significant factor affecting the mode of operation. The average superficial gas velocity for stable operation was 0.25 Nms^{-1}, with pyrolysis dominant operation occurring below about 0.20 Nms^{-1}, and gasification dominant operation above about 0.30 Nms^{-1}.

Two hypothesis are put forward to account for a turndown ratio of 1.3:1 found for the open-core gasifier; variation in temperature at the interface between the flaming pyrolysis zone and the unreacted feed; and variation in the surface area of the interface. Neither hypothesis was satisfactorily supported by the experimental test data obtained and further work in this area is recommended.

Particle size profiles, material proximate analysis profiles and temperature profiles of the reactor were obtained and related to the observations made. Increasing the height of the char bed was found to give a minor improvement in the product gas heating value due to a decreasing air/feed ratio with char bed height. A higher air/feed ratio is believed to be required in order to maintain a stable reaction zone when operating with lower char bed heights. A maximum in the energy conversion efficiency was found at a char bed height of about 10 cm as the increasing heat loss from the reactor offset the improvement in the product gas heating value.

Insulating the gasifier reduces the heat loss and increases the temperatures within the reactor leading to a higher energy conversion efficiency and a higher tar cracking efficiency. The performance of the insulated gasifier has been compared to open-core gasifiers reported in the literature.

The use of agitation has been found to improve feed flow, reduce voids within both the unreacted feed bed and reaction zones, reduces the pressure drop across the reactor, and reduces the fluctuations in the product gas composition. The improvement in performance is, however, minimal, with the conversion efficiency increased by 2.4% and there is no significant effect on tar output.

The gasification of 4.75-6.35 mm feed size has been found to have a higher energy conversion efficiency and product gas heating value than the base case feed due to a reduction in the air to feed ratio required. A higher specific capacity was obtained, as less time was required for pyrolysis and gasification of the smaller particles. Dried sewage sludge granules were found to be unsuitable for gasification due to the fusion of ash to form a large clinker within the reactor, preventing material flow. A stable reaction zone was not obtained with the rubberwood char, although gasification in a top stabilized mode may be possible.

Tar and char analysis have been carried out. The amount of tar produced during start-up was found to be up to four times greater than that produced during stable operation. The tar and particulate scrubbing efficiency of the venturi ejector has been determined to be about 90%.

8. HYBRID-THROATED GASIFIER RESULTS AND DISCUSSION

8.1 Introduction

In this chapter the observations and results from the hybrid-throated gasifier are presented. Early commissioning tests ended in failure to maintain a reaction zone are described along with the precautions taken to prevent failure. A qualitative description of the gasification process is given and the effects of insulation, feed size and type, and turndown are discussed. A mechanism for turndown is proposed.

8.1.1 Commissioning Tests

Test T1 was carried out without a grate since it was not known wether the bed would be supported by the throat, however, it was expected that a grate would be required to prevent small char particles from falling directly into the hot gas piping system. This was found to be the case as particles of wood, partially pyrolysed wood and char were carried into the product gas piping.

A grate was installed for test T2. However, the test was again aborted due to the failure to maintain the reaction zone at the throat. After ignition of the start-up material, there was a bed of flaming material at the throat with an active bed on the grate separated by a gap of 2 cm between the top of the bed to the throat. On further addition of feedstock, the ignited material at the throat fell through the constriction on to the reactive char bed supported by the grate. The unreacted wood blocks formed a bridge over the throat preventing additional material falling through to the reaction zone. The distance between the reacting bed and the un-ignited material at the throat increased as the bed was consumed by char gasification and/or char combustion. Attempts to dislodged the bridge at the throat failed and the feed on the grate was totally consumed. It was concluded from the test that in order to avoid similar occurrences a char bed height of at least 6 cm is required during start-up in order that material at the throat can begin to pyrolyse. Also, the addition of feed to the reactor needs to be controlled during start-up in order to limit the amount of material above the throat. This allows poker access if necessary to destroy un-ignited bridges at the throat until it is clear that the reaction zone is stabilized at the throat. The start-up procedure is discussed in the next section.

8.1.2 Start-Up of Hybrid-Throated Gasifier

In order to obtain a stable reaction zone at the throat the start-up conditions and procedure given here are followed. Char from a previous run sized between 3.35 and 12.7 mm is used to fill the reactor to within 1 cm of the throat followed by small pieces of paper and finally 1-2 g of small wood chips. This was lit using a match on a low air flow setting. As the char ignited, feed was added in small batches of about 50 g to

the reactor and the air flow rate adjusted to maintain a fire zone at the throat. Once the gasifier becomes stabilized, i.e. there is no movement of the reaction zone within the gasifier and the exit temperature and product gas composition show little variation, the reactor was filled with the feed and the test begins.

8.2 Description of Gasification Process in Hybrid-Throated Gasifier

In the hybrid-throated gasifier the gasification process on individual particles proceeds in much the same way as for a particle within the open-core system (Section 7.3.1). Figure 8.1 shows the hybrid-throated gasifier in operation. The flaming pyrolysis zone lies above the throat, with particles bridging across the constriction (see Figure 8.2). A void can be seen at the throat (see Figure 8.2), although this was not apparent when looking directly at the throat due to the presence of material on the ledge of the throat obscuring the view. The interface between the flaming pyrolysis zone and the unreacted feed material appeared to be dome-shaped, although there was difficulty in observing the precise shape of the pyrolysis front due to material obscuring the view. The domed shaped pyrolysis zone in the hybrid gasifier differs from the zonation observed within the open-core system in which the zones are relatively flat and horizontal (see Figure 7.3).

Below the throat there was usually a gap or void before the top of the char gasification zone (see Figures 8.1 and 8.2), which may suggest that a similar void exists within conventional throated gasifiers, although a void is not usually depicted (see Figure 2.9). The throat physically separates the flaming pyrolysis zone from the char gasification zone, this differs from the open-core system in which the zones are directly consecutive, although voids are present within the open-core gasifier (see Section 7.3; Figure 7.3). Within the gap flames from the flaming pyrolysis zone were observed to stream through the throat and fan out across the char bed, with turbulence forming swirls of flames below the edges of the throat indicating good mixing of the gases. Figure 8.2 shows the gas flow patterns below the throat. Within this region the average temperature was measured to be 1063°C with a maximum of 1213°C recorded (test T5.1).

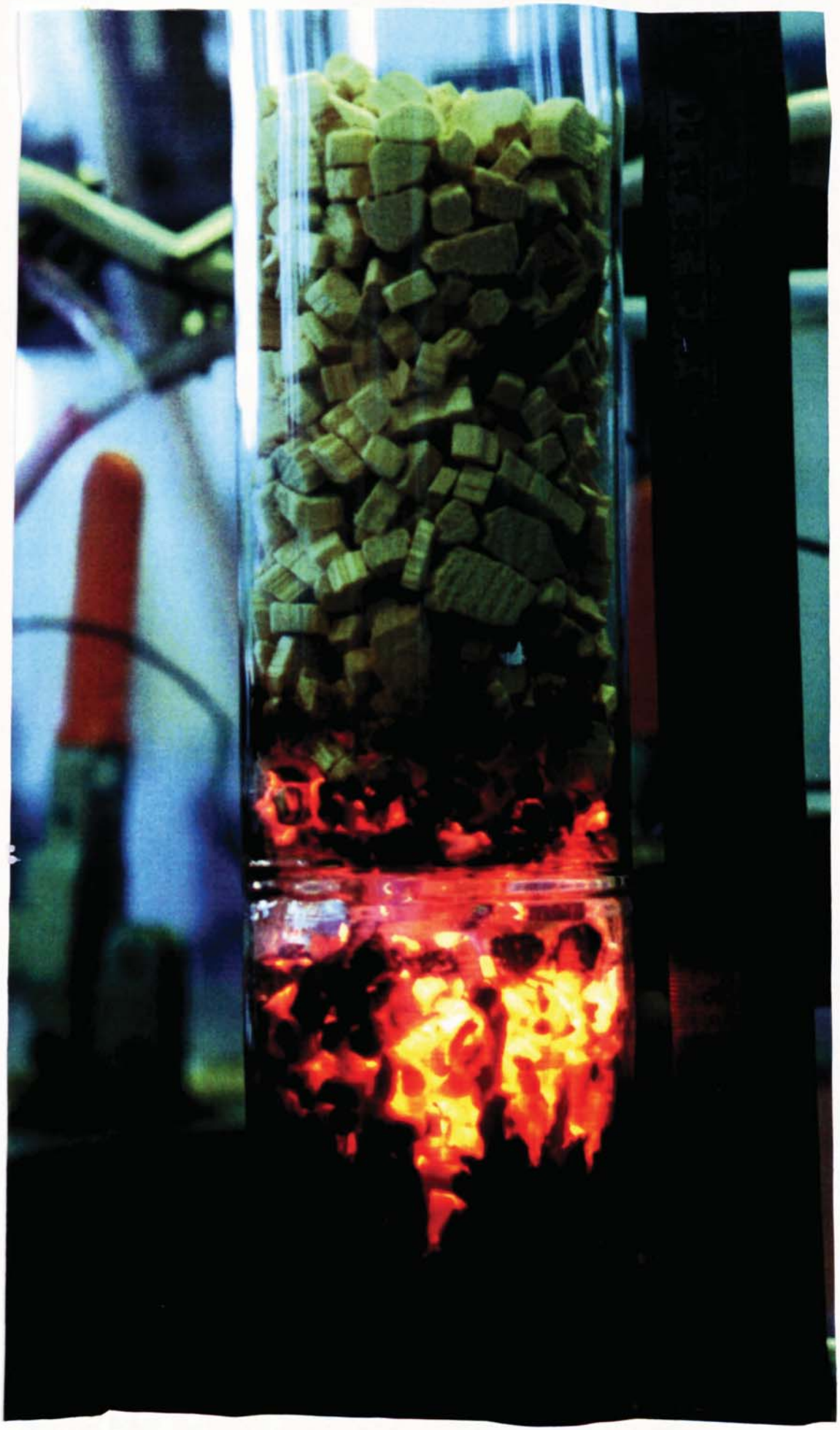

Figure 8.1 Hybrid-Throated Gasifier in Operation

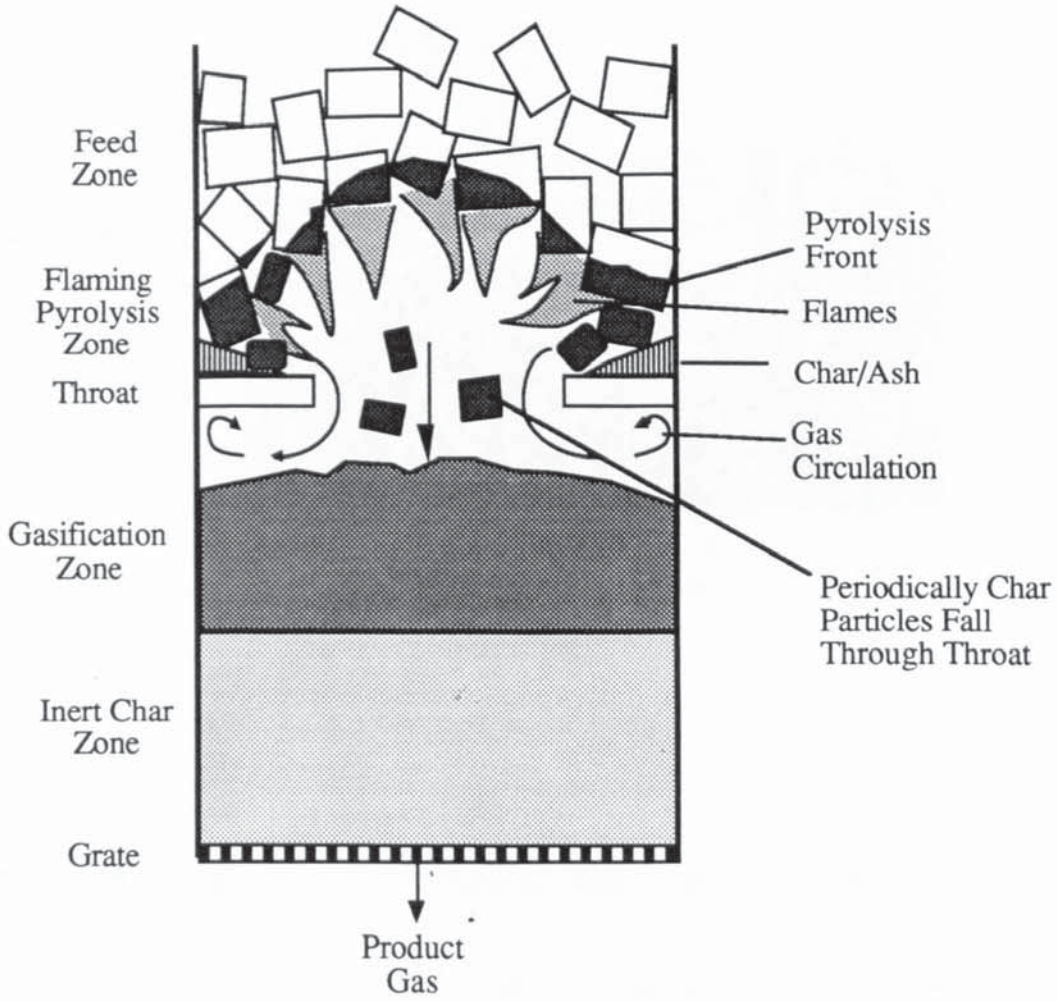

Figure 8.2 Cross-Section of the Hybrid-Throated Gasifier

Periodic collapses of the bridge across the throat occurred at randomly spaced intervals which resulted in particles dropping through the throat on to the reactive char bed below. Most particles passing through the throat were in a charred condition although on several occasions partially charred and unreacted wood particles were observed on top of the char bed after a collapse. The feed descends rapidly when a collapse occurs bringing unreacted material to bridge across the throat. The collapse of the bridge was followed by a period in which the pyrolysis front progresses upwards into the unreacted feed in a dome shape to give a cyclical effect. The frequency of the cycle is discussed later in this section. The void at the throat increases in size as particles are pyrolysed until the void becomes too big to support the feed above (see Figure 8.2).

Figure 8.3 shows the gas flow rate and the positions of the reaction zones during test T3 (from 14.25 to 27.5 minutes after start-up) and for the period directly afterwards where the reaction zone rises above the throat. The collapse of the throat bridge can be seen as a decrease in the flaming pyrolysis zone depth and an increase in the height of material below the throat, notably at about 15 and 16 minutes after start-up.

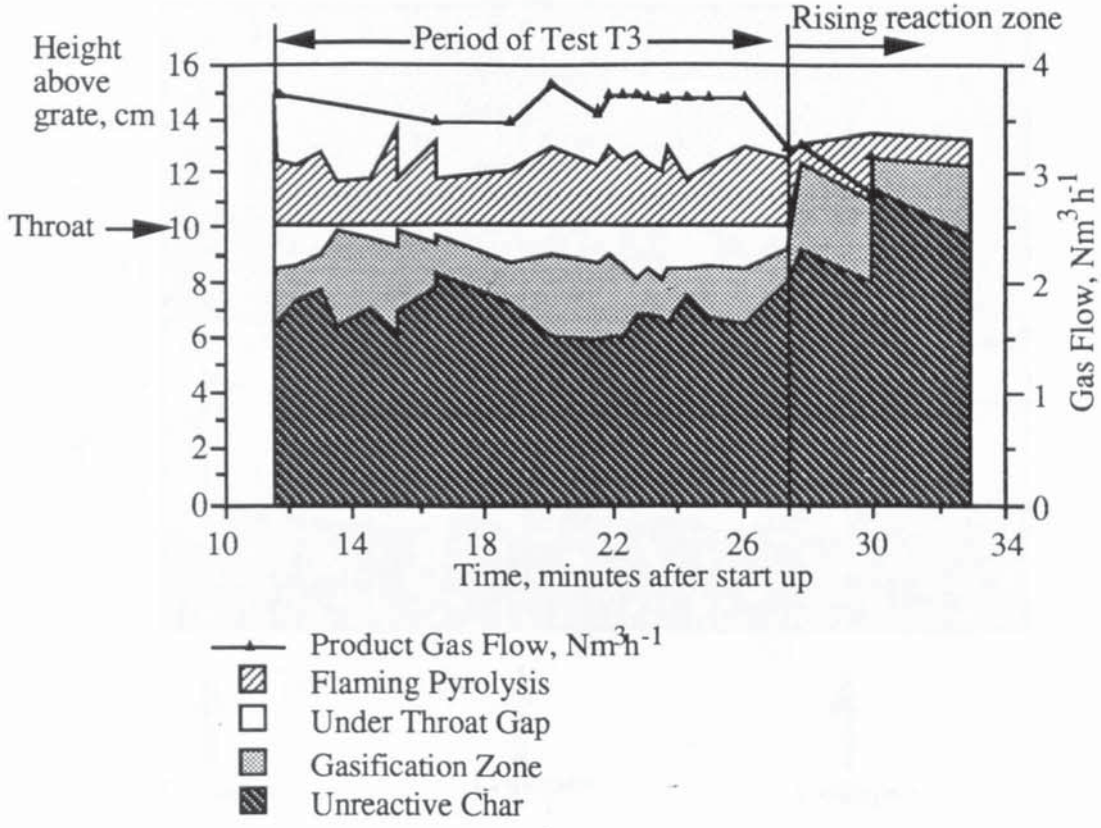

Figure 8.3 Reaction Zone Positions and Gas Flow During Test T3

The average char bed height measured from the video recording for test T3 during stable operation was 6.82 cm, with an average flaming pyrolysis depth of 2.5 cm, a gasification zone depth of 2.04 cm and a 1.14 cm gap between the throat and the top of the gasification zone. The measurements are within 0.6 cm of those taken by direct measurement during the run, taken at 2-3 minute intervals.

Figure 8.3 uses information from the figures given in Appendix I which were taken from a video recording of the run and shows the zonation as observed through the reactor wall. The actual zonation, however, is expected to have a radial function since temperatures are expected to decrease from the centre outwards as a result of heat loss from the reactor wall. Cool, apparently inert char may, therefore, be observed through the reactor wall, whilst at the reactor core a significant amount of gasification may occur. Due to the presence of the throat a radial temperature distribution search at and below the throat was not possible.

Voids were commonly seen at the interface between the unreacted feed zone and the flaming pyrolysis zone, and occasionally seen within the unreacted feed zone itself (see Appendix I). The voids were never greater than 2.5 cm across for the 6.35-12.7 mm feedstock, and less than about 1.5 cm for the 4.75-6.35 mm feedstock. Collapse of these voids were mostly initiated by the collapse of the bridge across the throat.

PAGE

NUMBERING

AS ORIGINAL

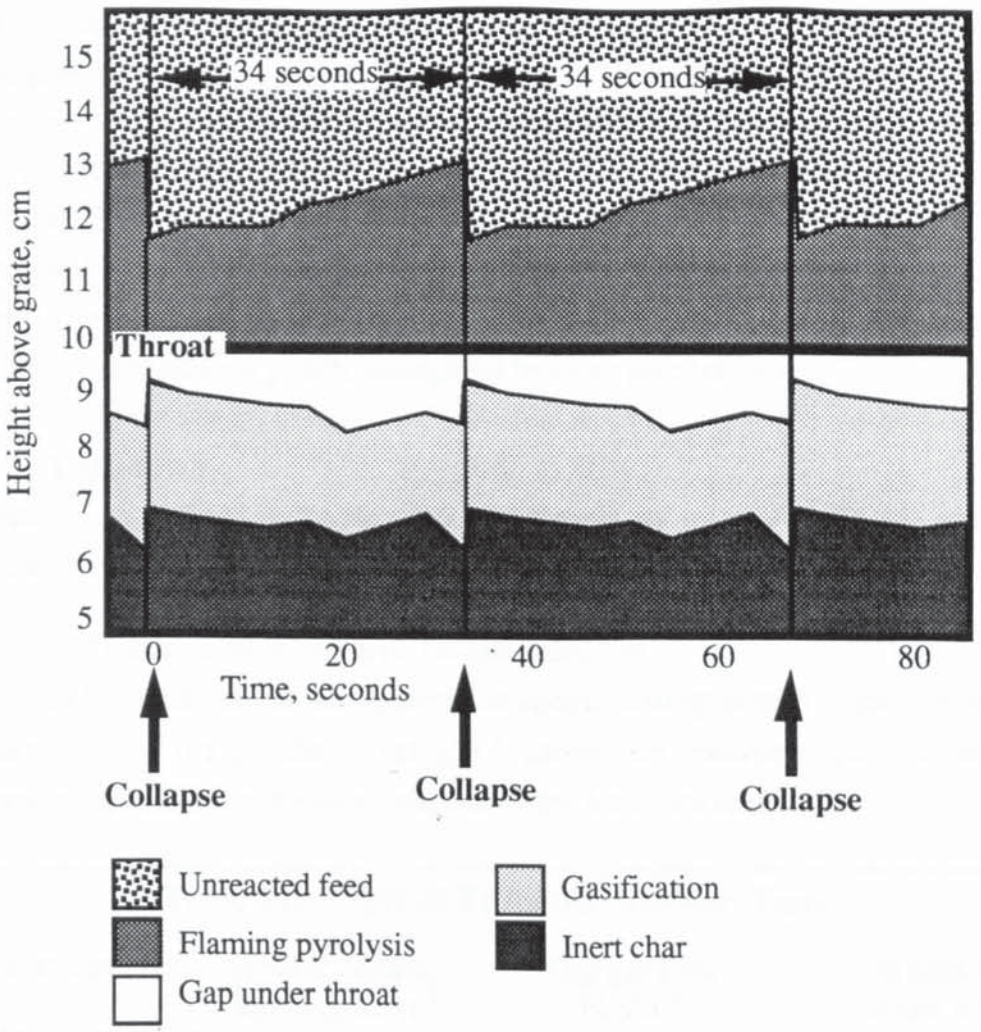

Figure 8.4 Flaming Pyrolysis Zone Bridge Collapse Cycle

The pulsating effect exhibited may be expected to cause fluctuations in the performance of the gasifier in terms of the product gas flow rate, composition and tar cracking efficiency, and may be important for practical applications. Fluctuations were not observed as the gas composition was recorded every 20-30 seconds by the data logger, and the tar content was determined over a period of 5-10 minutes.

Below the throat the remaining volatiles are released from any partially pyrolysed material. Char is consumed by gasification below the throat, with char arriving from above due to the collapse of the pyrolysis void.

8.2.1 Stability of the Hybrid-Throated Gasifier

Figure 8.3 shows a reduction in the product gas flow after the end of test T3. This was thought to be due to an increase in the pressure drop across the gasifier of about 1.1 kPa, probably due to an accumulation of fines in the lower part of the char bed near the grate. The increase in pressure drop would result in a reduction in the air flow rate into the reactor and cause the mode of operation to effectively change to the pyrolysis dominant mode. The accumulation of char within the gasifier caused the

reaction zone to rise above the throat, as shown in Figure 8.3. This suggests that the hybrid gasifier can only operate within certain air flow rate limits beyond which the gasifier is unstable with either pyrolysis or gasification becoming dominant as is the case with the open-core gasifier (Section 7.2.1). The limits are discussed in Section 8.3 below. The cycle of pyrolysis front growth above the throat and collapse of the resultant void may aid the stabilization of the reaction zone at the throat by limiting the growth of the pyrolysis zone and maintaining a hot (gasification) zone below the throat. This may allow a greater throughput range to give turndown.

8.3 Turndown

Turndown was defined in Section 2.6.3 as the ability to reduce the gas output as required by demand.

8.3.1 Turndown of the Hybrid-Throated Gasifier

The hybrid-throated gasifier was operated at various throughputs in order to determine the turndown of the gasifier. Table 8.2 shows the specific capacities and gas production rates for all uninsulated tests using the base case feed.

Table 8.2 Hybrid-Throated Gasifier Tests

Test number	Specific capacity $kgm^{-2}(grate)h^{-1}$	Dry gas flow Nm^3h^{-1}	Turndown minimum = 1.00
Stable operation			
T3	261.4	3.474	0.51
T4.1	405.2	5.498	0.80
T5.1	401.1	5.376	0.79
T5.3	477.4	6.841	1.00
T6.1	275.6	4.188	0.61
T6.2	332.8	4.265	0.62
T6.4	464.4	6.567	0.96
Unstable operation (direction of reaction zone movement in brackets)			
T5.2 (rising)	301.9[a]	2.877	0.83
T5.4 (falling)	583.4[a]	9.299	2.68
T6.3 (falling)	466.4[a]	7.777	2.24
Open-core gasifier (see Section 7.2.2)			
Base case, range	241.7 - 314.5	3.528 - 4.629	0.52 - 0.68[b]

Notes: a Approximate value due to short duration of tests (see Section 5.2).
b Turndown with respect to hybrid-throated reactor.

The specific capacities given in Table 8.2 are calculated over the grate area to enable direct comparisons with the results from the open-core gasifier (Section 8.4). The specific capacity per unit throat area, more commonly used in the literature, can be obtained by multiplying the values given in Table 8.2 by 3.06 (the ratio of grate area to throat area in the throated reactor). Turndown is expressed as the fraction of the maximum dry gas production rate achieved during stable operation (test T5.3), whereas the turndown ratio is the maximum to minimum gas production rate. Figure 8.5 shows specific capacity of the open-core and hybrid-throated gasifiers as a function of turndown (with respect to the maximum gas production rate from the hybrid-throated gasifier) using the values presented in Table 8.2.

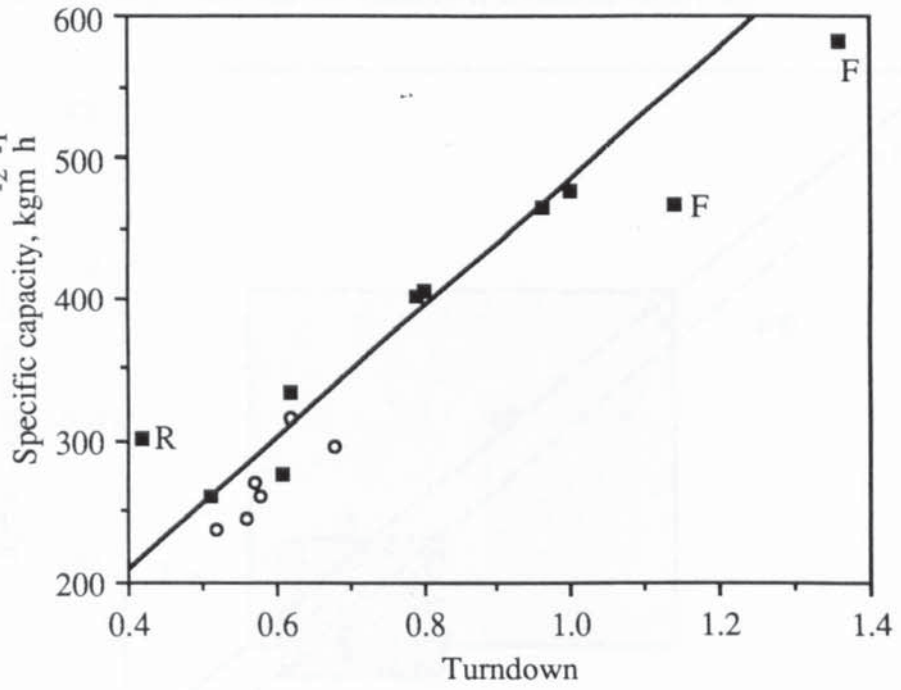

■ Hybrid-throated gasifier
o Open-core gasifier
F Falling (unstable) reaction zone
R Rising (unstable) reaction zone
—— Best fit line through hybrid-throated reactor data points during stable operation
No best fit line can be drawn through the open-core data points

Figure 8.5 Turndown of the Hybrid-Throated Gasifier and Comparison with the Open-Core Gasifier

The range of specific feed capacities measured for stable operation with the hybrid-throated gasifier is shown to be about 260-480 $kgm^{-2}h^{-1}$ compared to about 240-315 $kgm^{-2}h^{-1}$ for the open-core gasifier (Figure 8.5). Figure 8.5 shows that unstable operation is possible within the range of specific capacities obtained with stable operation.

The gas production rates given in Table 8.2 can be converted into superficial gas velocities using the same method as for the open-core (see Table 7.5, Section 7.2.1). Stable operation of the hybrid gasifier was achieved for superficial gas velocities at the grate in the range 0.218-0.430 Nms^{-1}, compared to 0.208-0.291 Nms^{-1} for the open-core reactor. For the hybrid gasifier a falling zone was obtained using a superficial gas velocity of 0.180 Nms^{-1} and a rising zone obtained with a velocity of 0.489 Nms^{-1}. Although the stable operative range differs, the result is similar to that obtained with the open-core and suggests the same mechanism for stability (Section 7.2.1). The hybrid gasifier is able to operate at higher superficial gas velocities than the open-core, which will later be related to an increase in the pyrolysis rate (Section 8.3.4). The influence of the air flow rate on stability is shown in Figure 8.6.

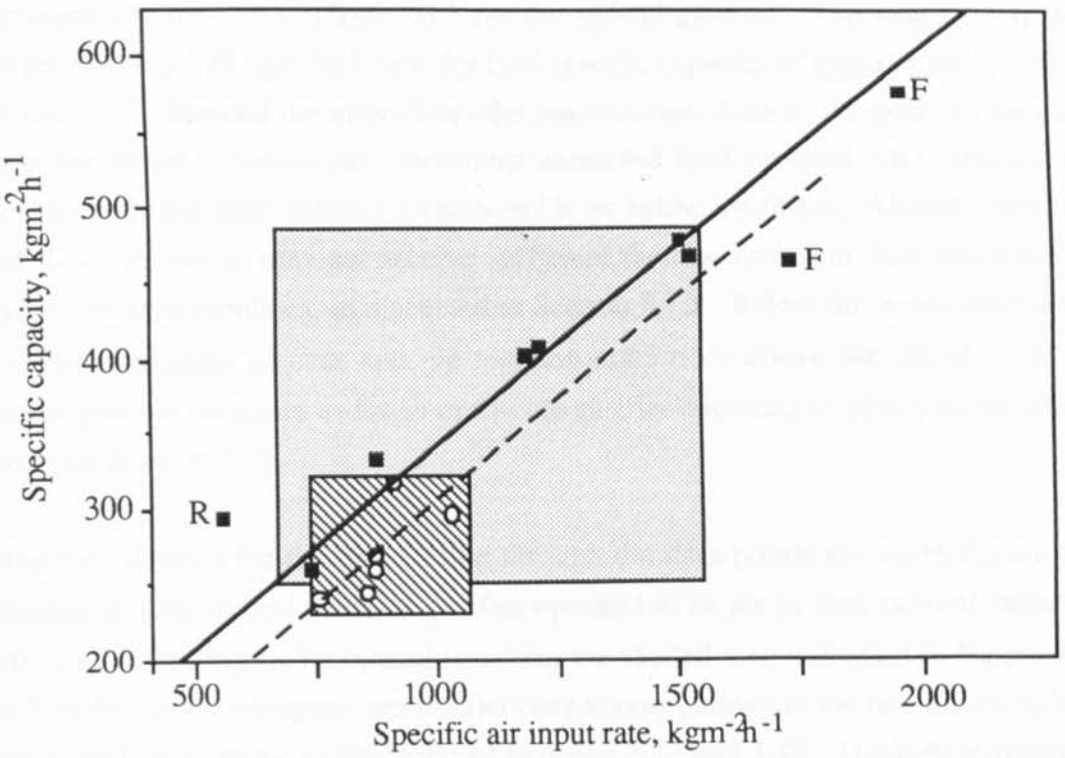

■ Hybrid-throated gasifier
o Open-core gasifier
Hybrid-throated gasifier: stable region of operation
Open-core gasifier: stable region of operation
F Falling (unstable) reaction zone
R Rising (unstable) reaction zone
—— Best fit line through hybrid-throated reactor data points during stable operation
– – – Best fit line through open-core reactor data points during stable operation

Figure 8.6 Operating Range of the Hybrid-Throated and Open-Core Gasifiers

The data points for the hybrid-throated gasifier during stable operation give a straight line best fit (see Figure 8.6), which is used to obtain the feed capacity limits for the gasifier (Equation 8.1; R^2 = correlation coefficient). A similar line can be drawn through the open-core data points (Equation 8.2), although the fit is less significant.

Hybrid-Throated Gasifier

$$\text{Feed } (kgm^{-2}h^{-1}) = 59.9 + 0.272 \times \text{Air } (kgm^{-2}h^{-1}) \qquad R^2 = 0.96 \qquad (8.1)$$

Open-Core Gasifier

$$\text{Feed } (kgm^{-2}h^{-1}) = 51.2 + 0.241 \times \text{Air } (kgm^{-2}h^{-1}) \qquad R^2 = 0.52 \qquad (8.2)$$

The upper specific air input rate limit for stable operation is indicated to lie between 1540 and 1760 $kgm^{-2}h^{-1}$ corresponding to a dry feed specific capacity of approximately 490 to 550 $kgm^{-2}h^{-1}$ for the hybrid gasifier. The lower limit lies between 600 and 770 $kgm^{-2}h^{-1}$, or a dry feed specific capacity of approximately 230 to 260 $kgm^{-2}h^{-1}$. Beyond the upper limit the reaction zone falls to the grate as the char below the throat is consumed. Incoming unreacted feed material falls through the throat towards the grate forming a unreacted layer below the throat. Alternatively, the feed above the throat may not receive sufficient thermal radiation from the reactive zone to continue pyrolysis, as discussed in Section 8.1.1. Below the lower limit there is net accumulation of char and the reaction zone rises above the throat, and the reaction process continues as for an open-core gasifier operating in pyrolysis dominant mode (see Section 7.2).

Using the equation for the best fit line through the data points shown in Figure 8.6 indicates that the hybrid-throated gasifier operates at an air to feed ratio of between 2.80 and 3.23 during stable operation within the shaded area indicated in Figure 8.6. The best fit line for the open-core gasifier runs almost parallel to the line for the hybrid gasifier and gives an air to feed ratio of between 3.23 and 3.47. The hybrid-throated gasifier requires less air in order to maintain stability which indicates that there is a lower heat loss from the reactor and, therefore, a higher energy conversion efficiency. The best-fit lines for both reactor types indicate that a slightly higher air to feed ratio is required as the capacity increases. The experimental data is discussed in Section 8.4.

Figure 8.6 shows that the hybrid-throated gasifier has a greater stable operating range compared to the open-core gasifier. The turndown ratio achieved using the hybrid-throated gasifier was 1.97:1 compared to 1.3:1 obtained for the open-core gasifier (see Section 7.3). The maximum turndown ratio for the hybrid-throated gasifier lies between 1.97:1 and 2.70:1. The first value is the highest experimental gas production ratio achieved for stable operation, and the second value is the gas production ratio between tests T5.2 (unstable operation below the lower limit) and T6.3 (unstable

operation above the upper limit). The open-core gasifier operates at the lower end of the specific capacity range obtained using the hybrid-throated gasifier. This may suggest that the hybrid-throated reactor is acting as an open-core reactor at low throughputs, and that the throat allows throughput to be turned-up. A mechanism giving turndown for the hybrid-throated gasifier is discussed in Section 8.3.3.

Turndown ratios for conventional throated downdraft gasifiers range from 2:1 for the Biomass Corporation gasifier to 5:1 for the Howden EE gasifier (Levelton, 1983). Performance for these gasifiers were given in Table 2.5 (the Biomass Corporation gasifier is listed under Forintek in Table 2.5). The turndown achieved for the hybrid-throated gasifier is within the lower end of the range for conventional systems; however, it is not known whether the quality of the product gas is adversely affected at low gas production rates for gasifiers claiming a higher turndown ratio.

8.3.2 Effect of Turndown on Gasifier Performance

In Section 2.8.3 it was stated that turndown should only apply to the range of gas production rates at which the gas quality was not adversely affected. The quality of the gas depends upon the heating value of the gas and its tar and particulate content. For all the stable tests listed in Table 8.2 above, the product gas higher heating values are in the range 3.25-4.15 $MJNm^{-3}$, with an average of 3.88 $MJNm^{-3}$.

Excluding test T6.4 the heating values range from 3.72 to 4.15 $MJNm^{-3}$ with an average of 3.99 $MJNm^{-3}$. The variation in gas heating values becomes less than ±7.5%. Test T6.4 was excluded as the product gas from test T6.4 was low in hydrogen at 6.5%, and a poor hydrogen balance closure of 70.9% (see Appendix G1) indicated a probable loss of hydrogen gas from the system. The poor closure was possibly a result of the increased pressure within the disentrainment tank during the test which developed weakness in the sealant to allow hydrogen gas to leak out. There was also a low energy balance closure of 90.9% (including heat loss) calculated for test T6.4, again indicating that the measurements were poor.

Figure 8.7 shows the product gas heating value plotted against turndown (test T6.4 excluded), and Figure 8.8 shows that the gas composition is virtually constant for all turndown values (test T6.4 excluded). The raw gas water content is also fairly constant over the turndown range (see Figure 8.9), with an average of 7.01%.

The results contradict the reported effect of operating at low turndown values lowering the amount of H_2 and CO in the product gas for conventional throated downdraft gasifiers (Kaupp, 1984). For conventional throated gasifiers at low throughputs poor distribution of the oxidant might occur resulting in a reduction in tar and char

conversion efficiency to give lower amounts of H_2 and CO in the gas. However, in the hybrid-throated gasifier there is a better distribution of oxidant (since it arrives via the feed bed), which may lead to the gas composition being less affected by turndown as shown by Figure 8.8.

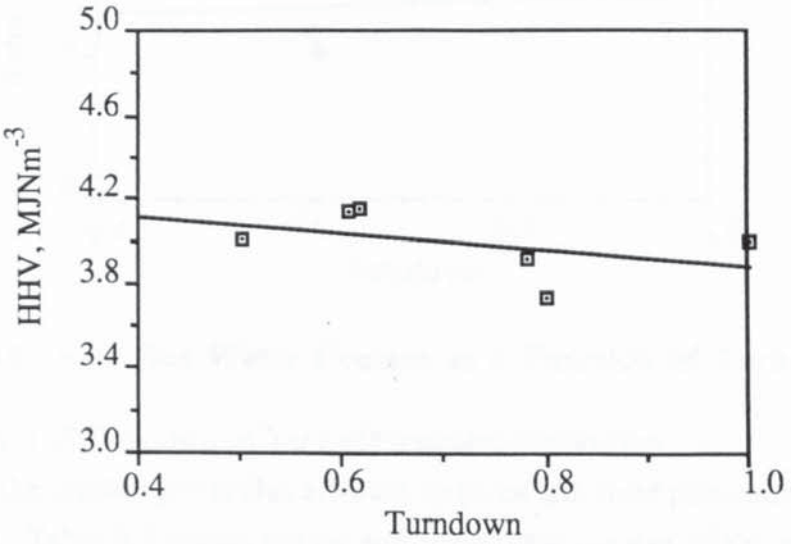

Figure 8.7 Gas Heating Value (HHV) as a Function of Turndown

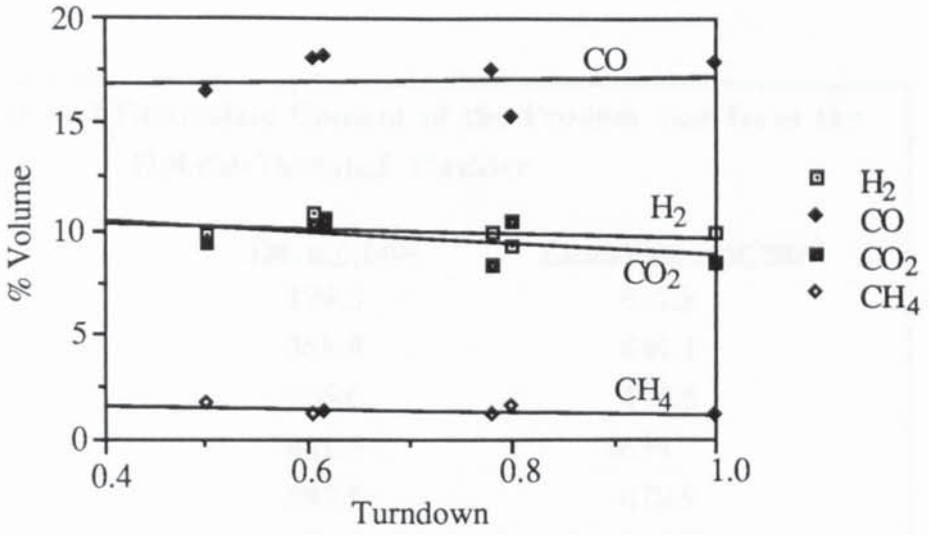

Figure 8.8 Dry Gas Composition as a Function of Turndown

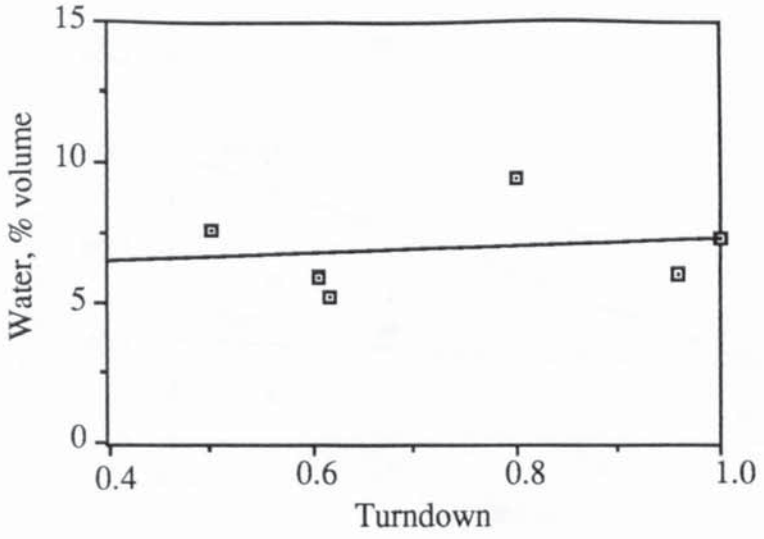

Figure 8.9 Raw Gas Water Content as a Function of Turndown

8.3.3 Effect of Turndown on Tar and Particulate Production

The quality of the product gas is also affected by its tar and solid particulate load (see Section 2.8.3). Table 8.3 shows the tar and particulate content of the product gas from the hybrid-throated gasifier. The average tar concentration for the stable tests listed in Table 8.3 is 347 $mgNm^{-3}$, and the average particulate content is 670 $mgNm^{-3}$. Figure 8.10 shows the variation in the tar and particulate content of the product gas with turndown.

Table 8.3 Tar and Particulate Content of the Product Gas from the Hybrid-Throated Gasifier

Test	Tar, $mgNm^{-3}$	Particulates, $mgNm^{-3}$
T3	179.3	667.8
T4.1	368.9	841.1
T5.3	426.6	276.6
T6.1	441.5	1654
T6.2	590.9	470.9
T6.4	74.8	112.1
Average	347.0	670.4
standard deviation	174.0	500.5
Excluding tests T6.1 & T6.4	391.4	564.1
standard deviation	147.1	211.4

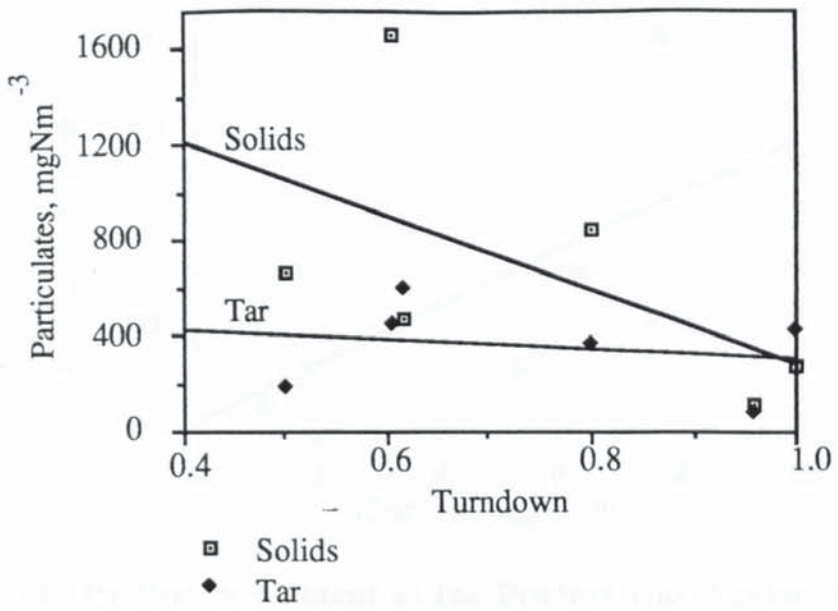

Figure 8.10 Tar and Particulate Production as a Function of Turndown

Although the spread of the results plotted in Figure 8.10 is great (±37.6%) the tar content of the product gas remains roughly constant as throughput is increased. A best fit line through the solid particulate data points suggests that there is a greater amount of solids in the product gas at low throughputs. There is a large variation in the measured solids content, which is thought to be due to the capture of a few large (>0.5 mm) particles that contribute a disproportionate amount of weight to the total mass captured by the filter as mentioned in Section 7.2.3. However, the trend remains the same even if the anomalously high solids content of 1654 $mgNm^{-3}$ measured for test T6.1 is excluded. A plot of the 'inert char' bed height against the solid particulate loading of the gas (Figure 8.11) indicates that there is a higher solids output for greater depths of inert char. The higher solids output may, therefore, be a result of lower conversion as the depth of the gasification zone is reduced. The observed inert char bed heights (i.e. the region of non-glowing char) may not, however, be the true height of inert char within the reactor (see Section 8.2).

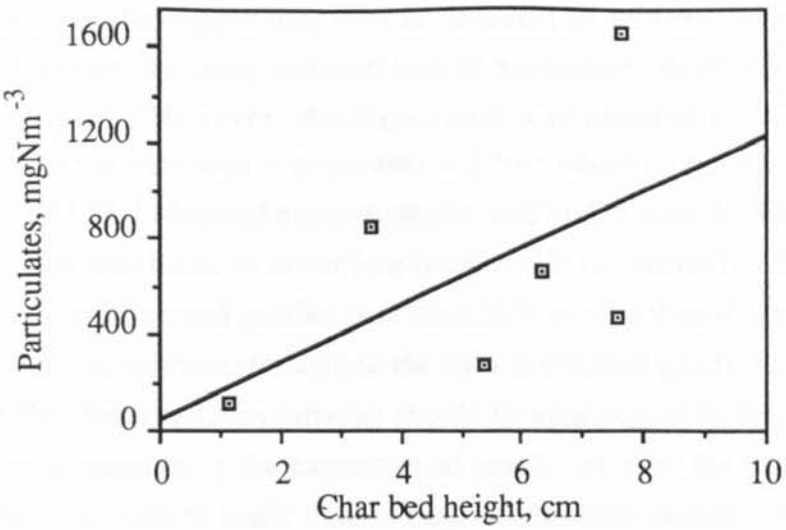

Figure 8.11 Particulate Content of the Product Gas Against Char Bed Height

8.3.4 Mechanism for Turndown

The rate of char production pyrolysis must approximately double with throughput in order that the observed turndown ratio for the hybrid-throated gasifier of 1.97:1 (Section 8.3.1) can be obtained. In Section 7.2.2 two possible mechanisms were put forward to explain the apparent turndown observed for the open-core gasifier. An increase in the temperature of the pyrolysis zone may increase the rate of radiative heat transfer for pyrolysis, and may also reduce the char yield, to give a limited turndown ratio for the open-core gasifier (Section 7.2.2). This may also be the case for the hybrid-throated reactor. Evidence for temperature variations within the flaming pyrolysis zone with throughput would be difficult to obtain due to difficulties in accurately measuring the temperature within the zone (see Section 7.2.2).

Increasing the area of the interface between the unreacted feed zone and the pyrolysis zone would increase the number of particles undergoing pyrolysis at any one time. For the open-core gasifier it was suggested that this could be achieved with a sloping reaction zone (Section 7.2.2), however due to the presence of the throat the formation of a sloping reaction zone within the hybrid-throated gasifier is restricted. A sloping reaction zone was never observed during operation. It was concluded that the placement of a throat within the reactor maintains a level reaction zone. The hybrid-throated gasifier, therefore, has an advantage of providing easier operation compared to the open-core for which a sloping reaction zone may cause poor distribution of oxidant and feed resulting in poor conversion.

Initially it was hypothesized that the minimum throughput may be obtained with pyrolysis operating at the throat with the area of the pyrolysis front equal to the throat

area. The maximum throughput may then be obtained by increasing the area of the pyrolysis front to cover the cross-sectional area of the reactor vessel (i.e. operating as a open-core gasifier). However, this hypothesis was rejected for three reasons. Firstly, the ratio of the grate area to throat area is 3.50:1 which is much higher than the turndown ratio of 1.97:1 obtained experimentally, and higher than the value of 2.70:1 at which instability was found to occur (see Section 8.3.1). Secondly, the maximum capacity in the hybrid-throated gasifier is at least 50% greater than that obtained with the open-core. If at maximum throughput the hybrid-throated gasifier operates as an open-core gasifier, the maximum capacity should be approximately the same in both types of reactor, contradicting the experimental result. Finally, the hypothesis does not support the observations made with the hybrid-throated gasifier, with the main objection being the observation of pyrolysis at the hybrid-throated reactor wall for all throughputs.

A second hypothesis is put forward (below) which is consistent with the observations and measurements obtained. In Section 8.2 the flaming pyrolysis zone was described to have a dome shape from observations made (see Figure 8.2). A turndown ratio of 2.0:1 is achieved for a flaming pyrolysis interface which is hemispherical at the maximum throughput and flat at the minimum throughput as shown by Equation 8.3.

$$\text{Turndown ratio} = \frac{\text{Maximum FP area}}{\text{Minimum FP area}} = \frac{2\pi r^2}{\pi r^2} = 2 \qquad (8.3)$$

It is hypothesized that at the minimum throughput, the pyrolysis front is a flat horizontal surface across the width of the reactor, and at maximum throughput the pyrolysis front expands to form a dome above the throat. At the minimum throughput, the hybrid gasifier operates in a similar way as the open-core, thereby having approximately the same specific capacity as the open-core. The hypothetical specific feed capacity of the hybrid-throated gasifier at maximum throughput is twice that of the open-core reactor. The experimental specific capacities obtained (see Table 8.2) support this hypothesis. The turndown ratio of 2.0:1 obtained using this hypothesis lies between the experimentally determined limits previously given in Section 8.3.1, and is very close to the maximum turndown ratio of 1.97:1 obtain using the hybrid gasifier. The hypothesis is, therefore, consistent with the experimental data and the observations made.

Figure 8.12 shows the hypothetical simplified radiative heat flux within the region of the throat. It is believed that the throat acts as a window to radiative heat transfer from the top of the char bed below the throat to the pyrolysing material above the throat (see Figure 8.12). The throat ledge obstructs the view from the hot char bed, which results

in a dome shaped pyrolysis front (see Figure 8.2). At maximum throughput there is an even distribution of heat to the pyrolysis front. The shape of the dome will depend upon the view factor which is dependant upon the distance from the throat to the top of the reactive char bed, the roughness and temperature of the emitting and receiving surfaces, reflection by the reactor walls and heat conductance through the reactor throat material and walls. There is insufficient experimental data for accurate calculation of the heat flux distribution to the flaming pyrolysis zone and further investigations are recommended. In addition, the throat gap distance is not constant for the duration of the test (see Section 8.2 and Figure 8.4) resulting in a continually changing heat flux.

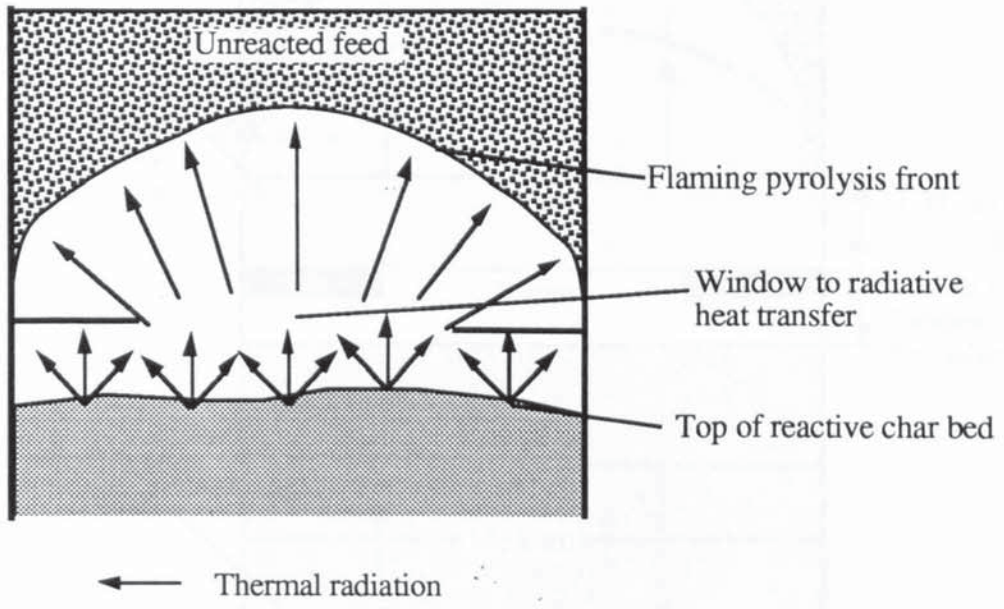

Figure 8.12 Thermal Radiation to the Flaming Pyrolysis Zone in the Hybrid-Throated Gasifier (Hypothetical)

The rate of production of char by pyrolysis is limited to the maximum surface area of the flaming pyrolysis front. The average position of the flaming pyrolysis front at the reactor wall was virtually constant for all tests at about 3.37 cm above the throat (see Figure 8.13). As the air input rate is increased the area of the flaming pyrolysis front increases as shown in Figure 8.13. This hypothesis differs from that of Hoi's (1991) expanding bubble theory (see Section 2.8.3), since the lower limit of turndown is set upon the cross-sectional area of the reactor (for the hypothesis put forward here) and not upon the cross-sectional area of the throat as hypothesized by Hoi.

A higher turndown ratio than 2:1 may be obtainable if the dome becomes more elliptical than the hemisphere described, with a dome twice as high as its diameter giving a turndown of 4:1. An elliptical dome may be produced by reducing the amount of radiation received close to the reactor wall by reducing the throat size.

Higher turndown ratios may also be achievable according to Hoi's expanding bubble theory (Section 2.8.3), although an air injector above the throat is believed to be necessary for this to occur. This is because the pyrolysis front will tend to move towards the air inlet (Section 2.5.6), which for the hybrid gasifier means across the reactor cross-section.

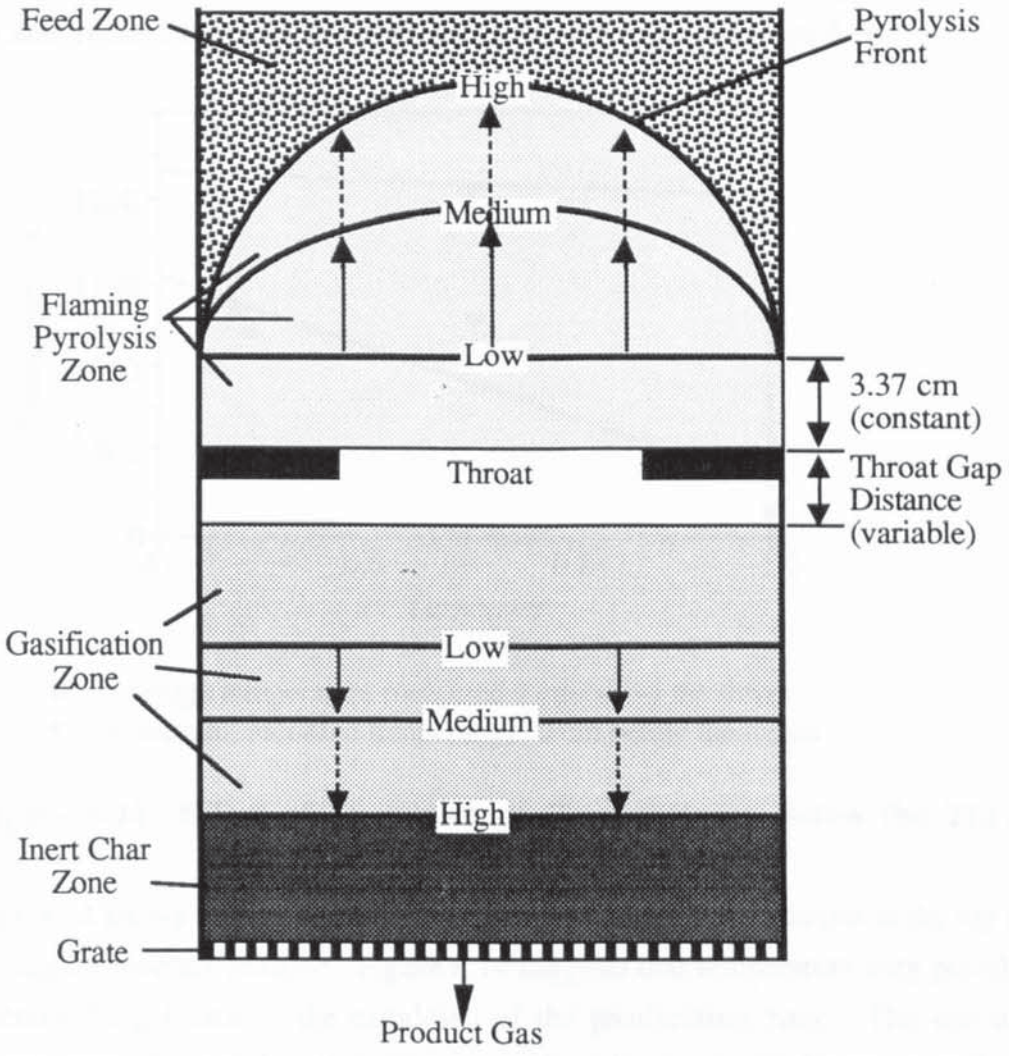

Specific Capacity	Turndown
Low	0.50
Medium	0.75
High	1.00

Figure 8.13 Mechanism for Turndown in the Hybrid-Throated Gasifier

For a turndown ratio of 2:1, the rate of char consumption by gasification must also vary by a factor of 2:1 to achieve stable operation, otherwise char will either accumulate in the gasification zone resulting in the reaction zone rising above the throat or the char will be depleted below the throat. The increase in the rate of char consumption by gasification may be achieved by an increase in the gasification zone

temperature, or an increase in the gasification zone depth. Increasing the temperature of the gasification zone increases the kinetic rate of char conversion as discussed in Section 2.4 (also see Section 9.6.3). The highest temperatures in the gasifier were believed to occur at the beginning of the gasification zone where the pyrolysis flames terminated. The temperature at a position of 2 cm below the throat (approximately the start of the gasification zone, see Section 8.2) were measured during tests T5.1, T5.3, T6.1 and T6.2. The results are plotted against turndown in Figure 8.14.

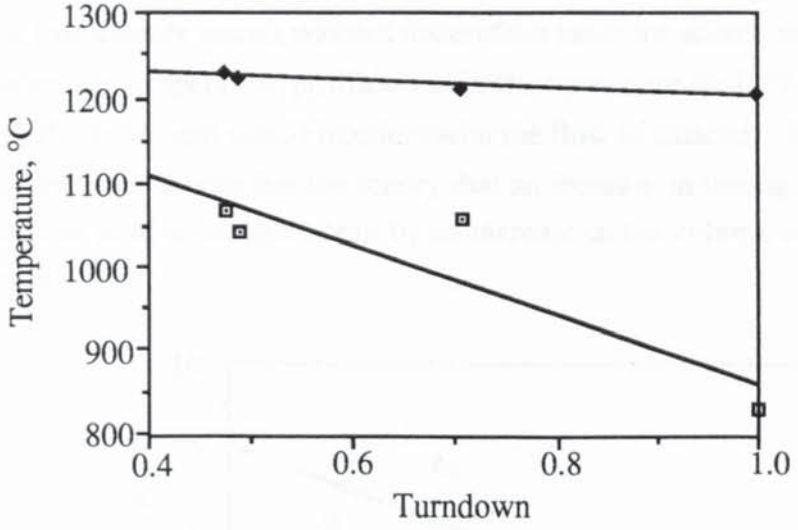

- Average temperature measured 2 cm below the throat
- Maximum recorded temperature, 2 cm below the throat

Figure 8.14 Effect of Turndown on Temperatures Below the Throat

Figure 8.14 shows that as the throughput is increased the temperatures at the top of the gasification zone are reduced. Figure 8.14 suggests that temperature may possibly be the controlling factor in the turndown of the gasification zone. The use of one measurement point within the reactor cross-section may not, however, reflect the average temperature within the gasification zone and an increase in the kinetic rate of gasification as gas production is increased can not be ruled out as the turndown control factor. The use of further thermocouples within the hybrid-throated gasifier was not possible since they would hinder material flow. It is recommended that further work should aim to measure the temperature distribution and temperature fluctuations within the reactor in order to eliminate temperature variation with gas production rates as the mechanism giving turndown.

Figure 8.15 shows the char bed height observed against turndown for the stable tests listed in Table 8.2. The height of inert char decreases as the gas production rate increases, indicating that as throughput increases the gasification zone depth increases. Using the best-fit line drawn the gasification zone depth (taken to be the distance from

the throat to the top of the inert char zone) at maximum gas production is about 7 cm compared to a depth of about 3 cm at minimum production. The volume of the gasification zone, therefore, varies by a factor of about 2.3 during stable operation, which compares to the turndown ratio of 1.97:1 obtained. Errors are involved in using the observed height of the inert char bed since only the outer portion of the reactor contents are visible (see Section 8.2). The errors may explain the discrepancy between the gasification zone depth within the hybrid (2.9 to 6.8 dp) and open-core gasifiers (5.8 to 7.7 dp; Section 7.3.1). Determination of the gasification zone depth using a temperature search was not undertaken since the search thermocouple used to determine the temperature profiles within the open-core gasifier would have to pass through the throat and would interfere with the flow of material. Further investigation is recommended to validate the theory that an increase in throughput within the char gasification zone is brought about by an increase in the volume of the zone as shown in Figure 8.13.

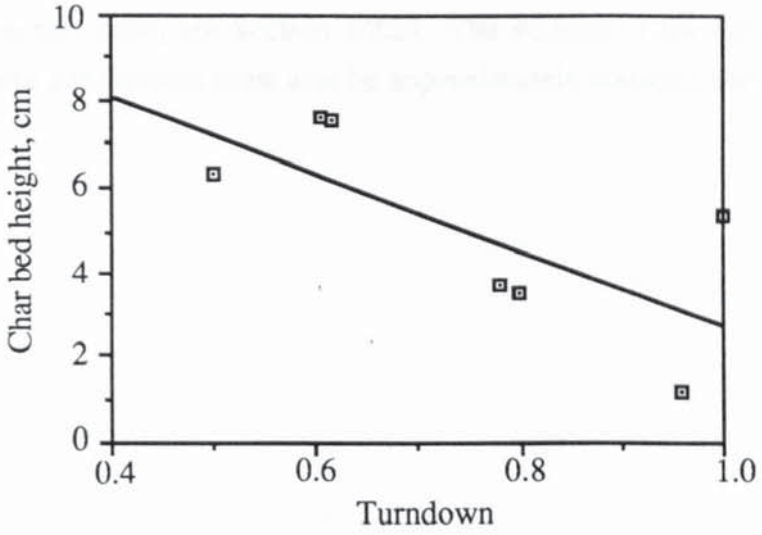

Figure 8.15 Char Bed Height Against Turndown

The volume of the gasification zone is restricted in the Aston hybrid-throated gasifier to the reactor volume between the throat and the grate. However, at the highest gas output rate achieved the gasifier was operated successfully with an inert char bed height suggesting that the maximum capacity was restricted by the production of char by pyrolysis as previously discussed in this section. A distance of 10 cm between the throat and the grate was, therefore, satisfactory for the throat size and feedstock size (6.35-12.7 mm) used in the experimental programme. For a larger reactor using a similar feedstock size, the proposed mechanism suggests that the height of the throat above the grate would be similar to that used here. For different sized feedstocks, however, the distance required may be different as indicated by the comparatively

short gasification zone depths observed using the 4.75-6.35 mm feedstock (see Section 8.6).

Instability (i.e. vertical movement of the reaction zone) occurs as changes in the air flow rate into the reactor causes the superficial gas velocity to move outside the range required for stability (see Section 8.3.1).

To summarize, the proposed mechanism enabling turndown in the hybrid-throated gasifier is considered in two parts. The turndown ability of the flaming pyrolysis zone is a function of the pyrolysis front area, which can expand to form the surface of a hemisphere above the throat as capacity is increased. The turndown ability of the gasification zone has been related to the volume of the gasification zone. The volume of the char gasification zone has been found to increase with capacity. This implies that for the open-core gasifier there is only one specific feed rate at which the gasification zone is stable, since the area of the pyrolysis front is constant (unless there is a sloping reaction zone; see Section 7.2.2). The volume of the gasification zone during open-core gasification must also be approximately constant for stability to be maintained.

8.4 Hybrid-Throated Gasifier Performance Comparison with the Open-Core Gasifier

The average results from the uninsulated hybrid-throated and open-core gasifiers are presented in Table 8.4 (test T6.4 is excluded due to uncertainties in the gas analysis, see Section 8.3.2).

Table 8.4 Hybrid-Throated and Open-Core Average Gasifier Performance Data Comparison

	Hybrid-Throated	Open-Core
Test numbers	T3, T4.1, T5.1, T5.3, T6.1, T6.2	(see Section 7.1)
Feed moisture, % wet basis	10.39	10.31
Specific capacity, $kgm^{-2}(grate)h^{-1}$	358.92	271.38
Gas volumetric yield, Nm^3kg^{-1}	3.59	3.37
Air/feed ratio	3.49	3.38
Gasifier exit temperature, °C	628.00	417.25
Dry gas composition, % volume		
H_2	10.03	9.45
CO	17.23	15.20
CO_2	9.63	10.53
CH_4	1.34	1.04
N_2	61.77	63.78
H_2/CO ratio	0.582	0.622
CO/CO_2 ratio	1.789	1.443
Raw gas water content, % vol.	7.19	11.93
Gas HHV, $MJNm^{-3}$	3.99	3.54
Cold gas efficiency, %	77.92	64.47
Tar content, $mgNm^{-3}$	347	665
Particulates, $mgNm^{-3}$	670	1002

The hybrid-throated gasifier gives a product gas with a higher H_2, CO and CH_4 content than the open-core gasifier, with a significantly higher energy content than that from the open-core gasifier. The product gas ratios given in Table 8.4 indicate that in the hybrid-throated gasifier thermodynamic equilibria (Section 2.3) has been reached at a higher temperature than for the open-core gasifier. For the open-core gasifier the maximum temperature recorded was 1023°C which compares to a maximum of 1231°C and an average temperature of 1071°C recorded during test T6.4 measured 2 cm below the throat. The higher temperatures occurring within the hybrid-throated gasifier promote the thermodynamics of conversion to the product gas. Higher temperatures

are obtained since there is less heat loss from the reactor. The average heat loss from the hybrid-throated gasifier was calculated to be 6.7% of the energy input compared to 28.0% (by difference) from the open-core. The reduction of heat loss in the hybrid-throated gasifier is thought to be due to a layer of char between the core and the walls of the gasifier, effectively insulating the high temperature region below the throat. The lower heat losses from the hybrid-throated gasifier lead to a higher cold gas conversion efficiency of about 78% compared to about 64% for the open-core gasifier.

The tar and particulate content of the product gas is lower for the hybrid-throated gasifier (see Table 8.4) indicating better conversion to gaseous products. The greater tar cracking efficiency is believed to be due to the high temperatures existing below the throat, and due to the circulation of the flaming pyrolysis products within this high temperature zone (see Section 8.2).

8.5 Insulated Hybrid-Throated Gasifier

The hybrid-throated gasifier fitted with insulation was operated in order to compare the results against the non-insulated hybrid-throated reactor, against the insulated open-core gasifier, and against other downdraft wood-fed gasifiers in the literature (Section 8.5.1). The quartz throat (Section 3.10.1) used for all previous runs was used in test T8. Due to breakage of the reactor vessel caused by thermal stress during the start-up period the test was aborted. A steel throat (Section 3.10.1) was used in test T11. No leakage at the reactor wall was believed to occur during the test since no gas streams were observed close to the wall and char/ash was deposited on the throat ledge. Observation of the reaction zone using the narrow sight strip was difficult owing to the semi-permanent ledge of char above the throat (see Section 8.2), and due to the opaqueness of the inner surface of the reactor caused by the high temperatures involved (see below). The results are presented in Table 8.5.

Insulating the hybrid-throated reactor improves the performance of the gasifier as was found for the open-core gasifier (Section 7.5.1). The average temperature 2 cm below the throat was 1107°C compared to an average of 1004°C for the uninsulated hybrid gasifier (tests T5.1, T5.3, T6.1 and T6.2; see Appendix G1). The maximum temperature recorded for the insulated hybrid gasifier was 1365°C; however, the significance of a single measurement is small. The tar content is reduced for the insulated gasifier as a result of improved tar cracking at the higher temperatures, although the result is not considered to be significant since only one sample was obtained. Comparison of the insulated hybrid-throated with the insulated open-core gasifier (Table 7.6) shows a similar improvement in the performance of the hybrid over the open-core to that found using uninsulated reactors (Section 8.5).

Table 8.5 Insulated Hybrid-Throated Gasifier Performance Compared to the Uninsulated Hybrid-Throated Gasifier

	Hybrid-throated insulated	Hybrid-throated uninsulated
Test numbers	T11	T5.1
Feed moisture, % wet basis	10.63	10.35
Specific capacity, $kgm^{-2}h^{-1}$	376.36	401.09
Gas volumetric yield, Nm^3kg^{-1}	2.72	3.50
Air input, kgh^{-1}	3.50	5.32
Air/feed ratio	2.11	3.47
Gasifier exit temperature, °C	669	650
Dry gas composition, % volume		
H_2	16.79	9.90
CO	19.71	17.49
CO_2	12.27	8.43
CH_4	1.96	1.13
N_2	49.28	63.06
Gas HHV, $MJNm^{-3}$	5.41	3.92
Cold gas efficiency, %	79.02	76.19
Heat loss, % input	4.77	6.63
Tar content, $mgNm^{-3}$	138	347
Particulates, $mgNm^{-3}$	251	670

8.5.1 Comparison with Downdraft Gasifiers in the Literature

The performance of the insulated hybrid-throated gasifier is used for comparisons with the selected downdraft gasifiers in the literature (presented in Tables 2.4 and 2.5) as the heat loss from the uninsulated gasifier would be comparatively high. The performance of the open-core gasifiers in Table 2.4 were discussed in Section 2.5.9 and compared with the results obtained from the insulated Aston open-core gasifier in Section 7.5.5. The throated gasifiers in Table 2.5 were discussed in Section 2.6.5.

The SynGas gasifier operated with a similar air to feed ratio and had a similar conversion efficiency to the hybrid-throated gasifier, but produced a higher heating value gas due to its greater methane content (see Table 2.4). The tar content of the gas from the hybrid-throated gasifier is lower than that produced from the KSU and SERI gasifiers (Table 2.4), indicating that the hybrid-throated gasifier has a better tar cracking efficiency due to the reasons discussed in Section 8.4, although the differences may be attributable to differences in the methods of tar measurement. The tar content of the product gas from the hybrid-throated gasifier is also about 55% of

that produced from the Twente throated gasifier (Table 2.5) which uses a central air injector above the throat, although the tar cracking mechanism is the same (Section 2.6.1). The lower tar level produced by the hybrid-throated gasifier may be due to the slightly higher temperatures existing within the hybrid gasifier of 1107°C compared to 1070°C in the Twente gasifier (Groeneveld, 1985a), or to differences in the method of measurement. The performance of the hybrid-throated gasifier is similar to the Howden EE gasifier (Table 2.5) in terms of gas composition, product gas heating value and conversion efficiency. The Howden EE gasifier is similar in design to the Twente gasifier since it uses a central air injector above the throat; thus air is delivered from the same direction as for the hybrid-throated gasifier. The similarity in performance is also due to the use of similar air to feed ratios with the Howden EE and hybrid-throated gasifiers. Other differences in the performance data are due to the reasons previously given in Sections 2.5.9, 2.6.5 and 7.5.5.

8.6 Effect of Feed Size

A feed size of 4.75-6.35 mm was used within the hybrid-throated gasifier to investigate the effect on size on the gasification process. In two tests a stable reaction zone was obtained, but in test T4.2 the reaction zone rose above the throat. Test T4.2 used 4.75-6.35 mm feed after the stable operation with the base case feed without altering the water flow through the venturi. Although the suction pressure remained the same it can be concluded that the additional pressure drop through the bed of smaller particles caused a reduction in the air flow into the gasifier. The increase in the pressure drop across the gasifier with time from start-up for the 4.75-6.35 mm (run T7) and the 6.75-12.7 mm (run T6) feed sizes are presented in Figure 8.16.

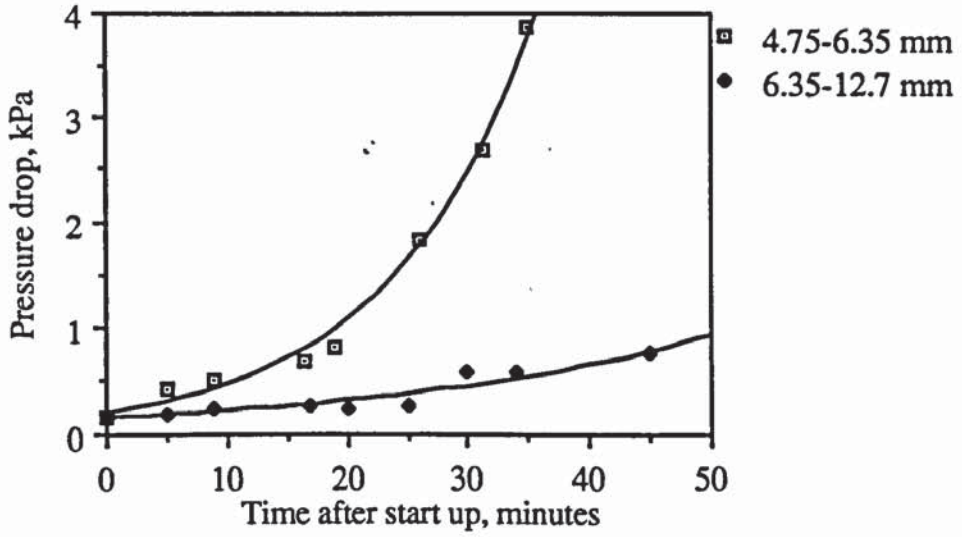

Figure 8.16 Pressure Drops Across the Hybrid-Throated Gasifier Operating on Different Feed Sizes

Figure 8.16 illustrates that the feed size is a critical operating parameter in the hybrid-throated gasifier. The pressure drop across the gasifier increases rapidly after 20 minutes of operation when using the 4.75-6.35 mm feed size. The water flow rate through the venturi had to be progressively increased to keep the air flow rate into the gasifier approximately constant to prevent the reaction zone rising above the throat.

The results presented in Table 8.6 show that there is a different operating range for the hybrid-throated gasifier using the 4.75-6.35 mm feed size compared to the 6.35-12.7 mm feed size. The lower specific air rate limit lies between 1018 and 1038 $kgm^{-2}h^{-1}$ compared to about 600-770 for the 6.35-12.7 mm feed. The gasifier was not operated to unstable conditions using high air input rates due to a shortage of feed in this size range, but the upper limit lies beyond 1267 $kgm^{-2}h^{-1}$. The difference in the operating range may be due to the higher throughput of particles since less time is required for pyrolysis and gasification of a particle. The turndown ratio of the gasifier using this feed size is at least 1.2:1; however, the maximum turndown ratio is expected to be about the same for all feed sizes since the rate of the pyrolysis process is limited by the reactor geometry. As is the case when operating with the base case feed size, the energy conversion efficiency to a cold gas is reduced at higher throughput.

Table 8.6 Hybrid-Throated Gasifier Using 4.75-6.35 mm Wood Feed Size Performance Data

	Rising Zone	Stable	
Test numbers	T4.2	T4.3	T7.1
Feed moisture, % wet basis	9.08	9.08	9.57
Specific feed capacity, $kgm^{-2}h^{-1}$	382.46	405.36	496.52
Gas volumetric yield, Nm^3kg^{-1}	3.26	3.21	3.14
Specific air rate, $kgm^{-2}h^{-1}$	1018.1	1038.5	1267.0
Air/feed ratio	3.07	2.96	2.95
Gasifier exit temperature, °C	541	628	646
Dry gas composition, % volume			
H_2	11.33	12.35	10.38
CO	16.65	17.44	19.50
CO_2	10.11	9.44	9.06
CH_4	1.74	1.84	1.37
N_2	60.18	58.94	59.78
Gas HHV, $MJNm^{-3}$	4.24	4.51	4.33
Cold gas efficiency, %	76.81	80.28	73.11
Heat loss, % input	5.19	6.50	5.94

Comparison of the data presented in Table 8.6 with the performance data in Table 8.4 using the 6.35-12.7 mm feed size shows that the energy content of the product gas is on average 11% higher with the smaller feed size. The conversion efficiency is approximately the same for both feed sizes. The findings are similar to the open-core gasifier operating on the different feed sizes (Section 7.7), and both sets of results are explained by the lower air to feed ratios required for stable operation using the 4.75-6.35 mm feed size.

8.7 Feed Type

The gasification of sewage sludge and rubberwood charcoal was attempted using the hybrid-throated gasifier.

8.7.1 Operation of Hybrid-Throated Gasifier on Sewage Sludge Granules

The attempt to gasify dried sewage sludge within the open-core gasifier was unsuccessful due to the fusion of the material within the reactor preventing the downwards flow of material (see Section 7.8.1). An attempt to gasify the sewage sludge using the hybrid-throated gasifier was conducted (test T7.2), although a similar result was expected. The gasifier was operated with a stable zone at the throat prior to the addition of the sewage sludge granules. Fusion of the sewage sludge occurred which effectively plugged the throat, thus confirming the conclusion that the feed was not suitable for use in a downdraft gasifier. The problems of using dried sewage sludge within downdraft gasifiers were discussed in Section 7.8.1.

8.7.2 Operation of Throated Hybrid Gasifier on Rubberwood Charcoal

The gasification of rubberwood charcoal within the open-core gasifier was unsuccessful (see Section 7.8.2). It was decided to attempt gasification of the charcoal within the hybrid-throated gasifier since the presence of throat may aid stabilization of the reaction zone by increasing the rate of pyrolysis relative to gasification by the formation of a domed pyrolysis front (see Section 8.2). The use of rubberwood charcoal was investigated in test T12, which is described below.

After achieving stable operation using the 6.35-12.7 mm wood feedstock rubberwood charcoal was added to the gasifier. Within a minute of the charcoal reaching the pyrolysis front the reaction zone was observed to be rising towards the open top of the gasifier. In order to maintain the reaction zone at the throat the air flow rate into the gasifier was progressively increased without significant effect. A blockage within the gasmeter then occurred which resulted in the tank pressure increasing until the relief manometer discharged and an emergency shut-down was implemented. Although the total test time was less than 3 minutes, the test indicated that a large air flow would be required in order to keep the reaction zone at the throat. Combustion of the char is

likely to play a significant role in consumption of char in addition to providing additional energy for a higher gasification rate in order to consume sufficient char to maintain a stable reaction zone. The high fixed carbon content of the charcoal leads to more char entering the gasification zone than can be consumed by gasification giving a rising reaction zone (see Section 7.8.2).

As with the open-core gasifier, the hybrid-throated gasifier may be operated in a top stabilized mode (see Section 7.2.1) with the reaction zone limited by the feed rate. However, in order to get full benefit from the presence of the throat, the depth of material above the throat has to be controlled by the feed rate in this case. Conventional downdraft gasifiers used during World War II gasified charcoal successfully for automotive power. In this case, however, the reaction zone is stabilized at the throat by using air injection into the throat. The reaction zone tends to move towards the point of air injection, thus in the conventional throated gasifier the reaction zone remains at the throat. With the hybrid-throated gasifier the reaction zone may also be stabilized at the throat by injecting a proportion of the air requirement into the throat. The proportion of air injected would depend primarily on the feed composition. Further work would be required in order to validate this suggestion and to provide guide-lines on the proportions of air injected into the throat and delivered through the feed bed for different types of biomass.

8.8 Scale-Up and Design of the Hybrid-Throated Gasifier

The bridging of material across the throat within the flaming pyrolysis zone is thought to provide turndown by the mechanism described in Section 8.3.4. Scale-up may be achieved by increasing the diameter of the throat and the diameter of the reactor vessel by the same ratio. However, this would eventually lead to an open-core operating condition in which material flow is not restricted by the throat and bridging does not occur. There may also be insufficient gas circulation within the vicinity of the throat in order to achieve the degree of tar cracking required. The successful gasification of the 4.75-6.35 and 6.35-12.7 mm feedstocks using a 40 mm throat indicates that a throat diameter of between 3.86 and 6.34 characteristic particle diameters is satisfactory. Further experimentation is required using different sized feedstocks to find the maximum and minimum throat size in terms of particle diameters. Using the 6.35-12.7 mm feed it is predicted that using a 65 mm throat would be successful by linear extrapolation. Reactor dimensions are calculated for different sized feedstocks using the following design calculations:

(a) a throat size of 6.34 dp (this Section).

(b) a reactor:throat diameter ratio of 1.88:1, i.e. the same as that used in the experimental work.

(c) a maximum flaming pyrolysis zone depth calculated using the model presented in Section 9.4.2 and assuming a maximum specific grate capacity of 477 $kgm^{-2}h^{-1}$ (i.e. the maximum obtained for stable operation using the experimental reactor, see Table 8.2) at maximum output. This gives the minimum height of reactor above the throat; additional reactor height is required to contain the unreacted feed.

(d) a maximum gasification zone depth of 6.8 dp (see Section 8.3.4)

(e) an inert char zone depth of 10 dp (Section 9.7). Together with the depth of the gasification zone, this gives the height of the throat above the grate.

Reactor dimensions for various feed sizes are presented in Table 8.7 below, where the characteristic particle diameter (dp) is calculated as described in Section 4.3.7. Feed sizes above 25 x 25 x 25 mm are not considered since carbon deposition within the particle is likely (Section 2.2.2) which is thought to increase the reaction time required for pyrolysis and increase the char yield, thus altering the stability of the reaction zone. A possible problem due to increasing the throat size is that the residence time within the hot void below the throat is reduced as a result of less disturbance to the gas flow by the throat, i.e. reduced gas circulation. This may lead to an increase in the tar load in the product gas due to a reduced tar cracking efficiency.

Table 8.7 Recommended Dimensions for Hybrid-Throated Reactor Vessels Using Feedstocks of Various Sizes

Particle size mm	dp mm	Throat diameter, mm	Reactor. diameter, mm	FP zone depth, mm	Throat height, mm
5 x 5 x 5	4.0	25	47	13	67
10 x 10 x 10	7.9	50	94	52	133
15 x 15 x 15	11.9	75	141	117	200
20 x 20 x 20	15.8	100	188	208	265
25 x 25 x 25	19.8	125	235	324	333

The turndown mechanism postulated for the hybrid-throated gasifier (Section 8.3.4) may suggest that the throat diameter can be kept constant whilst the reactor diameter is increased to give scale-up. However, the thermal heat transfer from below the throat to the pyrolysis zone would be limited due to the view factor, although the extent of this limitation is uncertain. Further research using different throat diameters and different throat to reactor area ratios is, therefore, recommended.

The hybrid gasifier may be scaled up by using a multiple throated system such as that shown in Figure 8.17. The multiple throated gasifier is expected to operate in a similar manner to the single throated hybrid, with feed material forming a bridge across each throat (i.e. each throat behaves as a cell equivalent to the hybrid-throated gasifier used in this research). The multiple throated gasifier may achieve turndown by the mechanism described in Section 8.3.4, resulting in a dome-shaped pyrolysis front above each throat as indicated in Figure 8.17. Additional turndown may also be achieved by closing a proportion of the cells using sliding gate valves.

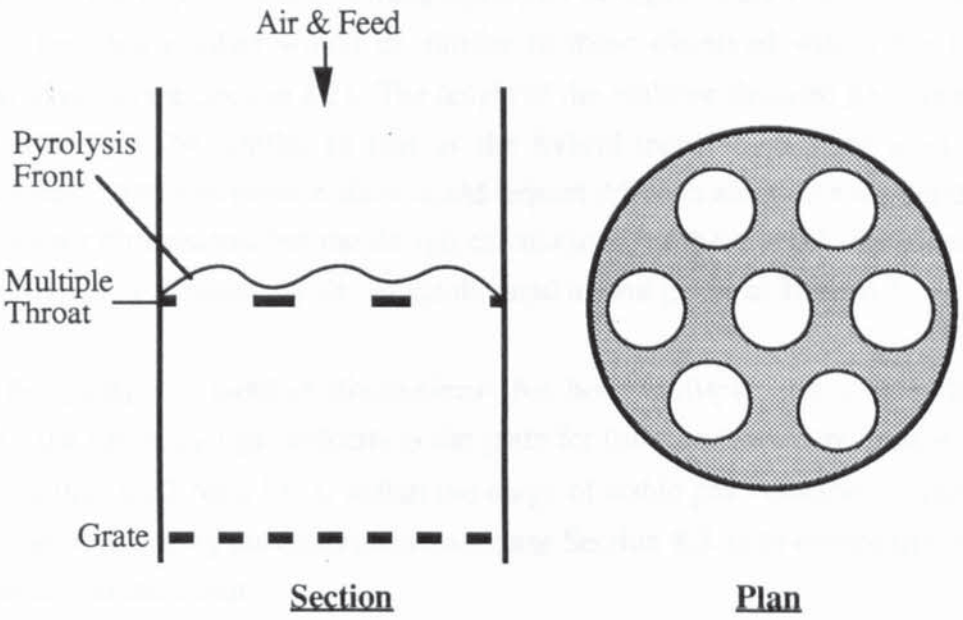

Figure 8.17 Multiple Throated Hybrid Gasifier

Turbulence within the high temperature region expected below the throat would result in good mixing of the gases and efficient tar cracking, whilst heat losses are reduced due to the presence of neighbouring cells.

The gas production rate per throat area for the insulated hybrid-throated gasifier (test T11; Section 8.5) is calculated by the specific capacity of the throat multiplied by the experimental gas yield (Appendix G1), as shown in Equation 8.4.

$$1323\ kgm^{-2}\ h^{-1}\ x\ 2.716\ Nm^3kg^{-1}\ =\ 3593\ Nm^3m^{-2}\ h^{-1} \qquad (8.4)$$

Using a throat diameter of 40 mm (i.e. the same as that used for the experimental work using the hybrid-throated gasifier in this Chapter) the production capacity of the multiple throated gasifier as shown in Figure 8.17 (with 7 throats) would be;

$$3593\ Nm^3m^{-2}\ h^{-1}\ x\ 1.257\ x\ 10^{-3}\ m^2\ x\ 7\ =\ 31.6\ Nm^3\ h^{-1} \qquad (8.5)$$

With a product gas heating value of 5.41 $MJNm^{-3}$ (test T11, Table 5), the energy output of the multiple throated gasifier (7 x 40 mm throats) is 171 MJh^{-1}. Maintaining the grate area to throat area ratio of 3.5:1 used for the hybrid-throated gasifier, the diameter of the multiple throated gasifier is 200 mm. The gasifier may be scaled-up to an unlimited size simply by increasing the number of throats. Since air is fed through the open top of the gasifier the distribution of oxidant is unlikely to be a problem; however, a stirrer within the feed bed may be necessary to distribute the feed over the multiple throat. Using the same feed size as used in the hybrid-throated gasifier programme, the depths of the flaming pyrolysis and gasification zones within the multiple throated gasifier would be similar to those observed within the hybrid-throated gasifier (see Section 8.2). The height of the multiple throated gasifier needed would, therefore, be similar to that of the hybrid-throated gasifier used in the experimental. Different particle sizes would require different reaction zone depths and, hence reactor dimensions, but the design calculations for these would be identical to those previously calculated for the single throated hybrid given in Table 8.7.

When designing the gasifier dimensions (for both multiple and single throated hybrids), the superficial gas velocity at the grate for full turndown is recommended to be greater than 0.22 Nms^{-1} (i.e. within the range of stable gas velocities obtained for stable operation during the experimentation; see Section 8.3.1) to ensure the reaction zone remains at the throat.

8.9 Summary

The operation of the hybrid-throated gasifier was investigated after start-up problems were resolved. The flaming pyrolysis zone is situated above the throat with particles bridging the constriction. Gas circulation takes place in a high temperature region below the throat (prior to the top of the gasification zone), in which tar cracking is believed to occur. The gasification zone is supported on a bed of inert char. The bridge over the throat periodically collapses producing a cyclical affect on the positions and depths of the reaction zones.

The gasifier was found to have a turndown ratio of at least 2:1. A mechanism giving turndown was proposed. The pyrolysis front is hypothesized to expand from a flat horizontal interface at low throughput to form a dome at high throughputs, thereby causing a doubling of the interfacial area. The gasification zone is thought to increase in depth in order to accommodate the increase in char production in order to maintain reaction zone stability. The hypothesis is supported by observations and experimental data. Turndown was found to have no significant affect on the product gas quality.

The hybrid-throated gasifier has been found to produce a gas with a higher heating value and a lower tar content than the open-core gasifier. The energy conversion efficiency to cold gas is about 78% using the uninsulated hybrid-throated gasifier compared to 64% for the uninsulated open-core gasifier. The improvements in gasifier performance are due to gas mixing and tar cracking in the high temperature zone below the throat, and because of reduced heat losses from the hybrid reactor.

Investigations on the effect of feed size, alternative feeds, and the use of insulation were also discussed, with the results showing similar effects to those reported for the open-core gasifier.

Limited scaled-up of the hybrid-throated gasifier may be achieved by increasing the diameter of the throat, and reactor dimensions are given for various feed sizes. A design for a multiple throated gasifier is presented based upon the hybrid-throated gasifier used in this research. The multiple throated design may have unlimited scale-up potential and the same tar cracking efficiency and gasifier performance of the insulated hybrid-throated gasifier used in the experimental work.

9. DOWNDRAFT GASIFIER MODELLING

9.1 Introduction and Objectives

Modelling of the gasification process in downdraft gasifiers has been carried out in order to provide information on how process variables affect gasification to allow prediction of performance. Modelling has also been carried out to obtain the length of reactor required in the design of a downdraft gasifier. Experimental data obtained during this research is used in the models developed. Modelling methods in the literature are also discussed and compared to the model presented here.

The models developed have two main objectives. The first objective concerns the calculation of the reactor height needed for each stage of the gasification process to reach completion. It is important that the feed is completely devolatilized within the pyrolysis zone, otherwise particles containing a significant amount of volatiles can pass through the oxidation zone. The oxidation zone is important for tar cracking by thermal and oxidative degradation (see Section 2.6.1), which, if by-passed, results in high product gas tar content. A sufficient gasification reaction zone depth is required in order to achieve the degree of char conversion needed to maintain a stable reaction zone and to obtain a high energy conversion efficiency. The second objective concerns the quality of the product gas in terms of its heating value by predicting the gas composition leaving the gasifier.

9.2 Outline of Modelling Study

Particles are characterized according to wood char structure and dimensions (Section 9.3) for use in the models. The following steps in the gasification process are then considered:

(a) Pyrolysis Wood + Heat $\rightarrow$ Char + Volatiles

(b) Oxidation Volatiles + Oxidant $\rightarrow$ CO, H_2, H_2O, CO_2, CH_4 + Tar

(c) Gasification Char + (H_2O + CO_2) $\rightarrow$ CO + H_2 (see Table 2.1)

The time for pyrolysis is based upon the time taken for the particle to reach the pyrolysis temperature by thermal conduction (Section 9.4). Oxidation of the volatiles is assumed to be instantaneous (Section 9.4.4), and steps (a) and (b) are combined to give the flaming pyrolysis zone. The product gases emerging from the flaming pyrolysis zone are assumed to be in water gas shift equilibrium (see Equation 2.6), allowing calculation of the flaming pyrolysis gas composition (Section 9.5). Mass and energy balances over the flaming pyrolysis zone are carried out to determine the mass flows of char, tar and gases into the gasification zone. A step-wise char gasification

model is then used to obtain a reaction profile of the char gasification zone (Section 9.6). The char gasification model is based upon external and internal mass transfer rates, mass and energy balances and reaction kinetics. Finally, the outlet product gas composition and temperature are predicted using an equilibrium model (Section 9.8).

9.3 Model Char Particle

The dimensions and internal structure of the wood char are required for calculations of the external and internal mass transfer of the reactant gas. Softwoods have a well defined pore structure, with pore diameters of about 20-80 μm and pore lengths of about 3-4 mm (Hillis, 1985). The fine structure of wood is said to be retained on charring (Hillis, 1985). Wood char is, therefore, assumed to have a structure made up of uniform cylindrical pores 20 μm in diameter (see Figure 9.1). The particles used in the experiments were formed by cutting across the grain (Section 4.2) to obtain a particle thickness of 5-6 mm along the direction of the grain. The thickness of the particle is, at most, twice the pore length described by Hillis (1985), suggesting that most of the internal surface of the char particle is accessible. For this reason it is assumed that the length of the pores are equal to the thickness of the particle, as indicated by L in Figure 9.1.

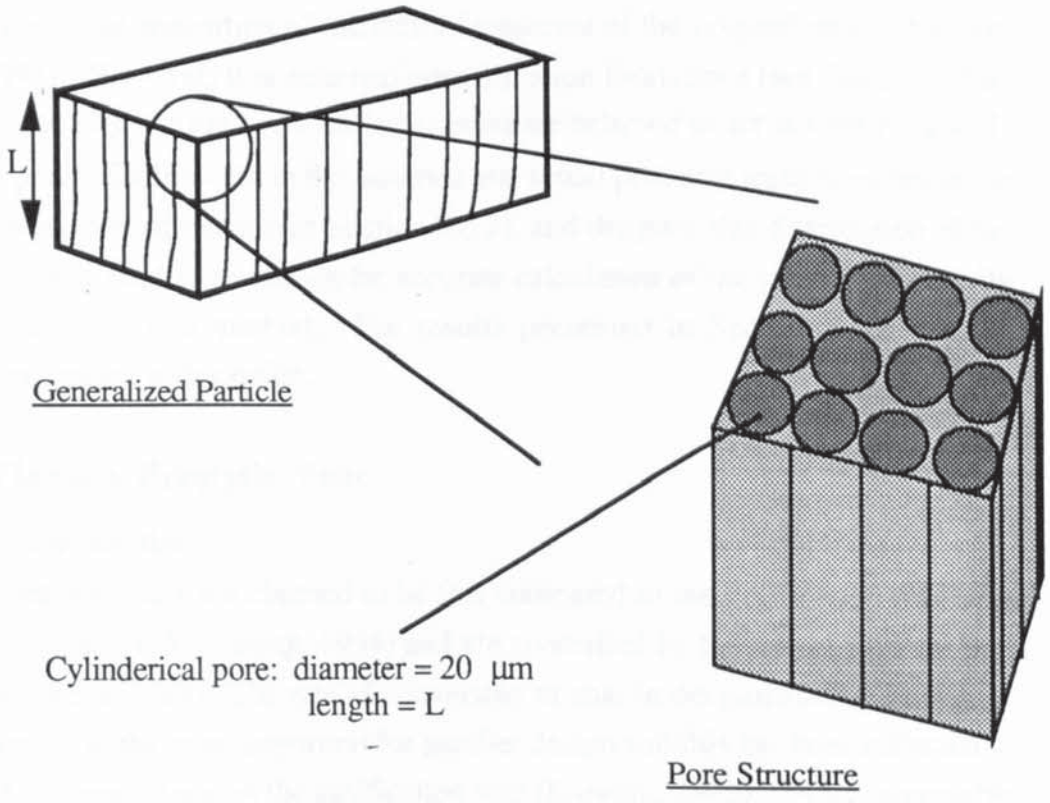

Figure 9.1 Model Particle Dimensions and Pore Structure

From the definition of the pore structure and dimensions the porosity of the char is calculated to be 0.79 m^3m^{-3}. For the base case feed used in the experimental work,

with a particle thickness of 5.5 mm (Section 4.3, Table 4.5), the external surface area is calculated to be less than 0.5% of the total surface area (Appendix J1). The external surface is therefore neglected. The internal surface area of the char is calculated to be 1.3 m^2g^{-1} (using a measured specific char density of 120 kgm^{-3}), which is much smaller than that measured by BET adsorption methods for various wood chars in the literature given in Table 9.1.

Table 9.1 Surface Areas of Biomass Chars in the Literature (Selected)

Char material	Surface area, m^2g^{-1}	Reference
Beech	271-388	van den Aarsen, 1985
Cottonwood	797	DeGroot, 1985
Douglas Fir	891	DeGroot, 1985
Jack Pine	676-836	Nandi, 1985
Maple	620-692	Nandi, 1985

The discrepancy between values in the literature and the calculated surface area cannot be attributed to the surface roughness of the pores alone, and indicates the presence of fine micro-pores. Fine micropores in the order of 10 nm are believed to be created on charring due to the separation of microfibril elements of the original wood structure (Smith, 1993). However, it is assumed pore diffusion limitations (see Section 9.6.2) only affect the 20 μm pores since the larger pores are believed to act as feeder channels to the fine pores. Differences in the assumed and actual pore size leads to errors in the calculation of pore diffusion (see Section 9.6.2), and the pore size distribution of the char used would need to be known for accurate calculation of the effective reactivity (Section 9.6.3) by this method. The results presented in Section 9.6.6 should, therefore, be treated with caution.

9.4 Flaming Pyrolysis Zone

9.4.1 Introduction

Pyrolytic reaction rates are claimed to be fast compared to the gasification reactions (e.g. DeGroot, 1984; Manurung, 1994) and are controlled by the rate of internal heat transfer (Buekens, 1985). The rate of conversion of char in the gasification zone may thus be viewed as the most important for gasifier design and this has been reflected in models which concentrate on the gasification step (Buekens, 1985). This is acceptable for coal gasifiers where the volatile content of the feed is low (e.g. Yoon, 1979), and for small particles where there are fast heat and mass transfer rates as is the case of fluidized bed gasifiers (Buekens, 1985). However, for larger particles in a moving bed gasifier the pyrolysis reaction step is significant in gasifier design and forms a

clearly recognizable zone within the gasifier (see Sections 2.5.2 and 7.3.2). For stable operation with a stationary reaction zone the rate of char production must, by definition, be equal to the rate of char consumption by gasification. This research has also shown that the rate of gasification can exceed the rate of pyrolysis (see Section 7.2.1). Both the pyrolysis and gasification steps should, therefore, be considered in gasification modelling studies.

9.4.2 Transient Heat Conduction Model

Estimation of the time for pyrolysis is carried out using a transient heat conduction model. The time for pyrolysis (complete devolatilization of wood particle) is obtained using temperature response charts (Schnieder, 1963) for point A in Figure 9.2 to reach the pyrolysis temperature. The pyrolysis temperature is assumed to be 450°C which is about the values given in the literature (e.g. Reed, 1988). Heat is assumed to travel with the grain since the thermal conductivity in this direction is 2.25-2.75 times greater than across the grain (Kollman, 1954). The wood particle is modelled in two ways:

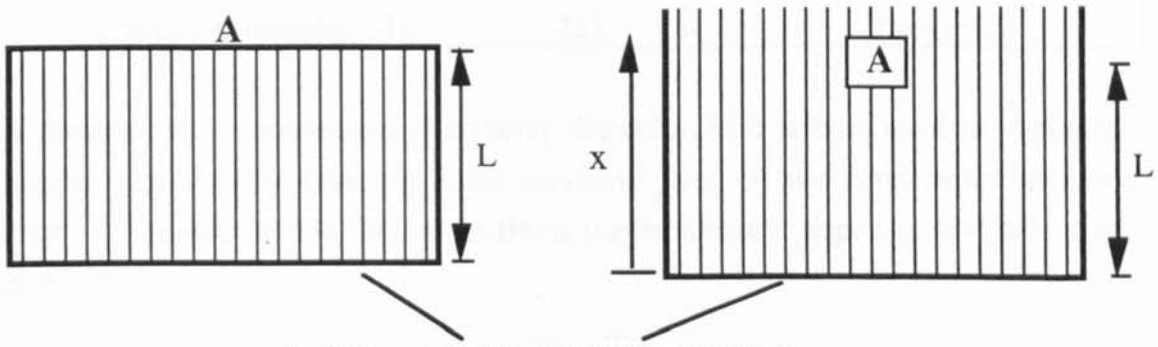

(a) Plate **(b) Semi-infinite solid**

Figure 9.2 Transient Heat Conduction Models

(a) Flat plate with the upper surface insulated, infinite in the horizontal and normal directions, and with L equal to the thickness of the particle as previously described in Figure 9.1.

(b) Semi-infinite (in the x direction indicated in Figure 9.1) block of solid wood, where A is at a distance equal to the thickness of the particle (L) from the heated surface.

The thermal diffusivity, α, is calculated using the data presented in Table 9.2 by Equation 9.1, where ρ is the specific density, λ is the thermal conductivity and C_p is the thermal heat capacity of the material.

$$\alpha = \frac{\lambda}{(\rho C_p)} \qquad (9.1)$$

Table 9.2 Data Used in the Estimation of the Heat Penetration Time for Pyrolysis

Specific density	497	kgm^{-3}	(measured)
Heat capacity	1380	$J\,K^{-1}kg^{-1}$	(Phillips, 1982)
Thermal conductivity	0.12	$Wm^{-2}s^{-1}$	(Phillips, 1982)
Thermal diffusivity	1.75×10^{-7}	m^2s^{-1}	(calculated)
Initial temperature, T_i	300	K	(measured)
External temperature, T_a	1323	K	(measured)
Pyrolysis temperature, T_p	723	K	(assumed)

A dimensionless temperature parameter (Equation 9.2) is then used to obtain the Fourier number (Fo) from the exact solutions given by the temperature response graphs (Schnieder, 1963). Equations fitting the temperature response curves are given in Appendix J2.

$$T = \frac{(T_p - T_i)}{(T_e - T_i)} \qquad (9.2)$$

T is the dimensionless temperature parameter, T_p is the temperature at which pyrolysis occurs, T_i is the initial temperature and T_e is the external temperature. A Fourier number of 0.3 is calculated using the data presented in Table 9.2. The time taken for the particle to reach the pyrolysis temperature is then calculated using the Fourier heat conduction equation (Equation 9.3).

$$\text{Time, seconds} = L^2 \frac{Fo}{\alpha} \qquad (9.3)$$

Results from the transient heat conduction calculations using the data given in Table 9.2 give a pyrolysis time of 53.1 seconds for case (a) and 128.6 seconds for case (b) for the base case feed size. From experimental mass flow velocities (calculated by Equation 9.4) for the open-core gasifier for the base case tests (Section 7.1), particles spend 55.5 ± 5.0 seconds within a 15 mm deep flaming pyrolysis zone (Section 7.3).

$$\text{Time in FP zone} = \frac{\text{Specific feed rate}}{\text{Bulk density x FP zone depth}} \qquad (9.4)$$

The result obtained experimentally is similar to that obtained using model (a), which was therefore chosen as the best method to model the effect of variables on the time required for pyrolysis. The result suggests that there is little heat lost from the upper surface of the particle during the pyrolysis process. The effect of initial, external and pyrolysis temperature on the time for pyrolysis is shown in Table 9.3. For the range of temperature variations shown in Table 9.3 there is a ±15% variation in the time to reach the pyrolysis temperature. It is concluded that given the measured initial and external temperatures, the assumed pyrolysis temperature of 450°C is sufficient to provide an estimation of the time required for pyrolysis.

Table 9.3 Effect of Temperature Variables on Pyrolysis Time

Particle thickness (L) = 5.52 mm

Temperature, K			Time to reach pyrolysis temperature, seconds
Initial	External	Pyrolysis	
300	1323	723	53.1
400	1323	723	45.5
300	1223	723	59.2
300	1423	723	48.6
300	1323	673	47.2
300	1323	773	59.8

Figure 9.3 shows the sensitivity of the transient heat conduction model to particle size (as defined in Section 9.3) using the data given in Table 9.2.

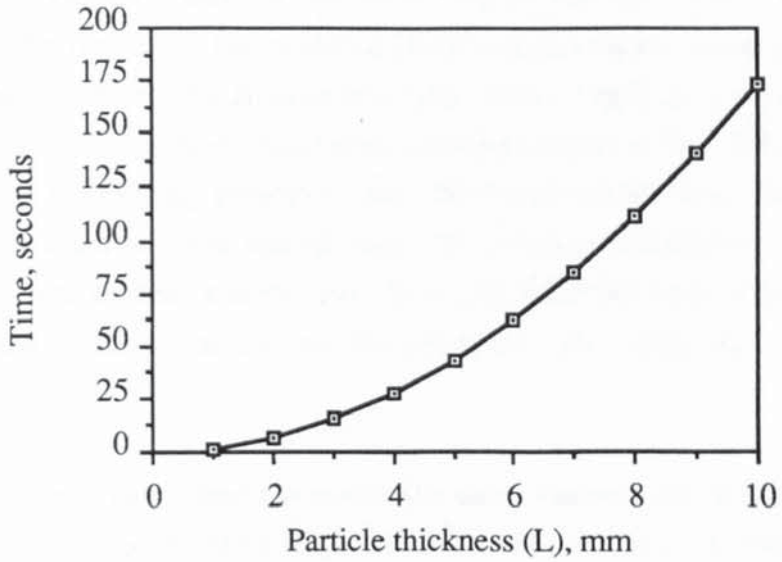

Figure 9.3 Predicted Pyrolysis Time as a Function of Particle Size

For the range of specific capacities obtained using the open-core gasifier under base case conditions (Section 7.1) and using a pyrolysis time of 53.1 seconds calculated by model (a), the depth of the flaming pyrolysis zone is calculated to be between 12.9 and 16.7 mm or 1.2-1.6 characteristic particle diameters (dp; see Section 4.3.7). The result agrees with the experimental observed flaming pyrolysis depth of 15 mm (see Section 7.3) for the base case feed. For the smaller feed size of 4.75-6.35 mm the pyrolysis time is 51.6 seconds, and the length of the flaming pyrolysis zone is calculated to 16.1 mm (equivalent to about 2.6 dp) for the specific feed rate measured during test 8 (Section 7). The similarity between the base case (6.35-12.7 mm) feed and the 4.75-6.35 mm feed is due to the similarity in particle thickness (see Table 4.4) since this is determined by the band sawing procedure (Section 4.2). For the smaller particle size heat transfer from the sides of the particle becomes more important and this would reduce the time required for pyrolysis. The observed flaming pyrolysis depth using the 4.75-6.35 mm feed size was about 10 mm which corresponds to a pyrolysis time of 32.2 seconds. The model presented uses a graphical solution of an infinite flat plate geometry and is therefore more applicable to larger particle sizes. For smaller sized particles errors will become significant.

9.4.3 Comparison with Other Models

Evans (1992) calculated the pyrolysis time using Reeds' modified Huff Equation (1983), which is based upon empirical relationships, to be 45.3 seconds for the 6.75-12.7 mm feed size (see Section 2.5.2). Using the characteristics of the feedstocks used in this research and a pyrolysis temperature of 600°C the pyrolysis time using Reeds' modified Huff equation was calculated to be 49.1 seconds for the 6.35-12.7 mm feed size, and 25.9 seconds for the 4.35-6.35 mm feed size. As previously mentioned in Section 2.5.2, the modified Huff equation under-estimates the time for pyrolysis, particularly for the smaller feed size. Reed (1988) used the modified Huff Equation and an assumed heat requirement during pyrolysis of 2000 $kJkg^{-1}$ to estimate the heat flux to the flaming pyrolysis zone. He found that the heat flux increased as the characteristic particle size was reduced. In the open-core gasifier there may be a limit for the rate of heat transfer which would limit the rate of pyrolysis, thus explaining the under-estimation of the pyrolysis time using the modified Huff equation.

Groeneveld (1980) calculated the minimum time required for pyrolysis using the Fourier heat conduction equation (Equation 9.3) with L equal to the particle diameter. His results were presented in Figure 2.5 (Section 2.5.2). Using the same Fourier number of 0.1 and thermal diffusivity of 2×10^{-7} m^2s^{-1} as Groeneveld and the characteristic diameters presented in Table 4.5 the time required for complete devolatilization is calculated to be 12.9 seconds for the 4.75-6.35 mm feed size, and

34.9 seconds for the 6.35-12.7 mm size. For both feed sizes the calculated pyrolysis time using the values used by Groeneveld is less than that observed during experimentation. As discussed in Section 2.5.2, Groeneveld does not state the external temperature to which the particle is exposed to or the temperature at which pyrolysis occurs. These factors are recognized in the calculation of the Fourier number described above. The differences in the calculated pyrolysis times are due to differences in the thermal diffusivity and Fourier number used by Groeneveld and those calculated here, and the use of the characteristic particle diameter by Groeneveld compared to the use of the particle thickness (L) in the calculations given here.

9.4.4 Oxidation of Pyrolysis Gases

The rate of oxidation of the primary pyrolysis gases is very rapid and is assumed to be instantaneous. The depth of the flaming pyrolysis zone is therefore identical to the length of reactor required for pyrolysis.

9.5 Flaming Pyrolysis Gas Composition Model

The gas composition leaving the flaming pyrolysis zone is required as an input for the char gasification zone model (Section 9.6). The model described below was developed for this purpose.

9.5.1 Model Assumptions

The composition of the gas leaving the flaming pyrolysis (FP) zone is calculated using the following assumptions:

(a) The feed composition is known and is represented as CH_aO_b. The composition of the feed used in the experimental programme was $CH_{1.46}O_{0.65}$ and this composition is used in the modelling studies. The nitrogen and ash content of the feed used in the experimental programme is less than 1% dry weight (see Table 4.2), and are assumed to be negligible. For feeds with a higher ash and nitrogen content (e.g. sewage sludge; see Table 4.2) this would lead to a considerable error. The application of the model is, therefore, limited to low ash (e.g. wood) feedstocks.

(b) The amount of char produced is assumed to be equal to the mass of the biomass material minus the volatile content. The actual amount of char produced will depend upon the heating rate and temperature (see Section 2.2.2); however, within the range of heating rates and temperatures expected under operational conditions within a gasifier little variation in the amount of char produced is expected. Particle size is also assumed to have no effect on the amount of char produced. The assumption is justified by the experimental analysis carried out after test 11 (see Section 7.3.4). The amount of char leaving the flaming pyrolysis zone was found to be approximately

equal to the fixed carbon content of the feed (see Table 4.3). The composition of the char is known by analysis (see Section 7.9.1).

(c) The amount of tar and methane exiting the flaming pyrolysis zone is assumed to be equal to the amount leaving the gasifier (i.e. there is no further degradation of tars in the gasification zone). Most of the tar cracking is thought to occur by oxidation within the flaming pyrolysis zone (Reed, 1988) and by thermal degradation at temperatures above 1000°C (see Section 2.6.1) which exist at the end of the flaming pyrolysis zone (although no data on the amount of tar entering the gasification zone was found in the literature). The amount of tar cracked within the gasification zone is, therefore, likely to be small and the error in the assumption is considered to be negligible. The tar composition is known by analysis (Section 7.9.2).

(d) The gases leaving the flaming pyrolysis zone are in water-gas shift equilibrium at the temperature existing at the bottom of the zone. The temperature at the base of the flaming pyrolysis zone corresponds to the maximum temperature in the reactor bed, which is justified by the experimental temperature profiles conducted (see Figures 7.4 and 7.15)

(e) The heat loss from the flaming pyrolysis zone is known. Experimental temperature profiles (Appendix G1) have been used to estimate the amount of heat lost by the gasifier above the interface between the flaming pyrolysis zone and the gasification zone (discussed in Section 9.5.2).

C, H, O and N elemental molar balances over the flaming pyrolysis zone are carried out over the flaming pyrolysis zone according to Equations 9.6-9.9, with the overall stoichiometry given in Equation 9.5. The energy balance is given in Equation 9.10.

$$CH_aO_b + W\,H_2O + A(0.79\,N_2 + 0.21\,O_2) = c(CH_{char}O_{char}) + t(CH_{tar}O_{tar}) + mCH_4 + qH_2O + xCO_2 + yCO + zH_2 + A(0.79N_2) \quad (9.5)$$

where:

W = water, mol mol^{-1} (daf feed)
c = char, mol mol^{-1} (daf feed)
t = tar, mol mol^{-1} (daf feed)
A = air, mol mol^{-1} (daf feed)

and m, q, x, y, z are the mol mol^{-1} (daf feed) of CH_4, H_2O, CO_2, CO, H_2 respectively.

Carbon Balance

$$1 = c + T + m + x + y \qquad (9.6)$$

Hydrogen Balance

$$a + 2W = c(char_H) + t(tar_H) + 4m + 2q + 2z \qquad (9.7)$$

Oxygen Balance

$$b + W + 2(0.21)A = c(char_O) + t(tar_O) + q + 2x + y \qquad (9.8)$$

Nitrogen Balance

$$2(0.79)A = 2(0.79)A \qquad (9.9)$$

Energy Balance

$$H_cFeed = H_cc + H_ct + H_cGas + H_sc + H_st + H_sGas + q \qquad (9.10)$$

where H_c = HHV, H_S = sensible heat.

At the reaction temperature the equilibrium constant for the water gas shift reaction (Equation 2.6) is calculated using the temperature dependency function given in Appendix J3.1. The equilibrium constant K is given by;

$$K = \frac{zy}{qx} \qquad (9.11)$$

The system of Equations 9.6-9.11 is then solved by an iterative search technique.

9.5.2 Calculated Composition of the Gas Leaving the Flaming Pyrolysis Zone

The calculated flaming pyrolysis gas compositions using base case feed for the uninsulated and insulated gasifier are presented in Table 9.4. The heat loss from the flaming pyrolysis zone is estimated to be about 48% of the total heat loss based on the external temperature profiles obtained (see Appendix G1). The amount of heat loss from the flaming pyrolysis zone seems quite high, which is believed to be due to the conduction of heat upwards along the reactor wall from the hottest region of the gasifier (i.e. at the start of the gasification zone). The average heat loss from the uninsulated and insulated open-core reactors (Table 7.7) was used in the calculations despite any error this may involve (see Section 7.5.2).

Table 9.4 Calculated Flaming Pyrolysis Gas Compositions

Input feed = $CH_{1.46}O_{0.65}$, 16.8 % fixed carbon, 10% moisture wet basis

	Uninsulated Gasifier	Insulated Gasifier
Air/feed ratio	2.87 (Test 13.2)	2.42 (Test 13.1)
Heat loss from FP zone	13.4	5.8
Gas composition, % volume		
H_2	3.1	5.0
CO	4.1	6.9
CO_2	14.6	13.5
CH_4	1.5	1.9
H_2O	20.4	20.2
N_2	56.3	52.4
Maximum temperature, °C	1022	1077
Tar (assumed), % weight daf feed	1.00	1.00

The effect of the air to feed ratio on the composition of the gas leaving the flaming pyrolysis zone is shown in Figure 9.4. As expected, increasing the air to feed ratio results in a greater proportion of combustion products (water and carbon dioxide).

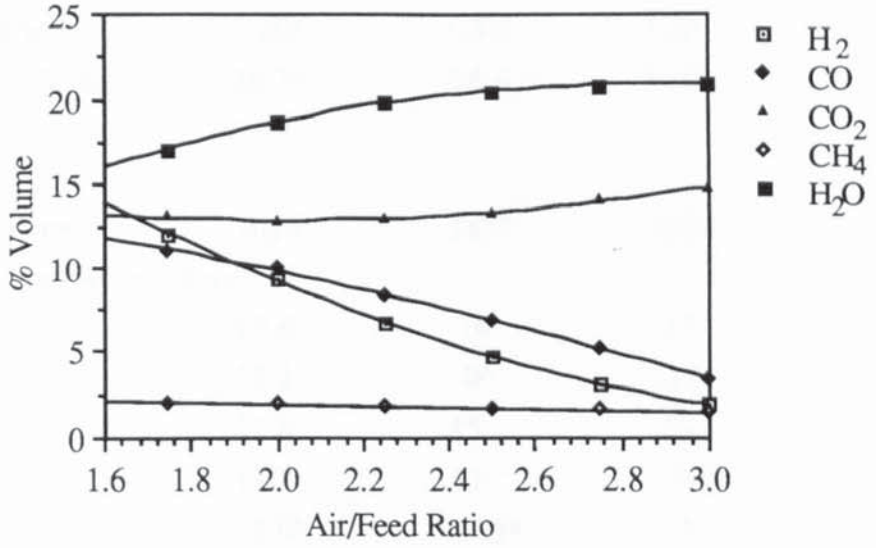

Figure 9.4 Calculated Gas Composition Leaving the Flaming Pyrolysis Zone as a Function of the Air to Feed Ratio

9.5.3 Comparison with Models in the Literature

Chen (1987) developed a gasifier model to predict the gas composition and temperature at the end of the oxidation zone using mass and energy balances. He assumed that the concentration of CO and H_2 were negligible at the end of the oxidation zone, and the methane and hydrocarbon output were assumed to be 2.5%

and 1.5 % respectively. His assumption that the CO and H_2 content of the flaming pyrolysis gas are negligible is considered to be an over-simplification since these gases are usually present (Reed, 1983) and would form by the water gas shift reaction (Equation 2.4) moving towards equilibrium at the predicted temperature. A typical gas composition prediction is given in Table 9.5 for a wood feedstock. The calculated temperature of the gases leaving the flaming pyrolysis zone is much greater than that measured during this research (see Figure 7.13) and by other workers (Evans, 1992; Reed, 1988; Walawender, 1987) for the open-core reactor (see Section 2.5.2); however, Groeneveld (1980) argues that temperatures may be as high as 1600°C. The high temperature obtained by Chen is probably due to his assumption of negligible CO and H_2 production which would result in a lower amount of chemical energy in the gas and therefore a higher sensible heat content for the gas in order to obtain a heat balance.

Table 9.5 Comparison of Predicted Flaming Pyrolysis Gas Compositions with Models from the Literature

	FP gas model	Chen (1987)	Chern (1988)	Evans (1992)
Moisture, % db	10[i]	10[i]	10[i]	0 (excluded)
Air/feed ratio	1.80[i]	1.82[i]	1.80[i]	2.74[e]
Char yield, % mass	16.7[e]	26.6	20.0[i]	12.2[e]
Tar yield, % mass	1.0[i]		-	1.0[a]
Zone exit temp. °C	1023	1477	1027	-
Wet gas composition, % vol*				
H_2	10.6	0[a]	13	19.5
CO	12.1	0[a]	13	16.2
CO_2	11.6	15	12	9.9[a]
H_2O	18.7	30	21	2.8
CH_4	2.0[b]	2.5[a]	0	0[a]
C_{2+}	-	1.5[a]	-	-
N_2	45.0	51	41	51.7

a = assumed, i = input variable, e = experimental, b = assumed yield of 3.5 kg per kg DAF, * = approximate values given for Chen (1987) and Chern (1988)

Chern (1989) used an equilibrium model to predict the char yield, gas composition and temperature at the end of the flaming pyrolysis zone. His model differs from that presented here since carbon deposition can take place increasing the char yield above the fixed carbon content of the feed. Chern points out that this provides a conceptual

means to account for incomplete devolatilization of the feed and that in reality carbon deposition is unlikely to occur. In addition, the char produced is assumed to be pure carbon, whereas the model given in this thesis uses the char composition determined by analysis. The predicted temperature (Table 9.5) is similar to those observed for the open-core reactor (see Figure 7.13). The FP gas model used here yields similar results to those of Chern.

Evans (1992) performed a theoretical mass balance over the flaming pyrolysis zone within an open-core gasifier to obtain a composition for the gas leaving the zone. He used experimental data for the char yield and equivalence ratio, and assumed a a tar yield of 1% mass, and a carbon dioxide yield of 0.35 moles per mole of dry ash free feed. His assumption for the carbon dioxide yield is invalid since the amount of carbon dioxide produced would certainly vary with changes in the air to feed ratio. Evans also failed to include the moisture content of the feed in his theoretical mass balance, which results in a calculated gas composition much lower in water content than that predicted by the models of Chen (1987), Chern (1988) or the FP gas model presented here.

9.5.4 Comparison of Predicted Flaming Pyrolysis Gas Compositions with Experimental Compositions in the Literature

Equation 2.30 (Reed, 1983) indicates a typical char yield of 20%, and a typical gas composition of 15% CO, 12% CO_2, 15% H_2, 8% water and 50% N_2. The predicted gas composition is similar to the typical composition given by Reed, with the exception of the water content which is predicted to be more than twice that given by Reed. However, Reed (1983) also points out that this may vary greatly according to the feed composition and moisture content. Reed neglected to indicate the feed composition and moisture content for the typical gas composition given (above). No experimental measurements of the flaming pyrolysis gas composition was found in the literature. No comparison between actual and predicted flaming pyrolysis gas compositions can therefore be made.

9.6 Char Gasification Zone Model

During stable operation there is no net change in the amount of char within the gasifier and the amount of char entering the gasification zone is equal to the amount produced in the flaming pyrolysis zone which has been discussed above. The amount of char leaving the gasifier with the product gas has been determined experimentally. The amount of char converted in the gasification zone can, therefore, be calculated. The depth of reactor bed required to achieve the calculated amount of conversion may be calculated if the temperature, mass transfer rates, kinetic parameters and decrease in

particle size and density with conversion are known. A step-wise model has been developed in order to estimate the depth of the gasification zone using the output data from the FP gas composition model described in Section 9.5. The char gasification zone model is based upon external mass transfer, internal mass transfer, reaction kinetics and mass and heat balances.

9.6.1 External Mass Transfer

The importance of mass transfer resistance is estimated for the process variables of temperature and particle size (see Section 2.4.1). Gas film diffusion of reactant gases is not expected to be rate limiting at operating temperatures of gasifiers (Buekens, 1985). The external mass transfer rate is expressed as;

$$\text{Mass Transfer Rate} = k_m \, \Delta C_g \, (\text{Area}) \qquad (9.12)$$

where k_m is the mass transfer coefficient, (Area) is the particle surface area and ΔC_g is the reactant concentration gradient between the surface and the bulk gas. The calculation of the mass transfer coefficient, k_m, is based upon the method given by Satterfield (1970) and is generally approved in the literature (e.g. Graboski 1979). The dimensionless group, j_D, is given by;

$$j_D = \frac{k_m \, \rho_m}{v} N_{Sc}^{2/3} \qquad (9.13)$$

and the correlation (Equation 9.14) is recommended for fixed bed operation (Satterfield, 1970).

$$\varepsilon j_D = \frac{0.357}{N_{Re}^{0.359}} \qquad \text{for } 3 < N_{Re} < 2000 \qquad (9.14)$$

where ρ_m is the molar density, v is the superficial gas velocity, N_{Sc} is the Schmidt number, ε is the bed voidage and N_{Re} is the Reynolds number. By combining Equations 9.13 and 9.14 the mass transfer coefficient can be estimated using Equation 9.15 (Graboski, 1979).

$$k_m = \frac{0.357 \, N_{Re}^{-0.359} \, (\rho_m \, v)}{\varepsilon N_{Sc}^{2/3}} \qquad (9.15)$$

A spreadsheet (Excel 2.2) was used to calculate k_m at various temperatures, gas flow rates and particle sizes (calculations given in Appendix J4). Results presented in Table 9.6 show the maximum gasification rate under mass transfer limitation given by Equation 9.12 per unit reactor volume. Particle size given is the length of a cubic particle.

Table 9.6 External Mass Transfer Limits of Gasification Reaction Rates

Temperature K	Particle size mm	k_m mol $m^{-2}s^{-1}$	Max. rate of char reaction, kmol $m^{-3}s^{-1}$
973	10	2.03	0.87
973	5	2.60	2.22
1373	10	2.27	0.97
1373	5	2.92	2.49
1573	10	2.39	1.02
1573	5	3.07	2.62

From Table 9.6 it is seen that temperature has a small effect on the external mass transfer rate. Smaller particles have a larger surface area to volume ratio than larger sized particles and this increases the amount of mass transfer per unit reactor volume as shown in Table 9.6. In a downdraft gasifier particle size can only decrease with conversion; therefore, it is assumed that if external mass transfer is non-limiting for the initial particle size then external mass transfer is non-limiting throughout the gasification zone. In Section 9.6.3 it will be shown that external mass transfer does not limit the rate of gasification for temperatures up to 1573 K.

9.6.2 Pore Diffusion

The rate of gasification may be limited by the mass transfer of reactant gases to the internal surface of the char by pore diffusion. Diffusion in a 20 μm pore is considered (see Section 9.3). The length of the pore is equal to the particle thickness as indicated in Figure 9.1. The reactant gas can, therefore, penetrate into the whole of the particle with reaction at the internal surface.

The diffusivity is calculated as a function of porosity, Equation 9.16. Knudsen diffusion (D_K) is calculated in Equation 9.17. The effective diffusivity (D_{eff}) is obtained from the approximation in Equation 9.18 (Satterfield, 1970).

$$D_{gas} = D\,\varepsilon_{char} \tag{9.16}$$

$$D_K = \frac{4}{3} r \sqrt{\frac{2RT}{\pi M}} \tag{9.17}$$

$$\frac{1}{D_{eff}} = \frac{1}{D_K} + \frac{1}{D_{gas}} \tag{9.18}$$

The effective diffusivity of carbon dioxide is plotted as a function of pore diameter in Figure 9.5 at 973 and 1273 K (i.e. the temperature range expected within the gasification zone, see Section 2.5.4). Figure 9.5 shows that diffusivity into the

particle decreases rapidly below a pore size of 2 μm, whilst above a pore size of about 5 μm the effect of Knudsen diffusion is negligible. Thus pore diffusion limitations become increasingly important to the rate of gasification below an approximate pore size of 5 μm. Accurate knowledge of the pore size distribution is, therefore, important for modelling studies which consider gasification taking place within the pore structure. The assumptions on the pore size of the char (see Section 9.3) may, if inaccurate, invalidate the results presented using the gasification zone model. At higher temperatures the effective diffusivity is increased; however, the increase is small compared to the increase in the intrinsic kinetic rate of the reaction (see Section 9.6.3).

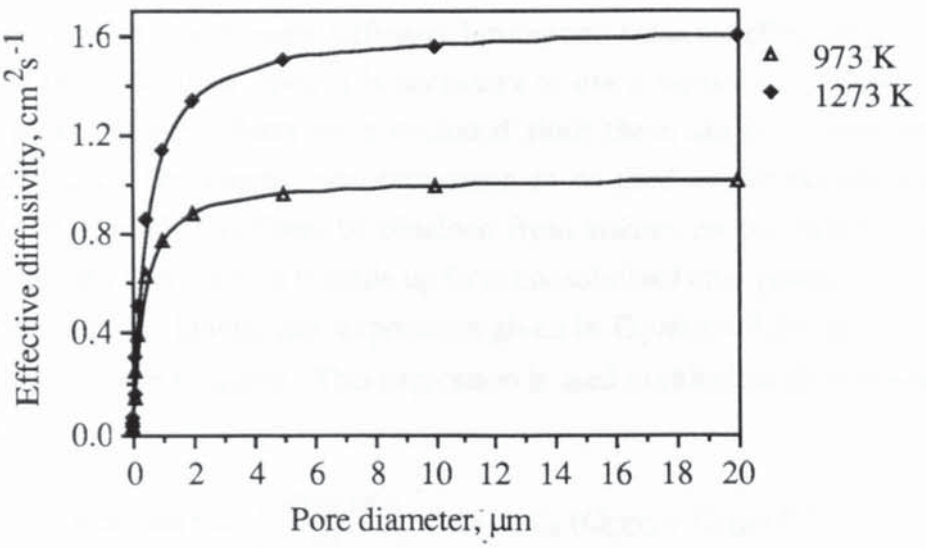

Figure 9.5 Effective Diffusivity of CO_2 as a Function of Pore Size

The effect of pore diffusion on the rate of gasification is determined by using the Thiele modulus. The Thiele modulus for a single pore is defined as (Petersen, 1965);

$$\text{Thiele modulus, } \phi = \sqrt{\frac{\text{Surface reaction rate}}{\text{diffusion rate}}} \qquad (9.19)$$

$$\phi = \sqrt{\frac{2\pi rLkC^n}{\pi r^2 D_{eff}(C/L)}} \qquad (9.20)$$

where r is the pore radius, L is the pore length, k is the intrinsic rate of reaction (see Section 9.6.3), C is the reactant concentration and n is the order of the reaction. For a first order reaction and a flat plate geometry the Thiele modulus is calculated using Equation 9.21 (Satterfield, 1970).

$$\phi = L\sqrt{\frac{k}{D_{eff}}} \qquad (9.21)$$

The Thiele modulus is used to calculate the effectiveness factor, η, using Equation 9.22 (Satterfield, 1970). The effectiveness factor is then used to calculate the effective gasification rate (Equation 9.23) from the char reaction rate obtained from kinetic calculations (Section 9.6.3).

$$\eta = \frac{\tanh \phi}{\phi} \tag{9.22}$$

$$\text{Effective rate} = \eta \text{ (Kinetic Rate)} \tag{9.23}$$

9.6.3 Reaction Kinetics

Some of the kinetic studies in the literature have been made using particles of a significant size in which pore diffusion limitations have an effect (e.g. Standish, 1988). In this modelling study it is necessary to use a kinetic expression in which internal mass transfer effects were excluded since these are calculated separately (Section 9.6.2). The kinetic rate expression to be used in the calculation of the reaction rate should, therefore, be obtained from studies on powdered char. It is assumed that the char particle is made up from consolidated char powder. Groeneveld (1980) obtained the kinetic rate expression given in Equation 9.24, for which mass transfer effects were excluded. This expression is used to calculate the intrinsic rate of reaction.

$$\text{Reaction rate } \left(\frac{-dchar}{dt}\right), -R = k\, C_s\, (C_{CO2} + C_{H2O})^{0.7} \tag{9.24}$$

where k is the rate constant given by;

$$k = A \exp\frac{-217100}{RT} \tag{9.25}$$

where Cs is the carbon concentration of the solid (mol m^{-3}), C_{CO2} and C_{H2O} are the concentration of CO_2 and H_2O in the gas stream (mol m^{-3}) and A is the pre-exponential factor and ranges from 10^6 to 10^7 $s^{-1}m^{2.1}mol^{-0.7}$ (Groeneveld, 1980), with a mid-range value of 5×10^6 used in the gasification zone model described here. The effective gasification rate is calculated using Equations 9.21-9.23 with the data listed below. It is assumed that the errors involved by using the first order solution (Equation 9.21) for the calculation of the effectiveness factor for a reaction order of 0.7 are negligible. The maximum error involved in this assumption has been estimated using the asymptotic solution for effectiveness factors given by Petersen (1965) to be about 8.5%. Errors are also believed to arise as a result of the pore size assumption (Section 9.3) as previously discussed (Section 9.6.2). The results are presented in Table 9.7, with the change in the effectiveness factor with temperature plotted in Figure 9.6.

Data Used in Calculation of Effective Gasification Rate

$A = 5 \times 10^6\ s^{-1}m^{2.1}mol^{-0.7}$

$Cs = 10000\ mol\ m^{-3}$, (specific density = $0.12\ gcm^{-3}$)

$(C_{CO2} + C_{H2O}) = 3.97\ mol\ m^{-3}$

Voidage = 0.5

Particle thickness = 0.055 m

Pore diameter = 20 μm

Table 9.7 Effectiveness Factors and Effective Gasification Rates

Temperature, K	Effectiveness Factor η	Effective Gasification Rate (per unit reactor volume) kmol $m^{-3}s^{-1}$
873	1.000	7.8×10^{-7}
973	0.997	1.6×10^{-4}
1073	0.974	1.7×10^{-3}
1173	0.857	0.0114
1273	0.585	0.0410
1373	0.330	0.1003
1473	0.189	0.1992
1573	0.142	0.3619

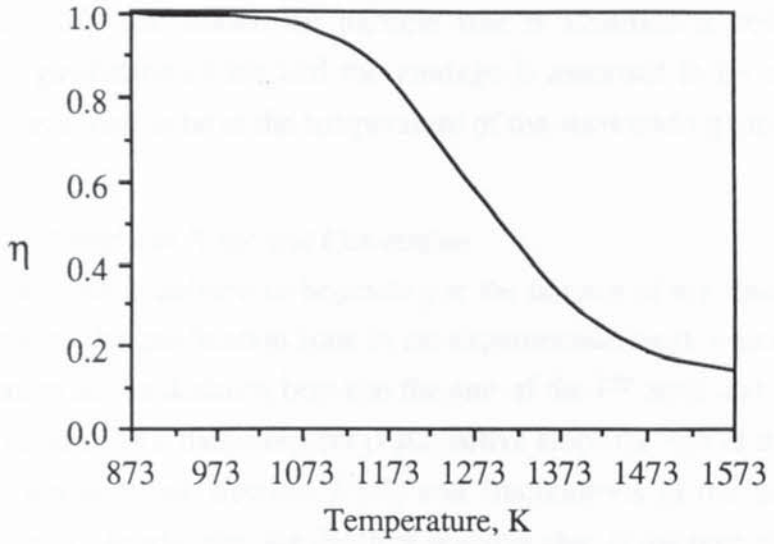

Figure 9.6 Effectiveness Factor (η) as a Function of Temperature

Figure 9.6 shows that internal diffusion becomes increasingly important above 1073 K. This agrees with the calculations carried out by Buekens (1985; see Section 2.4.3). The effective gasification rate at 1573 K is below the external mass transfer limit (see Section 9.6.1), so external mass transfer can be considered as non-limiting. (At 1573 K the gasification rate at the external surface is limited by external mass

transfer, however, as stated in Section 9.3 the external surface area is negligible to the internal surface area and can be ignored).

9.6.4 Particle Size Reduction with Conversion

The calculation of the char conversion profile within a downdraft gasifier is complicated by the change in particle size with conversion as a particle descends through the gasification zone. The reduction in particle size may be modelled by the loss of material below a minimum local carbon concentration (e.g. Groeneveld, 1980). The reduction in particle size reduces the particle velocity through the gasification zone and increases the amount of time spent at different temperatures, and therefore reduces the depth of bed required for complete gasification. At an effectiveness factor of 1 gasification occurs throughout the volume of a particle. As the effectiveness factor is reduced (i.e. at higher temperatures), the reactant gases are consumed before they diffuse further into the particle and gasification becomes increasingly confined to the outer regions of the particle. The reduction in particle size is therefore a function of temperature. The process is further complicated by the occurrence of voids immediately below the oxidation zone (see Sections 7.1 and 8.2) in the hottest part of the gasifier. Particles can fall through the voids reducing the residence time of the particle within the high temperature region. This may result in a greater depth of char being needed in order to maintain a stable reaction zone.

In order to simplify the model, the particle size is assumed to remain constant throughout the gasification zone and the voidage is assumed to be constant. The particle is also assumed to be at the temperature of the surrounding gases throughout its volume.

9.6.5 Char Residence Time and Conversion

The gasification zone is defined as beginning at the bottom of the flaming pyrolysis zone. The depth of the gasification zone in the experimental work was determined by visual observation as the distance between the end of the FP zone and the end of the glowing char region. This measurement is subjective since the end of the gasification is not sharply defined (see Section 7.3.1) and fluctuations in the position of the reaction zone occur. In addition, the depth of reactive char at the core of the reactor is believed to extend further than the depth of reactive char at the wall due to heat losses (see Section 8.2).

The gasification zone is treated as a succession of imaginary sub-zones of length l_g. The molar flowrate of char, tar and gases from the flaming pyrolysis zone are calculated from the FP gas model (see Section 9.5). The velocity of the char is

calculated in Equation 9.26, and the duration spent in each sub-zone is given by Equation 9.27;

$$\text{Char velocity} = \frac{\text{Specific molar flow rate of char}}{C_S\ \varepsilon} \qquad (9.26)$$

$$\text{Duration in sub-zone} = \frac{\text{Char velocity}}{l_g} \qquad (9.27)$$

where C_S is the carbon concentration within the particle and ε is the bed voidage. The degree of conversion within the sub-zone is then calculated using the effective reaction rate (Equation 9.23) at the temperature of the gases entering the sub-zone. The temperature and gas composition exiting the sub-zone are then calculated using the equilibrium model described in Section 9.6.7. The convective and radiative heat losses from each sub-zone are calculated in Equations 9.28-9.30;

$$q_{cg} = 1.18\ \pi\ d_r^{0.75}\ (T_g - T_{ref})^{1.25}.l_g \qquad (9.28)$$

$$q_{rg} = \pi\ d_r\ e\sigma\ (T_g^4 - T_{ref}^4)l_g \qquad (9.29)$$

$$\text{Heat loss from sub-zone, } q_g = q_{cg} + q_{rg} \qquad (9.30)$$

where q_{cg} and q_{rg} are the convective and radiative heat losses from sub-zone g of length l_g, d_r is the diameter of the reactor, T_g is the temperature of the sub-zone, T_{ref} is the temperature of the surroundings, e is the emissivity of charcoal (taken to be 1) and σ is the Stefan-Boltzman constant (5.67×10^{-12} $Wcm^{-2}K^{-4}$).

9.6.6 Simulation Profiles

Simulated gasification profiles were calculated using two scenarios, listed below. Three sub-zones 5.52 mm in length (l_g) were used, equivalent to the particle thickness used in the pyrolysis transient heat conduction model (see Section 9.4).

Simulation A: A heat loss of 5.8% from the FP zone. This is approximately equivalent to an overall heat loss of 12% from the gasifier from the experimental studies conducted; on this basis the heat loss from the FP zone is 48% of the total heat loss (see Section 9.5.2). The gas composition results are presented in Figure 9.7, the char conversion profile is presented in Figure 9.9 and the temperature profile presented in Figure 9.10.

Simulation B: No heat loss from the FP zone. The gas composition results are presented in Figure 9.8, with the char conversion profile presented in Figure 9.9 and the temperature profile presented in Figure 9.10.

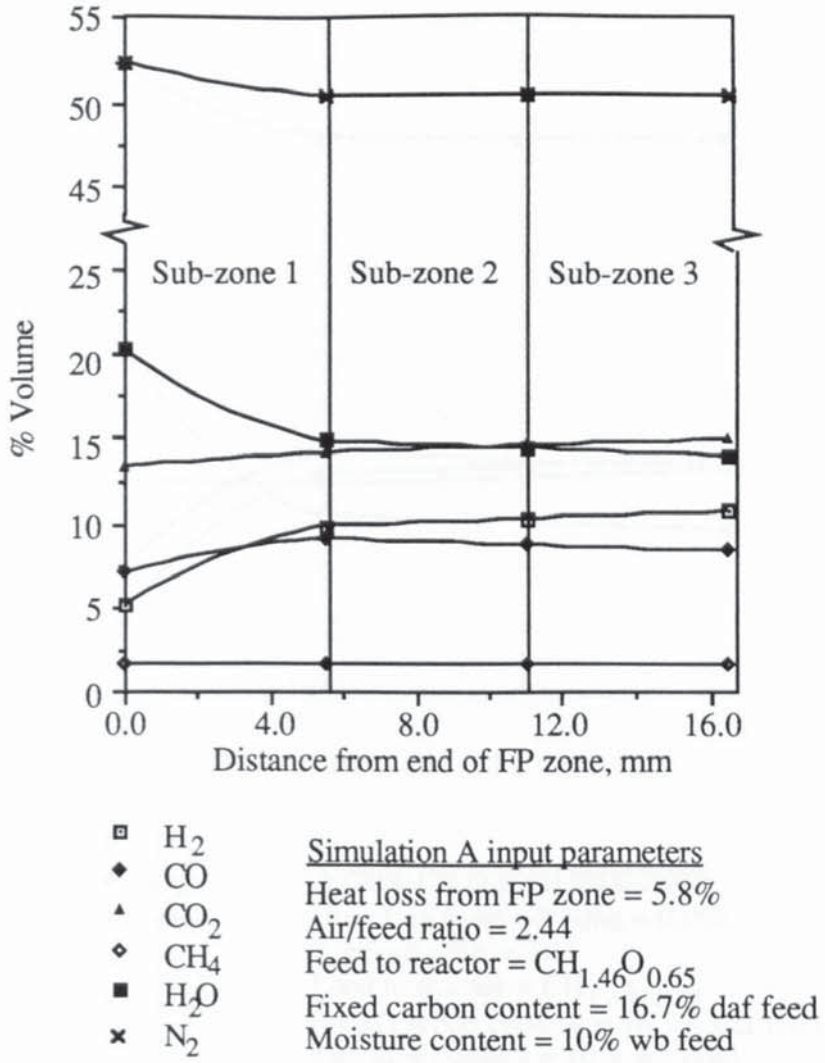

Figure 9.7 Calculated Gas Composition Profile for Simulation A (5.8% Heat Loss from FP Zone)

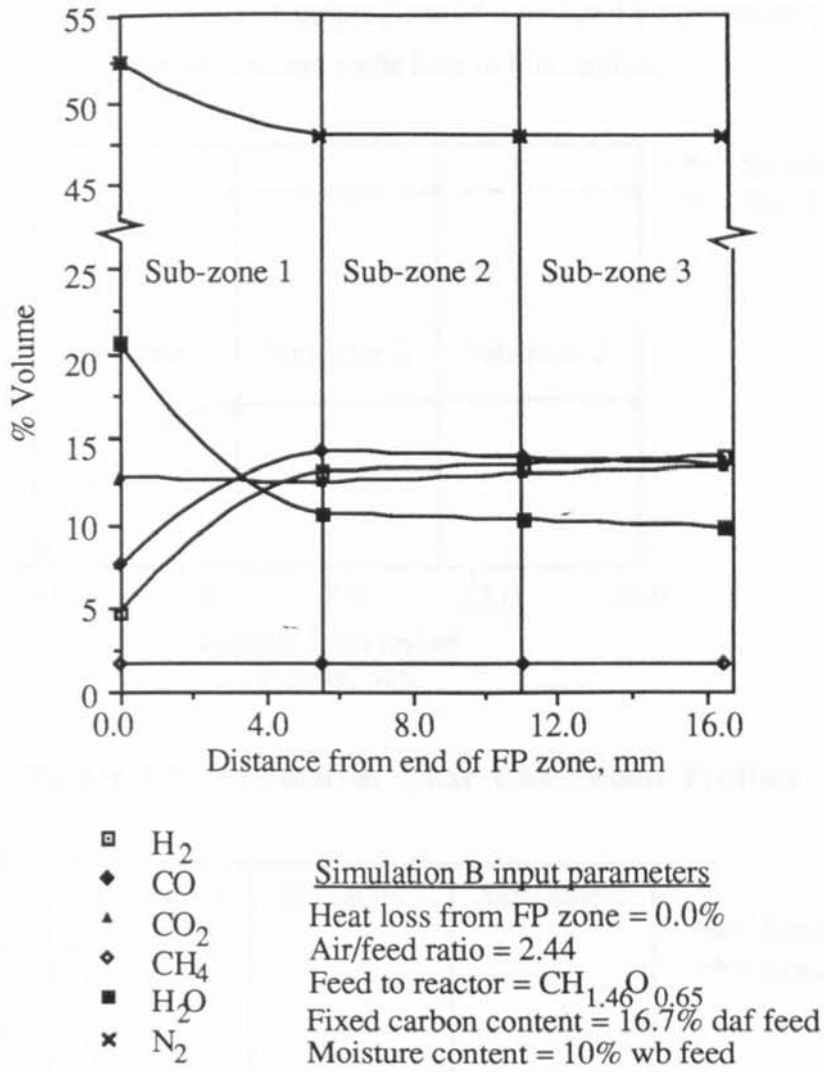

Figure 9.8 Calculated Gas Composition Profile for Simulation B (Zero Heat Loss from FP Zone)

Figures 9.7 and 9.8 both indicate that the gas composition changes rapidly within one particle width, and thereafter only slight changes occur. Figure 9.9 (below) shows that the degree of char conversion follows the same pattern. Simulation B has a final char conversion of about 90%, whilst in simulation A only about 35% of the char is converted. The differences in the two simulations are due to the temperatures at the top of the zone (see Figure 9.10). In simulation B with no heat losses from the FP zone the initial temperature is calculated to be about 1200°C at the start of the gasification zone (see Figure 9.10), whereas for simulation A the FP heat losses have resulted in an initial temperature of about 1075°C. This leads to a much faster conversion rate for simulation B. In both simulations it can be seen from Figure 9.10 that the temperature drops to about 800°C within the first sub-zone due to the amount of heat used by the endothermic char reactions and also by heat losses from the sub-zone. The rate of conversion is significantly reduced, thereby explaining the low amount of further conversion and the small amount of change in the gas composition

curves after the first sub-zone. Comparisons of simulated temperature profiles with experimental temperature profiles are made later in this section.

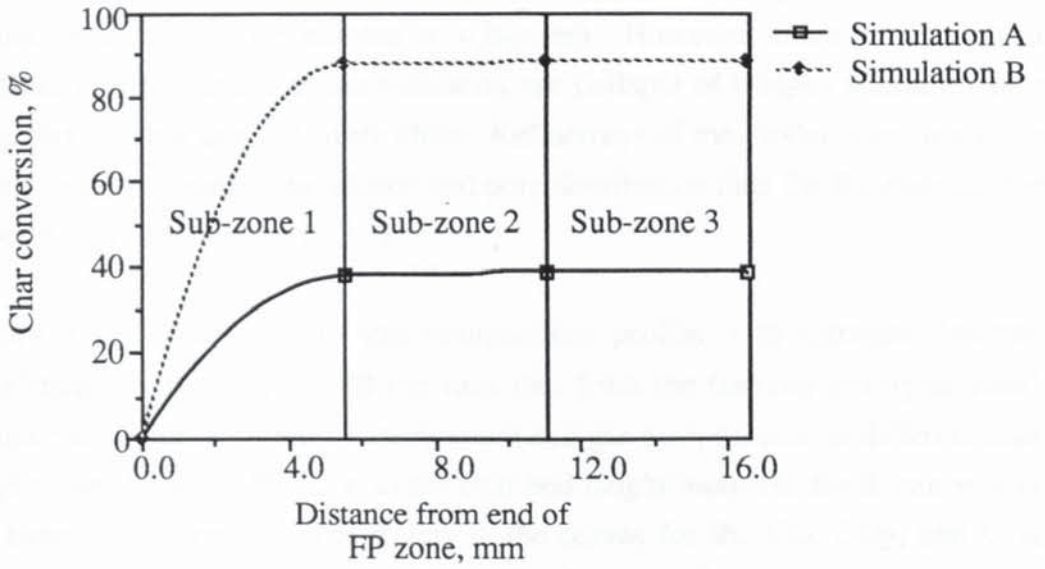

Figure 9.9 Simulation Char Conversion Profiles

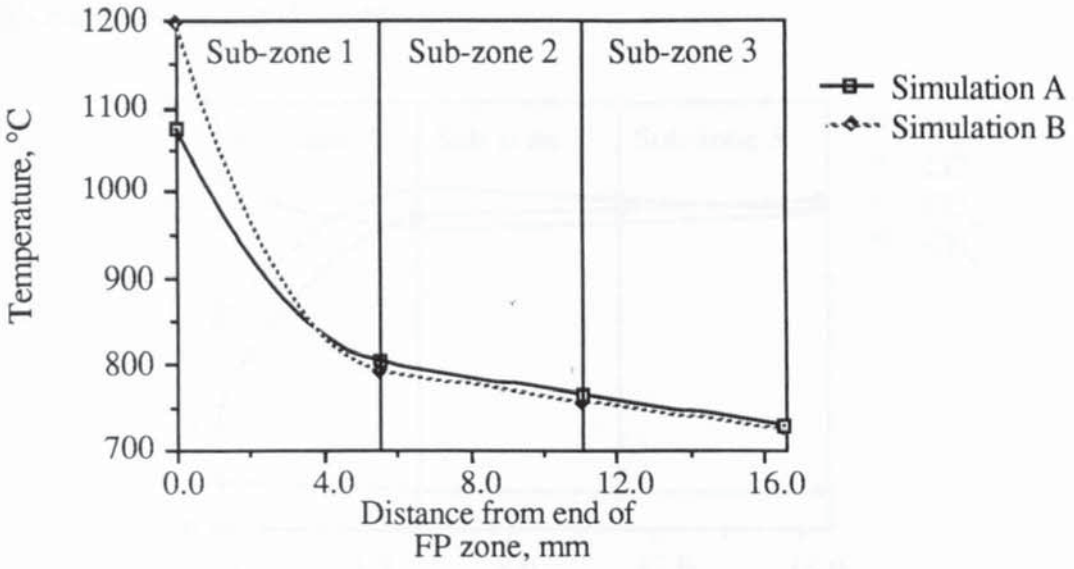

Figure 9.10 Simulation Temperature Profiles

The model indicates that most conversion occurs within a distance of three particle widths or 1.6 cm. This compares with to an observed gasification zone depth of 6-8 cm (Section 7.1.2). The disparity between the simulated and observed gasification zone depths may be due to: using an inaccurate kinetic expression (Equation 9.24); inaccuracies in the assumed pore size distribution (see Section 9.3); or errors in the estimation of heat losses from the flaming pyrolysis and gasification zones (Section 9.5.3, and Equations 9.28 and 9.29). The degree of conversion is sensitive to the degree of heat loss from the flaming pyrolysis zone (see Figure 9.9). The amount of

heat lost from the flaming pyrolysis zone is an input variable and an accurate description of the heat loss distribution would be required in order to model the gasifier adequately. The model may be made more accurate by reducing the length of l_g and by increasing the number of sub-zones. However, since the motion of the particles is irregular due to the formation and collapse of bridges within the reaction zone this was not thought worthwhile. Refinement of the model is recommended to begin with determining the kinetic and pore distribution data for the char used in the experiments (see Section 11.3.3).

Figure 9.11 shows the dry gas composition profile with nitrogen omitted for simplification of simulation B (no heat loss from the flaming pyrolysis zone). A comparison is made with the experimental exit gas compositions at different char bed heights (see Figure 7.6), since as the char bed height increases the distance from the FP zone also increases. The trends in the curves for the CO, CO_2, and CH_4 gas compositions are similar for both the simulation and experimental results. The proportion of H_2 increases with distance from the FP zone in the simulation, whilst the opposite effect was obtained from the experimental results with decreasing H_2 content with increasing char bed height.

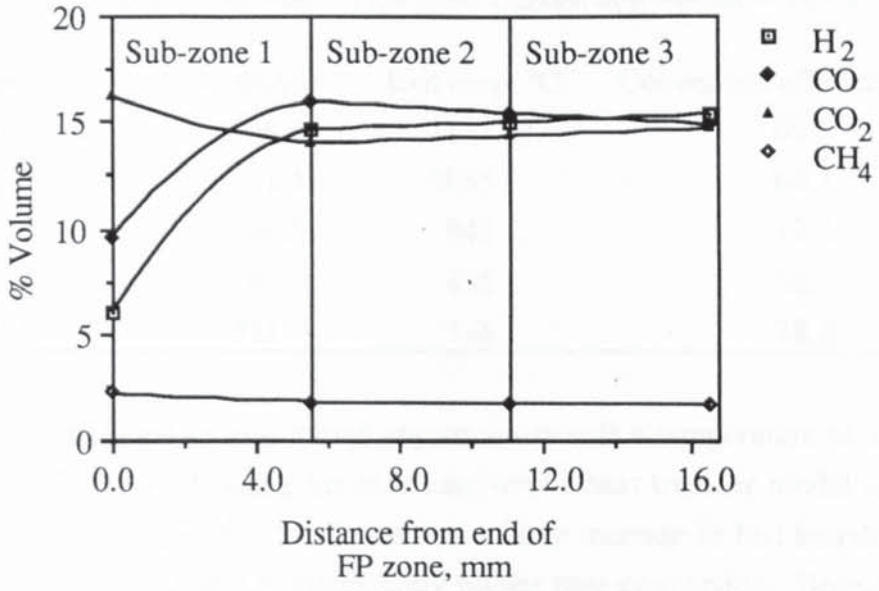

Figure 9.11 Dry Gas Composition Profile for Simulation B

A comparison of the simulated temperature profiles obtained (see Figure 9.10) with the experimental profiles previously presented in Figures 7.2 and 7.14 is difficult to make since temperature measurements in the experimental profiles were taken at 2 cm intervals. Figures 7.2 and 7.14, however, indicate that the reduction in temperature with depth is greatest within the first half of the gasification zone; thereafter, the rate of temperature reduction decreases until near the grate. This is in general agreement with

the simulated results. The greater rate of temperature reduction close to the grate in the experimental results may be explained by heat losses through the base of the reactor via the grate and reactor collar.

9.6.7 Simulation Models in the Literature

Groeneveld (1980) developed a co-current moving bed gasifier simulation model in order to calculate reactor dimensions as a function of the characteristics of the feed. For about 95% conversion his model gives a reactor length of about 3.5 cm for 5 mm diameter particles, and a length of about 6 cm for 12.4 mm particles with no heat losses from the reactor. Heat losses increased the length of reactor required. The air to feed ratio had a significant effect upon the calculated reactor length (see Table 9.8). As the air to feed ratio increases the depth of the gasification zone required decreases. Groeneveld (1980) suggests that a reactor length of 50 cm would be sufficient under practical conditions.

Table 9.8 Influence of Air to Feed Ratio on the Calculated Depth of the Char Gasification Zone Required (after Groeneveld, 1980)

Reed (1988) predicted an asymptotic approach towards a temperature of about 800-850°C, (see Figure 9.12) using his char carryover - heat transfer model of the char gasification zone. Figure 9.12 indicates that a large increase in bed length would be required in order to achieve a significantly higher char conversion. Because of this, Reed (1988) arbitrary chooses a reaction time of 100 seconds for char gasification in order to calculate the depth of gasification zone required using Equation 9.27;

$$\text{Gasification zone depth (cm)} = \text{Feed velocity (cm s}^{-1}\text{)} \times 100 \text{ (s)} \quad (9.27)$$

For 25 x 20 x 6 mm pine wood chips and a feed velocity of 0.26 cm s^{-1}, Reed calculates a reaction zone depth of 25.8 cm.

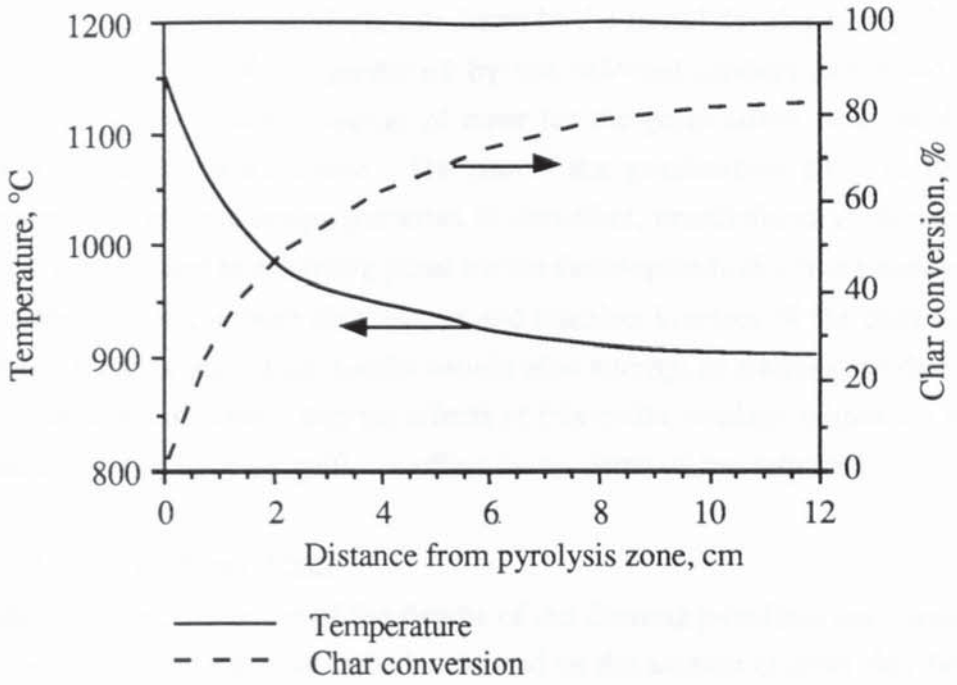

Figure 9.12 Gas Temperature and Char Conversion Profiles Predicted by Reed's Char Carryover - Heat Transfer Model

Reed's use of the feed velocity does not take into account the effects of particle size reduction with conversion or of changes in bed voidage within the gasifier. The simulated profiles given in Figure 9.12 are similar in shape to those presented in Figures 9.9 and 9.10 using the model developed during this research. However, in the simulation model presented here the asymptotes are achieved within a much shorter distance.

Manurung (1993) developed a chemical reaction engineering model based upon mass and energy balances, chemical reaction kinetics, heat and mass transfer rates and fundamental thermodynamic relations. The model was used to predict rice husk gasification profiles for different char bed heights. Good agreement between experimental and simulated data were achieved. Heat loss from the reactor was found to have a large effect on gasifier performance, and led to a reduction in char conversion and lower thermal efficiencies. Increasing the height of the char bed from 50 to 75 cm was found to slightly improve the gas heating value and char conversion efficiency. For a bed height of 50 cm the model predicts a specific capacity of 180-200 $kgm^{-2}h^{-1}$ for the optimum energy efficiency whilst for a 75 cm bed height a specific capacity of 130-150 $kgm^{-2}h^{-1}$ is predicted. The simulation model indicates that optimum performance is a function of specific capacity and char bed height. It is not clear from the paper how the air to feed ratio used in the simulations varies as a function of the capacity. Manurung does not suggest the minimum depth required for the gasification zone.

The gasification reaction zone depth calculated by the model developed here is at least ten times shorter than those predicted by the selected models described above. Explanations of the possible sources of error for the gasification zone model were discussed in Section 9.6.6.above. The use of the gasification zone model in its present form for reactor design purposes is, therefore, unsatisfactory. Nevertheless the model can be used as a starting point for the development of a more sophisticated model after data on the pore distribution and reaction kinetics of the char has been obtained. Development of the model should also attempt to address the decrease in particle size with conversion and the affects of this on the voidage within the reaction zone since this may have a significant effect on the depth of bed required.

9.7 Depth of Inert Char

In addition to the calculation of the depths of the flaming pyrolysis and gasification zones, the height of the reactor will also depend on the amount of inert char bed. The inert char zone is important since it acts as a buffer to fluctuations in the position of the reaction zone within the gasifier. It may also adsorb tars to give a cleaner product gas as discussed in Section 7.4. However, as the height of inert char increases the pressure drop across the gasifier also increases which may cause difficulties in obtaining the required air flow rate into the reactor in order to maintain a stable reaction zone. In addition, the heat loss from the reactor will increase as the char bed height is increased which will reduce the energy content (as sensible heat) of the gas. In Section 7.4.2 it was suggested that a char bed height of about 10 cm provided the optimum energy conversion efficiency using the base case feed. This is about 10 characteristic particle diameters (dp). Generally, no operational problems were encountered as a result of pressure drop across the gasifier with char bed heights under 25 cm (see Chapter 5). It is, therefore, recommended that an inert char bed height of about 10 dp would be satisfactory in most applications. This would allow fluctuations of 5 dp in the height of the reaction zone above the grate to be absorbed by the inert char zone without adversely affecting gasifier performance.

9.8 Equilibrium Model

In equilibrium modelling the output stream is assumed to reach equilibrium at the gas exit temperature allowing prediction of the product gas composition. The equilibrium approach to modelling is made possible at a sufficient residence time of the char in the high temperature reaction zone (Chern, 1985); however, there is the possibility that equilibrium will not be attained due to the kinetic rates of the reactions involved (discussed in Section 2.4). The feed composition, moisture content, air to feed ratio and gasifier heat loss are usually the input parameters used in equilibrium modelling.

9.8.1 Modelling Assumptions

The gasification equilibrium model used here to predict the outlet gas composition is similar to that described in Section 9.5 for the prediction of the composition of the gas from the flaming pyrolysis zones. The assumptions are;

(a) The feed composition is known and is represented as CH_aO_b; the nitrogen and ash content of the feed are assumed to be negligible (see Section 9.5, assumption (a)).

(b) The amount of char leaving the gasifier (or accumulated within the gasifier) is known (see Appendix G1). The composition of the char is assumed to be the same as that found experimentally (Section 7.9.2).

(c) The amount of tar exiting the gasification zone is known (Appendix G1). The tar composition is assumed to be the same as that found experimentally (Section 7.9.1).

(d) The amount of methane produced is known (Appendix G1). Methane producing reactions (Table 2.1) are slow since they are multi-molecular and, therefore, can be neglected.

(e) The gases leaving the gasification zone are in water-gas shift equilibrium at the predicted exit temperature from the zone.

(f) The heat losses from the reactor are known.

The elemental balances (Equations 9.2-9.5) are used along with the energy balance (Equation 9.23) for the gasifier. The water gas shift reaction equilibrium constant was previously given in Equation 9.7. The system of equations 9.3-5, 9.7 and 9.28 are then solved by a two dimensional iterative search to obtain the exit temperature and outlet gas composition.

$$H_cFeed = H_cc + H_ct + H_cGas + H_sc + H_st + H_sGas + q \qquad (9.28)$$

where;

H_c = heating value
H_s = sensible heat

Other workers have developed equilibrium models for downdraft gasifiers that are based upon similar assumptions to those used here. For example, Chern (1988) calculates the gas composition from mass and energy balances and thermodynamic equilibrium of the char and wet gas at the predicted outlet temperature. As the method

is similar to that used in the prediction of the flaming pyrolysis gas composition (see Section 9.5.3), further comparisons are unnecessary.

9.8.2 Predicted Effect of the Air to Feed Ratio on Gasifier Performance

The gasifier equilibrium model has been used to predict the effects of varying the air to feed ratio. The predicted output gas composition (using the input parameter values listed below) are presented in Figure 9.13 as a function of the air to feed ratio. The predicted exit temperature from the gasifier are shown in Figure 9.14. The results from the model (giving the effect of the air to feed ratio) cannot be directly compared to the experimental results obtained due to the variation in the estimated heat losses (see Appendix G1 and Section 7.5.2). The model is directly compared to the experimental results in the following section using the experimental measurements obtained as the input parameters in the model (see Section 9.7.3).

Input Parameters to Gasifier Equilibrium Model (Effect of Air to Feed Ratio)

Input feed composition = $CH_{1.46}O_{0.65}$

Feed moisture content = 10% wet basis

Heat loss = 10% of feed energy input

Methane yield = 3.5% weight daf feed

Char yield = 0% weight daf feed

Tar yield = 1% weight daf feed

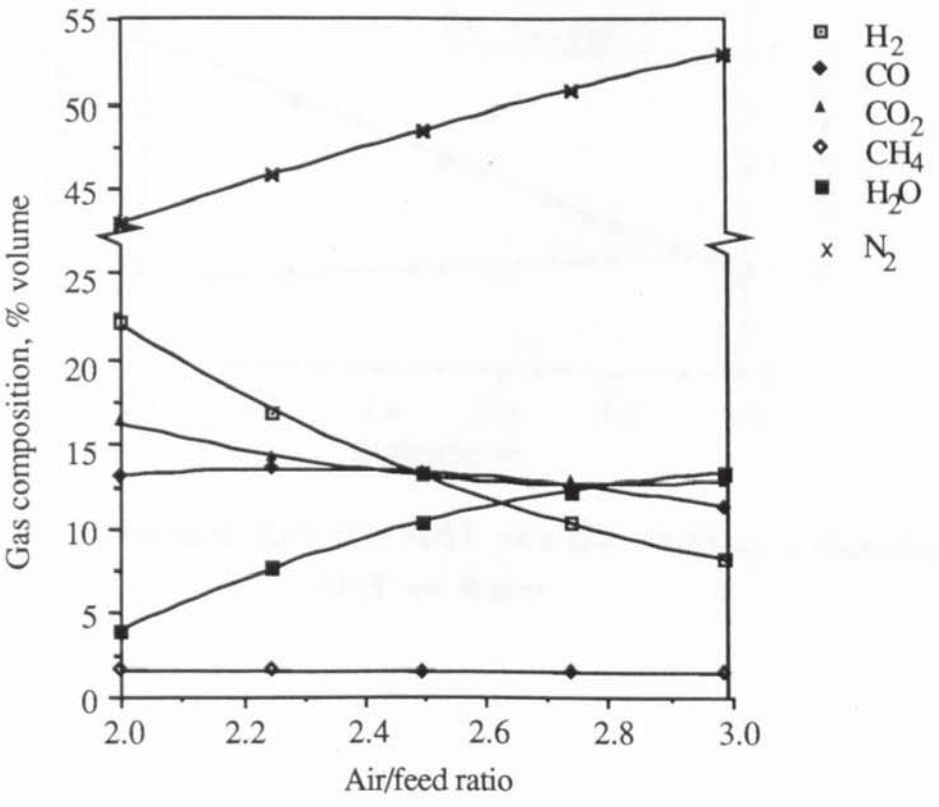

Figure 9.13 Calculated Gas Compositions as a Function of Air/Feed Ratio

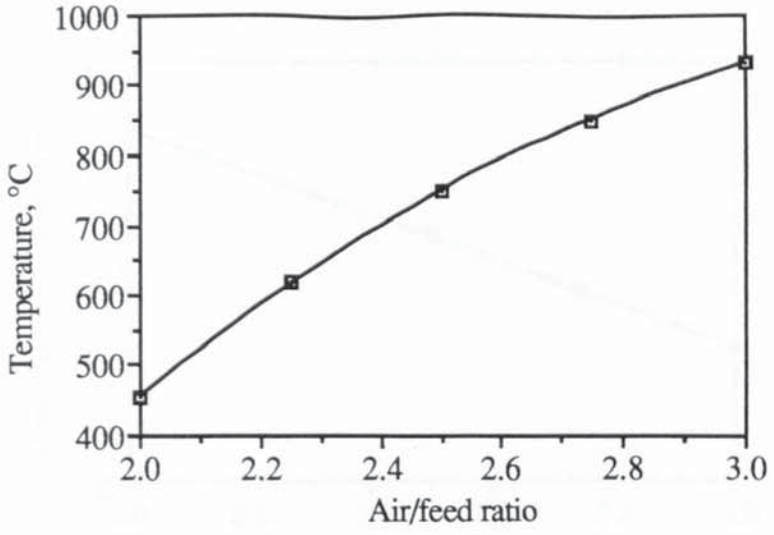

Figure 9.14 Calculated Gasifier Exit Temperature as a Function of Air/Feed Ratio

Increasing the air to feed ratio from 2 to 3 decreases the proportion of H_2 and CO in the product gas. This results in the decrease in the product gas heating value from 5 to 3 $MJNm^{-3}$ (see Figure 9.15). The cold gas conversion efficiency also decreases from 74 to 55% (Figure 9.16).

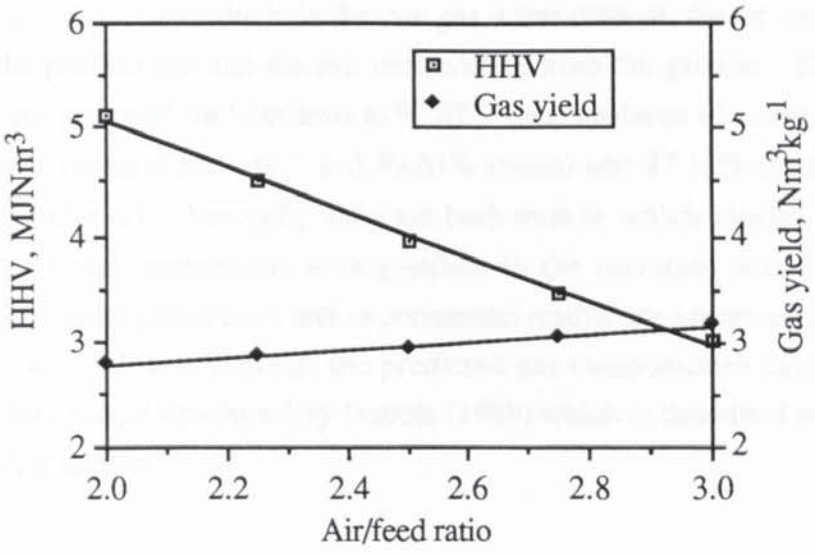

Figure 9.15 Calculated Raw Gas HHV and Gas Yield as a Function of Air/Feed Ratio

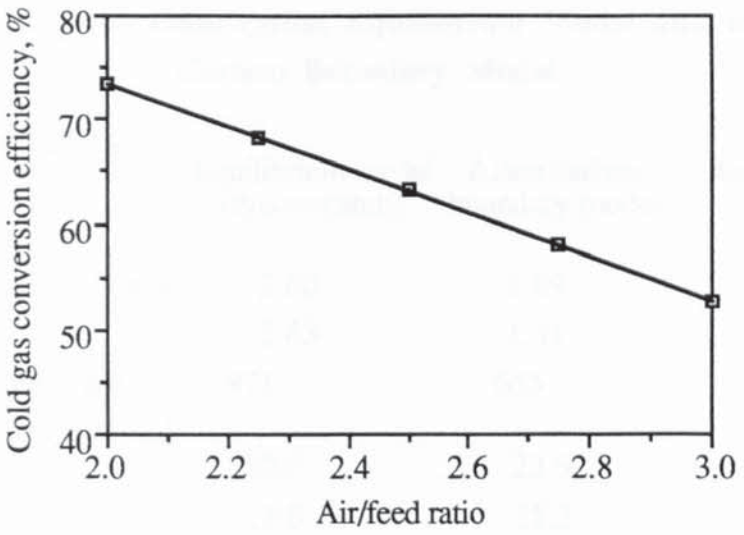

Figure 9.16 Calculated Cold Gas Conversion Efficiency as a Function of Air/Feed Ratio

9.8.3 Comparison with Experimental Results

The experimental results obtained for test 7 and test T11 are compared with the predicted results from the equilibrium model used in this research. These tests were selected for comparison for two reasons. Firstly, the results obtained during these tests are complete since they include the raw gas water content, the tar and particulate contents of the product gas and the exit temperature from the gasifier. The mass and energy balances are good for both tests at 97.27% (mass balance closure) and 99.99% (energy balance closure) for test 7, and 99.61% (mass) and 97.12% (energy) for test T11 (see Appendix G1). Secondly, they are both tests in which insulation was used which enables better comparison with gasifiers in the literature which are usually insulated. The model predictions and experimental results are presented in Table 9.9. In addition, Table 9.9 also presents the predicted gas compositions using the Aston carbon boundary model developed by Double (1988) which is described and discussed in the following section.

Table 9.9 Comparison of Experimental Test Data with Predicted Results Using the Gasification Equilibrium Model and the Aston Carbon Boundary Model

	Equilibrium model (this research)	Aston carbon boundary model	Experimental results
Test 7: Insulated open-core			
Gas volumetric yield, Nm^3kg^{-1}	3.00	1.89	3.03
Air/feed ratio	2.63	1.31	2.63
Gasifier exit temperature, °C	971	655	702
Dry gas composition, % vol.			
H_2	12.0	22.9	13.1
CO	17.0	21.3	21.7
CO_2	12.8	11.9	8.9
CH_4	1.8	1.1	1.7
N_2	56.3	42.8	54.6
Raw gas water content, % vol.	12.8	6.0	6.6
Gas HHV, $MJNm^{-3}$	4.39	6.05	5.09
Cold gas efficiency, %	63.5	76.1	77.6
Test T11: Insulated hybrid-throated			
Gas volumetric yield, Nm^3kg^{-1}	2.81	1.94	2.72
Air/feed ratio	2.11	1.42	2.11
Gasifier exit temperature, °C	609	649	669
Dry gas composition, % vol.			
H_2	19.1	21.4	16.8
CO	18.3	20.0	19.7
CO_2	13.4	12.4	12.3
CH_4	1.9	1.1	2.0
N_2	47.2	45.1	49.3
Raw gas water content, % vol.	7.3	6.0	6.6
Gas HHV, $MJNm^{-3}$	5.50	5.69	5.41
Cold gas efficiency, %	76.4	73.2	79.0

For test 7 the model predicts 4.7% less CO and 3.9% more CO_2 than found experimentally. This may indicate that a equilibrium has not been achieved. However, since the predicted exit gas temperature is 269°C higher than the experimental result it is likely that the heat losses from the experimental reactor are higher than that measured (1.87%). A higher heat loss from the model would result in a reduction in the exit temperature of the gas and consequently alters the equilibrium

gas composition. This point illustrates the importance of obtaining accurate heat loss data when comparing gasification systems.

The predicted gas composition for test T11 is fairly similar to that found experimentally with a maximum difference of 2.3% (H_2) in the values. This indicates that the experimental measurements used as input data to the model are more accurate than the example described above. The model gives a satisfactory prediction of the product gas heating value to within 2% and the predicted energy conversion efficiency is within 2.6% of the experimental value for test T11.

9.8.4 The Aston Carbon Boundary Model

The Aston carbon boundary model predicts the equilibrium gas composition at the carbon boundary. At the carbon boundary the consumption of char by gasification is equal to the amount produced by pyrolysis, with no char accumulation within the reactor or char outflow from the reactor. The model uses the minimum oxidant requirement in order to gasify the material. As a consequence, the model predicts the gas composition for optimum operation. Table 9.9 compares the predictions from the model with the predictions using the equilibrium model presented in this thesis, and with experimental results obtained for tests 7 and T11.

The results for test 7 show that the carbon boundary model predicts a significantly lower air to feed ratio than that obtained during the experiment. This results in a lower predicted nitrogen content of 42.8% by the carbon boundary model compared to the predicted value of 56.3% using the gasification equilibrium model, and also to the experimental result (54.6% nitrogen). The gas has a higher energy content than that predicted using the gasification equilibrium model and that obtained experimentally. The Aston carbon boundary model indicates that the gasifier is operating at a higher air to feed ratio than is required. The high air to feed ratio may be necessary in order to maintain a stationary reaction zone by increasing the temperatures within the zone, thereby increasing the rate of the char gasification to equal the rate of char production. The under-estimation of the heat loss from the reactor during test 7 (discussed in Section 9.7.3) would invalidate the comparison between the carbon boundary model predictions and the experimental results.

The carbon boundary prediction for test T11 are similar to those predicted by the equilibrium model developed in this work and to the experimental results. The predicted air to feed ratio is lower than that obtained during the experiment and this results in a slightly lower nitrogen content and a slightly higher energy content in the product gas.

The Aston carbon boundary model assumes that all the carbon in the feedstock is converted to gas. The equilibrium model presented here allows the char and tar outflows from the gasifier to be included as an input variable, which affects the predicted product gas composition. In addition, the equilibrium model uses the actual air to feed ratio as an input variable and, therefore, calculates the gas composition from non-ideal conditions which may be occurring within the gasifier in order to maintain reaction zone stability.

9.9 Summary

Modelling of the downdraft gasifier has been done in order to estimate the length of reactor needed for each stage of the gasification process and to predict the product gas composition.

The depth of the flaming pyrolysis zone is calculated from the time taken to heat particles to the pyrolysis temperature by transient heat conduction. The results are similar to those obtained during experimentation and give a flaming pyrolysis depth of between 1.29 and 1.67 cm for the base case feed used in the experimental tests. The flaming pyrolysis gas composition has been predicted and comparisons made with models in the literature.

A step-wise gasification model is used to give the gas composition, char conversion and temperature profiles within the gasification zone. The model is based upon external and internal mass transfer, mass and energy balances, reaction kinetics and thermodynamic equilibria. Simulations indicate that most char gasification takes place within three particle widths of the flaming pyrolysis zone. The distance is less than that observed during experimentation and less than that given by models in the literature. The model gives unsatisfactory results which may be due to errors in the assumed pore size distribution, kinetic expression and voidage within the reaction zone.

An equilibrium model has been developed in order to predict the product gas composition and comparisons to the Aston carbon boundary model and experimental results have been made. The equilibrium model has been shown to predict gas compositions similar to those obtained during the experimental programme.

Nomenclature for Chapter 9

A	Arrhenius constant
α	Thermal diffusivity (m^2s^{-1})
C_g	Reactant gas concentration
Cp	Specific heat capacity
C_s	Reactant solid concentration
c	Char yield ($mol.mol^{-1}$ daf feed)
D	Diffusivity
D_K	Knudsen diffusivity
D_{eff}	Effective diffusivity
ε	Bed voidage
ε_{char}	Char voidage
e	Emissivity
Fo	Fourier number
H_c	HHV
H_s	Sensible heat
η	Effectiveness factor
j_D	Dimensionless group
k	Reaction rate constant
k_m	Mass transfer coefficient
K	Equilibrium constant
L	Particle width, pore length
l	Length of gasification sub-zone
λ	Thermal conductivity ($Wm^{-2}s^{-1}$)
m	Methane yield ($mol.mol^{-1}$ daf feed)
M	Molar weight
n	Reaction order
N_{Sc}	Schmidt number
N_{Re}	Reynolds number
ϕ	Thiele modulus
$q_{r,c}$	Heat loss
R	Gas constant ($8.314\ JK^{-1}mol^{-1}$)
$-R_{eff}$	Effective gasification rate
ρ	Specific density
ρ_m	Molar density
σ	Stefan-Boltzman constant ($5.67 \times 10^{-12}\ Wcm^{-2}K^{-4}$)
T	Temperature (K)
T	Dimensionless temperature parameter

t Tar yield (mol.mol^{-1} daf feed)

v Superficial gas velocity

W Water inputs (mol.mol^{-1} daf feed)

q, x, y, z H_2O, CO_2, CO and H_2 yields respectively (mol.mol^{-1} daf feed)

Subscripts

p pyrolysis

a,b Feed composition

i initial

e external

ref reference

g sub-zone g

c convective

r radiative

10. CONCLUSIONS

10.1 Gasification System

The gasification system has given reliable performance after several modifications were made to improve the ease of operation of the equipment. A raw gas sampling system has allowed the water, tar and particulate content of the product gas to be determined to give greater accuracy in calculation of the mass and energy balances than Evans (1992). The use of a contact thermocouple to measure the external temperature of the reactor has improved the estimation of heat losses.

A hybrid-throated reactor has been designed and used in the experimental programme (Section 10.3). The hybrid gasifier combines the inherent simplicity of the open-core gasifier (i.e. both the feed and air enter through the open top of the reactor) with the throat of conventional downdraft gasifiers.

10.2 Open-Core Experimental Programme

The following conclusions can be made from the experimental work using the uninsulated open-core gasifier unless otherwise stated:

(1) From direct observations of the pyrolysis process, radiative heat transfer from the zones below is concluded to be the main method of pyrolysis propagation (Section 7.2.1), confirming previous observations (Earp, 1988).

(2) The mode of operation (Section 2.5.6) depends upon the relative rates of char production by pyrolysis and char consumption by gasification. Stable operation with a stationary reaction zone is obtained when the rate of char production by pyrolysis is equal to the rate of char consumption by gasification. It has been found that the mode of operation does not depend upon the air factor as believed by previous workers (Earp, 1988; Evans, 1992), but upon the superficial gas velocity within the gasifier (Section 7.2.1). For the 6.35-12.7 mm feedstock stable operation was achieved for superficial gas velocities in the range of 0.208 to 0.291 ms^{-1}, and insulation was found not to have a significant effect on the superficial velocity (Section 7.6.2). It is concluded that as the air flow into the gasifier is increased, convective cooling reduces the temperature at the pyrolysis front reducing the rate of pyrolysis. The rate of char production by pyrolysis is then reduced relative to char consumption resulting in the reaction zone falling to the grate (gasification dominant operation). Conversely, at low air flow rates into the reactor the rate of char gasification is reduced resulting in pyrolysis dominant operation. A stable reaction zone is achieved when the rate of char production is equal to the rate of char consumption.

(3) In principle turndown can be achieved by increasing the rate of char production by pyrolysis without altering its relative rate to gasification. The open-core gasifier was operated with a stable reaction zone over a range of throughputs giving a turndown ratio of 1.3:1 (Section 7.2.2). Two hypotheses were put forward to account for the turndown achieved in terms of the pyrolysis process: (a) as a result of temperature variation at the pyrolysis front; (b) as a result of variations in the interfacial area of the pyrolysis front caused by sloping reaction zones. Neither hypothesis was satisfactorily supported by the experimental test data obtained and more work is recommended (Section 11). An increase in the rate of char gasification may, in theory, be achieved by an increase in the kinetic rate of reaction due to higher temperatures, or by an increase in the reaction zone depth.

(4) The flaming pyrolysis zone was measured to be about 15 mm deep using the 6.35-12.7 mm feedstock (equivalent to 1.4 particle diameters) within the uninsulated gasifier, which is comparable to 2 particle diameters measured by Earp (1988) and 1.2 particle diameters measured by Evans (1992). Flaming pyrolysis resulted in a 60% decrease in particle volume and a 83% decrease in mass (Section 7.3.2). The loss in mass is approximately equal to the volatile content of the feed (Section 7.3.4).

(5) The maximum temperatures within the gasifier are at the bottom of the flaming pyrolysis zone (Section 7.3.3) where the oxidant is used up. For the uninsulated gasifier the maximum temperature measured was 1023°C, which was increased to 1128°C when the gasifier was insulated (Section 7.5.3).

(6) The end of the gasification zone had a char ash content of 8% (Section 7.3.4) suggesting that there is an accumulation of ash in this region as the char particle is consumed. The depth of the gasification zone is about 6-8 cm (5.8-7.7 characteristic particle diameters) deep for the 6.35-12.7 mm feed size (Section 7.3.1).

(7) The total reaction zone depth (flaming pyrolysis plus char gasification) is between 7 and 9 characteristic particle diameters for both the 6.35-12.7 mm and 4.75-6.35 mm feedstocks (Section 7.7). A combined reaction zone depth of 7-8 particle diameters together with an inert char depth of 10 particle diameters (see item 8 below), allows the reactor height to be calculated for any given feedstock size. Additional height would be required to accommodate the unreacted feed zone, which, since it serves to distribute the oxidant, is important, and a minimum depth of 5 particle diameters is suggested based upon operational experience.

(8) Increasing the height of the char bed led to a minor improvement in the product gas heating value due to a decrease in the air/feed ratio. A maximum in the energy conversion efficiency was found at a char bed height of about 10 cm (about 10 characteristic particle diameters) as the increasing heat loss from the reactor offset the improvement in the product gas energy content (Section 7.4.2) The inert char also serves as a buffer zone between the reaction zone and the grate to absorb fluctuations in the position of the reaction zone.

(9) Insulating the open-core gasifier reduces the heat loss from 28% to 12% of the energy inputs on average (Section 7.5.2) resulting in an improvement in the product gas heating value from 3.54 to 5.04 $MJNm^{-3}$ and the cold gas energy conversion efficiency from 64% to 70%.

(10) Using insulation reduced the tar content of the product gas by 50% on average to 336 $mgNm^{-3}$. The reduction in tar output is believed to be due to the higher temperatures within the insulated gasifier leading to a greater tar cracking efficiency (Section 7.5.4).

(11) The amount of tar produced during start-up was found to be up to four times greater than that produced during stable operation (Section 7.9.3).

(12) The tar and particulate scrubbing efficiency of the venturi ejector has been determined to be about 90% (Section 7.10).

(13) Agitation of the reactor bed by vibration was found to;

- improve the flow of solids
- reduce the amount of voidage within the feed bed and the reaction zones
- reduce the pressure drop across the reactor
- reduce the degree of fluctuation in the product gas composition
- give a minor improvement in the gas heating value by 5% and increase the cold gas conversion efficiency by 2.4%.

It is concluded that the main advantage of using reactor bed agitation is the reduction of the pressure drop across the bed (Section 7.6.3) which may allow the gasifier to be operated for longer periods up to about 12 hours (limited by the size of the char catchpot). Operation using the vibrator did not adversely affect gasifier performance.

(14) The gasification of 4.75-6.35 mm feed size has been found to give a higher energy conversion efficiency and a higher product gas heating value than the base case

feed (6.35-12.7 mm), due to a reduction in the air to feed ratio required with the smaller feed size (Section 7.7). A 27% higher specific capacity was obtained, as less time was required for pyrolysis and gasification of the smaller particles.

(15) Dried sewage sludge granules were found to be unsuitable for gasification within downdraft gasifiers due to the fusion of ash to form a large clinker within the reactor, preventing material flow (Section 7.8.1).

(16) Gasification of char with a feed bed above a stable reaction zone can not be achieved due to its low volatile content (7.8.2). Char could be gasified in top stabilized operation; however, heat losses from the top of the bed would reduce the conversion efficiency. The use of air injection into the reactive bed may allow gasification of the char.

10.3 Hybrid-Throated Experimental Programme

The hybrid-throated gasifier (uninsulated unless stated otherwise) was operated successfully with a reaction zone at the throat, allowing the following conclusions to be made:

(1) The throat separates the flaming pyrolysis and gasification zones (Section 8.2), with a 0.5-1.5 cm gap or void between the throat and the top of the gasification zone. This differs from the common view of zonation within conventional gasifiers, since a void below the throat is not usually depicted, although the pyrolysis and gasification zones are separated by the throat (Section 2.6). The zonation also differs from that in the open-core gasifier, in which the zones are consecutive.

(2) Gas circulation was observed within the gap between the throat and the top of the gasification zone. After passing through the throat the gases were observed to spread across the top of the char bed and roll back up towards the throat, eddying within the gap. The circulatory currents are believed to carry tars back to the hottest part of the gasifier, in which temperatures of about 1070°C were measured for the uninsulated reactor, thereby increasing the residence time for tar cracking (Section 8.2).

(3) The gasifier exhibits a pulsating affect due to the periodic collapse of bridges over the throat resulting in the flow of solids through the throat and a shifting in the positions of the reaction zones (Section 8.2). Pulses occur with an average period of 34 seconds. After a bridge collapse the pyrolysis front above the throat progresses upwards into the unreacted feed bed. The mechanical integrity of the material

supporting the bridge is reduced as pyrolysis progresses resulting in collapse of the bridge. The cycle may cause fluctuations in the tar and gas output of the gasifier (Section 8.2).

(4) A turndown ratio of 2:1 was obtained for the hybrid-throated gasifier (Section 8.3.1), giving three times more turndown than the open-core gasifier.

(5) A turndown mechanism is proposed (Section 8.3.4) which has been validated by experimental observations. In the proposed mechanism the pyrolysis front is a flat horizontal interface at maximum turndown (i.e. minimum gas production) which expands to form a hemispherical dome at higher throughputs, causing a doubling of the interfacial area, thereby explaining the turndown ratio achieved (see item 4). The rate of pyrolysis is therefore directly related to the area of the pyrolysis front. The throat is believed to act as a window to radiative heat transfer from the hot char surface below the throat to the pyrolysis front, giving the dome-shaped heat distribution. Higher turndown ratios may be attained if an elliptical dome can be formed by altering the throat to reactor diameter ratio (to give different radiative heat distributions), or by using air injection to form a bubble as proposed by Hoi (1991).

(6) The rate of gasification has been shown to match the rate of char production by pyrolysis (thereby giving a stable, stationary reaction zone) as a result of changes in the reaction zone volume. This hypothesis is supported by experimental observations, although the observed gasification zone depth may not correspond to the actual depth at the reactor core and validation of the hypothesis using temperature measurements is required (see 11.3.4).

(7) A stable (stationary) reaction zone was achieved for superficial gas velocities in the range 0.218 to 0.430 Nms^{-1} at the grate for the hybrid gasifier. The upper limit is higher than that of the open-core gasifier (see Section 10.2, item 2) and is believed to be due to the ability of the pyrolysis front to form a dome as discussed in item 5 above.

(8) It was found that the product gas composition and energy content did not vary significantly for the range of turndown values obtained (Section 8.3.2). Thus turndown will not adversely affect the performance of the application using the gas.

(9) The uninsulated hybrid-throated gasifier produces a gas with an average higher heating value of 3.99 $MJNm^{-3}$, 13% greater than the uninsulated open-core gasifier. The cold gas energy conversion efficiency of the hybrid gasifier is 78% on average,

greater than that of the open-core gasifier with an average efficiency of 64% (Section 8.4). The improvements in gasifier performance are believed to be due to better gas mixing and tar cracking (supported by the experimental results, see item 10 below) in the high temperature zone below the throat, and because of reduced heat losses from the hybrid reactor due to a layer of char between the hot core of the reactor and the reactor wall (Section 8.4) as a result of focussing the reaction zone at the centre of the reactor by the throat.

(10) The hybrid-throated gasifier produces about 50% less tar than the open-core gasifier as a result of gas circulation below the throat and higher reactor temperatures (Section 8.4).

(11) Insulating the hybrid-throated gasifier reduces tar output by 60% to 138 $mgNm^{-3}$, improves the product gas energy content by 36% to 5.41 $MJNm^{-3}$ and increases the energy conversion efficiency by 1% to 79%. The improvements in performance are a result of reduced heat losses and higher temperatures, with a maximum of 1365°C measured 2 cm below the centre of the throat (Section 8.5). Temperatures at the wall and throat are believed to be significantly lower (i.e. below about 850°C) than at the core since no damage was observed; thus, the throat permits the use of materials with a lower recommended temperature limit than that which occurs within the gasifier.

(12) Operation of the hybrid-throated gasifier with the 4.75-6.35 mm feedstock indicates that there is a different specific capacity range for stable operation compared to using the 6.35-12.7 mm feedstock. A different range could be due to a faster reaction time for the smaller particles allowing greater throughput (Section 8.6). In addition, higher product gas energy content was obtained for the for the 4.75-6.35 mm feedstock since operation was achieved at a lower air to feed ratio compared to the 6.35-12.7 mm feed. However, the pressure drop across the reactor when using the 4.75-6.35 mm feedstock was found to increase at more than twice the rate than when using the 6.35-12.7 mm feedstock, which can lead to operational problems (e.g. in maintaining the reaction zone at the throat as the superficial gas velocity is progressively reduced). An optimum feed size may, therefore, exist for the hybrid dependant upon the trade-off between the increasing gasifier pressure drop and the improvements in gasifier performance with smaller feed sizes. There is insufficient data to suggest the optimum feed size for the hybrid gasifier.

(13) The use of dried sewage sludge in the hybrid reactor was unsuccessful due to fusion of the material (Section 8.6.1) as previously concluded for the open-core gasifier.

(14) The gasification of rubberwood charcoal using the hybrid gasifier was unsuccessful due to an inability to maintain the reaction zone at the throat (Section 8.6.2), although charcoal is typically used with a conventional downdraft gasifier. As the reaction zone tends to move towards the air inlet the reaction remains at the throat within the conventional downdraft. However, it quickly moves to the open-top of the hybrid-throated gasifier, thus explaining the difference in the ability to gasify char.

(15) Limited scale-up of the hybrid gasifier is possible by increasing the throat diameter. The results indicate that a throat diameter of between 4 and 7 characteristic particle diameters can be used. The hybrid-throated gasifier may also be scaled-up by using a multiple throated design (Section 8.7), with the same tar cracking efficiency and gasifier performance of the insulated hybrid-throated gasifier used in the experimental work.

10.4 Downdraft Gasification Modelling Studies

The following conclusions on the models used in Chapter 9 have been made:

(1) A two stage design model for calculating the height of a downdraft reactor vessel is partially successful. The calculation of the pyrolysis zone depth using a transient heat conduction model is satisfactory (see item 2); however, a step-wise gasification zone model produced unsatisfactory results compared to the experimental work. The gasification zone depth obtained using the model was shorter than experimental measurements made and shorter than values in the literature (Section 9.6.6). The assumed pore size of 20 μm and kinetic data used in the model may be responsible for the poor correlation to experimental zone depths since:

- The internal surface area of wood char cannot be accounted for using the primary pore dimensions of the original wood and a simple cylindrical pore structure (Section 9.3). Fine micro-pores are, therefore, believed to be produced on devolatilization leading to an increase in the internal surface area.
- Pore diffusion limitations to the rate of gasification become increasingly important below a pore diameter of 5 μm over the temperature range found within the gasification zone (Section 9.6.2).
- Internal diffusion becomes increasingly important at temperatures above 1073 K for a pore size of 20 μm (Section 9.6.3).

Using the determined pore size and kinetic data for the char used in the experimental work within the model would improve the authenticity of the model by removing two major assumptions (see recommendations; Section 11.4). There may also be errors in the heat loss data from the reaction zone, and because bed voidage within the reaction zones was not accounted for due to the lack of sufficient data (see Section 11.4).

(2) The transient heat conduction model gives a pyrolysis time of 53 seconds giving a flaming pyrolysis zone depth of of between 1.29 and 1.67 cm for the 6.35-12.7 mm feedstock, in good agreement with the experimental results. For smaller sized particles the agreement is less good since heat transfer to the sides of the particle become significant (Section 9.4.2).

(3) The agreement with the transient heat conduction model suggests that little heat is lost from the upper surface of a particle during pyrolysis for the 6.35-12.7 mm feedstock (Section 9.4.2). As little heat progresses into the feed zone little drying of the unreacted particles would occur, suggesting that modelling for a drying zone within the reactor is unnecessary.

(4) The predicted flaming pyrolysis gas composition (Section 9.5) is comparable to that predicted using a similar model by Chern (1988). The accuracy of the prediction cannot be determined due to a lack of experimental data in the literature; however, a method of obtaining a gas composition is proposed in Section 11.2.2.

(5) The equilibrium model developed to predict the outlet product gas composition compares well with the experimental results (Section 9.8.3). Comparisons to the Aston carbon boundary model suggest that both the open-core and hybrid-throated gasifiers operate at a higher air to feed ratio than that required for optimum operation (Section 9.8.4). The higher air to feed ratio may be necessary to give a sufficient superficial gas velocity in order to maintain a stable reaction zone (see 10.2, item 2).

11. RECOMMENDATIONS

11.1 Introduction

The gasification system was found to be generally reliable and easy to operate, however, a number of improvements to the instrumentation are recommended in Section 11.2. Further investigations using the open-core and hybrid throated reactor vessels are given in Section 11.3, whilst recommendations for modelling studies are described in Section 11.4.

11.2 Experimental Equipment

11.2.1 Temperature Measurements

Using a contact thermocouple to measure the external temperature of the reactor wall has been found to improve the estimation of heat losses from the reactor (see Section 7.5.2). However, measurement of the external temperature profile was time consuming taking at least 25 minutes for three readings at 2 cm intervals along a 30 cm high reactor. Permanent contact thermocouples connected to a data-logging system are recommended to allow continuous measurement of the external temperature allowing more time for other operator duties and increasing the accuracy in the calculation of heat loss. Accurate calculation of the heat loss is required since heat losses affect the air to feed ratio and is also important in the energy balance.

An accurate method of measuring temperatures within the reactor is also required in order to improve the understanding of the stability and operating range of the gasifier (as discussed in Section 11.3 below). The possible sources of error in measuring the temperature profile are discussed in Section 7.2.1. Using the search thermocouple without a sheath may reduce errors, although the positioning of the thermocouple may be more difficult. Temperature measurements within the hybrid-throated gasifier are discussed in Section 11.3.4.

11.2.2 Gas Analysis

In addition to the gas analysers used in this research (see Section 3.7), an oxygen analyser for the product gas would be useful to check for the ingress of air into the gasification system. An inward leak of air would affect the N_2 content of the product gas found by difference. Since the mass of N_2 entering the gasifier is calculated from its approximate equality to the mass of N_2 leaving the gasifier (Appendix F) this leads to errors in the calculation of the air intake into the reactor, although the difference in the total mass balance may be insignificant.

The measurement of the gas composition profile along the length of the reactor using a probe adjustable to sample at different bed depths is recommended. This would allow comparison with the results from the flaming pyrolysis gas model (Section 9.5) and the step-wise gasification model (Section 9.6).

11.2.3 Tar Sampling

Measurement of the tar content of gas samples taken from within the reactor bed (see Section 11.2.2) is recommended. Equipment similar to that described in Section 3.8 may be used, although a heated sample line may be necessary to prevent condensation within the line. Other collection methods should also be considered, such as using a separate heated solids filter and a tar adsorption bed, to enable comparisons on the method of collection to be undertaken. The tar measurements will allow the tar cracking efficiency of the char bed to be investigated. In addition, the amount of water in the sample can be determined using the dryer assembly used in this work to provide further data for comparison with the models as discussed in Section 11.2.2.

11.2.4 Removal of Ash and Fines

The use of a agitator within the gasifier has been found to reduce the pressure drop across the reactor bed (Section 7.6.3). A vibrating grate is recommended for this purpose, especially if the gasification of feedstocks with a higher ash content than the wood used in the experimental programme is to be investigated. Rods attached to the grate would allow the agitating effect of the vibrations to be carried upwards into the reaction zone. The vibrating grate would then aid removal of fines and ash from the char bed, and may also help solids flow through the reactor.

11.2.5 Data-Logging and Data Transfer

A new data-logging system is required since the VAX mainframe (Section 3.7) is now obsolete, and the BBC micro-computer used is unreliable.

11.3 Investigations Recommended for Further Work

11.3.1 Reaction Zone Stability

Further investigation into the relationship between the superficial gas velocity within the reactor and the rates of heat transfer to the flaming pyrolysis and gasification zone are recommended. This may lead to the understanding of the stability of the reaction zone within the open-core gasifier (Section 7.2.1) and hybrid-throated gasifier (Section 8.2.1). The stability of the insulated open-core gasifier is recommended for further investigation to confirm that heat loss has little significance on the superficial gas velocity required for stability, as indicated by the results given in Section 7.5.1. In addition, the determination of superficial gas velocities for different feed sizes under

different modes of operation would validate the theory of stability as a function of the superficial velocity.

11.3.2 Turndown of the Open-Core Gasifier

In Section 7.2.2 the apparent turndown of the open-core gasifier during stable operation was discussed. As turndown is of important practical use (e.g. for automotive power) confirmation of the turndown ability of the open-core gasifier (both with and without insulation) is required and the possible explanations for turndown investigated. Accurate measurement of temperatures within the gasifier as proposed in Section 11.2.1, would be required to support the hypothesis of increased throughput as a result of higher temperatures (described in Section 7.2.2).

Investigation of turndown as a result of altering the interfacial area between the unreacted feed and pyrolysis zone is also recommended. This may be attained by sloping the reaction zone (Section 7.2.2), although maintaining a sloped reaction zone may be difficult and no methods of achieving this can be suggested. However, the affect can be created by altering the angle of the reactor from the vertical, although this would require a flexible gas piping system capable of withstanding temperatures up to 600°C and, possibly, a flexible section of the reactor to accommodate the unreacted feed. Other methods of altering the surface area of the interface include using a variable geometry reactor in the form of an inverted cone for which the throughput progressively increases as the reaction zone moves upwards from the grate, or by using air injection as discussed in Section 11.3.6.

11.3.3 Tar Cracking Efficiency

Measuring the tar content of the gas along the length of the reactor bed (Section 11.2.3) would allow the tar cracking efficiency of the flaming pyrolysis and gasification zones to be investigated. This may confirm the existence of a tar cracking region below the throat in the hybrid-throated gasifier. In Section 7.6.4 it was suggested that the occurrence of voids below the flaming pyrolysis zone may create a high temperature region for tar cracking. The effect of the voids in the open-core gasifier would, therefore, be similar to that of the void observed below the throat in the hybrid-throated gasifier in which tar cracking is believed to take place (Section 8.2). This contradicts the theory of voids as cold spots through which tars could pass uncracked (Earp, 1988), and the observations of gases channelling through the voids (Section 7.3.1) which suggest poor mixing of the oxidant with the pyrolysis gases carrying the tars. Further investigations of tar production from the open-core gasifier using the vibrator to reduce the occurrence of voids is recommended.

The tar cracking efficiency of both types of gasifiers using secondary air injection below the primary oxidation zone also warrants investigation (also see Section 11.3.6). In addition, the use of a secondary thermal or catalytic tar cracking unit connected below the grate may also be considered in order to further reduce the tar content of the product gas. This improves the gas for use in applications requiring a clean fuel (e.g. gas turbines) while minimizing the need for a downstream cleaning system.

11.3.4 Zonation Within the Hybrid-Throated Gasifier

It is recommended that the temperature distribution (both vertical and radial) within the hybrid-throated gasifier is measured to aid identification of the reaction zones. Using the search thermocouple used in the open-core experimental programme, the flaming pyrolysis zone may be identified as the region in which temperatures rise above 300°C to the maximum temperature in the reactor (indicating the end of the oxidation zone), and the gasification zone can be identified as the region between the end of the FP zone and a temperature of about 700°C (at which the kinetic rate of gasification becomes negligible).

The probe may help confirm the presence of a dome-shaped pyrolysis front and may also be used to investigate the change in depth of the gasification zone with turndown. However, the presence of the temperature probe may affect the process within the gasifier which should become apparent by comparing observations against those made without the search thermocouple in place.

11.3.5 Turndown of the Hybrid-Throated Gasifier

The turndown of the hybrid-throated gasifier should be further investigated to confirm the turndown ratio obtained during this research and to provide evidence for the mechanism proposed in Section 8.3.4 by determination of the heat transfer rate to the pyrolysis front. In addition, the turndown of the gasifier using insulation should be investigated. The turndown ratio obtained by this investigation should correspond to the turndown ratio of the uninsulated gasifier (although the range of throughputs may differ) if the mechanism proposed in Section 8.3.4 is accurate, since the ratio is defined by geometry of the flaming pyrolysis front and gasification zone depth. Problems in observing the positions of the reaction zones (see Section 8.5) may be overcome by temperature measurements as discussed in Section 11.3.4.

The turndown of the gasifier should also be investigated using different feed sizes, since in Section 8.6 it was concluded that the range of air flow rates required for stable operation is different for the 4.75-6.35 mm feedstock compared to the 6.35-12.7 mm feedstock.

11.3.6 Investigations Involving the Use of Air Injection

In Section 8.7.2 it was suggested that a proportion of the air requirement injected into the throat of the hybrid gasifier would provide a means of stabilizing the reaction zone at the throat for feedstocks with different compositions. It is recommended that investigations using a variety of feedstocks and a hybrid-throated gasifier equipped with a method of injecting a variable proportion of the air requirement into the throat is suitable for research. A simple pipe extending from the top of the feed bed to the throat may be used, with the proportion of air delivered becoming a function of the relative cross-sectional area of the pipe (compared to the cross-sectional area of the reactor) and the pressure drop through the feed bed. The proportion of air delivered can then be increased by using a pipe with a larger diameter whilst keeping the height of the unreacted feed bed constant. This may, however, alter the solids flow as a result of bridging. Alternatively, the air may be pumped under positive pressure into the reactor, although the air flow should not exceed the air requirement of the reactor in order to avoid pyrolysis vapours travelling up through the unreacted feed bed. The air flow delivered by injection can be measured using a rotameter, with the air flow delivered through the bed calculated by difference in the nitrogen balance. The research may enable the design of a widely versatile gasifier with the ability to gasify a variety of feedstocks by adjusting the proportion of air injected into the throat.

Air injection may be similarly carried out using the open-core gasifier. This may allow the reaction zone to become stabilized (i.e. stationary) at a variety of throughputs, thereby giving turndown according to the bubble theory described by Hoi (1991). Secondary air injection below the primary oxidation zone may also increase the tar cracking efficiency of the gasifier as recommended in Section 11.3.3. Air injection into the open-core gasifier whilst using a sealed feeder (e.g. through a star valve), would also allow investigations of a throatless hybrid gasifier (described in Section 2.7.2) to be carried out.

11.3.7 The Effect of Throat Size

Investigating the effect of different throat sizes and different throat to reactor area ratios on the gasification process, gasifier performance and turndown ratio should be considered. This information is important when considering scale-up of the hybrid-throated gasifier (Section 8.8).

11.3.8 Hybrid-Throated Reactor Design

The design for a multiple throated gasifier (Section 8.8) is recommended for development. Successful operation of this gasifier would indicate that the reactor can be scaled-up to whatever size required simply by increasing the number of throats within the gasifier.

11.4 Modelling Studies

In order to develop the char gasification model (Section 9.6) determination of the pore size distribution and kinetics of the char gasification reactions should be carried out. In addition the effect of voidage within the zone is recommended to be incorporated in order to provide a more accurate estimation of the gasification zone depth required. The voidage within the gasification zone may be calculated using the volume reduction of the material within the pyrolysis zone, of which measurements were presented in Section 7.3.2. In addition, more accurate calculation of the heat loss from the zones from external measurements (recommended in Section 11.2.1) would improve the accuracy of the model. The model would then allow the height of the reactor required to be calculated.

Modelling studies should also consider the rates of heat transfer within the gasifier which may provide information leading to a better understanding of the stability and operating range of the open-core gasifier and of turndown in the hybrid-throated gasifier, in conjunction with the related experimental work recommended in Sections 11.3.1 and 11.3.2. The study should aim to provide information that will lead to better design of downdraft gasifiers, to enable the calculation of the superficial gas velocities required for different feed sizes and compositions, and to enable the design of a hybrid-throat to give higher turndown ratios than that obtained during this research.

REFERENCES

Adschiri, T., Nozaki, T., Furusawa, T. and Zi-bin, Z., "Characterization of Coal Char Gasification Rates", AIChE Journal, Vol. 37, 6, 897 - 904, 1991.

Airflow, "Pitot Static Tube", Information Brochure AI 133/984, Airflow Developments Ltd, High Wycombe, UK, undated.

Airflow, "Precision Manometer Test Sets", Information Brochure AI 134/984, Airflow Developments Ltd, High Wycombe, UK, undated b.

Anonymous, "Balston Coalescing Filters", Balston Filter Products, Bulletin P-100K, 1989.

Anonymous, "Drying Agents", Encyclopedia of Chemical Technology 3rd Edition, Vol. 8, Kirk-Othmer, Wiley, NY, 1979.

Anonymous, "Generator Gas : The Swedish Experience, 1939-1945", Swedish Gas Producer Reports, SERI SP33 - 40, 1979.

Anonymous, "Quantitive Filter Papers", Whatman Technical Literature, 1980.

Antal, M.J., "Biomass Pyrolysis: A Review of the Literature, Part 1 - Carbohydrate Pyrolysis", Advances in Solar Energy, Vol 1, Boer, K.W. and Duffie, J.A. (eds), American Solar Energy Society, Boulder, USA, 1982.

Antal, M.J., "Biomass Pyrolysis: A Review of the Literature, Part 2 - Lignocellulose Pyrolysis", Advances in Solar Energy, Vol 2, Boer, K.W. and Duffie, J.A. (eds), American Solar Energy Society, Plenum Press, NY, 1985.

ASTM D1792 - 84, "Standard Methods for Chemical Analysis of Wood Charcoal", ASTM, 1984.

ASTM D2395 - 83, "Standard Test Methods for Specific Gravity of Wood and Wood-base Materials", ASTM, 1983.

Becker, H.A., Phillips, A.M. and Keller, J., "Pyrolysis of White Pine", Combustion and Flame Vol. 58, 163-189, 1984.

Beenackers, A.A.C.M. and Bridgwater, A.V., "Gasification and Pyrolysis of Biomass in Europe", in Pyrolysis and Gasification, Ferrereo, G. L., Maniatis, K., Buekens, A. and Bridgwater, A. V., (eds), Elsevier Applied Science, London, 1989.

Beenackers, A.A.C.M. and van Swaaij, W.P.M, "Gasification of Biomass, a State of the Art Review" (Keynote paper) in Thermochemical Processing of Biomass, Bridgwater A .V. (ed), Butterworths, London, 1984.

Bilbao, R., Salvador, M.L., Arauzo, J. and Murillo, M.B., "Modelling of the Product Distribution in the Pyrolysis of Lignocellulosic Wastes", 6th European Conference, Biomass for energy , Industry and the Environment, 22-26 April 1992, Athens.

Bridgwater, A.V. and Evans, G.D., "An Assessment of Thermochemical Conversion Systems for Processing Biomass and Refuse", ETSU B/T1/00207/REP, ETSU, 1993.

Bridgwater, A.V. "Catalysis in Thermal Biomass Conversion", to be published in Applied Catalysis, 1993a.

Bridgwater, A.V., "Review of Thermochemical Biomass Conversion", Contractor Report, ETSU B 1202, Department of Energy, 1991.

Brown, M.D., Baker, E.G. and Mudge, L.K., "Environmental Design Considerations for Thermochemical Biomass Energy", Biomass, Vol. 11, 255-270, 1986.

Brown, M.D., Baker, E.G. and Mudge, L.K., "Evaluation of Processes for the Removal of Particulates, Tars and Oils from Biomass Product Gases", in Energy from Biomass and Wastes 10, Klass, D.L., (ed), Elsevier Applied Science, London, 1987.

BS 893: 1978, "Method for the Measurement of Concentration of Particulate Material in Ducts Carrying Gases", British Standards Institute, HMSO, 1978.

BS 1042: Section 2.1: 1983, "British Standard Measurement of Fluid Flow in Closed Conduits: Section 2.1, Method Using Pitot Static Tubes", British Standards Institute, HMSO, 1983.

BS 3405: 1983, "British Standard Method for the Measurement of Particulate Emission Including Grit and Dust (Simplified Method)", British Standards Institute, HMSO, 1983.

Buekens, A.G and Schoeters, J.G., "Modelling of Biomass Gasification", in Fundamentals of Thermochemical Biomass Conversion, Overend, R.P., Milne, T.A., and Mudge, L.K. (eds), Elsevier Applied Science, 1985.

Buekens, A.G and Schoeters, J.G., "Valuable Products from the Pyrolysis of Biomass", in Biomass for Energy and Industry, 4th E.C Conference, Grassi, G., Delmon, B., Molle, J.-F. and Zibetta, H. (eds) Elsevier Applied Science, London, 1987.

Chan, W.C.R., Kelbon, M. and Krieger B.B., "Modelling and Experimental Verification of Physical and Chemical Processes During Pyrolysis of a Large Biomass Particle", Fuel Vol. 65, 1505-1513, 1985b.

Chan, W.C.R., Kelbon, M. and Krieger B.B., "Product Formation in the Pyrolysis of Large Particles", in Fundamentals of Thermochemical Biomass Conversion, Overend, R.P., Milne, T.A., and Mudge, L.K. (eds), Elsevier Applied Science, 1985a.

Chee, C.S., Walawender, W.P. and Fan, L.T., "Material Balance Analysis of Prototype Commercial Downdraft Gasifiers", in Research in Thermochemical Biomass Conversion, Bridgwater, A.V. and Kuester, J.L. (eds), Elsevier Applied Science, 1988.

Chen, J.-S. and Gunkel, W.W., "Modeling and Simulation of Co-Current Moving Bed Gasification Reactors - Part II. A detailed Gasifier Model", Biomass Vol. 14, 75-98, 1987

Chern, S-M., "Equilibrium and Kinetic Modeling of Co-Current (Downdraft) Biomass Gasifiers", PhD Thesis, Kansas State University, 1989.

Chowdhury, R, Chakravarty, M.and Bhattacharya, P., "Prediction of Venturi Scrubber Efficiency Used in an Updraft Gasifier Cleaning Train", International Journal of Energy Research, 16, 731-741, 1992.

Cornish, D.C., Jepson, G. and Smurthwaite, M.J., "Sampling Systems for Process Analysis", Butterworths, London, 1981.

Coulson, J.M. and Richardson, J.F., "Chemical Engineering, Vol. II", 3rd Edition, Pergamon, 1989.

Coulson, J.M. and Richardson, J.F., "Chemical Engineering, Vol. 1", 3rd Edition, Pergamon, 1977.

Crane, T.H., "Production of Low - BTU Gases Via a Downdraft Gasifier", in Technology and Economics of Wood Residue Gasification , Proceedings: Texas Industrial Wood Seminar, Rogers, K. E., (ed), Texas Forest products Lab, 1979.

Davis, K.G. and Manchanda, K.D., "Drying Gases and Liquids - Unit Operations for Drying Fluids", Chemical Engineering, 81, 102 - 110, 1974.

Deglise, X. and Magne, P., "Pyrolysis and Industrial Charcoal", in Biomass Regenerable Energy, Hall D.O, and Overend, R.P. (eds), Wiley, Chichester, 1987.

DeGroot, W.F. and Shafizadeh, F., "Kinetics of Wood Gasification by Carbon Dioxide and Steam" in Fundamentals of Thermochemical Biomass Conversion, Overend, R.P., Milne, T.A., and Mudge, L.K. (eds), Elsevier Applied Science, 1985.

DeGroot, W.F., and Shafizadeh, F., "Kinetics of Gasification of Douglas Fir and Cottonwood Chars by Carbon Dioxide", Fuel, Vol. 63, 210-216, Feb. 1984.

Delikouras, E.A. and Perlmutter, D.D., "Combined Effects of Mass Transfer and Inaccessible Porosity in Gasification Reactions", AIChE Journal, 39, 829-836, 1993.

Desrosiers, R. "Thermodynamics of Gas-Char Reactions", Chapter 6, Vol. 2, in A Survey of Biomass Gasification, SERI Report No. TR-33-239, 1979

Diebold, J. and Stevens, D., "Progress in Pyrolysis and Gasification of Biomass: an Overview of Research in the United States", in Pyrolysis and Gasification, Ferrereo, G. L., Maniatis, K., Buekens, A. and Bridgwater, A. V., (eds), Elsevier Applied Science, London, 1989.

Double, J.M., Smith, E.L. and Bridgwater, A.V., "Computer Modelling of Fluidised Gasification" in Pyrolysis and Gasification, Ferraro, G.L., Maniatis K., Buekens, A. and Bridgwater, A.V. (eds), Elsevier Applied Science, London, 1989.

Double, J.M., "The Design, Evaluation and Costing of Biomass Gasifiers", PhD Thesis, Aston University, Birmingham, UK, 1988.

Earp, D.M., "Gasification of Biomass in a Downdraft Reactor", PhD Thesis, Aston University, Birmingham, UK, 1988.

Earp, D.M., Reyes-Nunez, L.R., Evans, G.D. and Bridgwater, A.V., "Mass and Energy Balances Over an Open-Core Downdraft Gasifier", in Biomass for Energy and Industry, Volume 2. EC Conference 9-13 Oct 1989, Lisbon. Grassi, G., Gosse, G. and dos Santos, G. (eds), Elsevier Applied Science, London, 1990.

Edrich, R., Bradley, T. and Graboski, M.S., "The Gasification of Ponderosa Pine Charcoal", in Fundamentals of Thermochemical Biomass Conversion, Overend, R.P., Milne, T.A. and Mudge, L.K. (eds), Elsevier, London, 1985.

Eoff, C.M., "Operating Parameters for a Small, Stratified Bed, Gasifier-Engine System", Energy from Biomass and Wastes X, Klass, D.L. (ed), IGT, Chicago, 1987.

Eoff, C.M., Private communication to Reyes, L.R, 4th October 1988.

Espenäs, B-G., "Reactivity of Biomass and Peat Chars Formed and Gasified at Different Conditions", in Advances in Thermochemical Biomass Conversion, Vol. 1, (Conference Proceedings, 11-15 May 1992, Interlaken,Switzerland), Blackie Academic & Professional, 1994.

Esplin, G.J., Fung, D.P.C. and Hsu, C.C., "Development os Sampling and Analytical Procedures for Biomass Gasifiers", Canadian Journal of Chemical Engineering, 63, 946-953, 1985.

Esplin, G.J., Fung, D.P.C. and Hsu, C.C., "A Comparison of the Energy and Product Distribution from Biomass Gasifiers", Canadian Journal of Chemical Engineering, 64, 651-662, 1986.

Evans, G.D., "Development and Operation of an Open-Core Downdraft Gasifier", PhD Thesis, Aston University, Birmingham, UK, 1992.

Ginesi, D. and Grebe, G., "Flow Meters a Performance Review", Chemical Engineering, 102-118, 1987.

Ginesi, D., "Choices Abound in Flow Measurement", Chemical Engineering, 88-100, 1991.

Graboski, M. and Bain, R., Properties of Biomass Relevant to Gasification", in "A Survey of Biomass Gasification, Vol. 2 - Principles of Biomass Gasification", Reed, T.B. et al. (eds), SERI report No. SERI/TR-33-239, Colorado, USA, 1980.

Graboski, M. "Kinetics of Char Gasification Reactions", Chapter 7, Vol. 2, in "A Survey of Biomass Gasification", SERI Report No. TR-33-239, 1979.

Graboski, M.S. and Brogan, T.R., "Development of a Downdraft Modular Skid Mounted Biomass/Waste Gasification System", Energy from Biomass and Wastes XI, Orlando , Florida, 1987.

Graham, R.G. and Bergougnou, M.A., "The Production of Pyrolytic liquids, Gas and Char from Wood and Cellulose by Fast Pyrolysis", in Research in Thermochemical Biomass Conversion, Bridgwater, A.V. and Kuester, J.L. (eds), Elsevier Applied Science, 1988.

Graham, R.G. and Huffman, D.R., "Gasification of Wood in a Commercial-Scale Downdraft Gasifier", in Energy from Biomass and Wastes V, Klass, D.L.(ed), IGT, 1981.

Graham, R.G., "A Characterization of the Fast Pyrolysis of Cellulose and Wood Biomass", PhD thesis, University of Western Ontario, Canada, 1993.

Groeneveld, M.J. and van Swaaij, W.P.M, "Gasification of Char Particles with CO_2 and H_2O", Chemical Engineering Science, Vol. 35, 307-313, 1980a.

Groeneveld, M.J. and van Swaaij, W.P.M, "The Design of Co-current Moving Bed Gasifiers Fuelled by Biomass", Chemical Age of India, Vol. 31, 171-178, 1980b.

Groeneveld, M.J., Gellings, P.E. and Hos, J.J., "Production of a Tar-Free Gas in an Annular Co-Current Moving Bed Gasifier", in Energy from Biomass and Wastes VII, IGT, Chicago, 1983.

Groeneveld, M.J., "The Co-Current Moving Bed Gasifier", PhD thesis, Twente University of Technology, The Netherlands, 1980.

Groeneveld, M.J., van Amerogen, J. and Hos, J.J., "Production of a Tar-Free Gas in an Annular Co-Current Moving Bed Gasifier", Symposium on Forest Products Research - International Achievements and the Future, CSIR, Pretoria, RSA, 22-26 April, 1985.

Grover, P.D., "Thermochemical Characterisation of Biomass Residues for Gasification", Indian Institute of Technology, Delhi, 1989.

Gumz, W., "Gas Producers and Blast Furnaces: Theory and Methods of Calculation", Wiley, New York, 1950.

Harker, J.H. and Allen, D.A., "Fuel Science", Oliver & Boyd, 1972.

Harris, L.S., "Fume Scrubbing with the Ejector Venturi System", Chemical Engineering Progress, 62 (4), 55-59, 1966.

Hawley, C., Boyd, M., Anderson C.and DeVera, A., "Gasification of Wood Char and The Effects of Intraparticle Transport", Fuel, Vol. 62, 213-216, Feb. 1983.

Hellgren, R., Lindblom, M., Andersson, L. and Bjerle, I., "High Temperature Pyrolysis of Biomass", in Energy from Biomass and Wastes XV, Klass, D.L. (ed), Institute of Gas Technology, Chicago, USA, 1991.

Hillis, W.E., "Wood and Biomass Ultrastructure", in Fundamentals of Thermochemical Biomass Conversion, Overend, R.P., Milne, T.A. and Mudge, L.K. (eds), Elsevier, London, 1985.

Hoi, W.K. and Bridgwater, A.V. , "Development of a Rubberwood Gasifier", in Biomass for Energy and Industry, proceedings of the 5th EC Conference, Lisbon, 9-13 October 1989, Grassi, G., Gosse, G., dos Santos, G. (eds), Elsevier Applied Science, 1990.

Hoi, W.K., "Gasification of Rubberwood in a Downdraft Gasifier," PhD Thesis, Aston University, Birmingham, UK, 1991.

Hos, J.J, and Groeneveld, M.J., "Biomass Gasification" in Biomass Regenerable Energy, Hall D.O, and Overend, R.P. (eds), Wiley, Chichester, 1987.

Howard, J.B., "Fundamentals of Coal Pyrolysis and Hydropyrolysis", in Chemistry of Coal Utilization, Second Supplementary Volume, Elliot, M.A. (ed), Wiley, NY, 1981.

Huff, E.R., "Effect of Size, Shape, Density, Moisture and Furnace Wall Temperature on Burning Times of Wood Pieces", in Fundamentals of Thermochemical Biomass Conversion, Overend, R.P., Milne, T.A. and Mudge, L.K. (eds), Elsevier, London, 1985.

JANAF, "Thermochemical Tables", 2nd Edition, Hull, D.R. and Prophet, H. (Project Directors), NSRDS - NBS 37, Washington, 1971.

Kannan, M.P. and Richards, G.N., "Gasification of Biomass Chars in Carbon Dioxide: Dependence of Gasification Rate on the Indigenous Metal Content", Fuel, Vol. 69, 747-753, June 1990.

Kasaoka, S., Sakata, Y., Kayano, S. and Masuoka, Y., "The Development of Rate Expressions and the Evaluation of Reactivity for Gasification of Coal Chars with Steam and Oxygen", International Chemical Engineering, 23, 477-485, 1983.

Kaupp, A. and Goss, J.R., "State of the Art for Small Scale (to 50 kW) Gas Producer-Engine Systems", Final Report, US Department of Agriculture, N0. 53-319R-0-141, Tipi Workshop, Colorado, USA, 1984 .

Kaupp, A., "Air Blown Gasification of Rice Hulls: Dependence of Gas and Solid Properties on Operating Variables", PhD Thesis, University of California, Davies USA, 1983.

KnitMesh, "KnitMesh Demister Catalogue", KnitMesh Ltd., South Croydon, undated.

Knoef, H.A.M., Stassen, H.E.M., Hovestad, A. and Visser R., "Environmental Aspects of Condensates from Biomass Gasifiers", 4th EC Conference, Orleans, France, 11-15 May, 1987, in Biomass for Energy and Industry, Grassi, G., Delmon, B., Molle, J.-F. and Zibetta, H. (eds), Elsevier Applied Science, London, 1987.

Knoef, H.A.M., "UNDP/World Bank Monitoring Program on Biomass Gasifiers in Indonesia", 6th EC Conference on Biomass for Energy, Industry and the Environment, 22-26 April, 1991

Kollman, F.F.P. and Côté, "Principles of Wood Science and Technology I: Solid Wood", Springer-Verlag, Berlin, 1968.

Kutz, L.J., Barrett, J.R., Richey, C.B. & Jacko, R.B., "Downdraft Channel Gasifier Operation and Particulate Emissions", Transactions of the American Society of Agricultural Engineers, 26, 1614-1618, 1983.

L'Ecuyer, A. and Huffman, D.R., "Operation of a Fixed-Bed Downdraft Gasifier on Low Quality Residue Fuels", Canadian Bioenergy R & D Seminar, Vol 3, 205-208, 1981.

Levelton, B.H., Edwards, W.C., Shaw, A.J. and Rogerson, D.E., "Data Book of Unit Processes for Primary Conversion by Thermal, Chemical, and Biological Methods", Volume V of ENFOR Project C-258 "A Comparative Assessment of Forest Biomass Conversion to Energy Forms, Contractors Final Report, DSS Contract 43SS.KN107-1-4416, Energy, Mines and Resources, Canada, December, 1983.

Li, Z., Capart, R. and Gelus, M., "Study of Catalytic Effects of Alkali Metal Salts in the Gasification of Charcoal", in Biomass for Energy and Industry, Volume 2. EC Conference 9-13 Oct 1989, Lisbon. Grassi, G., Gosse, G. and dos Santos, G. (eds), Elsevier Applied Science, London, 1990.

Liinanki, L., Svenningsson, P-J. and Thessen, G., "Gasification of Agricultural Residues in a Downdraft Gasifier", Energy from Biomass, 3rd EC Conference, Palz, W., Coombs, J. and Hall, D.O. (eds), Elsevier Applied Science, 1985.

Maniatis, K. and Buekens, A., "Fast Pyrolysis of Biomass", in Research in Thermochemical Biomass Conversion, Bridgwater, A.V. and Kuester, J.L. (eds), Elsevier Applied Science, 1988.

Manurung, R. and Beenackers, A.A.C.M., "Gasification of Rice Husk in a Small Downdraft Gasifier", in Energy from Biomass, 3rd EC Conference, Venice, Italy, Palz, W., Coombs, J. and Hall, D.O. (eds), Elsevier Applied Science, London, 1985.

Manurung, R., "Gasification and Pyrolytic Conversion of Agricultural and Forestry Wastes", Renewable Energy Review Journal, Vol. 3 (1), 1-21, 1981.

Manurung, R.K. and Beenackers, A.A.C.M., "Modeling and Simulation of an Open Core Down-Draft Moving Bed Rice Husk Gasifier", in Advances in Thermochemical Biomass Conversion, Vol. 1, (Conference Proceedings, 11-15 May 1992, Interlaken,Switzerland), Blackie Academic & Professional, 1994.

Milne, T., "Pyrolysis - the Thermal Behaviour of Biomass Below 600°C", Chapter 6, Vol. 2, in "A Survey of Biomass Gasification", SERI Report No. TR-33-239, 1979.

Morganite, "Triton Kaowool Ceramic Fibre - High Strength Paper", product information brochure, Morganite Ceramic Fibres Limited, undated.

Moilanen, A., Saviharju, K. and Harju, T., "Steam Gasification Reactivities of Various Fuel Chars", in Advances in Thermochemical Biomass Conversion, Vol. 1, (Conference Proceedings, 11-15 May 1992, Interlaken,Switzerland), Blackie Academic & Professional, 1994.

Mudge, L.K., Weber, S.L., Mitchell, D.H., Sealock, L.J. and Robertus, R.J., "Investigations on Catalysed Steam Gasification of Biomass", Report for U.S Dept. of Energy, Pacific Northwest Laboratory, PNL-3695/UC-11, Jan., 1981.

Nandi, S.P. and Onischak, M., "Gasification of Chars Obtained from Maple and Jack Pine Woods", in Fundamentals of Thermochemical Biomass Conversion, Overend, R.P., Milne, T.A., and Mudge, L.K. (eds), Elsevier Applied Science, 1985.

Pakdel, H. and Roy, C., "Hydrocarbon Content of Liquid Products and Tar from Pyrolysis and Gasification of Wood", Energy and Fuels, 5, 427-436, 1991.

Parikh, P.P., Paul, A., Bhave, A.G. and Uma, R., "Tar in Producer gas - How Much and Why?", Energy from Biomass and Wastes X, IGT, Chicago, 1987.

Perma Pure, "Perma Pure Sampling Systems", Bulletin 120, undated.

Perry, R.H., Green, D., "Perry's Chemical Engineer's Handbook", 6th Edition, McGraw Hill, 1985.

Petersen, E.E., "Chemical Reaction Analysis", Prentice-Hall, NJ, USA, 1965.

Phillips, A.M. and Becker, H.A., "Pyrolysis and Burning of Single Sticks of White Pine in a Uniform Field of Temperature, Gas Composition and Gas Velocity", Combustion and Flame, Vol. 46, 221-251, 1982.

Radovic, L.R., Jiang, H.and Lizzio, A.A., "A Transient Kinetics Study of Char Gasification in Carbon Dioxide", Energy and Fuels, Vol. 5, 68-74, 1991.

Rajvanshi, A, K. and Joshi, M.S., "Development and Operational Experience with a Topless Wood Gasifier Running a 3.75 kW Diesel Engine Pumpset", Biomass 19, 47-56, 1989.

Rajvanshi, A.K. and Jorapur, R.M., "Leafy Biomass Gasifier for 15 kVA Diesel Genset", in Advances in Thermochemical Biomass Conversion, Vol. 1, (Conference Proceedings, 11-15 May 1992, Interlaken,Switzerland), Blackie Academic & Professional, 1994.

Raman, P., Walawender, W.P., Fan, L.T and Howell, J.A., "Thermogravimetric Analsis of Biomass. Devolatilization Studies on Feedlot Manure", Ind. Eng. Chem. Process Des. Dev., Vol. 20, 630-636, 1981.

Reed T.B. and Das A., "Handbook of Biomass Downdraft Gasifier Engine Systems", SERI Report SERI/SP-271-3022, Golden, Colorado, USA, March 1988a.

Reed, T.B. and Markson, M., "A Predictive Model for Stratified Downdraft Gasification of Biomass", in Proceedings of the 15th Biomass Conversion Contractors Meeting, March 16-17, 1983, CONF 830323 PNL-SA-11306, 1983.

Reed, T.B. and Markson, M., "A Predictive Model for Stratified Downdraft Gasification of Biomass", in Progress in Biomass Conversion, Volume IV, Tillman D A, Jahn E C (eds), Academic Press, New York, 1983a.

Reed, T.B. and Markson, M., "Biomass Gasification Reaction Velocities" in Fundamentals of Thermochemical Biomass Conversion, Overend, R.P., Milne, T.A., and Mudge, L.K. (eds), Elsevier Applied Science, 1985.

Reed, T.B., Graboski, M.S. and Levie, B., "Fundamentals, Development and Scaleup of the Air-Oxygen Stratified Gasifier". Report no SERI/PR-234-2571, Biomass Energy Foundation Press, Golden, Co. USA, 1988.

Reed, T.B., Levie, B., Das, A., "Biomass Gasification for Power, Fuels, and Chemicals", 5th Canadian Bioenergy R&D Seminar, Ottawa, Hasnain, S. (ed), Elsevier, 1984.

Reines, R.G., "The Gasification of Carrot Fibre in a Cast Refractory Micro-Gasifier", in Thermochemical Processing of Biomass", Bridgwater, A.V. (ed), Butterworths, 1984.

Reyes-Nuñez, L.R., "Downdraft Gasification and Opportunities in Chile", M.Phil. Thesis, Aston University, Birmingham, UK, 1989.

Richard, J.R., Cathonnet, M. and Rouan, J.P., "Gasification of Charcoal: Influence of Water Vapour", in Fundamentals of Thermochemical Biomass Conversion, Overend, R.P., Milne, T.A., and Mudge, L.K. (eds), Elsevier Applied Science, 1985.

Roberts, A.F., "A Review of Kinetics Data for the Prolysis of Wood and Related Substances", Combustion and Flame, 14, 261-272, 1970.

Rolin, A., Richard, C., Martin, G. and Deglisse, X., "Influence of Catalysts on Gasification of Biomass at Short Residence Time", in Energy from Biomass, 2nd EC conference, Strub, A., Chartier, P. and Schleser, G. (eds), Applied Science Publishers, London, 1983.

Rosemount, Technical Literature, 1991.

Satterfield, C.N., "Mass Transfer in Heterogeneous Catalysis", MIT Press, Massachusetts, 1970.

Schimdt, F.W., Henderson, R.E. and Wolgemuth, C.W., "Introduction to Thermal Sciences: Thermodynamics, Fluid Dynamics, Heat Transfer", Wiley, NY, 1984.

Schneider, P.J., "Temperature Response Charts", Wiley, NY, 1963.

Seigal, R. and Howell, J.R., "Thermal Radiation Heat Transfer", McGraw Hill, NY, 1972.

Shafizadeh, F., "An Introduction to the Pyrolysis of Biomass", Journal of Analytical and Applied Pyrolysis, 3, 283-305, 1982.

Shafizadeh, F., "Pyrolytic Reactions and Products of Biomass", in Fundamentals of Thermochemical Biomass Conversion, Overend, R.P., Milne, T.A., and Mudge, L.K. (eds), Elsevier Applied Science, 1985.

Shamsuddin, A.H. and Williams, P.T., "Devolatilization Studies of Oil-Palm Solid Wastes by Thermo-Gravimetric Analysis", Journal of the Institute of Energy, 65, 31-34, 1992.

Shaw, L.N., "A Biomass-Energized Crop Dryer", American Society of Agricultural Engineers, CONF-821257--1, Chicago, December 14-17, 1982

Simmons G.H. and Lee, W.H., "Kinetics of Gas Formation from Cellulose and Wood Pyrolysis", in Fundamentals of Thermochemical Biomass Conversion, Overend, R.P., Milne, T.A., and Mudge, L.K. (eds), Elsevier Applied Science, 1985.

Smith, E.L. and Shand, R.N., "Design and Evaluation of Biomass Gasification Systems", in Biomass for Energy and Industry, 4th EC Conference, Orleans, France 11-15 May 1987, Grassi, G., Delmon, B., Molle, J.-F. and Zibetta, H. Elsevier Applied Science, 1987.

Smith, E.L., Private communication, Aston University, August, 1993.

Sonnenberg, R. Zerbin, W.O. and Krispin, T., "1.4 and 4.8 MW Woodgas Power Plants in Operation", in Energy from Biomass, 3rd EC Conference, Venice, Italy, Palz, W., Coombs, J. and Hall, D.O. (eds), Elsevier Applied Science, London, 1985.

Standish, N. and Tanjung, A.F.A., "Gasification of Single Wood Charcoal Particles in CO_2", Fuel, Vol. 67, 666 - 672, May 1988.

Susanto, H., Beenackers, A.A.C.M and van Swaaij, W.P.M, "Moving Bed Gasifier with Internal Recycle of Pyrolysis Gas", in Energy from Biomass, 2nd EC conference, Strub, A., Chartier, P. and Schleser, G. (eds), Applied Science Publishers, London, 1983.

van den Aarsen, F.G., Beenakers, A.A.C.M and van Swaaij, W.P.M., "Wood Pyrolysis and Carbon Dioxide Char Gasification Kinetics in a Fluidized Bed", in Fundamentals of Thermochemical Biomass Conversion, Overend, R.P., Milne, T.A., and Mudge, L.K. (eds), Elsevier Applied Science, 1985.

Vigil, S.A., Bartley, D.A., Healy R. and Tchobanoglous, G., "Operation of a Downdraft Gasifier Fuelled with Source-Separated Solid Waste", in Thermal Conversion of Solid Wastes and Biomass, Jones, J.L. (ed), American Chemical Society, Washington, USA, 1980.

Walawender, W.P., Chee, C.S. and Fan, L.T., "Operating Parameters Influencing Downdraft Gasifier Performance" Energy from Biomass and Wastes XI, IGT, Chicago, 1988.

Walawender, W.P., Chee, C.S. and Geyer, W.A., "Influence of Tree Species and Wood Deterioration on Downdraft Gasifier Performance", Biomass vol. 17, 51-64, 1988.

Walawender, W.P., Chern, S.M. and Fan, L.T., "Influence of Operating Parameters on the Performance of a Wood-Fed Downdraft Gasifier" Energy from Biomass and Wastes X, IGT, Chicago, 1987.

Walawender, W.P., Chern, S.M. and Fan, L.T., "Wood Chip Gasification in a Commercial Downdraft Gasifier", in Fundamentals of Thermochemical Biomass Conversion, Overend, R.P., Milne, T.A., and Mudge, L.K. (eds), Elsevier Applied Science, 1985.

Wallace, J.B., "Technical Summary of the American Power and Waste Management Gasifier System", report prepared by NovaTec Consultants Inc, Vancouver for American Power and Waste Management Ltd, Vancouver, File: 1185.02, March, 1991.

Wang, Y. and Kinoshita, C.M., "Temperature Field and Reaction Zones in Biomass Gasification", Journal of Solar Engineering, Transactions of ASME, Vol. 113, 224 - 227, Nov. 1991.

Weiner, A.L., "Drying Gases and Liquids - Dynamic Fluid Drying", Chemical Engineering 81, 92 - 101, 1974.

Wessex Water Laboratories, "Analysis by Wessex Water Laboratories of Avonmouth Granules from a Swiss Combi Drying Plant", Ref: SCIA5554, unpublished, Jan. 1991.

Whatman, "Whatman Labsales Filtration and Chromatography Products", Whatman Labsales Ltd., Maidstone, 1991.

Williams, R.O. and Goss, J.R., "An Assessment of the Gasification Characteristics of Some Agricultural Residues Using a Laboratory Scale Gas Producer", Resource Recovery and Conservation, 3, 317-329, 1979.

Williams, R.O. and Horsfield, B., "Generation of Low-BTU Fuel Gas from Agricultural Residues. Experiments with a Laboratory Scale Gas Producer", in Food, Fertilizer and Agricultural Residues, Loehr, R.C. (ed), Ann Arbor Sci. Publ., Mich., USA, 1977.

Winship, R.D., "Evaluation of Fuels for Operation of a Fixed Bed, Downdraft, Commercial Gasifier", Bioenergy R & D Seminar, Vol. 2, 221-5, 1980.

Yoon, H., Wei, J. and Denn, M.M., "Transient Behavior of Moving Bed Coal Gasification Reactors", AIChE Journal, 25, 429-439, 1979.

Zerbin, W.O., "Generating Electricity from Biomass with Imbert Gasifier", 3rd EC Conference, Venice, Italy, 25-29 March, 1985.

APPENDIX A PUBLISHED WORK

(i) Evans, G.D., Milligan, J.B. and Bridgwater, A.V., "The Development of an Open-Core Downdraft Gasifier", in Biomass for Energy, Industry and Environment, 6th EC Conference, Grassi, G. Collina, A. and Zibetta, H. (eds), Elsevier, 1992.

(ii) Milligan, J.B., Evans, G.D. and Bridgwater, A.V., "Results from an Open-core Downdraft Gasifier", presented at Advances in Thermochemical Biomass Conversion Conference, Interlaken, Switzerland, May 11-15, 1992.

(iii) Milligan, J.B. and Bridgwater, A.V., "Downdraft Gasification of Biomass in an Open-Core and a Hybrid-Throated Gasifier", The 1994 IChemE Research Event, University College London, 5-6 January, 1994.

The Development of a Transparent Open-Core Downdraft Gasifier

G D Evans, J B Milligan and A V Bridgwater
Energy Research Group
Department of Chemical Engineering and Applied Chemistry
Aston University, Aston Triangle
Birmingham B4 7ET
UK

Abstract

This paper describes the modifications which have been made to a transparent open-core downdraft gasifier. A venturi ejector has been added to pull, clean and cool the gas in one process stage. This system is more reliable than the previous design and has made the control and operation of the gasifier simpler. The experimental system is described with some preliminary results and plans for future work.

Introduction

The open-core downdraft gasifier used in this project consists simply of an open topped quartz tube through which the biomass feed and oxidant move down to a narrow reaction zone on a bed of char supported on a grate [1]. Biomass is pyrolysed and gasified in this hot reaction zone. This system is simple, robust and eases the problems of scale-up associated with throated downdraft gasifiers. However, the open-core downdraft gasifier is difficult to turn-down and is thought to produce more tars than the throated type.

The objectives of this project were to realize the following:

i) Carry out mass and energy balances over the system,
ii) Investigate the effectiveness and control of the venturi ejector system,
iii) Investigate the effects of feed characteristics on the gasification process,
iv) Study the operability of the gasification system,
v) Investigate the effects of turn-down on reactor performance.

Equipment

The gas cooling, pumping and scrubbing system used previously [1],[2] with a 50mm venturi water ejector system which would cool, clean and move the product gas prior to its analysis for CO_2, CO, CH_4 and H_2 using dedicated infra red gas analysers [1] and subsequent disposal in a flare. The 75mm internal diameter transparent quartz glass gasifier has been retained and has been previously described [1],[2]. Figure 1 shows a schematic of the modified experimental rig.

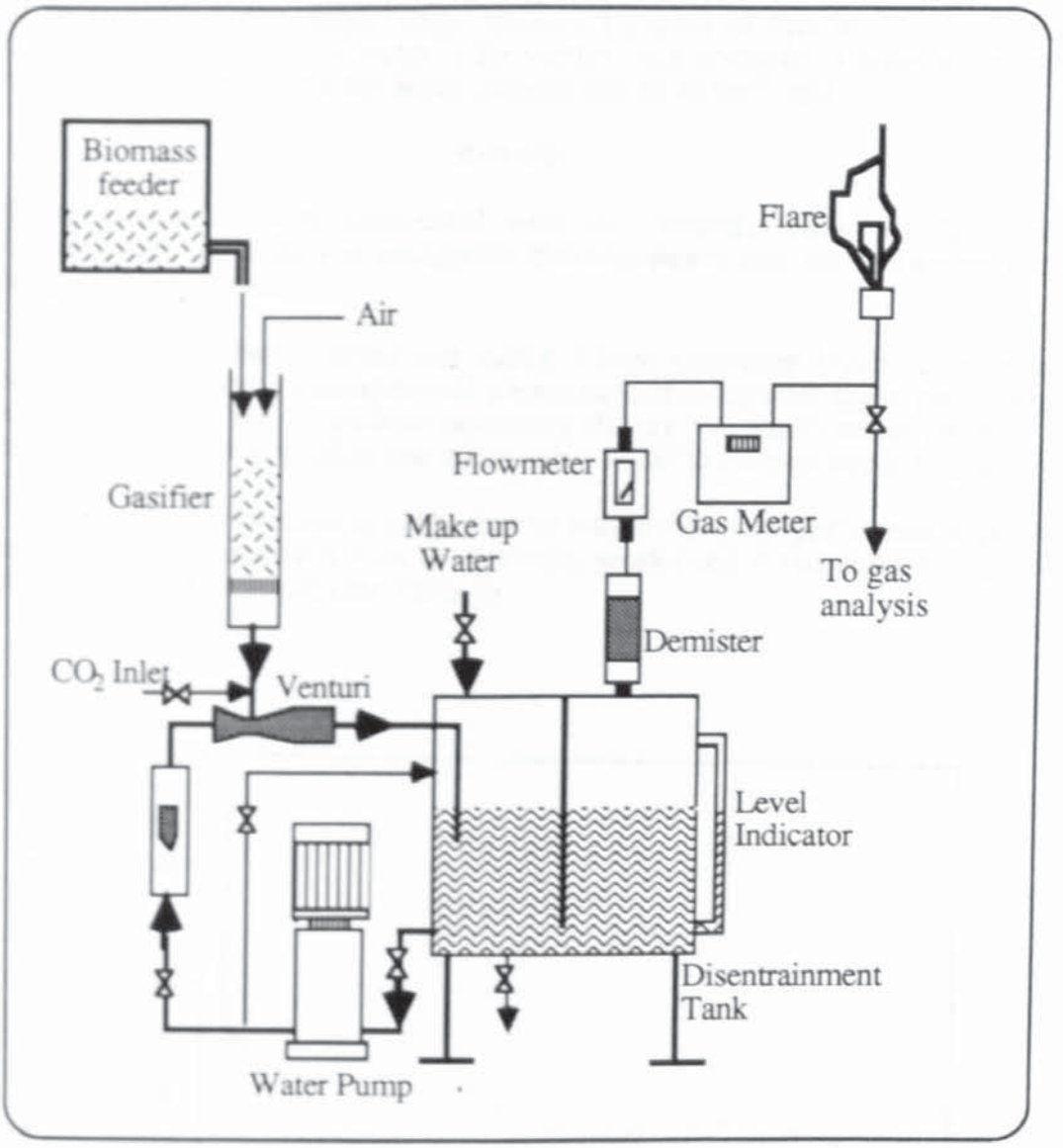

Figure 1 Open-Core Downdraft Gasification System

Description of Operation and Control

It has been shown [2] that an open-core downdraft gasifier can be operated in three modes:

i) Pyrolysis dominant, ie, the char bed below the reaction zone is increasing in size,

ii) Gasification dominant, ie the rate of gasification is greater than the rate of pyrolysis resulting in a reduction in char volume,

iii) Rate of pyrolysis equals the rate of gasification and the reaction zone position and the height of the char bed are both constant.

The third case above is taken as steady state operation for the purposes of carrying out mass and energy balances although during some runs such as during the investigation of turn down, this was not the case. The mode of operation of the gasifier is controlled by the air to fuel ratio within the gasifier which is in turn controlled by the water flowrate to the venturi ejector.

Venturi ejectors work by expanding a fluid, in this case water, at high pressure through a nozzle. The conversion of velocity energy into pressure energy [3] reduces the pressure in a suction chamber and the fluid from the system to be evacuated is sucked in at the throat of the ejector [4]. Suction pressures of down to 50 mmHg (abs)

should be possible using single stage ejectors [5] such as that in this application. Hence, by altering the flow of water to the venturi it is possible to draw more or less air through the gasifier's open top hence altering the air to fuel ratio.

Results

Significant problems were associated with the commissioning of the revised gasification system especially in sealing the disentrainment tank lid. However, once a suitable gasket was found.

One run has been varied out using 15mm diameter birch spheres as a feedstock. This run was videotaped and photographed using time lapse photography to illustrate in detail the operations occurring during the gasification process. A temperature profile of the gasifier was taken using a search thermocouple (Figure 2).

23 runs have been carried out to date of which five were performed to provide base case data for comparison with the previous work carried out using this gasifier and that found in the literature (see Table 1)

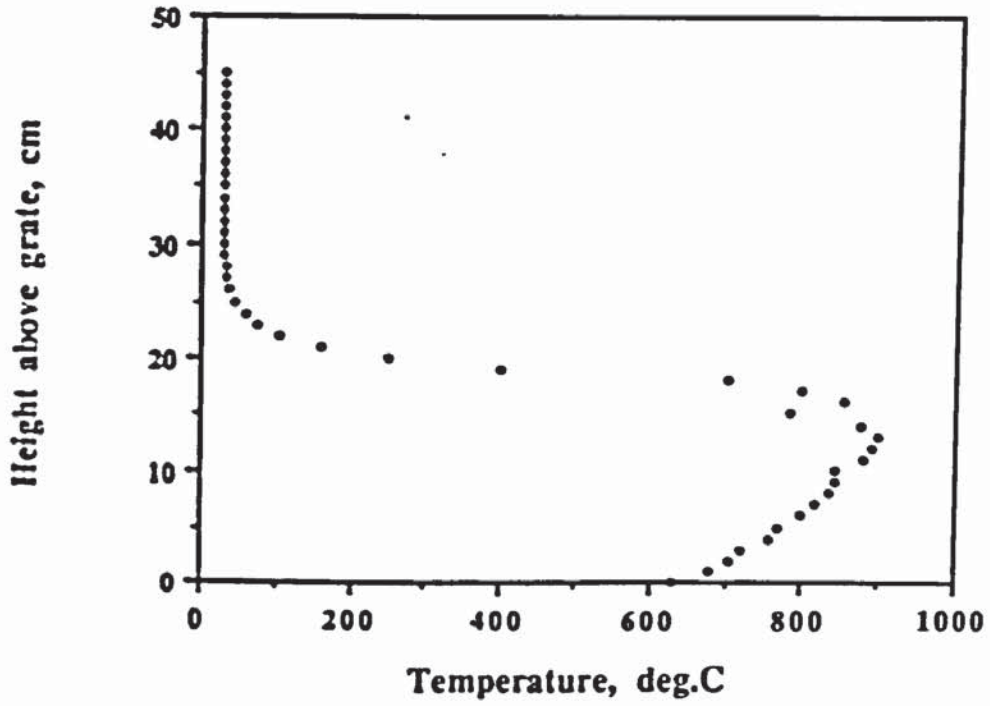

Figure 2 Temperature Distribution Within Gasifier

Although it was found that it was possible to operate this open-core gasifier in the three modes described above, in practice it was found difficult to operate in the gasification dominant regime. This was often found to be because of clogging of the reactor by small particles causing the pressure drop to rise to levels to high for the previous system to operate. However, due to the larger air moving capacity of the venturi ejector compared with the previous gas pump, some results from operating in this mode have been obtained (Figures 3 and 4).

Table 1
Comparison of Typical Results from the Present and Previous Aston Gasifier Designs

	Present Design	Previous Design [6]
Grate diameter, mm	75	75
Specific capacity, dry $kgm^{-2}h^{-1}$	348.49-376.49	290-415
Feedstock type	Wood chips	Wood chips
Feedstock moisture content, % dry basis	9.71-12	10
Feedstock size, mm	6.35-9.5	4.75-6.35
Operational pressure, mmHg	760	760
Maximum temperature, °C	935-1200	900-100
Outputs		
H_2	9.155-12.49	10.3
CO	12.97-16.85	18.6
CO_2	11.756-17.236	11.9
CH_4	0.8-1.63	1.4
N_2	55.339-60.808	57.8
Higher heating value, MJm^{-3}	3.1245-4.194	4.00
Gas production rate, $Nm^3m^{-2}h^{-1}$	902.26-1022.8	850-1050
Gas yield, Nm^3kg^{-1}	2.4139-3.0495	2.53-2.93
Exit temperature, °C	391.02-551.1	450-750

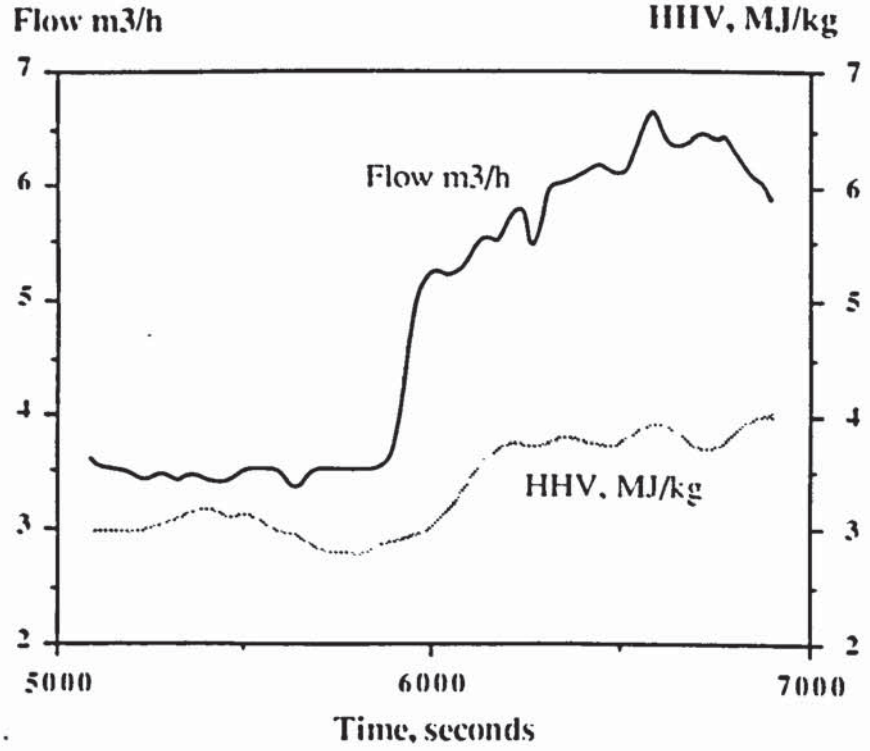

Figure 3
Effect of Increasing Air Flow Through Reactor on Gas Flow and Heating Value

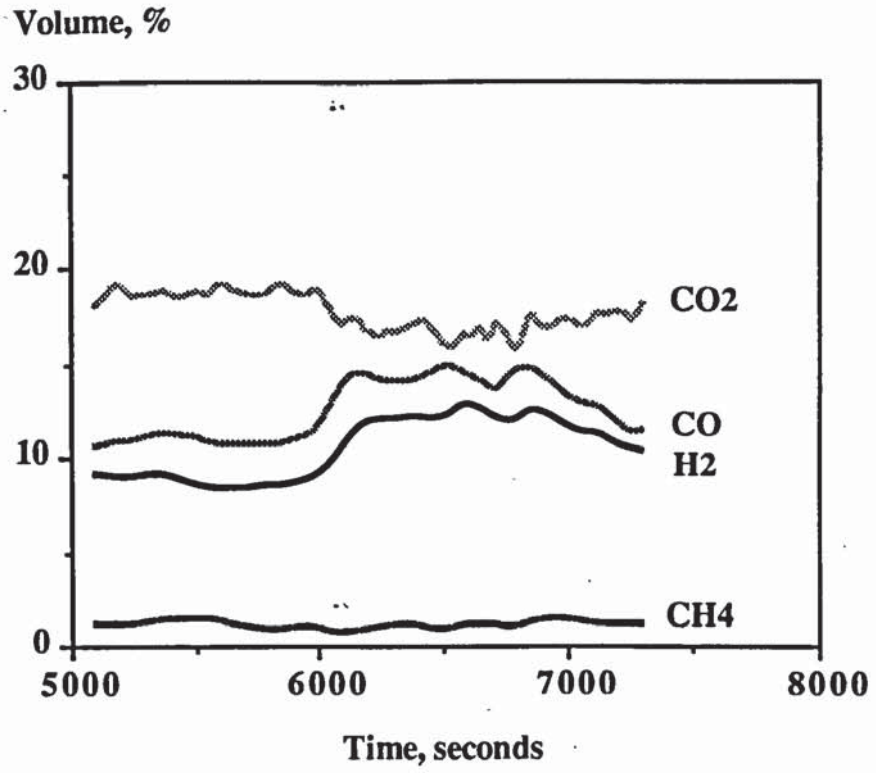

Figure 4
Gas Composition vs Time During Gasification Dominant Mode Period

Discussion

The results from Table 1 show that the gasifier is operating correctly and can be used further as a research tool for the investigation of the gasification process in an open-core downdraft gasifier.

A physical model of the gasification process occurring within an open-core downdraft gasifier has been presented by Reed [7]. However, this has been shown to be flawed in several areas [1]. and was further modified by Earp from his experimental experience. However, this work using a spherically shaped feed would tend to disagree in several areas with Earp's model [1]. In order to describe the gasification process, the gasifier is split into various zones through which each biomass particle travels during the gasification process.

On entry to the reactor, the biomass enters the unreacted feed zone where it falls towards the reaction zone due to the consumption of biomass in the reaction zone. As the draught in the reactor is drawing air down to the reaction zone, no convection currents transfer heat to the particles and since wood is poor conductor of heat, the particles are not heated to any significant extent by conduction until they are within approximately one particle's diameter of the reaction zone [1]. The temperature in this zone, however, (see Figure 2) is about 10-15°C above room temperature (15°C) due to convective heat transfer from outside the reactor as a result of heat losses to the surrounding air from the reaction zone below. As the particle approaches to within six particle diameters of the hottest part of the reaction zone, its temperature rises sharply, though not instantaneously, from approximately 30°C to approximately 900°C (as measured using a search thermocouple; 1000°C using a disappearing filament pyrometer).

The particle then enters the flaming pyrolysis zone where it pyrolyses - the volatiles released burning to provide energy for the system. Earp suggests that following the FP zone, the particles fall through a void of burning gases and on to the

gasifying char bed. However, using the video film and time lapse photography, no void area was noted at any time and flaming gases were clearly seen (especially in negative) occupying the voids occurring naturally between the particles. It is thought that any voids which have been seen previously were as a result of the poor flow characteristics of the non uniformly shaped biomass not pushing unreacted biomass down to compensate for the consumption of biomass.

Following flaming pyrolysis, the particle falls into the char gasification zone where the endothermic gasification reactions occur and thus start to cool the system down (Figure 2). In this run, gasification probably stopped at approximately 5 cm above the grate where the temperature fell below about 750°C. The particles then enter the hot char zone where the temperature is not high enough to sustain gasification though it is thought that some tar cracking may occur.

The work showing the effects of operating in the gasification dominant mode of operation presented show that increasing the air flow rate through the reactor increases the gas production rate as would be expected. The increase in gas heating value is attributed to the increased gas solid reactions occurring in the char bed as indicated by the higher carbon monoxide and hydrogen levels and corresponding lower carbon dioxide levels during this period.

Future Work

A sampling system has been fitted to the gasifier which will allow mass determination of the components of the product gas stream at sub-micron level. With the current gasifier this has been previously achieved by removal of the tar and solid deposits from the tank and pipework after a run. The new sampling system will allow differentiation between tars produced during start-up and those from steady-state operation and measurements of the components including water during operational investigations.

Future work will also include placing a constriction within the quartz reactor to observe and investigate the operation of a throated gasifier and using wood/dried sewage sludge mixes as a feed. In addition, the efficiency of the venturi ejector as a gas scrubber will be determined.

Conclusions

The gasifier system has been modified to increase the efficiency of the system, allow a more accurate degree of control, allow simpler operation thus increasing operator safety, to permit more accurate mass and energy balances to be realized and to allow a study of the operability of the system to be carried out.

Studies have been conducted to obtain base case data for comparison with the work previously carried out using this gasifier and with the results presented in the literature. Video tape film of a run using a spherically shaped feed have helped to refine physical modelling of the gasifier.

It has now been possible to carry out more runs in the gasification dominant mode of operation - the effects of which on gas heating value and flowrate have been presented in this paper. Further analysis work is now required to investigate the effects of turn down on this reactor's performance.

References

1 Earp D M, Gasification of Biomass in a Downdraft Reactor, PhD Thesis, Aston University, 1988

2 Earp D M, Reyes-Nunez, L R, Evans G D, Bridgwater A V., Mass and Energy Balances Over an Open-Core Downdraft Gasifier, 5th E.C. Conference,

Biomass for Energy and Industry, Grassi G, Gosse G, dos Santos G (eds), Lisbon, 1989

3 Perry R H, Green D, Perry's Chemical Engineer's Handbook, 6th Edition, McGraw Hill, 1985

4 Coulson J M, Richardson J F, Chemical Engineering, Volume 2, Unit Operations, Pergammon, 3rd edition, 1978

5 Harker J H, Backhurst J R, Process Plant Design, Heinemann Educational Books, London, 1983

6 Earp D M, Bridgwater A V., Research into a Transparent Open Core Downdraft Gasifier, 4th E.C. Conference, Biomass for Energy and Industry, Grassi G, Delmon B, Molle J-F Zibetta H (eds), Orleans, France, 1987

7 ReedT B, Graboski M S, Levie B, Fundamentals, Development and Scaleup of the Air-Oxygen Stratified Downdraft Gasifier, The Biomass Energy Foundation Press, Box 1392, Golden, CO 80402, USA. SERI Report SERI/PR-234-3571. 1988

RESULTS FROM A TRANSPARENT OPEN-CORE DOWNDRAFT GASIFIER

J B MILLIGAN, G D EVANS AND A V BRIDGWATER
Energy Research Group
Department of Chemical Engineering and Applied Chemistry
Aston University
Birmingham B4 7ET, UK

ABSTRACT

A transparent quartz reactor has allowed observations on the process of gasification of biomass within an open-core gasifier. This has enabled the individual stages in the gasification process to be qualitatively and quantitatively described. Results achieved using the gasifier are presented which show the effects of insulating the reactor on the performance of the gasifier. Insulation has the effect of improving the heating value of the product gas by 33%, and the cold gas efficiency of the gasifier is improved from 46.7% to 63.5%. The results are compared to those obtained using an equilibrium model for an ideal gasifier.

INTRODUCTION

Open-core downdraft gasification operates without the throat of a conventional downdraft gasifier. The bed is supported by a grate within the reactor. Air and feed enter through the open top of the reactor and travel downwards to the reaction zone. Gasification is a three step process, (drying, pyrolysis and gasification), which can be seen as horizontal stratified zones within the reactor [1].

The feed bed remains unaltered until it approaches the reaction zone where back radiation from reaction zone causes the feed to heat and dry. As the temperature rises above 250 °C pyrolysis of the feed occurs in a narrow band at the reaction zone front. Here thermal degradation takes using the radiative energy released by the partial oxidation of the pyrolysis products in the zone below. The products from the flaming pyrolysis zone consisting of char, a complex liquid fraction comprising of tars and oils, and a gaseous phase including water vapour, CO, CO_2, H_2 and hydrocarbons then pass into the gasification zone. In the gasification zone thermochemical conversion takes place at about 1000 °C.

The char is converted into the product gas by the following reactions;

Boudouard reaction	$C + CO_2 = 2CO$
Water gas reaction	$C + H_2O = H_2 + CO$

The above reactions are endothermic and energy contained in the hot gases and char from the partial-oxidation zone above is required to drive the reactions. As the reactions proceed the temperature progressively decreases reducing the rate of the reactions until they become insignificant below 700°C [2]. The extent of char reduction is, therefore, dependant upon the amount of energy entering the reduction zone [3]. Heat losses from a gasifier are, therefore, to be avoided as they decrease the heating value of the product gas [4]. In addition tar cracking in the gasification zone is reduced at lower temperatures.

Finally the product gases pass through an inert char zone in which temperatures are too low for any further significant gasification to take place.

The gasifier can be basically operated in three modes [5];

1) Gasification dominant, where the rate of char consumption is greater than the rate of char deposition by pyrolysis. This results in movement of reaction zone towards the grate.
2) Pyrolysis dominant, where pyrolysis occurs at a faster rate than that of gasification resulting in char accumulation (increase in char bed height).
3) Stable reaction zone, where the rate of char deposition by pyrolysis equals the rate of char depletion by gasification.

The mode of operation is dependant upon the equivalence ratio which is about 0.25 for gasification without heat losses [4]. At equivalence ratios less than 0.25 the gasifier operates in the pyrolysis dominant mode and char is continually generated. Stable mode operation at the carbon boundary is the thermodynamic optimum for gasification [6] giving the maximum output of chemical energy as product gas. Because of their fixed geometry it is likely that open-core gasifiers can only operate continually with a stable reaction zone at a fixed set of operating parameters for a given feedstock, however small changes in any operating parameter may cause the zone to drift [7].

EQUIPMENT

Granulated wood chips of 6.35-12.7 mm in size and approximately 10% moisture content (wet basis) are used as the standard feed during investigations.

A diagram of the open-core gasifier is shown in Figure 1. Gasification of the wood chips takes place within a 75mm ID open topped quartz cylinder. A venturi ejector provides the driving force to pull air into the reactor and the product gas from the reactor. The gas is cooled and cleaned by the venturi before passing into a baffled water tank where gas disentrainment takes place. The tank also provides a reservoir for the water circulation system flowing through the venturi. The gas then passes through a demister to remove water before passing through the flow metering devices.

A continuous sample is drawn off for gas analysis after passing through filters to remove particulates and tar and a silica gel column to dry the gas. The gas composition is determined using infra-red (CO, CO_2, and CH_4) and thermal conductivity (H_2) gas analysers with the balance assumed to be N_2. The gas is then flared off in a lean gas burner.

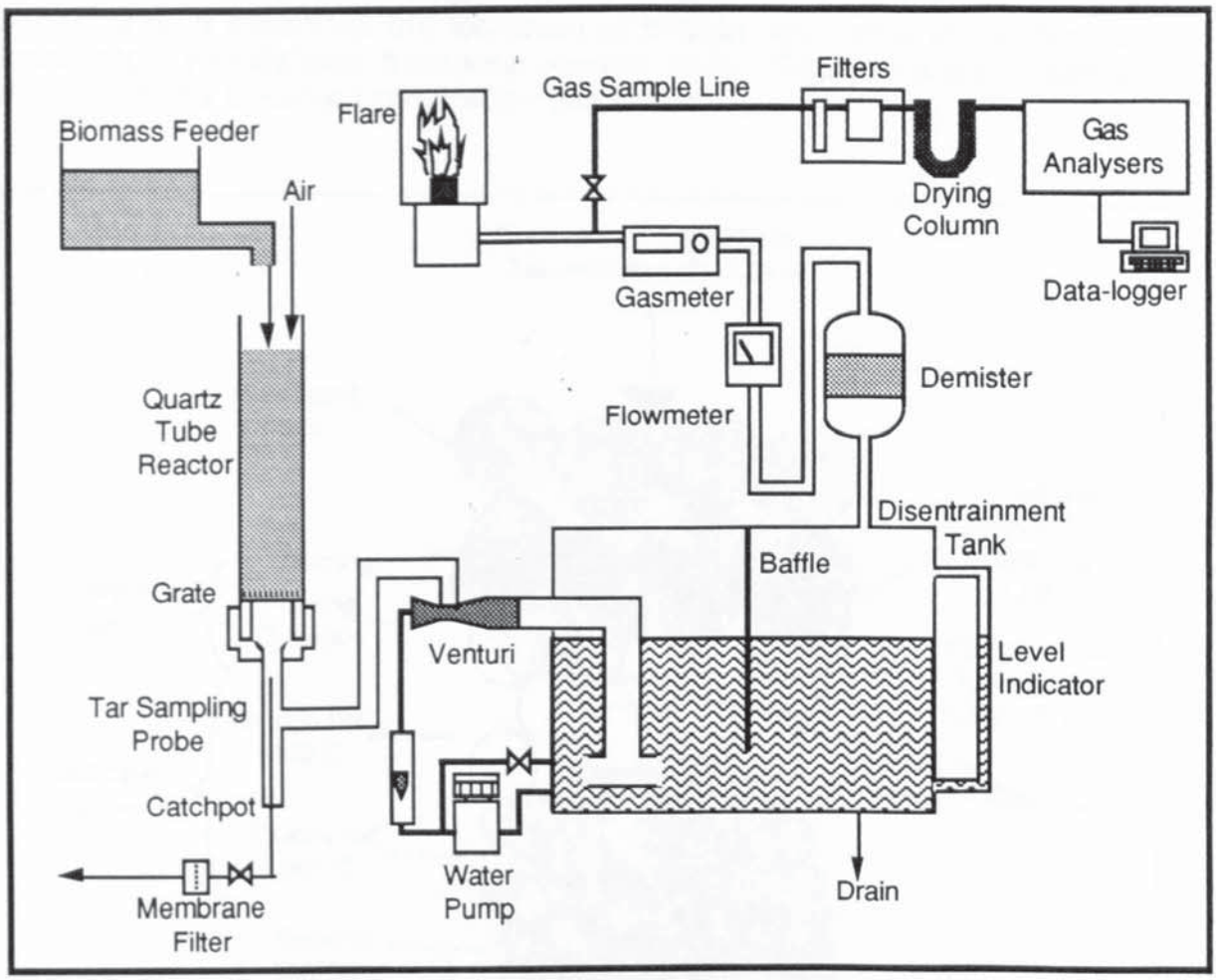

Figure 1: Gasifier Configuration

A representative sample of the gas (12% of the total product gas volume) is taken from below the grate using an isokinetic probe to permit the tar and solid particulate loading of the gas to be determined. The particulates are collected on a 0.1μm nylon membrane filter for gravimetric analysis. Tar and solid deposits are also washed out of the system using acetone and added to the results from the filter analysis. Using the measured gas sampling rate enables calculation of the particulate load in the product gas.

The reactor can be insulated with Kaowool mineral fibre leaving 10% of the reactor surface free in a narrow vertical strip for observation and measurement of the reaction zone. Temperature profiles within the gasifier were measured using a thermocouple that could be moved up and down the length of the reactor within a close-fitting sheath. A disappearing filament pyrometer was also used to measure temperatures between 800 and 1200 °C in the gasification zone.

RESULTS AND DISCUSSION

QUALITATIVE DESCRIPTION OF GASIFICATION

The transparency of the quartz reactor has allowed qualitative examination of the processes which individual particles undergo during gasification in an open-core downdraft gasifier. Observations of the behaviour of single spherical particles were made during steady state operation as the spherical feed minimises the formation of bridges and voids in the reactor leading to a well defined, horizontal reaction zone. Figure 2 is a conceptual diagram of the observed gasification processes.

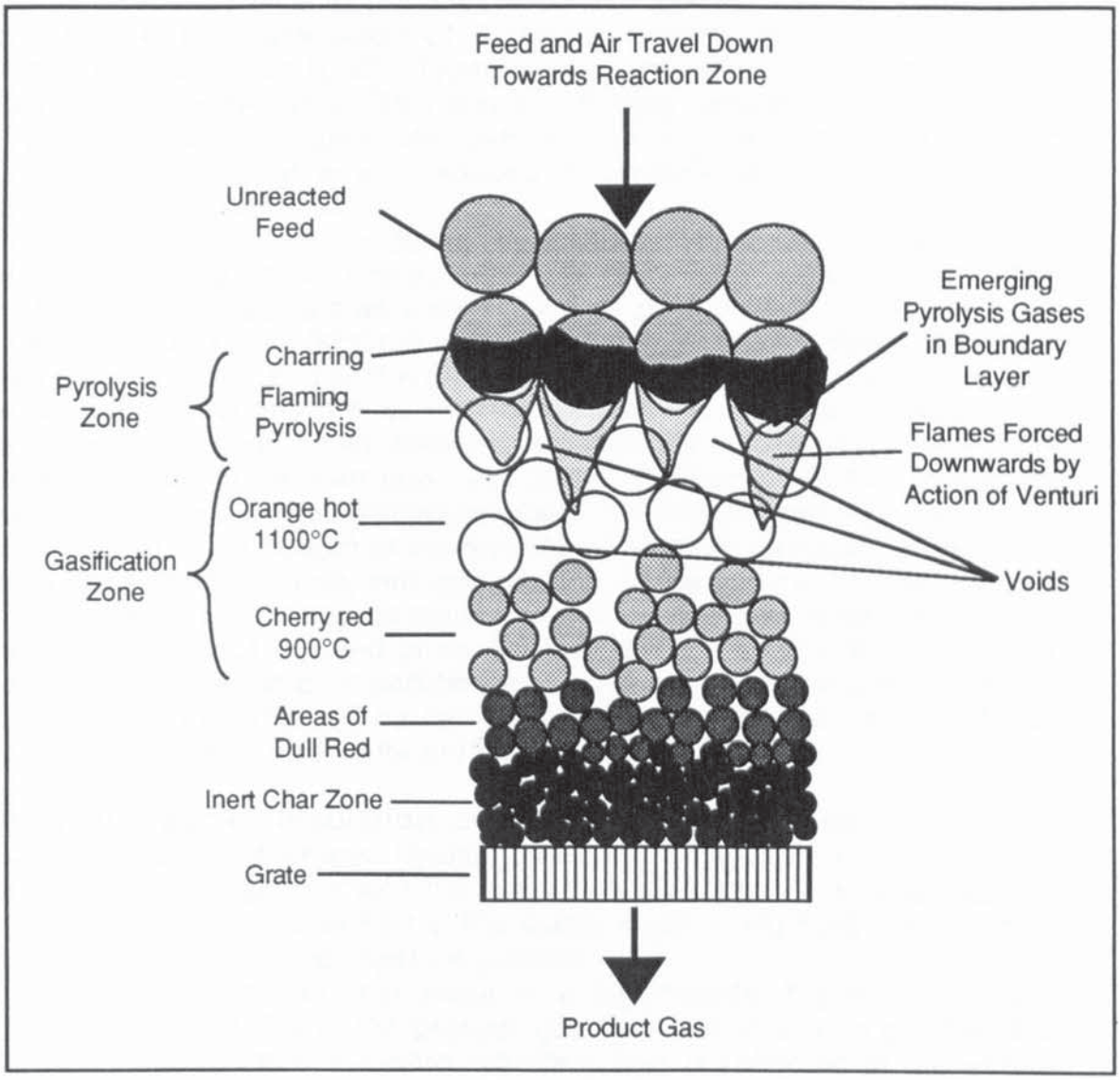

Figure 2: Zonation Within the Open-Core Gasifier

The feed travels down the reactor as biomass is consumed in the reaction zones below. As a single particle descends towards the reaction zone, the base of the particle begins to char due to back radiative heat transfer from below and the particle is progressively charred as it passes through the pyrolysis zone. Directly after this wave of charring, flames can be seen evolving from the particle as the pyrolysis products are oxidized. This is the "flaming pyrolysis" zone described by Reed [1], which observations show to be approximately one particle diameter in depth.

The particle is enveloped by a flame separated from the particle itself by a boundary layer of emerging pyrolysis gases. The flames are drawn downwards in forced convection by the suction from the venturi. Jets of flame can occasionally be seen streaming through the reaction zone. This indicates the channelling of gases through voids resulting in poor oxidant distribution across the reaction zone and allowing pyrolysis products to pass directly through the zone below without completely reacting, thereby reducing gasification efficiency.

In the flaming pyrolysis zone visible shrinking of the particle occurs which results in a reduction in particle volume. This causes an increase in voidage towards the bottom end of the zone. Voids are particularly prominent when using irregular shaped wood chips. When a bridge over a void collapses pyrolysing particles may fall directly into the gasification zone before the completion of pyrolysis. However, due to the high temperatures of about 1000°C found in the gasification zone, such particles rapidly complete pyrolysis. This may significantly reduce the residence time for particles that have fallen into voids within the gasification zone resulting in incomplete gasification and reduced tar cracking leading to a higher tar loading in the product gas.

Flaming pyrolysis ends as the emission of burning volatiles dies away and the particle moves into the char gasification zone. The gasification zone appears as a bright orange zone (indicating temperatures of between 900 and 1100°C) of incandescent char, approximately 6 to 8 cm deep. Towards the end of the glowing orange zone, the colour of the char darkens through cherry red, dull red to black as the temperature decreases. Gasification reaction rates become significantly slower as temperature decreases prior to an inert cool char zone. A sharply defined end to the gasification zone is not distinguishable. Individual particles cannot be distinguished at the bottom of the reaction zone since gasification has either totally consumed or greatly reduced the size of the particle. An ash residue is left some of which may become entrained in the gas stream along with charcoal dust (soot). Reed gives approximately 2 to 5% of the charcoal leaving the gasifier as char particles entrained in the product gas stream [1]. Further measurements will be carried out to determine the amount of char leaving the gasifier under different operating conditions.

Effect of Gasifier Insulation on Gasifier Performance

Table 1 compares averaged results from 2 stable reaction zone runs using the non-insulated gasifier with the average results of 4 runs obtained from the insulated gasifier operated in the stable mode using runs with a similar char bed height and feed moisture content.

The table shows that there is a significantly higher percentage volume of H_2 and CO in the product gas from the insulated gasifier than from the non-insulated standard reactor. This is reflected in the energy content of the product gas being 33% higher for the insulated gasifier. In addition, the hot and cold gas conversion efficiency of the gasifier is improved and the tar loading in the product gas is decreased when using insulation. These results can be explained using the temperature profiles within the insulated and non-insulated gasifier presented in Figure 3.which also gives the positions of the reaction zones at the time of measurement. The profile for the insulated reactor is from a single set of results from a run given in Table 1.

TABLE 1
Gasifier Performance Data (Averaged)

	Insulated Gasifier	Non-Insulated Gasifier
Run numbers used	1,29,30,31	28,32
Average run duration, mins.	46.6	58.5
Feed moisture content, %	9.42	9.49
Char bed height, cm	18.97	17.23
Specific capacity, $kgm^{-2}h^{-1}$	320.57	276.39
Volumetric yield, Nm^3kg^{-1}	2.98	2.94
Equivalence ratio	0.361	0.392
Dry gas HHV, $MJNm^{-3}$	4.25	3.20
H_2/CO ratio	0.77	0.66
CO/CO_2 ratio	1.46	1.07
Product gas exit temperature, °C	637.38	440.39
Hot gas efficiency, %	77.44	55.40
Cold gas efficiency, %	63.52	46.69
Gas composition, % volume;		
H_2	13.25	9.25
CO	17.41	14.22
CO_2	12.36	13.69
CH_4	1.50	1.01
N_2	55.48	61.82
Tar Loading, $mgNm^{-3}$	522.8	746.6

Heat losses from the gasifier are reduced by 50% when using insulation. This results in higher temperatures throughout the reactor. The high temperatures measured in the unreacted feed bed for the insulated gasifier are believed to be misleading since pyrolysis, which begins at 250-350 °C, was not observed. This is believed to be due to back conductance of heat from the reaction zone along the thermocouple sheath.

In the unreacted feed zone, the feed has a longer drying time before it reaches the flaming pyrolysis zone. Within the flaming pyrolysis zone less energy is therefore required for pyrolysis since there is less moisture to be evaporated. The flames from the oxidation of pyrolysis products are drawn downwards by the pull of the venturi and supply the heat energy required to drive the gasification reactions. Figure 3 shows the reduction in temperature downwards through the gasification zone due to the endothermic reactions. Heat loss from the reactor reduces the amount of gasification taking place. This can be seen from the gas compositions and the ratios of H_2 to CO and CO to CO_2.

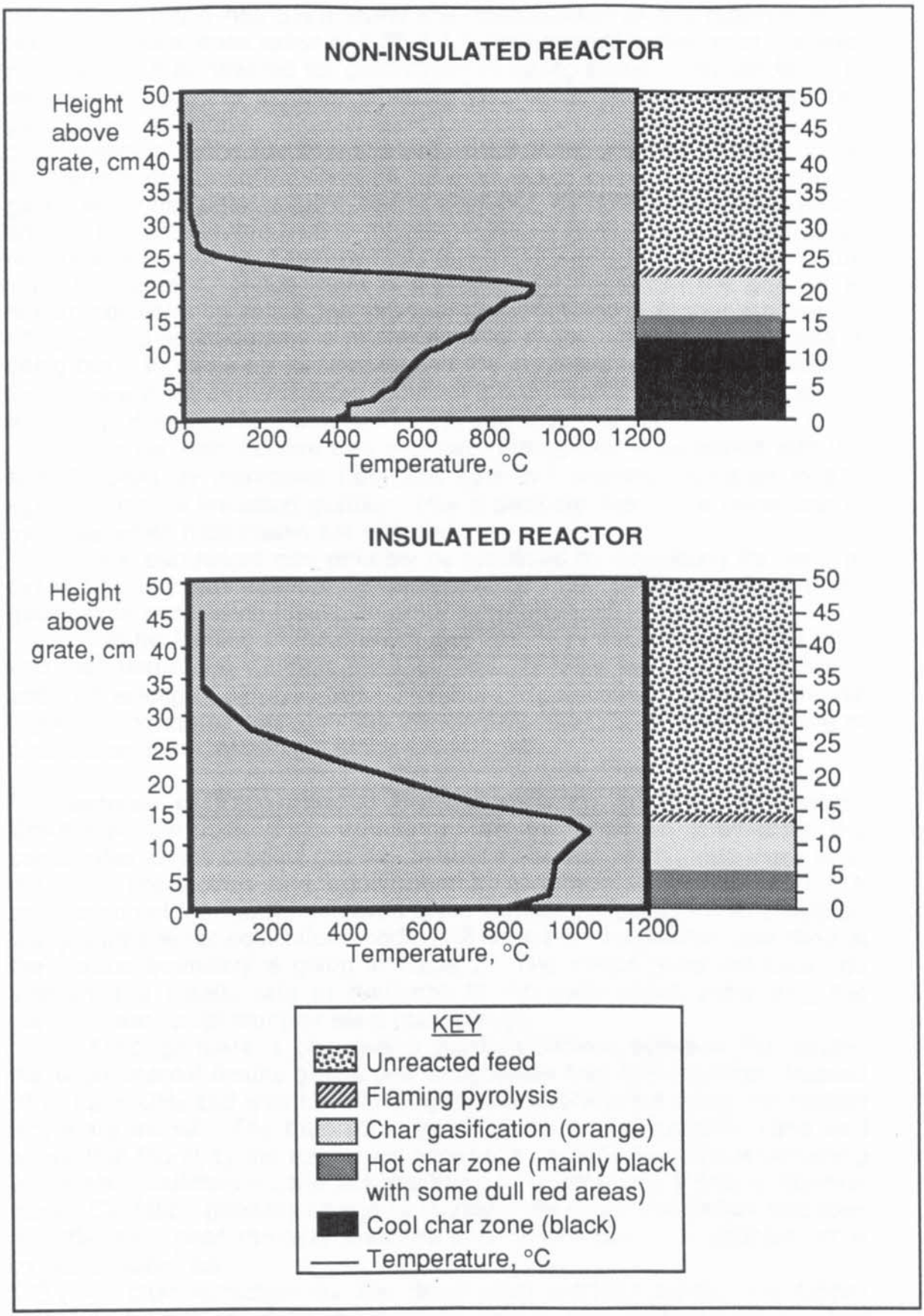

Figure 3: Vertical Temperature Profiles for Non-insulated and Insulated Reactors

Generally it has been found that stabilization of the reaction zone occurs at equivalence ratios of 0.35-0.4 indicating that oxidation of the feed in excess of that required for gasification is taking place. This oxidation is required in order to achieve a stable bed by providing energy for the gasification reactions. Char oxidation occurs in the gasification zone, as char oxidation in the flaming pyrolysis is not thought to be possible since the particle has been observed to be enveloped in the evolving pyrolysis gases which has been noted in earlier work [8]. As heat losses increase the amount of oxidation required to maintain a stable zone also increases. This results in a higher equivalence ratio for the standard as compared to the insulated reactor. Since there is a greater air input into the gasifier at higher equivalence ratios the product gas contains a higher fraction of nitrogen and consequently a poorer heating value. As less of the feed is being burnt to make up for heat loss in the insulated reactor this results in the improvement in the heating value of the product gas and the cold gas efficiency of the gasifier observed for the insulated gasifier.

Results also indicate that a greater throughput is achieved with the specific capacity increased from 276 $kgm^{-2}h^{-1}$ without insulation to 321 $kgm^{-2}h^{-1}$ for the insulated gasifier. This is possibly due to the faster rate of pyrolysis when heat losses are reduced.

Char bed height may possibly be stabilized by equalizing the rates of pyrolysis and gasification by maintaining high temperatures in the gasification zone using insulation around the gasification zone.

The tar loading of the product gas from the insulated gasifier is 30% less than that of the standard case tar load. At lower temperatures there is poorer cracking of pyrolytic tars. Therefore in the insulated reactor, where higher temperatures exist, the tars are cracked to a greater extent leading to a reduction in the tar content of the product gas.

Comparison of Experimental Results with an Equilibrium Model

Chemical thermodynamic equilibria can be used in predicting the composition of the product gas [9]. In stable reaction zone mode there is no net char production and equilibrium is assumed to be reached. A comparison of the results achieved using insulation against those predicted using a theoretical equilibrium model [10] based on the gasifier operating at the carbon boundary is given in Table 2. The model does not take into account the kinetic rate of reactions in the gasification zone only the thermodynamic optimum for ideal operation [6].

Although there is generally a good agreement between the results, the experimental results give a gas composition that has a greater fraction of CO and CH_4 and less H_2 and CO_2 than that predicted using the carbon boundary model. The theoretical model gives an equivalence ratio well below that found by the results indicating that oxidation reactions occurring within the gasification zone are important in maintaining a stable reaction zone. Oxidation provides energy to increase the rate of reduction reactions in order that char removal matches char production. In addition, char oxidation provides
CO_2 for char reduction by the Boudouard reaction hence the higher CO/CO_2 ratio in the product gas compared to that predicted for an ideal gasifier. The gas compositions achieved may not, however, have reached equilibrium on leaving the hot gasification zone. Rate models have also been developed for example by Groeneveld [11] and Reed [1] in the prediction of gasifier performance. Further work may include modelling of

the system based upon the observations made and the stagewise mechanisms deduced.

TABLE 2
Comparison of Experimental Results from the Insulated Reactor with the Theoretical Results from the Equilibrium Model [10]

	Equilibrium Model	Experimental Results
Model Input		
Heat loss, % (by calculation)	16.6	16.6
Feed analysis, CHO	$C_6H_{8.25}O_{3.39}$	
Moisture, % wet basis	9.49	
Ash, %	0.07	
Inlet temperature, °C	20	
Model Output		
Dry gas composition, % volume;		
H_2	16.34	13.25
CO	15.52	17.41
CO_2	13.67	12.36
CH_4	0.84	1.50
N_2	53.63	55.48
Dry gas HHV, $MJNm^{-3}$	4.15	4.25
H_2/CO ratio	1.05	0.77
CO/CO_2 ratio	1.14	1.46
Equivalence ratio	0.272	0.361
Product gas exit temperature, °C	624.57	637.38
Cold gas efficiency, %	61.79	63.52

The investigation of the effect of process parameters on gasification performance will continue with the measurement of tar and solid particulate loading of the raw product gas under a variety of conditions such as feed moisture content, feed size and the use of insulation. In addition to this, a means of measuring the raw product gas moisture content will be developed enabling mass balances to be carried out to a greater degree of accuracy.

A stirrer will be introduced in order to reduce the occurrence of voids and bridging within the reaction zone which may reduce the efficiency of gasification, to investigate its action on the reaction zone and the effect on gasification. A stirring device would also increase the removal of fines from the char bed which cause an increasing pressure drop across the bed leading to instability of the reaction zone.

The use of a transparent quartz throat within the reactor is to be investigated. This will allow the observation of individual particles undergoing gasification within the throat of the gasifier providing an understanding of the processes involved. The performance of the throated gasifier is to be compared with the open-core system using identical feeds. An investigation on the turndown of the throated gasifier will be carried out.

CONCLUSIONS

A greater understanding of the processes occurring during gasification has been achieved using the detailed observations obtained with the transparent reactor. This information will be useful in directing future investigations aiming to improve gasification performance such as the use of a stirrer to reduce voids in the reaction zone. The effect of using insulation on improving gasifier performance and product gas quality has been explained with attention to thermodynamics. For an un-insulated reactor, a higher air to fuel ratio is required to maintain a stable reaction zone to compensate for heat loss. This results in product gas with a lower energy content than that achieved with insulation. Considerable improvements to cold gas efficiency and reduced tar loading of the product gas are also achievable with the use of insulation. The experimental results obtained deviate from the ideal predicted using the carbon boundary model since a higher air to feed ratio is required in order to maintain a stable reaction zone. Further studies using a throated transparent reactor will provide information on throated gasification performance.

REFERENCES

1. Reed, T.B. and Markson, M., A Predictive Model for Stratified Downdraft Gasification of Biomass, in Proceedings of the 15th Biomass Conversion Contractors Meeting, March 16-17, 1983, CONF 830323 PNL-SA-11306.
2. Reed, T.B., Levie, B., Markson, M.L. and Groboski, M.S., A Mathematical Model for Stratified Downdraft Gasifiers. Symposium on Mathematical Modelling of Biomass Pyrolysis Phenomena, Division of Fuel Chemistry 28, 5. American Chemical Society, Washington, 1983.
3. Chern S-M., Equilibrium and Kinetic Modeling of Co-Current (Downdraft) Biomass Gasifiers, PhD Thesis, Kansas State University, 1989. pg 2-6.
4. Reed, T.B., Graboski, M.S. and Levie, B., Fundamentals, Development and Scaleup of the Air-Oxygen Stratified Gasifier. The Biomass Energy Foundation Press. SERI/PR-234-2571, 1988.
5. Earp, D.M., Reyes-Nunez, L.R., Evans, G.D. and Bridgwater, A.V., Mass and Energy Balances Over an Open-Core Downdraft Gasifier, Biomass for Energy and Industry, Volume 2. EC Conference 9-13 Oct 1989, Lisbon. Grassi, G., Gosse, G. and dos Santos, G. (eds), Elsevier Applied Science, London, 1990.
6. Double, J.M., Smith, E.L. and Bridgwater, A.V., Computer Modelling of Fluidised Gasification in Pyrolysis and Gasification, Ferraro, G.L., Maniatis K., Buekens, A. and Bridgwater, A.V. (eds), Elsevier Applied Science, London, 1989.
7. Reed, T.B. and Markson, M., Biomass Gasification Reaction Velocities in Fundamentals of Thermochemical Biomass Conversion, Overend, R.P., Milne, T.A., and Mudge, L.K. (eds), Elsevier Applied Science, 1985.
8. Earp, D.M., Gasification of Biomass in a Downdraft Reactor, PhD thesis, Aston University, Birmingham, UK, 1988.
9. Gumz, W., Gas Producers and Blast Furnaces: Theory and Methods of Calculation, Wiley, New York, 1950.
10. Double, J.M., The Design, Evaluation and Costing of Biomass Gasifiers, PhD thesis, Aston University, Birmingham, UK, 1988.

12. Groeneveld, M.J., The Co-Current Moving Bed Gasifier, PhD thesis, Twente University of Technology, The Netherlands, 1980.

DOWNDRAFT GASIFICATION OF BIOMASS IN AN OPEN-CORE AND A HYBRID-THROATED GASIFIER

J.B. MILLIGAN, A.V. BRIDGWATER
Energy Research Group, Department of Chemical Engineering and Applied Chemistry, Aston University, Aston Triangle, Birmingham, B4 7ET

ABSTRACT

The gasification of 6.35-12.7 mm wood blocks has been studied within an existing transparent open-core gasifier. The reactor was modified by placing a throat within the reactor to create a hybrid-throated downdraft gasifier. The hybrid gasifier is a simpler construction than the conventional downdraft gasifier since a gas tight feeding system and air injection at the throat are not required. For a similar throughput to the open-core, the hybrid-throated gasifier produces a gas with a higher energy value and a reduced tar content. Temperatures greater than 1200°C below the throat improve the tar cracking performance of the gasifier. The hybrid gasifier has been found to have a turndown capability of 2:1.

INTRODUCTION

Biomass is in principle a CO_2 neutral energy resource and is the only renewable source of fixed carbon. Biomass fuels typically have a lower sulphur content than fossil fuels. Gasification is one of several thermochemical methods for the conversion of biomass into more useful and valuable fuels and chemical feed stocks.

There are two basic types of downdraft gasifiers (see Figure 1). The conventional downdraft requires an air tight lid with air introduced just above the throat. The restriction is claimed to create a high temperature zone in which tars are cracked, as discussed by Groeneveld (1). In addition, the throat may be responsible for turndown, ie the ability to reduce output on demand, although how this is achieved is not fully understood.

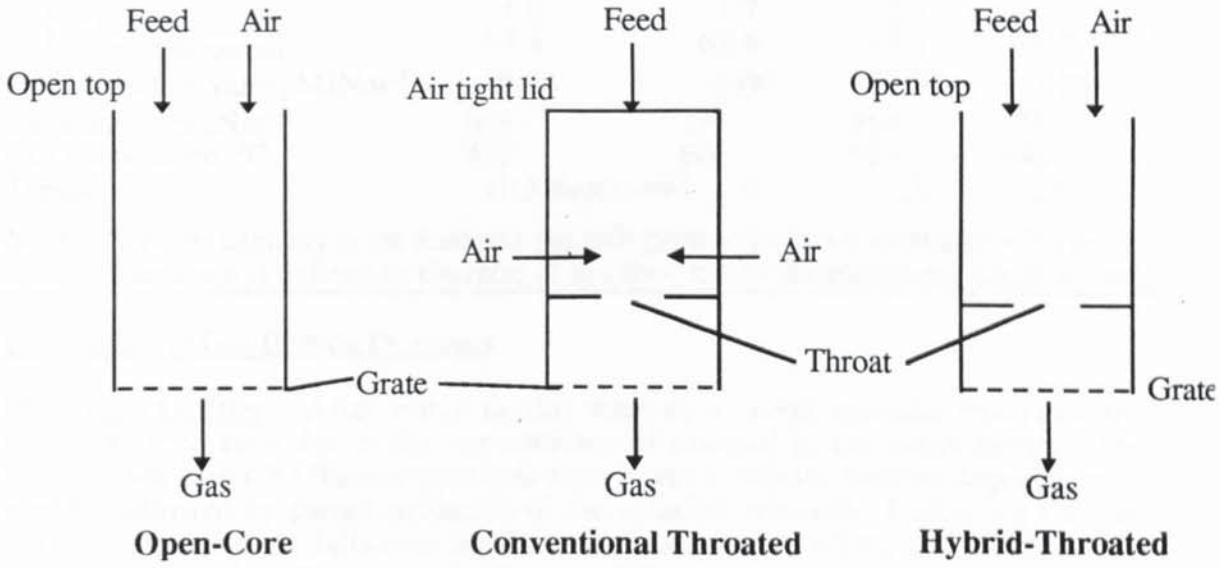

Figure 1: Downdraft Gasifier Types

The open-core downdraft gasifier, developed by Reed (2) in 1980, consists of an open topped tube through which the biomass and oxidant descend towards a reaction zone. The open-core downdraft gasifier is claimed by Earp (3) to have only one throughput at which the reaction zone is stable (with a stationary reaction zone), ie there is no turndown.

The introduction of the throat of the conventional gasifier to the open-core reactor creates a hybrid gasifier as shown in Figure 1, with the objective of giving turndown and reducing the tar content of the product gas whilst retaining the simplicity of construction of the open-core.

EQUIPMENT

A 75 mm diameter transparent quartz reactor is used in the gasification of 6.75-12.7 mm wood blocks having a moisture content of about 10 % (wet basis). For hybrid-throated tests a 40 mm restriction is placed within the reactor. A water based venturi ejector is used to cool, clean and pull the product gas. On-line CO_2, CO and CH_4 infra-red and H_2 thermal conductivity gas analysers measure the gas composition. The product gas is then disposed in a flare. A raw gas sampling system is fitted which is used to determine the water, tar and solid particulate content of the gas.

RESULTS

Table 1 gives the averaged results obtained from 6 open-core runs and results obtained with the hybrid reactor at different throughputs.

TABLE 1: Experimental Results Obtained Using Downdraft Gasifiers

	Open-core	Hybrid-throated		
Throughput	average	low	medium	high
Specific capacity, dry $kgm^{-2}h^{-1}$ (high)	271	261 (low)	401	464
Maximum temperature, °C	1134	1231	1213	1225
Dry gas composition, % v/v				
H_2	9.5	9.8	9.9	6.5
CO	15.2	16.5	17.5	15.8
CO_2	10.5	9.4	8.4	10.4
CH_4	1.0	1.7	1.1	1.1
N_2 *(by difference)*	63.8	62.6	63.1	66.2
Higher heating value, $MJNm^{-3}$	3.54	4.00	3.92	3.25
Tar loading, $mgNm^{-3}$	665	179	369	75
Exit temperature, °C	417	606	628	650
Turndown	(1.3 maximum)	1.0	1.5	2.0

Notes: Specific capacity is the feed rate per unit grate area, (grate diameter = 7.5 cm).
Turndown is defined as the ratio of gas flow rate to the minimum gas flow rate.

Description of Gasification Processes

Open-Core Gasifier After entry to the reactor, a wood particle descends the unreacted feed zone due to the consumption of material in the zones below. The particle then enters the flaming pyrolysis zone where pyrolysis, thermal degradation, is rapidly followed by partial oxidation of the volatiles released. Following flaming pyrolysis, the particle falls into the char gasification zone where endothermic char gasification reactions take place resulting in a fall in temperature within the zone from about 1050°C to 700°C. Finally, the particle enters an inert char zone where the kinetic rate of gasification is negligible due to temperatures falling below 700°C.

Hybrid-Throated Gasifier In the hybrid gasifier the flaming pyrolysis zone is supported by the throat. Below the throat there is a gap of about 1.5 cm before the

gasification zone bed of char within which the product gases can be seen to fan outwards across the top of the char bed and circulate within the region indicating good mixing. Periodically, the material bridging over the throat collapses as a result of a reduction in volume due to pyrolysis of the supporting material, and char falls through to the gasification zone below.

DISCUSSION

The operational limits of the open-core and the hybrid-throated gasifier are indicated in Figure 2.

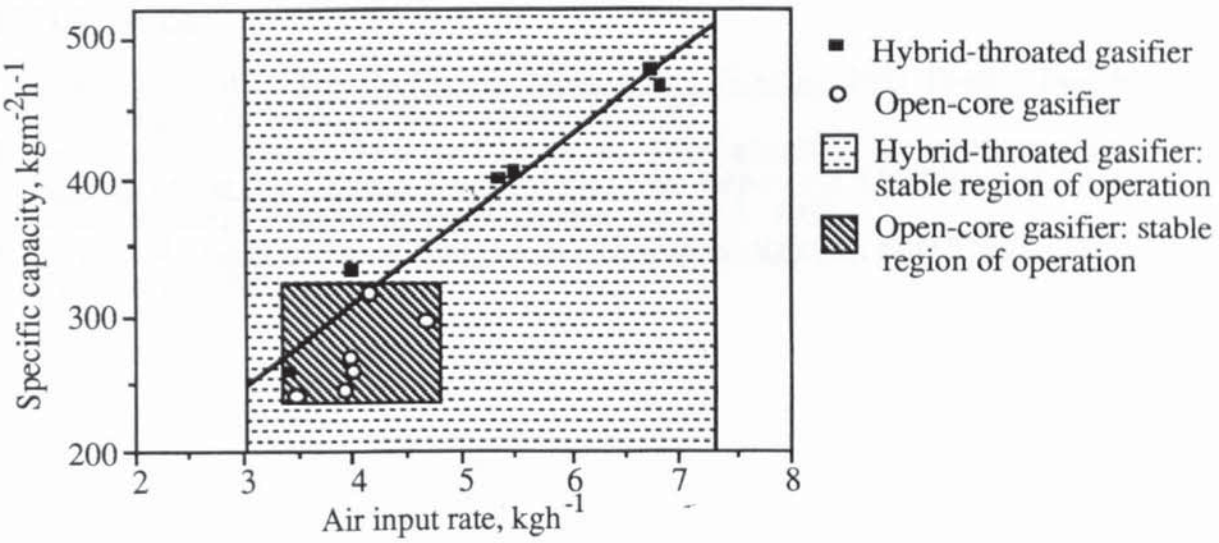

Figure 2: Operating Range of the Open-Core and Hybrid-Throated Gasification Systems

In the open-core gasifier, stable operation is achievable over a narrow range of throughputs. The observed turndown of 1.3 is thought to be an aberration caused by the reaction zone sloping thereby increasing the surface area available for flaming pyrolysis. Small variations in the feed size, moisture content and shape will also affect the apparent turndown of the gasifier.

For the hybrid-throated gasifier the air to feed ratio is approximately constant throughout the operating range. The turndown can be explained in terms of simple geometry of the surface area of the flaming pyrolysis interface. At low throughputs the interfacial area is equal to the cross-sectional area of the reactor. At high throughputs there is a hemispherical flaming pyrolysis zone. The shape of the flaming pyrolysis zone can be attributed to the radiation view factor from the surface of the hot char bed below the throat. The char gasification step is regulated by the fall through of material from the flaming pyrolysis zone.

For a similar throughput as the open-core gasifier, the tar content of the product gas from the hybrid is only 27% of that from the open-core. The region between the throat and the top of the char bed has a temperature greater than 1200°C to give a greater degree of tar cracking confirming the claim that the presence of a throat induces tar cracking. In the open-core system there is the possibility of 'cold spots' within the bed through which tars can pass uncracked.

CONCLUSIONS

The hybrid-throated gasifier has been found to have the following attributes:

- Simple construction without the need for an air-tight feeding system or air injection.
- Double the capacity of the open-core gasifier.
- A turndown capacity of 2:1.
- A lower product gas tar content compared with that of the open-core gasifier.
- A higher gas energy content compared to the open-core gasifier except at high throughput.

REFERENCES

1. Groeneveld, M.J., The Co-Current Moving Bed Gasifier, PhD Thesis, Twente University of Technology, The Netherlands, 1980.
2. Reed, T.B., Graboski, M.S. and Levie, B., Fundamentals, Development and Scaleup of the Air-Oxygen Stratified Gasifier. Report no SERI/PR-234-2571, Biomass Energy Foundation Press, Golden, Co. USA, 1987.
3. Earp, D.M., Gasification of Biomass in a Downdraft Reactor, PhD Thesis, Aston University, 1988.

APPENDIX B DESIGN CALCULATIONS

B 1 Demister Size

The size of the demister was calculated using Equation B1.1 (KnitMesh, undated).

$$v = K\sqrt{\frac{D - d}{d}} \qquad (B1.1)$$

where:

v = Maximum superficial velocity, ms^{-1}

K = Constant = 0.107 ms^{-1} for clean conditions.

D = Liquid density at operating temperature and pressure, kgm^{-3}

d = Vapour density at operating temperature and pressure, kgm^{-3}

Taking the liquid density to be 1000 kgm^{-3} and the gas density as 1.1 kgm^{-3} (approximating the product gas to air) at operational temperature and pressure (298 K and 780 mm Hg), this yields a maximum superficial gas velocity of 3.22 ms^{-1}. A demister pad diameter of 2.7 cm is calculated for a gas flow of 6.4 m^3h^{-1}, the highest experimental gas flow rate for a run reported by Evans (1992). KnitMesh (undated) recommend a minimum superficial velocity 30% of v, giving a minimum gas flow rate of 1.92 m^3h^{-1}.

B1.1 Collection Efficiency of Demister

The total mass of water in an air stream exiting the tank was found by placing an adsorption column containing silica gel and dry cotton wool after the tank and measuring the mass gain. The mass of water present as vapour was determined from the vapour pressure of water at the temperature of the gas stream. The mass of water carried by the gas stream as droplets could then be calculated as the difference between the measured total water content and the calculated water vapour content. It was found that on average 86 % of the water carried was in the form of vapour, or 10.59 gNm^{-3}, with 1.75 gNm^{-3} of water carried as mist. Collection efficiencies for a 22 cm and a 2.7 cm demister pad were calculated (Table B1.1).

Table B1.1 Demister Collection Efficiencies and Pressure Drops

Pad Diameter cm	Flow Rate Nm3h-1	Mass Collected gNm-3	Collection Efficiency, %	Pressure Drop mm Hg
22	4.77	0.063	3.59	5
22	8.50	0.461	26.39	8
2.7	4.31	0.004	0.24	7
2.7	8.22	0.062	3.53	17

The collection efficiency is very low for all cases compared to a value of over 99% that is possible (KnitMesh undated). This may be due to the KnitMesh pad, being unsaturated at the start of the experiment, retaining an unknown amount of water. Higher collection efficiencies are obtained at higher flow rates indicating better impingement at higher velocities, however, the results also show that the 22 cm pad removed more water than a 2.7 cm pad (see Section 3.4.5).

B 2 Design of Gas Drying Unit for Water Content Measurement

B2.1 Dessicant Characteristics

Various characteristics for three commonly used dessicants are presented in Table B2.1.

Table B2.1 Characteristics of Solid Dessicants (Anonymous, 1979)

	Alumina A	Silica Gel	Molecular Sieve 4A
Surface Area, m^2g^{-1}	320	832	750
Bulk Density, kgm^{-3}	800	720	670
Heat of Adsorption, $Jg^{-1}(H_2O)$	1400	930	4180
Reactivation Temp., °C	150-315	125-275	200-315
Porosity, %	50	55	48
Pore Size, nm	1-7.5	1-40	0.42
Pore Volume, cm^3kg^{-1}	400	430	290
Sorptive Capacity[a], $kgkg^{-1}$	0.25-0.33	0.35-0.5	0.22-0.26

a: from Perry, (1985)

The use of adsorption isotherms (Figures B2.1-2) provides the best information for the design of a packed bed column (Anon., 1979).

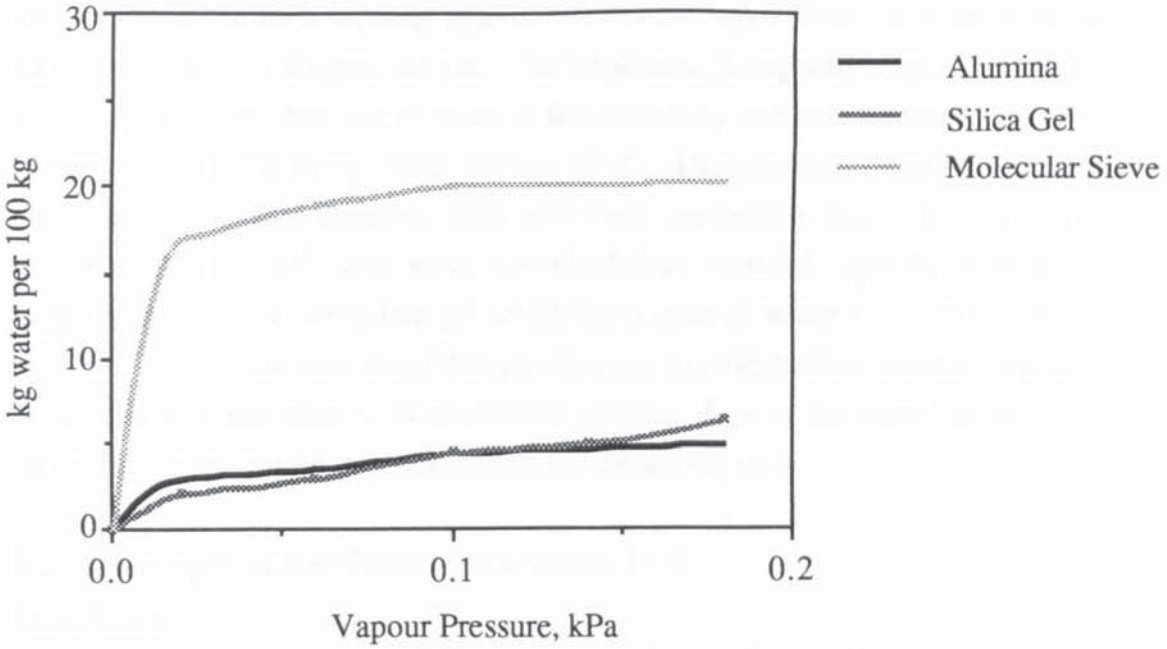

Figure B2.1 Water Adsorption Isotherms of Dessicants up to 0.2 kPa Vapour Pressure (Anonymous, 1979)

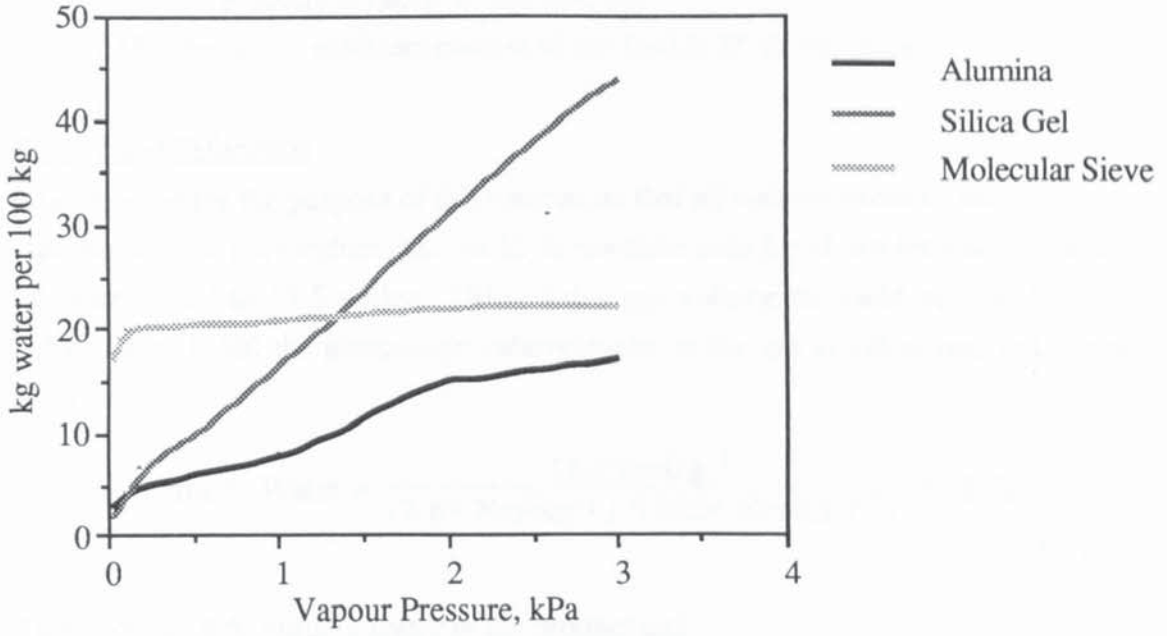

Figure B2.2 Water Adsorption Isotherms of Dessicants up to 4 kPa Vapour Pressure (Anonymous, 1979)

B2.2 Exit Gas Humidity

The humidity of the gas leaving the drying unit is dependant upon the amount of water adsorbed per unit mass of adsorbent and may be calculated assuming equilibrium has been reached. Adsorption isotherms can be used to obtain the vapour pressure of the water in equilibrium with the gas (Anonymous, 1979). In addition, adsorption isoteres may be used at temperatures for which isotherms are not available. Since equilibrium may not of been reached, the gas leaving the unit could contain water

vapour. Breakthrough capacity is a measure of the amount of water adsorbed before moisture appears in the product gas. The breakthrough capacity improves with factors increasing the mass transfer of water to the adsorbate and on the adsorbent properties (Anonymous, 1979; Perry, 1985; Davies 1974). Thus the adsorbent with the highest equilibrium sorbtive capacity may not have the best useful capacity. This is demonstrated by molecular sieve 4A which has a useful capacity to equilibrium capacity ratio of 0.9 over silica gel which has a ratio of about 0.5. For the dessicants in Table 3.1 it can be seen that although silica gel has the greatest sorptive capacity, the driest gas is obtainable with molecular sieves. It was therefore decided to use molecular sieve type 4A as the dessicant for the drying unit.

B2.3 Drying Unit Size Calculation (Weiner, 1974)

Design data

1) Inlet gas temperature of the product gas is just above ambient temperatures as measured at the sampling rotameter and will be taken as 25°C.
2) The maximum gas sample volume is 135 litres at the sample rotameter.
3) System pressure is taken as 760 mm Hg.
4) The maximum moisture content of the feed is 25 % wet basis.

Water Load Estimation

It is assumed for the purpose of this estimation that all water present as moisture in the feed passes into the product gas. At 25 % moisture each kg of dry feed will yield 0.33 kg water equal to 18.5 moles. Using a dry gas volumetric yield of 2.69 Nm^3kg^{-1} DAF (Earp, 1988) the percentage volume water in the gas is calculated in Equation B2.1

$$\text{Volume \% Water} = \frac{18.5\ molkg^{-1}}{(2.69\ Nm^3kg^{-1} / 0.0224\ Nm^3mol^{-1})} \times 100\% \qquad (B2.1)$$

This gives 15.4 % volume water in the product gas.

A maximum design gas volume of 135 litres at 25°C is used in calculating the total amount of water that the dessicating unit will be designed to cope with. The volume is equivalent to 0.124 Nm^3.

$$\text{Mass of water} = 18\ gmol^{-1} \frac{0.154 \times 0.124\ Nm^3}{0.0224\ Nm^3mole^{-1}} = 15.3\ g \qquad (B2.2)$$

Dessicant Mass and Unit Size Required

The mass of dessicant required to adsorb the water is calculated using the sorptive capacity in $kgkg^{-1}$ (B2.3). The volume of the drying unit is calculated using the bulk density of the dessicant.

$$\text{Mass of Dessicant} = \frac{15.3\ \text{g}}{\text{Sorptive Capacity}} \qquad \text{(B2.3)}$$

The mass and volume of drying units using each of the three dessicants in Table B2.1 have been calculated in Table B2.2

Table B2.2 Size of Drying Units Using Various Dessicants

	Alumina,A	Silica Gel	Molecular Sieve, 4A
Mass required, g	53	36	64
Volume, cm^3	66	50	96

Using 4A molecular sieve requires a volume of 96 cm^3. A 25 cm length of plastic piping of 2.25 cm diameter gives the required volume. Cotton wool is used at either end of the packing to prevent loss of small particles to the gas stream.

APPENDIX C PRODUCT GAS FLOW METERING

C1 Gas Flow Metering Devices

U16 Gasmeter

Used in previous system by Evans (1992), discussed in Section 3, cost .£161 (1991).

Range Measures cumulative gas flow.

Accuracy ±2% (manufactures claim); <1.5% compared with the rotameter (see below), however can only be read to 5 cu. ft. which is equivalent to a 5% error for a 30 min test at 6 m^3h^{-1}.

Suitability See Section 3.4.1.

Platon Gapmeter

Used in previous system by Evans (1992), discussed in Section 3.4.1, cost £414 (1989)

Range 0.8-8 m^3h^{-1}

Accuracy ±35% of flow rate measured using the U16 gasmeter (above), very erratic performance.

Suitability Becomes heavily fouled with tarry deposits.

Pitot Static Tube

Originally installed to measure the product gas velocity for iso-kinetic sampling (Section 3.). Differential pressure primary element. Cost £102 (from Airflow Developments Ltd. Bucks., 1991)

Range See Section 3.4.1.

Accuracy 2% (BS 1042, 1983); Calibrated using U16 gasmeter (see above).

Suitability Limited use with a dirty gas (Ginesi, 1987); no blockages encountered during velocity measurements.

Rotameter

Used in previous system by Evans (1992). Problems were encountered due to condensation within the rotameter after approximately 20 minutes operation.

Range 1.2-10.8 m^3h^{-1}

Accuracy 0.5-5%

Suitability Unsuitable due to condensation in tube.

Concentric Orifice Plate

Differential pressure primary element.

Range 3:1 (Ginesi, 1987)

Accuracy 0.5-3%

Suitability Problems may occur due to build up of deposits on face of the plate (Perry, 1985), and is therefore unsuitable for measurement of the tarry gas.

Eccentric Orifice Plate

Differential pressure primary element. Eccentric orifice reduces problems of fouling and is therefore suitable for use with a dirty gas (Ginesi, 1987).

Range 3:1 (Ginesi, 1987)

Accuracy Unknown

Suitability Recommended minimum pipe diameter of 10 cm (Perry, 1985), which is too large for the product gas flow

Segmental Wedge

Differential pressure primary element, performs as an eccentric orifice plate.

Range 3:1 (Ginesi, 1987)

Accuracy 0.5-5%

Suitability Suitable for use with the product gas (Ginesi, 1991), however there no suppliers of the device were found and there are no details of sizing/construction in British Standards.

Venturi Meter

Differential pressure primary element. Low pressure drop across meter compared to orifice plate.

Range 3:1 (Ginesi, 1987)

Accuracy 0.5-1.5% (Ginesi, 1991)

Suitability Suitable for limited use with the product gas (Ginesi, 1991), low pressure loss would benefit the system. Minimum pipe size of 5 cm diameter needed (Ginesi, 1991) would mean altering the product gas piping after the demister.

Ultrasonic Vortex

Range 20:1 (Ginesi, 1987)

Accuracy 1% (Ginesi, 1987)

Suitability Suitable for limited use with dirty gases (Ginesi, 1987), unreliable since it is sensitive to vibration.

Coriolis Mass Meter

Cost £3000 (Rosemount, 1991)

Range 25:1 (Ginesi, 1987)

Accuracy 0.25% (Ginesi, 1987)

Suitability Requires at least 10 bar pressure (Rosemount, 1991) and is therefore unsuitable.

Thermal Gradient Mass Meter

Cost £550 (Rosemount, 1991)

Range 50:1 (Rosemount, 1991)

Accuracy 1% (Rosemount, 1991)

Suitability Minimum flow of 30 $lmin^{-1}$ required, equivalent to 1.8 m3h-1. Flowrates below this value, which may be encountered, would not be measured accurately.

Target Meter

Range 3:1 (Ginesi, 1987)

Accuracy 0.5-2% (Ginesi, 1987)

Suitability Mechanism would be susceptible to clogging.

C2 Gas Velocity Calculations Using the Pitot Static Tube (BS 1042, 1983)

The velocity of the gas is given by;

$$v = \alpha (1 - \varepsilon) \sqrt{\frac{2\ \Delta P}{\rho}} \qquad \text{(C2.1)}$$

The difference between the total and static pressure is calculated by;

$$\Delta P = \rho_m\, g\, h + \partial(\Delta P) \qquad \text{(C2.2)}$$

$\partial(\Delta P)$ is the correction required for stem flow blockage which may not be neglected since the ratio d/D is greater than 0.02.

$$\partial(\Delta P) = -0.7\ k_b \frac{S}{A} \Delta P \qquad \text{(C2.3)}$$

The density of the gas is determined using the ideal gas law, Equation.C2.4, for estimations however, the gas density is taken as 1.2 kgm^{-3} at 273 K.

$$\rho = \frac{R\,M}{Z\,T} \qquad \text{(C2.4)}$$

The compressibility correction factor $(1 - \varepsilon)$ is calculated by ;

$$(1-\varepsilon) = \left(1 - \left(\frac{\Delta P}{2}\lambda P\right)\right) + \lambda - \frac{1}{6}\lambda^2 . \left(\frac{\Delta P}{P}\right)^2 \qquad \text{(C2.5)}$$

giving a value of 0.99995 at maximum $\Delta P/P$. Since this value is close to unity this factor is omitted from the calculation.

Condition 1.

ΔP must be greater than ;

$$\frac{2 \times 10^4}{\rho(\mu^2 / \alpha d_i)} \qquad \text{(C2.6)}$$

which is equal to 0.067 Pa.

Condition 2.

$(\Delta P/P)_{max}$ must always be less than a limiting value which varies with λ, the ratio of the specific heat capacities of the gas. For the product gas λ is assumed to be 1.40 which is consistent with the values for the main constituents, CO, N_2 and H_2 between 293 K and 523 K. Using this value $(\Delta P/P)_{max}$ should never exceed 0.046.

Nomenclature

Symbol	Quantity	Value	Units
$(1 - \varepsilon)$	Compressibility correction factor	1	
α	Pitot calibration factor	calibrate	
d_i	Diameter of pressure hole	0.001	m
d	Diameter of pitot tube stem	0.004	m
D	Diameter of pipe	0.022	m
g	Gravitational constant	9.81	ms^{-2}
k_b	Blockage constant	0.922	
A	Cross-sectional area of pipe	3.88×10^{-4}	m^2
S	Cross-sectional area of pitot stem	1.26×10^{-5}	m^2
h	Manometer fluid height	measure	m
λ	Ratio of specific heat capacities	1.40	
M	Average molecular mass	calculate	
μ	Dynamic viscosity	20×10^7	Nsm^{-2}
P	Absolute pressure	measure	Pa
R	Gas constant	8.314	$Jmol^{-1}K^{-1}$
ρ	Gas density	calculate	kgm^{-3}
ρ_m	Manometer fluid density	785	kgm^{-3}
T	Temperature	measure	K
v	Velocity	calculate	ms^{-1}
Z	Ideal gas law deviation factor	1	
$\partial(\Delta P)$	Correction for stem blockage	calculate	Pa
ΔP	Differential pressure	calculate	Pa

APPENDIX D PIPING AND INSTRUMENTATION

A piping and instrumentation diagram is given in Figure D1

Key

Miscellaneous Items

B1	Burner
R1	Gasifier
P1	Water circuit pump
P2	Sampling system vacuum pump
F1	Membrane filter
F2	Dessicant unit
S1	Char catchpot
S2	Disentrainment tank
S3	Demister
VE1	Venturi ejector
PT	Pitot tube

Flowmeters

FI1	Water circuit flowmeter(Series 1000 Rotameter 65S metric)
FI2	Sampling system gas Rotameter (Type 10P metric)
FI3	Water flowrate into disentraiment tank
XI	Gasmater (cumulative flow)

Valves

	Function	**Type**
V1	Water circuit isolation	Gate
V2	Water circuit by-pass	Gate
V3	Water circuit control	Needle
V4	Sampling system isolation	Ball
V5	CO_2 purge	Ball
V6	Tank drain	Ball
V7	Gas sampling system isolation	Ball
V8	Tank water filling control	Gate
V9	Sampling system control valve	Ball
V10	Demister drain	
V11	Pressure relief manometer make-up	Gate
V12	Pressure relief manometer drain	Gate
V13	Char catchpot exit port	Ball
V14	Pilot light (natural gas) control	Needle

Pressure Instruments

PI1 Pressure transducer at gasmeter

PI2 Pitot and reactor pressure drop manometer (not shown)

PI3 Water circuit Bourdon gauge (psig)

PI4 Disentrainment tank Bourdon gauge (psig)

Thermocouples

TI1 Undergrate temperature

TI2 Disentrainment tank temperature

TI3 Raw gas pipe temperature

TI4 Room temperature

TI5 Search thermocouple (within sheath)

TI6 Wet gas temperature at flowmeter

TI7 Reactor temperature

TI8 Reactor temperature

TI9 Reactor temperature

TI10 Sampling system gas temperature

TI11 Contact thermocouple

TIA Pilot light alarm thermocouple

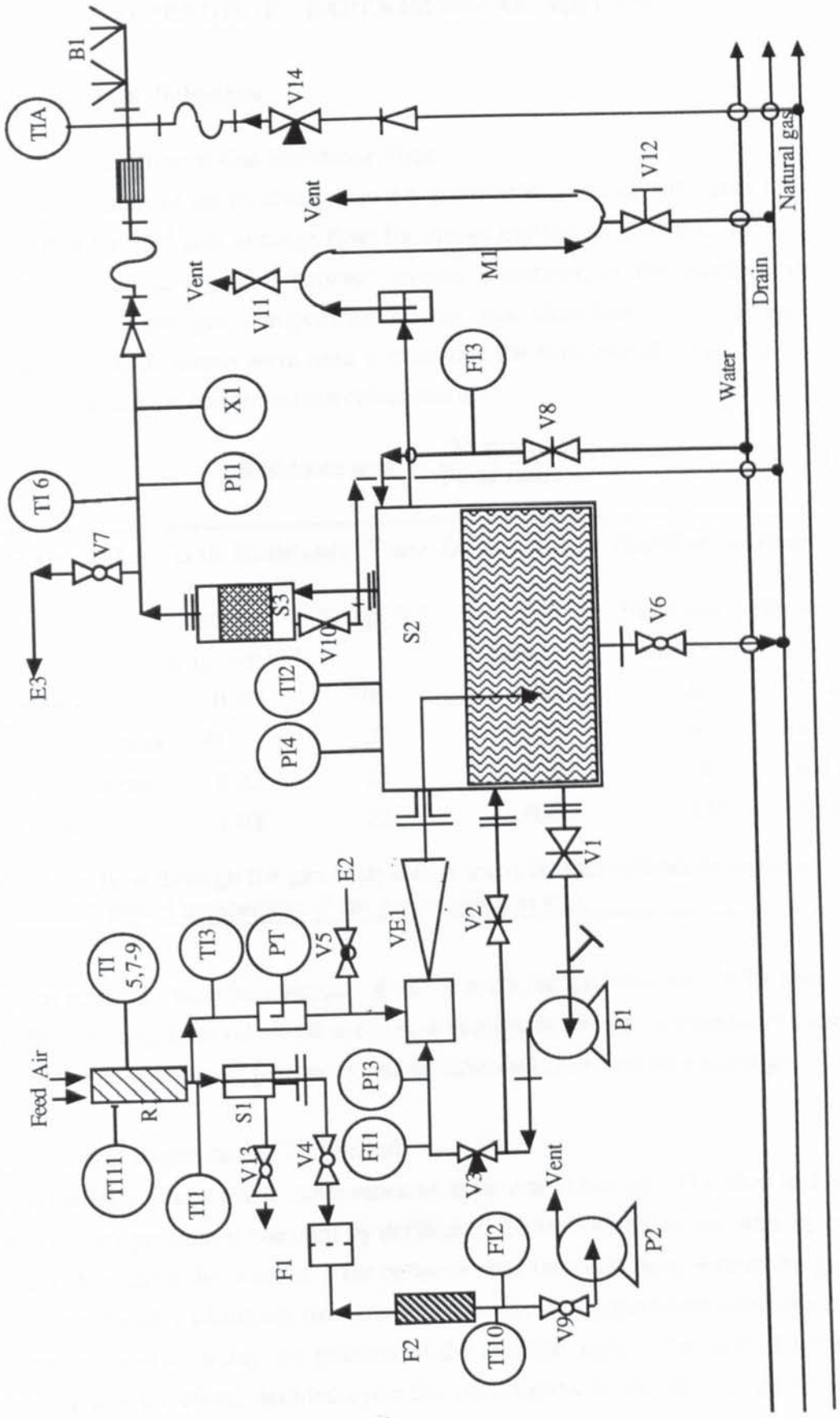

Figure D1 P&I Diagram

APPENDIX E EXPERIMENTAL METHODS

E1 Test Data Selection

E1.1 Calculation of Gas Residence Time

The residence times of the product gas in the gasification rig was calculated for a flow rate of 4.408 Nm^3h^{-1} (the average flow for Aston gasifier in previous work; Evans, 1992) to obtain the lag-time between events occurring in the gasifier and the measurement of the gas composition in the gas analysers. The average run temperatures and pressures were used to calculate the flow rate through the different parts of the rig and the residence time calculated as;

$$\text{Residence time} = \frac{\text{Volume}}{\text{Flow rate}} \qquad \text{(E1.1)}$$

Table E1.1 Gas Residence Time in the Aston Gasifier System

	Volume x 10^{-3} m^3	Temp., °C	Pressure, kPa	Flow rate, m^3h^{-1}	Residence time, s.
Hot gas pipe	0.49	390	1000	10.85	0.16
Disentrainment tank	81	30	1058	4.68	62.29
Demister & piping	5.23	25	1038	4.70	4.01
Gas sample lines	1.08	22	1009	0.43*	8.96

Note: * the flow through the gas analysers is set at an approximately constant value of 7.2 $lmin^{-1}$ irrespective of the gas production rate.

The total residence time for a sample of gas to reach the gas analysers is 76.1 seconds. At a data reading interval of 20 seconds a change in the gas composition after an alteration in an operational parameter will be indicated after four data readings.

E1.2 Start of Experimental Test Period

Before the start of any test a stable reaction zone was achieved. The char bed height during stable operation is constant by definition. However, during the start-up period or when stabilizing the reaction zone between tests the conditions within the gasifier may be continually changing (for example the reactor temperature increases during start-up) without affecting the position of the reaction zone. The start of the stable operation was therefore, decided upon the consistency of the gas composition and gasifier exit temperature data. Since a change in the experimental gas composition becomes apparent after about 80 seconds (see Appendix E1.1) a series of 4-5 consistent data points indicates that stability is reached. The reactor was then filled to a pre-determined level within the reactor to allow accurate determination of the amount

of feed used during a test, and the data reading set number recorded used as the start of the test. For test involving a *falling or rising reaction zone* the test period began immediately after the air flow rate into the reactor was changed from that *given a stable* reaction zone.

E1.3 Test Duration

During stable operation the char bed height is a parameter that is constant by definition. For a data set to be included as part of a test, the data must be relatively consistent without significant drift in the gas compositions. As an example, Figure E2.1 shows that for test T4.3 the gas composition is steady, although fluctuations exist (in particular for CO_2).

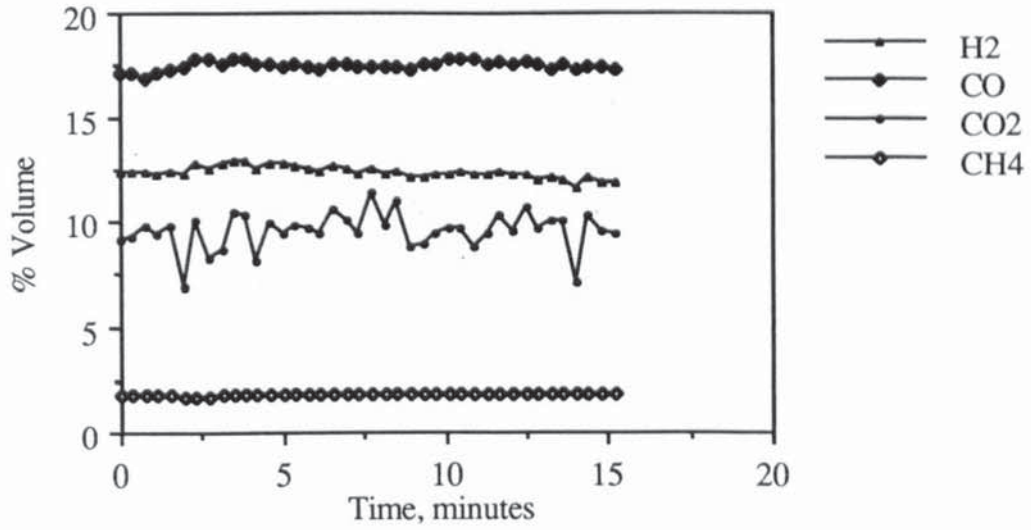

Figure E1.1 Gas Compositions During Stable Operation (Test T4.3)

Test durations of longer than 15 minutes were considered to be satisfactory since errors due to fluctuations in the char bed height are averaged out.

E1.4 End of Experimental Test Period

For stable operation tests were ended if one of the following occurred:

the reaction zone could no longer be controlled at a fixed height above the char bed

a test of satisfactory duration was achieved and another test or reactor shut-down was to be carried out

a problem with the operational equipment occurred resulting in shut-down of the reactor.

The reactor was then filled to the same level as at the start of the test to allow the feed rate to be calculated (Appendix F1). For tests involving rising or falling reaction zones

the test was ended before the reaction zone reached the reactor top or the grate respectively.

APPENDIX F MASS AND ENERGY BALANCE CALCULATIONS

F1 Mass Balance

F1.1 Gasifier Inputs

The wet feed rate is calculated as the sum of the feed batch additions for the length of a test starting directly after the addition of a batch that fills the reactor to the brim (or to some other pre-determined level) and ending directly after the addition of a batch returning to the same level. In addition to this, any change in height of the reaction zone has to be considered since wood is consumed if the reaction zone rises and accumulates in the reactor if the zone falls. The zone height is defined in this calculation as the height from the grate to the centre of the reaction zone. The wet feed rate is calculated as;

$$F_w\ (kgh^{-1}) = \frac{\text{Mass of feed consumed}}{\text{Duration of test}} \qquad (F1.1)$$

From the wet feed rate, the dry feed rate (F_d) and the dry ash free (F_{DAF}) feed rate are obtained;

$$F_d = F_w - W_F \qquad (F1.2)$$

$$F_{DAF} = F_d - F_a \qquad (F1.3)$$

where f_{H2O} and F_a are the mass flow rate of water and the mass flow rate of ash calculated in Equations F1.4 and F1.5.

$$W_F = F_w.f_{H2O} \qquad (F1.4)$$

$$F_a = F_d.f_a \qquad (F1.5)$$

The nitrogen content in the product gas is used to determine the air intake, kgh^{-1};

$$N_{2Air} = N_{2gas} - N_{2feed} \qquad (F1.6)$$

$$N_{2feed} = f_N.Fd \qquad (F1.7)$$

where N_{2feed} is the fraction of nitrogen in the feed (f_N) multiplied by the dry feed rate, Equation F1.7. The composition for air is assumed to be 77% N_2 and 23% O_2 by mass, giving the mass of oxygen as;

$$O_{2air} = \frac{N_{2air}}{0.77} - N_{2air} \qquad (F1.8)$$

The dry and wet bulb temperatures are taken during a run, from which the amount of water (Air_{H2O}, $kgkg^{-1}$) in the air can be obtained using psycometric charts (Perry, 1985).

$$W_A = \text{Mass of air} \times Air_{H2O} \qquad (F1.9)$$

F1.2 Gasifier Outputs

The raw product gas consists of; the gaseous components H_2, CO, CO_2, N_2 and CH_4; condensates, tars and water; and solid particulates, ash and char. The dry gas composition is measured at the gas analysers. This differs from the raw product gas composition since it is moisture free. After the raw gas has passed through the venturi and disentrainment tank the term wet gas is used since it contains moisture from the venturi circuit.

The raw gas flow rate is calculated using the velocity of the gas measured by a pitot tube (see Section 3.5.1) multiplied by the cross-sectional area of the hot gas pipe, Equation F1.10. The normalized raw gas flow in Nm^3h^{-1} is calculated in Equation F1.11.

$$Q_r = 3600\ A_p.v \qquad \text{(F1.10)}$$

The normal raw gas flow = $G_{r\,n}$, Nm^3h^{-1}

$$Q_{r\,n} = \frac{G_r\ P_r\ 273}{101325\ T_r} \qquad \text{(F1.11)}$$

where P_r is the pressure (Pa) in the raw gas pipe, and T_r is the temperature (K).

In addition to this the gas flow through the sample line is calculated and added to the flow rate. The mass flow rate of the sample gas is calculated using Equation F1.12.

$$G_S = \frac{Q_S\ P_S\ M_{wr}}{1000\ R\ T_S} \qquad \text{(F1.12)}$$

Hence the mass flow rate of raw gas G_r, kgh^{-1}

$$G_r = \frac{Q_r\ P_r\ Mw_r}{1000\ R\ T_r} + G_S \qquad \text{(F1.13)}$$

The flow rate is then checked against the wet gas flow rate measured by the gas meter. As the fraction of water in the raw gas is measured the dry gas mass flow rate is obtained in Equation F1.14. The molecular weight of the dry gas composition is obtained using Equation F1.15.

$$G_d = G_w\ (1 - W_w) \qquad \text{(F1.14)}$$

$$Mw_d = \Sigma(Mw_i.x_{di}) \qquad \text{(F1.15)}$$

where Mw_i is the molecular weight of component i in the gas and x_{di} is the molar fraction of component i.

The amount of water, tars and solid particulates in the raw product gas are calculated from measurements obtained using the sampling system. The sampling system collects all water using a drying unit (see Appendix B2). The mass of water collected in the sampling system and dessicant unit is converted into moles. This is divided by the number of moles of raw gas sampled to give the molar faction of water in the product gas which is equivalent to the volume fraction assuming ideal gas behaviour (Equation F1.16).

$$W_r = \left(\frac{\text{Mass collected}}{18}\right)\left(\frac{1}{n_s+1}\right) \qquad \text{(F1.16)}$$

The difference between the dried used filter weight and the dried acetone washed filter weight gives the weight of tar collected by the filter (see Section 3.7.5). The total tar collected by the sampling system is the sum of the tar collected by the paper and nylon filters, and the tar washed out of the sample probe and filter holder at the end of sampling. The tar loading of the raw product gas is given by Equation F1.17 in units of $mgNm^{-3}$.

$$c_{tar} = \frac{M_{tar}}{V_s} \qquad \text{(F1.17)}$$

The tar production rate, kgh^{-1};

$$\text{Tar} = c_{tar} \times Q_{rn} \times 10^{-3} \qquad \text{(F1.18)}$$

The solid particulate loading of the gas is calculated in a similar manner;

$$c_{solids} = \frac{M_{solids}}{V_s} \qquad \text{(F1.19)}$$

$$\text{Char} = c_{solids} \times Q_{rn} \times 10^{-3} \qquad \text{(F1.20)}$$

F1.3 Mass Balance Closure and Elemental Balance

The closure for the mass balance is calculated and presented as a percentage of outputs divided by the inputs using Equation *F1.21;*

$$\text{Closure, \%} = \frac{(F_{DAF} + F_{ash} + F_{H_2O} + \text{Air} + W_A)}{(\sum x_{di}.Mw_i + \text{Tar} + F_{ash} + \text{Char} + W_r)} \times 100\% \qquad \text{(F1.21)}$$

The mass input rates, mass output rates and closures for carbon, hydrogen, oxygen and nitrogen are calculated in Equations F1.22-F1.30. The closure for nitrogen is always exactly 100% as the input rate is directly obtained from the output rate (see Equation F1.6).

Carbon Balance

$$\text{Carbon Input} = f_C F_d \quad \text{(F1.22)}$$

$$\text{Carbon Output} = \left(\frac{12}{28} x_{CO} + \frac{12}{44} x_{CO_2} + \frac{12}{16} x_{CH_4}\right) Gd + \text{char}_C.\text{Char} + \text{tar}_C.\text{Tar}) \quad \text{(F1.23)}$$

$$\text{Closure, \%} = \frac{\text{Carbon Inputs}}{\text{Carbon Outputs}} \times 100\% \quad \text{(F1.24)}$$

Hydrogen Balance

$$\text{Hydrogen Inputs} = f_H + \frac{2}{18}(W_F + W_A) \quad \text{(F1.25)}$$

$$\text{Hydrogen Outputs} = \left(\frac{4}{16} x_{CH_4} + 2x_{H_2}\right) G_d + \text{char}_H.\text{Char} + \text{tar}_H.\text{Tar} + \frac{2}{18} W_r \quad \text{(F26)}$$

$$\text{Closure, \%} = \frac{\text{Hydrogen Inputs}}{\text{Hydrogen Outputs}} \times 100\% \quad \text{(F1.27)}$$

Oxygen Balance

$$\text{Oxygen Inputs} = f_O.F_d + \frac{16}{18}(W_F + W_A) + O_{2air} \quad \text{(F1.28)}$$

$$\text{Oxygen Outputs} = \left(\frac{16}{28} x_{CO} + \frac{32}{44} x_{CO_2}\right) G_d + \text{tar}_O.\text{Tar} + \text{char}_O\text{Char} + \frac{16}{18} W_r \quad \text{(F1.29)}$$

$$\text{Closure, \%} = \frac{\text{Oxygen Inputs}}{\text{Oxygen Outputs}} \times 100\% \quad \text{(F1.30)}$$

F 2 Energy Balance

F2.1 Energy Inputs

The gross heating value of the wood is used (i.e the enthalpy of combustion to products at 0°C) which is calculated using a form of the Dulong formula, the IGT equation (see Chapter 4). This is given in Equation F2.1, where the dry feed analysis is used.

$$\Delta H_{C(Feed)} = 0.341 f_C + 1.322 f_H - 0.12(f_O + f_N) - 0.0153 f_A + 0.0686 f_S \quad \text{(F2.1)}$$

This is used to obtain the energy input from the feed when multiplied by the feed rate (Equation F2.2).

$$E_F = \Delta H_{C(Feed)}.F_d \quad \text{(F2.2)}$$

The specific heat capacity of the feed, CpF, is calculated using Kopp's rule (Coulson, 1989) to be about 1.35 $kJkg^{-1}\ K^{-1}$. However since the feed temperature at the inlet (T_F) is identical to the reference temperature (T_{Ref}), set as the ambient temperature, the sensible heat input from the feed is zero (Equation F2.3).

$$E_{sF} = F_d.(T_F - T_{Ref}).Cp_F = 0 \qquad (F2.3)$$

for the same reason there is no sensible heat input from the feed moisture or from the air, however the latent heat of the moisture in the air is considered. The latent heat of water is 2548.4 $kJkg^{-1}$ giving an energy input of;

$$E_{lAir}\ (kJh^{-1}) = 2548.4\ W_A \qquad (F2.4)$$

F2.2 Energy Outputs

The energy outputs from the gasifier are as follows: chemical energy in the product gas, tars and char; latent heat of condensation of water and the tars; sensible heat carried by the gasification products and heat losses from the gasifier.

The heating value of the dry gas is calculated in Equation F2.5 from the gross heating values of the component gases which are given in Table F2.1 (Perry, 1985) and their molar fractions in the product gas, x_{di}.

$$HHV_d = \sum(HHV_i x_{di}) \qquad (F2.5)$$

Table F2.1 Energy Values of Product Gases at 288 K

Gas	HHV, MJm^{-3}
Carbon monoxide	11.97
Hydrogen	12.10
Methane	37.69

The energy content of the gas is the HHV multiplied by the gas flow rate to give the energy flow of the product gas.

$$E_{Gd} = HHV_d.Q_d \qquad (F2.6)$$

The sensible heat content of the gas is calculated using Equation F2.7.

$$\Delta H_g,\ kJkg^{-1} = \frac{\int_{T_{Ref}}^{T} Cp_g\ dT}{Mw_D} \qquad (F2.7)$$

The specific heat capacity at constant pressure of the product gas is dependant upon the temperature, usually expressed as an empirical power series equation (F2.8).

$$Cp = a + bT + cT^2 + dT^3 \qquad \text{(F2.8)}$$

The temperature-independent coefficients (a, b, c and d) for the gaseous components of the gas are available from tabulated data (Coulson, 1989). The mean heat capacity is obtained using Equation F2.9;

$$Cp_m = \frac{\int Cp\ dT}{T - T_{Ref}} \qquad \text{(F2.9)}$$

on integration this gives;

$$Cp_m = \frac{a(T - T_{Ref}) + b/2(T^2 - T_{Ref}^2) + c/3(T^3 - T_{Ref}^3) + d/4(T^4 - T_{Ref}^4)}{(T - T_{Ref})} \qquad \text{(F2.10)}$$

For the product gas the coefficients are obtained as;

$$a_g = \sum x_{di}.a_i \qquad \text{(F2.11)}$$

$$b_g = \sum x_{di}.b_i \qquad \text{(F2.12)}$$

$$c_g = \sum x_{di}.c_i \qquad \text{(F2.13)}$$

$$d_g = \sum x_{di}.d_i \qquad \text{(F2.14)}$$

where x_{di} is the volume fraction of the i^{th} component (H_2, CO, CO_2, CH_4, N_2) and a_i, b_i, c_i and d_i are their corresponding coefficients. The mean specific heat capacity for the dry gas, Cp_m, is then calculated as in Equation F2.10 using the coefficients obtained in Equations F2.11 to F2.14.

The energy output as sensible heat carried by the gas is therefore;

$$E_{sGd} = Gd.\Delta H_g \qquad \text{(F2.15)}$$

The sensible heat calculation for water is considered separately as there is a change of state between the gas temperature and the reference temperature.

$$\Delta H_{H_2O} = \frac{\int_{T_b}^{T} Cp_1\ dT + \int_{T_{Ref}}^{T_b} Cp_2\ dT}{18} \qquad \text{(F2.16)}$$

T_b is the boiling point of water, and Cp_1 is a power series of the form given in Equation F2.10. The specific capacity of water in the liquid phase, Cp_2, is 4.184 $kJkg^{-1}K^{-1}$. The energy output as sensible heat carried by water in the product gas is;

$$E_{sW} = W_r.\Delta H_{H_2O} \qquad \text{(F2.17)}$$

The tar loading ($mgNm^{-3}$) of the gas is calculated in Equation F1.7 and the mass flow rate of tar (kgh^{-1}) in Equation F1.8. The heating value of the tars is calculated using Equation F2.18.

$$\Delta H_{C(Tar)} = 0.341\ tar_C + 1.322\ tar_H - 0.12\ tar_O \qquad (F2.18)$$

The chemical energy of the tars is calculated by multiplying the heating value of the tar with the tar mass flow rate as in Equation F2.19.

$$E_{Tar} = \Delta H_{c(Tar)}.Tar \qquad (F2.19)$$

The specific heat capacity of the tars is 1.568 $kJkg^{-1}K^{-1}$ using Kopp's rule (Coulson, 1989). The sensible heat of the tars is calculated using Equation F2.20

$$E_{sTar} = Cp_{tar}\,(T_r - T_{Ref})Tar \qquad (F2.20)$$

In addition to this, there is the latent heat of condensation of the tars which is not considered due to the complex nature of the tars produced. Since the tars represent only a small fraction of the products this is not expected to be significant. Similarly, the chemical and sensible heat energy of the char output is calculated.

Heat is lost from the gasifier by convection and radiation. The outside surface temperature of the reactor is measured in order to calculate the losses from the two mechanisms. The gasifier is divided along its length into sections for which the temperature was assumed to be constant for the duration of the run.

Convective Heat Loss

Heat loss by convection is calculated by

$$q_c = h_c.A.(T - T_{Ref}) \qquad (F2.21)$$

where h_c is the convective heat transfer coefficient which, for the case of convection from a hot body to air with streamline flow, is given by (Coulson, 1977);

$$h_c = 1.18 \sqrt[4]{\frac{(T - T_{Ref})}{d_r}} \qquad (F2.22)$$

Combining Equations F2.21 and F2.22, the convective heat transfer rate is obtained. For each section of the gasifier, k, of length l_k the rate of heat loss is given by (Coulson, 1977);

$$q_{ck} = 1.18\ \pi\ d_r^{0.75}\ (T_k - T_{Ref})^{1.25}.l_k \qquad (F2.23)$$

The total convective heat loss in watts is;

$$q_{c(Total)} = \sum q_{ck} \qquad \text{(F2.24)}$$

Radiative Heat Loss

The radiative heat loss from the gasifier are calculated in a similar way to the convective heat loss. Radiative heat transfer is calculated using the Stefan-Boltzman law in Equation F2.25 (Schmidt, 1984).

$$q_r = A\varepsilon\,\sigma(T^4 - T_{Ref}^4) \qquad \text{(F2.25)}$$

A is the surface area of the gasifier, ε is the emissivity of the reactor wall and σ is the Stefan-Boltzman constant which is equal to 5.699 x 10-8 $Wm^{-2}K^{-4}$. The emissivity of the quartz glass tube is taken as 0.935 (Reyes, 1988), and that of the insulation as 0.93 (Evans, 1992).

For a section of gasifier l_k in length, the radiative heat loss is:

$$q_{rk} = \pi\, d_r\, \varepsilon\sigma\, (T_k^4 - T_{Ref}^4) l_k \qquad \text{(F2.26)}$$

The total radiative heat loss in watts is;

$$q_{r(Total)} = \sum q_{rk} \qquad \text{(F2.27)}$$

The total heat loss is therefore;

$$E_{loss} = qc(Total) + qr(Total) \qquad \text{(F2.28)}$$

For insulated runs, the heat losses are calculated for both the insulated reactor and the uninsulated observation strip at the measured temperatures. In this case Equation F2.28 becomes;

$$E_{loss} = I(q_{c(ins)} + q_{r(ins)}) + B(q_{c(B)} + q_{r(B)}) \qquad \text{(F2.29)}$$

where the fraction of reactor surface insulated is I, and the fraction uninsulated is B.

F2.3 Energy Balance Closure

The energy inputs (feed and air moisture) are divided by the sum of the energy outputs in order to get a measure of the energy closure presented as a percentage (Equation F2.30).

$$\text{Closure, \%} = \frac{E_F + E_{l\,Air}}{E_{Gd}+E_{sGd}+E_{sH_2O}+E_{lH_2O}+E_{Tar}+E_{sTar}+E_{Char}+E_{sChar}+E_{loss}} \times 100\% \qquad \text{(F2.30)}$$

F3 Equivalence Ratio

The equivalence ratio is a measure of the degree of oxidation occurring. From the ultimate feed analysis the relative number of moles in the feed of each element C, H, O, N and S are obtained. The stoichiometric oxygen requirement is calculated using the formula (Harker, 1972)

$$C_6H_aO_bS_cN_d + xO_2 = yCO_2 + zH_2O + qSO_2 + rN_2 \qquad (F3.1)$$

a, b, c & d are number of moles of H, O, S and N respectively per six moles of carbon (i.e. 1 mole of wood) and y = 6, z = a/2, q = c, r = d/2. The number of moles of oxygen required, x, is given by;

$$x = \frac{2y + z + 2q - b}{2} \qquad (F3.2)$$

The mass of oxygen required for stoichiometric combustion ($kgkgmol^{-1}$), and the mass of 1 kgmol of feed are calculated in Equations F3.3 and F3.4.

$$O_2 = 32x \qquad (F3.3)$$

$$Mw_F = 12 \times 6 + a + 16b + 32c + 14d \qquad (F3.4)$$

The stoichiometric oxidant to feed ratio, $\{O_2:Feed\}_s$, is given by the equation;

$$\{O_2:Feed\}_s, = \frac{O_2}{Mw_F} \qquad (F3.5)$$

The actual oxidant to feed ratio is;

$$\{O_2:Feed\}_a = \frac{O_{2air}}{F_d} \qquad (F3.6)$$

$$\text{Equivalence ratio, } \% = \frac{\{O_2:Feed\}_a}{\{O_2:Feed\}_s} \times 100\% \qquad (F3.7)$$

Nomenclature

a, b, c, d	Coefficients in gas heat capacity equation	
A	Surface area of reactor	cm^{-2}
A_{pipe}	Cross-sectional area of raw gas pipe	m^2
$A_{reactor}$	Cross-sectional area of reactor	cm^2
Air	Air intake rate	kgh^{-1}
B	Fraction of uninsulated reactor	
$char_j$	Mass fraction of j in char	$kgkg^{-1}$
Cp	Specific heat capacity	$Jkg^{-1}K^{-1}$
Cp_m	Mean specific heat capacity of gas	$Jkg^{-1}K^{-1}$
c_{solids}	Solids loading of raw product gas	gNm^{-3}
c_{tar}	Tar loading of raw product gas	gNm^{-3}
d_r	Diameter of reactor	cm
E	Energy flow rate (chemical)	MJh^{-1}
E_l	Latent energy flow rate	MJh^{-1}
E_{loss}	Energy lost by convection and radiation	MJh^{-1}

E_s	Sensible heat energy flow rate	MJh^{-1}
f_j	Mass fraction of j (j = C, H, O, N, ash) in feed	$kgkg^{-1}$
F	Mass feed rate	kgh^{-1}
F_{Ash}	Feed ash input rate	kgh^{-1}
G	Product gas mass flow rate	kgh^{-1}
h_c	Convective heat transfer coefficient	
HHV	Higher heating value	$MJNm^{-3}$
Ins	Fraction of reactor insulated	
l_k	Length of section k	cm
M	Mass	g
Mw	Molecular weight	$gmol^{-1}$
N_2	Nitrogen flow rate	kgh^{-1}
n	Moles	moles
O_{2air}	Intake rate of O_2	kgh^{-1}
P	Pressure	Pa
q_c	Convective heat transfer rate	W
Q	Volumetric gas flow rate	m^3h^{-1}
Q_n	Volumetric gas flow rate (normalized)	Nm^3h^{-1}
q_r	Radiative heat transfer rate	W
R	Universal gas constant	$JK^{-1}mol^{-1}$
T	Temperature	K
Tar	Tar mass flowrate in product gas	kgh^{-1}
tar_j	Mass fraction of j in tar	$kgkg^{-1}$
T	Temperature	K
V	Volume of gas sampled	Nm^3
v	Velocity	ms-1
W	Water flow rate	kgh^{-1}
x_{di}	Molar fraction of i in dry product gas	$molmol^{-1}$
ΔH_C	Heat of combustion of feed	$kJkg^{-1}$
ΔH_g	Sensible heat of product gas	$kJkg^{-1}$
ε	Emissivity of outer reactor wall	
ρ	Gas density	kgm^{-3}
ρ_b	Bulk feed density	gcm^{-3}
σ	Stefan-Boltzman constant	$Wm^{-2}K^{-4}$

Subscripts

w	Wet
d	Dry
DAF	Dry ash free
s	Sample
i	Gaseous component of product gas (H_2, CO, CO_2, CH_4, N_2)
r	Raw product gas
k	Section of gasifier
A	Air
F	Feed
G	Gas
Ref	Reference Temperature
j	Component, (C, H, O, N, ash)
C	Carbon
H	Hydrogen
O	Oxygen
N	Nitrogen
a	Ash
H2O	Water

APPENDIX G EXPERIMENTAL TEST SUMMARIES

G 1 Test Summaries

All tests for which a mass and energy balance was carried out are listed in test order.

Notes:

(a) average value for insulated open-core gasifier.

(b) average value for uninsulated open-core base case test

(R) char accumulated in reactor vessel

Test:	1.1	Date:	20/9/91	Duration, mins:	41.02	
Objectives:	Insulated run			**Specific**	Tar	Assumed (a)
	Temperature profile			**Measurements:**	Water	Assumed (a)
	Measurement of time				Temperature	Core and insulation
	for pyrolysis				Gas flow	Gasmeter

Feed			**Bed Conditions**		
Type	Wood blocks (batch 1)				
Size	6.35 - 12.7	mm	Char bed height	8.33	cm
Moisture, % wet basis	9.31	%	Zone depth, cm	6.81	cm
Wet feed rate, kg/h	1.39	kg/h	Rate of zone rise	2.94	cm/h
Dry specific capacity	285.39	kg/m2h	Max. temperature	1128	°C
Equivelence ratio	0.327				
Air/fuel ratio	2.312				

Dry Gas Composition, %vol.		**Sampling Measurements**	
H2	13.427	Tar output	mg/Nm3
CO	19.542		% wt DAF
CO2	10.950		
CH4	1.539	Solids output	mg/Nm3
balance N2	54.542		% wt DAF
Dry gas flow	3.384 Nm3/h		
H2/CO	0.688	Raw gas water content, %vol.	
CO/CO2	1.801		
Dry gas HHV	4.793 MJ/Nm3		
Dry gas yield, DAF basis	2.685 *Nm3/kg*		
Exit temp.°C	643 °C		

Mass Balance

Input stream	kg/h	Output stream, kg/h	
DAF wood	1.260	H2	0.041
Ash	0.001	CO	0.826
Water, wood	0.129	CO2	0.728
O2, air	0.618	CH4	0.037
N2, air	2.296	N2	2.307
Water, air	0.029	Water	*0.175*
TOTAL	4.333	Tar	*0.012*
		Ash	*0.001*
		Char (R)	0.010
		Char (gas)	*0.010*
		TOTAL	4.147

Mass & Elemental Balance Closures, %

Mass	95.71
C	90.34
H	75.23
O	92.23

Figures in Italics are calculated from assumptions

Energy Balance		**Temperature Profile °C**		
Energy bal. (no heat loss)	78.42 [81.93]	cm above grate	Core	Insulation
Energy bal. + heat loss	88.14 [92.09]	30	23	23
Heat loss, % calculated	9.72	21		59
Heat loss, % by difference	21.59	14	789	120
[Figures in brackets, normalized for mass bal.]		12	1046	
		10	1055	
Conversion Efficiencies, %		8	1001	
Cold gas	62.03 [70.38]	7		177
Hot gas (at exit temp.)	74.93 [85.03]	6	953	
Raw (incuding tar + char)	79.26 [89.22]	4	950	
		2	928	
[Figures in brackets are normalized to closure]		0	797	

Test:	1.2	Date:	20/9/91	Duration, mins:	42.65	
Objectives:	Base case run Temperature profile			**Specific Measurements:**	Tar Water Temperature Gas flow	Assumed (b) Assumed (b) Core Gasmeter

Feed		**Bed Conditions**	
Type	Wood blocks (batch 1)		
Size	6.35 - 12.7 mm	Char bed height	17.11 cm
Moisture, % wet basis	9.31 %	Zone depth, cm	7.65 cm
Wet feed rate, kg/h	1.177 kg/h	Rate of zone rise	-2.81 cm/h
Dry specific capacity	241.678 kg/m2h	Max. temperature	1090 °C
Equivelence ratio	0.460		
Air/fuel ratio	3.256		

Dry Gas Composition, %vol.		**Sampling Measurements**	
H2	8.748	Tar output	mg/Nm3
CO	15.563		% wt DAF
CO2	12.050		
CH4	0.929	Solids output	mg/Nm3
balance N2	62.710		% wt DAF
Dry gas flow	3.538 Nm3/h		
H2/CO	0.562	Raw gas water content, %vol.	
CO/CO2	1.296		
Dry gas HHV	3.451 MJ/Nm3		
Dry gas yield, DAF basis	3.315 Nm3/kg		
Exit temp.°C	392 °C		

Mass Balance

Input stream	kg/h	Output stream, kg/h	
DAF wood	1.067	H2	0.028
Ash	0.001	CO	0.682
Water wood	0.110	CO2	0.829
O2, air	0.737	CH4	0.023
N2, air	2.738	N2	2.748
Water, air	0.035	Water	*0.348*
TOTAL	4.686	Tar	*0.020*
		Ash	*0.001*
		Char (R)	0.000
		Char (gas)	*0.026*
		TOTAL	4.704

Mass & Elemental Balance Closures, %

Mass	100.38
C	100.75
H	91.74
O	101.59

Figures in Italics are calculated from assumptions

Energy Balance		
Energy bal. (no heat loss)	69.87	[69.61]
Energy bal. + heat loss	125.35	[124.88]
Heat loss, % calculated	55.49	
Heat Loss, % by differenc	30.14	
[Figures in brackets, normalized for mass bal.]		

Conversion Efficiencies, %		
Cold gas	55.24	[44.07]
Hot gas (at exit temp.)	64.01	[51.06]
Raw (including tar + char)	70.14	[55.95]
[Figures in brackets are normalized to closure]		

Temperature Profile °C

cm above grate	Core
40	26
26	443
24	496
22	850
20	779
12	703

Test:	2.1	Date: 15/10/91	Duration, mins:	52.62
Objectives:	Insulated run Tar sampling		**Specific Measurements:**	Tar Sampled Water Assumed (a) Temperature Core as test 1.1 Insulation temperature measured Gas flow Gasmeter

Feed		**Bed Conditions**	
Type	Wood blocks (batch 1)		
Size	6.35 - 12.7 mm	Char bed height	19.37 cm
Moisture, % wet basis	8.86 %	Zone depth, cm	4.16 cm
Wet feed rate, kg/h	1.166 kg/h	Rate of zone rise	1.14 cm/h
Dry specific capacity	240.576 kg/m2h	Max. temperature	
Equivelence ratio	0.335		
Air/fuel ratio	2.372		

Dry Gas Composition, %vol.		**Sampling Measurements**	
H2	14.747	Tar output	522.76 mg/Nm3
CO	20.547		1.47 % wt DAF
CO2	9.680		
CH4	1.949	Solids output	245.00 mg/Nm3
balance N2	53.077		0.69 % wt DAF
Dry gas flow	3.007 Nm3/h		
H2/CO	0.718	Raw gas water content, %vol.	
CO/CO2	2.189		
Dry gas HHV	5.252 MJ/Nm3		
Dry gas yield, DAF basis	2.831 Nm3/kg		
Exit temp.°C	556 °C		

Mass Balance

Input stream	kg/h	Output stream, kg/h	
DAF wood	1.062	H2	0.040
Ash	0.001	CO	0.772
Water, wood	0.103	CO2	0.572
O2, air	0.534	CH4	0.042
N2, air	1.985	N2	1.995
Water, air	0.026	Water	*0.154*
TOTAL	3.712	Tar	0.016
		Ash	0.004
		Char (R)	0.039
		Char (gas)	0.004
		TOTAL	3.637

Mass & Elemental Balance Closures, %

Mass	97.97
C	99.54
H	88.47
O	93.78

Figures in Italics are calculated from assumptions

Energy Balance		
Energy bal. (no heat loss)	88.77	[90.61]
Energy bal. + heat loss	100.10	[102.18]
Heat loss, % calculated	11.34	
Heat loss, % by difference	11.23	
[Figures in brackets, normalized for mass bal.]		

Conversion Efficiencies, %		
Cold gas	69.56	[69.49]
Hot gas (at exit temp.)	80.67	[80.59]
Raw (including tar + char)	89.03	[88.94]
[Figures in brackets are normalized to closure]		

Temperature Profile °C

cm above grate	Insulation
26	21
21	60
14	120
7	173

Test:	2.2	Date: 15/10/91	Duration, mins:	40.22
Objectives:	Base case run Temperature profile		**Specific Measurements:**	Tar: Assumed (b) Water: Assumed (b) Reactor tem: Core Gas flow: Gasmeter

Feed		**Bed Conditions**	
Type	Wood blocks (batch 1)		
Size	6.35 - 12.7 mm	Char bed height	22.16 cm
Moisture, % wet basis	8.86 %	Zone depth, cm	7.45 cm
Wet feed rate, kg/h	1.525 kg/h	Rate of zone rise	1.49 cm/h
Dry specific capacity	314.524 kg/m2h	Max. temperature	1023 °C
Equivelence ratio	0.421		
Air/fuel ratio	2.982		

Dry Gas Composition, %vol.		**Sampling Measurements**	
H2	10.081	Tar output	mg/Nm3
CO	15.909		% wt DAF
CO2	11.184		
CH4	1.149	Solids output	mg/Nm3
balance N2	61.677		% wt DAF
Dry gas flow	4.249 Nm3/h		
H2/CO	0.633	Raw gas water content, %vol.	
CO/CO2	1.433		
Dry gas HHV	3.752 MJ/Nm3		
Dry gas yield, DAF basis	3.060 Nm3/kg		
Exit temp.°C	353 °C		

Mass Balance

Input stream	kg/h	Output stream, kg/h	
DAF wood	1.389	H2	0.039
Ash	0.001	CO	0.845
Water, wood	0.135	CO2	0.933
O2, air	0.878	CH4	0.035
N2, air	3.263	N2	3.276
Water, air	0.043	Water	*0.364*
TOTAL	5.710	Tar	*0.029*
		Ash	*0.001*
		Char (R)	0.005
		Char (gas)	*0.043*
		TOTAL	5.571

Mass & Elemental Balance Closures, %

Mass	97.57
C	95.04
H	87.58
O	94.38

Figures in Italics are calculated from assumptions

Energy Balance		
Energy bal. (no heat loss)	71.04	[72.81]
Energy bal. + heat loss	139.14	[142.61]
Heat loss, % calculated	68.09	
Heat loss, % by difference	28.96	

[Figures in brackets are normalized to closure]

Conversion Efficiencies, %		
Cold gas	56.06	[40.29]
Hot gas (at exit temp.)	63.46	[45.61]
Raw (including tar + char)	66.85	[48.05]

[Figures in brackets are normalized to closure]

Temperature Profile °C	
cm above grate	Core
40	46
38	57
36	56
34	178
32	388
30	693
28	921
26	903
24	935
22	923
18	843
14	733
12	730
10	702
8	703
6	652
4	621
2	552
0	466

Test:	2.3	Date: 15/10/91	Duration, mins:	18.92

Objectives: Pyrolysis dominant run; Tar sampling

Specific Measurements:

Tar	Sampled
Water	Assumed (b)
Temperature	As test 4
Gas flow	Gasmeter

Feed

Type	Wood blocks (batch 1)	
Size	6.35 - 12.7	mm
Moisture, % wet basis	8.86	%
Wet feed rate, kg/h	0.752	kg/h
Dry specific capacity	155.032	kg/m2h
Equivelence ratio	0.469	
Air/fuel ratio	3.315	

Bed Conditions

Char bed height	11.39	cm
Zone depth, cm	3.11	cm
Rate of zone rise	28.42	cm/h
Max. temperature		°C

Dry Gas Composition, %vol.

H2	6.317	
CO	17.190	
CO2	8.563	
CH4	1.425	
balance N2	66.506	
Dry gas flow	2.158	Nm3/h
H2/CO	0.388	
CO/CO2	5.543	
Dry gas HHV	3.543	MJ/Nm3
Dry gas yield, DAF basis	3.153	Nm3/kg
Exit temp.°C	371	°C

Sampling Measurements

Tar output	822.73	mg/Nm3
	2.89	% wt DAF
Solids output	380.27	mg/Nm3
	1.34	% wt DAF

Raw gas water content, %vol.

Mass Balance

Input stream	kg/h
DAF wood	0.685
Ash	0.000
Water, wood	0.067
O2, air	0.481
N2, air	1.788
Water, air	0.024
TOTAL	3.045

Output stream, kg/h	
H2	0.012
CO	0.464
CO2	0.363
CH4	0.022
N2	1.794
Water	*0.300*
Tar	0.020
Ash	*0.000*
Char (R)	0.099
Char (gas)	0.009
TOTAL	3.083

Mass & Elemental Balance Closures, %

Mass	101.27
C	111.76
H	109.32
O	98.90

Figures in Italics are calculated from assumptions

Energy Balance

Energy bal. (no heat loss)	83.66	[82.61]
Energy bal. + heat loss	102.33	[101.05]
Heat loss, % calculated	18.68	
Heat loss, % by difference	16.34	

[Figures in brackets, normalized for mass bal.]

Conversion Efficiencies, %

Cold gas	49.10	[47.98]
Hot gas (at exit temp.)	56.28	[54.99]
Raw (including tar + char)	84.01	[82.09]

[Figures in brackets are normalized to closure]

Temperature Profile °C

cm above grate

Test:	3	Date:	24/4/92	Duration, mins:	39.22

Objectives:	Base case run Tar and water sampling

Specific Measurements:		
	Tar	Sampled
	Water	Sampled
	Temperature	External
	Gas flow	Pitot tube

Feed		
Type	Wood blocks (batch 2)	
Size	6.35 - 12.7	mm
Moisture, % wet basis	11.62	%
Wet feed rate, kg/h	1.302	kg/h
Dry specific capacity	260.368	kg/m2h
Equivelence ratio	0.535	
Air/fuel ratio	3.490	

Bed Conditions		
Char bed height	7.61	cm
Zone depth, cm	10.06	cm
Rate of zone rise	0	cm/h
Max. temperature		°C

Dry Gas Composition, %vol.		
H2	8.883	
CO	15.355	
CO2	11.202	
CH4	0.868	
balance N2	63.693	
Dry gas flow	3.983	Nm3/h
H2/CO	0.579	
CO/CO2	1.385	
Dry gas HHV	3.418	MJ/Nm3
Dry gas yield, DAF basis	3.479	Nm3/kg
Exit temp.°C	446	°C

Sampling Measurements		
Tar output	665.36	mg/Nm3
	2.628	% wt DAF
Solids output	1001.62	mg/Nm3
	3.957	% wt DAF
Raw gas water content, %vol.	11.934	

Mass Balance

Input stream	kg/h
DAF wood	1.145
Ash	0.006
Water, wood	0.151
O2, air	0.847
N2, air	3.148
Water, air	0.037
TOTAL	5.334

Output stream, kg/h	
H2	0.032
CO	0.759
CO2	0.870
CH4	0.025
N2	3.149
Water	0.468
Tar	0.030
Ash	*0.006*
Char (R)	0.000
Char (gas)	0.040
TOTAL	5.378

Mass & Elemental Balance Closures, %

Mass	100.82
C	110.32
H	102.91
O	98.80

Figures in Italics are calculated from assumptions

Energy Balance		
Energy bal. (no heat loss)	89.57	[88.84]
Energy bal. + heat loss	98.68	[97.88]
Heat loss, % calculated	9.11	
Heat loss, % by difference	10.43	

[Figures in brackets, normalized for mass bal.]

Conversion Efficiencies, %		
Cold gas	67.81	[68.71]
Hot gas (at exit temp.)	80.74	[81.82]
Raw (including tar + char)	89.94	[91.14]

[Figures in brackets are normalizedto closure]

Temperature Profile, °C

External temperatures using contact thermocouple

cm above grate	External
30	33
28	38
26	40
24	50
22	54
20	81
18	120
16	282
14	363
12	498
10	453
8	433
6	360
4	305
2	275
0	249

Test:	4	Date:	20/5/92	Duration, mins:	73.07

Objectives: Base case run
External temperature profile

Specific Measurements:

Tar, start-up	Measured
Water, start-up	Measured
Tar	Assumed (b)
Water	Assumed (b)
Reactor tem	External
Gas flow	Pitot tube

Feed

Type	Wood blocks (batch 2)	
Size	6.35 - 12.7	mm
Moisture, % wet basis	9.76	%
Wet feed rate, kg/h	1.448	kg/h
Dry specific capacity	295.716	kg/m2h
Equivelence ratio	0.549	
Air/fuel ratio	3.578	

Bed Conditions

Char bed height	12.19	cm
Zone depth, cm	6.65	cm
Rate of zone rise	2.46	cm/h
Max. temperature	1131	°C

Dry Gas Composition, %vol.

H2	9.096	
CO	15.728	
CO2	10.169	
CH4	1.005	
balance N2	64.003	
Dry gas flow	4.629	Nm3/h
H2/CO	0.579	
CO/CO2	1.547	
Dry gas HHV	3.547	MJ/Nm3
Dry gas yield, DAF basis	3.560	Nm3/kg
Exit temp.°C	478	°C

Sampling Measurements

Start-up tar	1850.30	mg/Nm3
		% wt DAF
Start-up solids	1947.80	mg/Nm3
		% wt DAF
Start-up water content, %vol.	5.632	

Mass Balance

Input stream	kg/h
DAF wood	1.300
Ash	0.006
Water, wood	0.141
O2, air	0.986
N2, air	3.667
Water, air	0.038
TOTAL	6.139

Output stream,	kg/h
H2	0.037
CO	0.901
CO2	0.915
CH4	0.033
N2	3.667
Water	*0.530*
Tar	*0.029*
Ash	*0.006*
Char (R)	0.009
Char (gas)	*0.033*
TOTAL	6.179

Mass & Elemental Balance Closures, %

Mass	100.33
C	109.36
H	108.95
O	97.11

Figures in Italics are calculated from assumptions

Energy Balance

Energy bal.(no heat loss)	93.39	[93.08]
Energy bal. + heat loss	104.00	[103.66]
Heat loss, % calculated	10.61	
Heat loss, % by difference	6.61	

Figures in brackets are normalized for mass bala

Conversion Efficiencies, %

Cold gas	71.50	[68.75]
Hot gas (at exit temp.)	85.46	[82.18]
Raw (hot gas with tar/char	93.74	[90.14]

[Figures in brackets are normalized to closure]

Temperature Profile °C

cm above grate	External
30	46
24	83
22	185
20	295
18	565
16	595
14	415
12	390
10	325
8	308
6	277
4	270
2	249
0	257

Test:	5	Date:	21/9/92	Duration, mins:	17.97

Objectives: Base case run; Reaction temp. measurement

Specific Measurements:

Tar	Assumed (b)
Water	Assumed (b)
Exit Temp.	As test 4
Temperature	Bed thermocouples
Gas flow	Pitot tube

Feed

Type	Wood blocks (batch 2)	
Size	6.35 - 12.7	mm
Moisture, % wet basis	11.16	%
Wet feed rate, kg/h	1.347	kg/h
Dry specific capacity	270.876	kg/m2h
Equivelence ratio	0.513	
Air/fuel ratio	3.346	

Bed Conditions

Char bed height	3.7	cm
Zone depth, cm	7.3	cm
Rate of zone rise	-1.67	cm/h
Max. temperature	1129	°C

Dry Gas Composition, %vol.

H2	10.282	
CO	13.715	
CO2	9.889	
CH4	1.225	
balance N2	64.890	
Dry gas flow	3.899	Nm3/h
H2/CO	0.747	
CO/CO2	1.437	
Dry gas HHV	3.531	MJ/Nm3
Dry gas yield, DAF basis	3.274	Nm3/kg
Exit temp.°C	478	°C

Sampling Measurements

Tar output	mg/Nm3
	% wt DAF
Solids output	mg/Nm3
	% wt DAF
Raw gas water content, %vol.	

Mass Balance

Input stream	kg/h
DAF wood	1.191
Ash	0.006
Water, wood	0.150
O2, air	0.845
N2, air	3.140
Water, air	0.041
TOTAL	5.373

Output stream, kg/h	
H2	0.036
CO	0.664
CO2	0.752
CH4	0.034
N2	3.141
Water	*0.432*
Tar	*0.024*
Ash	*0.006*
Char (R)	0.000
Char (gas)	*0.027*
TOTAL	5.116

Mass & Elemental Balance Closures, %

Mass	95.20
C	92.72
H	101.18
O	85.96

Figures in Italics are calculated from assumptions

Energy Balance

Energy bal. (no heat loss)	85.02	[89.3]
Energy bal. + heat loss	96.70	[101.57]
Heat loss, % calculated	11.68	
Heat loss, % by difference	14.98	

[Figures in brackets, normalized for mass bal.]

Conversion Efficiencies, %

Cold gas	65.45	[67.69]
Hot gas (at exit temp.)	78.80	[81.49]
Raw (including tar + char)	85.39	[88.31]

[Figures in brackets are normalized to closure]

Temperatures in bed

cm above grate	7.5	10
Average	957	360
Standard deviation	89	201
Minimum	644	94
Maximum	1129	691

Test:	6	Date: 24/9/92	Duration, mins:	102.7

Objectives:	Base case run Reaction temp. measurement	Specific Measurements:	Tar	Assumed (b)
			Water	Assumed (b)
			Exit Temp.	Assumed as run4
			Temp., 7.5 cm above grate	
			Gas flow	Pitot tube

Feed			Bed Conditions	
Type	Wood blocks (batch 2)			
Size	6.35 - 12.7	mm	Char bed height	5.39 cm
Moisture, % wet basis	11.16	%	Zone depth, cm	7.91 cm
Wet feed rate, kg/h	1.219	kg/h	Rate of zone rise	-2.34 cm/h
Dry specific capacity	245.141	kg/m2h	Max. temperature	1134 °C
Equivelence ratio	0.559			
Air/fuel ratio	3.646			

Dry Gas Composition, %vol.		Sampling Measurements	
H2	9.593	Tar output	mg/Nm3
CO	14.932		% wt DAF
CO2	8.705		
CH4	1.091	Solids output	mg/Nm3
balance N2	65.678		% wt DAF
Dry gas flow	3.802 Nm3/h		
H2/CO	0.649	Raw gas water content, %vol.	
CO/CO2	1.947		
Dry gas HHV	3.544 MJ/Nm3		
Dry gas yield, DAF basis	3.527 Nm3/kg		
Exit temp.°C	487 °C		

Mass Balance

Input stream	kg/h	Output stream, kg/h	
DAF wood	1.078	H2	0.033
Ash	0.005	CO	0.704
Water, wood	0.136	CO2	0.645
O2, air	0.833	CH4	0.029
N2, air	3.098	N2	3.098
Water, air	0.038	Water	*0.423*
TOTAL	5.189	Tar	*0.024*
		Ash	*0.005*
		Char (R)	0.000
		Char (gas)	*0.027*
		TOTAL	4.988

Mass & Elemental Balance Closures, %

Mass	96.14
C	99.54
H	105.22
O	86.12

Figures in Italics are calculated from assumptions

Energy Balance		
Energy bal. (no heat loss)	91.76	[95.45]
Energy bal. + heat loss	104.62	[108.82]
Heat loss, % calculated	12.86	
Heat loss, % by difference	8.24	
[Figures in brackets, normalized for mass bal.]		

Conversion Efficiencies, %		
Cold gas	70.77	[67.65]
Hot gas (at exit temp)	85.03	[81.28]
Raw (including tar + char)	92.18	[88.11]

[Figures in brackets are normalized to closure]

Temperatures in bed		
cm above grate	7.5	10
Average	874	941
Standard deviation	66	74
Minimum	724	757
Maximum	1124	1134

Test:	7	Date: 21/10/92	Duration, mins:	72.63

Objectives:	Insulated run Tar and water sampling	**Specific Measurements:**	Tar Water Temperature Gas flow	3 samples Sampled External Pitot tube

Feed		**Bed Conditions**	
Type	Wood blocks (batch 2)		
Size	6.35 - 12.7 mm	Char bed height	7.85 cm
Moisture, % wet basis	12.08 %	Zone depth, cm	7.18 cm
Wet feed rate, kg/h	1.836 kg/h	Rate of zone rise	0.83 cm/h
Dry specific capacity	365.240 kg/m2h	Max. temperature	°C
Equivelence ratio	0.403		
Air/fuel ratio	2.627		

Dry Gas Composition, %vol.		**Sampling Measurements**		
H2	13.073	Tar output	1	210.03 mg/Nm3
CO	21.701		2	270.05 mg/Nm3
CO2	8.866		3	339.78 mg/Nm3
CH4	1.721		average	274.64 mg/Nm3
balance N2	54.638			0.891 % weight
Dry gas flow	4.869 Nm3/h	Solids output	1	420.06 mg/Nm3
H2/CO	0.609		2	282.16 mg/Nm3
CO/CO2	3.032		3	258.52 mg/Nm3
Dry gas HHV	5.093 MJ/Nm3		average	321.67 mg/Nm3
Dry gas yield, DAF basis	3.032 Nm3/kg			1.044 % weight
Exit temp.°C	702 °C	Raw gas water content, %vol.		6.55%

Mass Balance

Input stream	kg/h	Output stream, kg/h	
DAF wood	1.606	H2	0.057
Ash	0.008	CO	1.321
Water, wood	0.222	CO2	0.848
O2, air	0.895	CH4	0.060
N2, air	3.325	N2	3.326
Water, air	0.031	Water	0.274
TOTAL	6.086	Tar	0.014
		Ash	*0.008*
		Char (R)	0.003
		Char (gas)	0.009
		TOTAL	5.920

Mass & Elemental Balance Closures, %

Mass	97.27
C	107.17
H	82.54
O	88.91

Figures in Italics are calculated from assumptions

Energy Balance

Energy bal. (no heat loss)	98.14	[100.90]
Energy bal. + heat loss	99.99	[102.80]
Heat loss, % calculated	1.85	
Heat loss, % by difference	1.86	

[Figures in brackets, normalized for mass bal.]

Conversion Efficiencies, %

Cold gas	77.56	[77.57]
Hot gas (at exit temp.)	95.77	[95.78]
Raw (including tar + char)	98.39	[98.40]

[Figures in brackets are normalized to cosure]

Temperature Profile, °C

External temperatures using contact thermocouple

cm above grate	Quartz	Insulation
30	93	27
28	109	27
26	115	28
24	147	31
22	152	33
20	191	36
18	288	39
16	440	39
14	655	40
12	575	42
10	570	48
8	515	47
6	470	48
4	465	60
2	430	49
0	400	48

Test:	8	Date: 4/11/92	Duration, mins:	92.43
Objectives:	Run on small feed Temperature profile Tar and water sampling		**Specific Measurements:**	Tar Sampled Water Sampled Temperature Core and external Gas flow Pitot

Feed		**Bed Conditions**	
Type	Wood blocks (batch 2)		
Size	4.75 - 6.35 mm	Char bed height	5.77 cm
Moisture, % wet basis	10.79 %	Zone depth, cm	5.49 cm
Wet feed rate, kg/h	1.525 kg/h	Rate of zone rise	0 cm/h
Dry specific capacity	312.386 kg/m2h	Max. temperature	1009 °C
Equivelence ratio	0.465		
Air/fuel ratio	3.032		

Dry Gas Composition, %vol.		**Sampling Measurements**	
H2	9.841	Tar output	455.22 mg/Nm3
CO	17.894		1.61 % wt DAF
CO2	10.005		
CH4	1.401	Solids output	486.89 mg/Nm3
balance N2	60.859		1.73 % wt DAF
Dry gas flow	4.347 Nm3/h		
H2/CO	0.551	Raw gas water content, %vol.	10.671
CO/CO2	1.802		
Dry gas HHV	4.073 MJ/Nm3		
Dry gas yield, DAF basis	3.165 Nm3/kg		
Exit temp.°C	526 °C		

Mass Balance

Input stream	kg/h	Output stream, kg/h	
DAF wood	1.374	H2	0.038
Ash	0.007	CO	0.965
Water, wood	0.167	CO2	0.848
O2, air	0.883	CH4	0.043
N2, air	3.282	N2	3.283
Water, air	0.034	Water	0.456
TOTAL	5.747	Tar	0.022
		Ash	*0.007*
		Char (R)	0.000
		Char (gas)	0.017
		TOTAL	5.679

Mass & Elemental Balance Closures, %

Mass	98.82
C	102.73
H	95.94
O	95.04

Figures in Italics are calculated from assumptions

Energy Balance		
Energy bal. (no heat loss)	90.60	[91.69]
Energy bal. + heat loss	94.68	[95.81]
Heat loss, % calculated from external temperature	4.08	
Heat loss, % by difference	9.40	

[Figures in brackets, normalized for mass bal.]

Conversion Efficiencies, %		
Cold gas	72.48	[76.55]
Hot gas (at exit temp.)	86.43	[91.28]
Raw (including tar + char)	90.89	[96.00]

[Figures in brackets are normalized to closure]

Temperature Profile °C

cm above grate	Core	External
30		24
26		25
20		42
18		53
16	31	50
14	39	65
12	71	68
10	200	306
8	397	430
6	809	308
4	980	336
2	962	276
0	664	318

Test:	9	Date: 19/11/92	Duration, mins:	96.95
Objectives:	Agitated base case run		**Specific Measurements:**	Tar Assumed (b) Water Assumed (b) Temperature External Gas flow Pitot tube Vibro-mixer Duration of use

Feed		
Type	Wood blocks (batch 2)	
Size	6.35 - 12.7	mm
Moisture, % wet basis	11.15	%
Wet feed rate, kg/h	1.168	kg/h
Dry specific capacity	234.908	kg/m2h
Equivelence ratio	0.565	
Air/fuel ratio	3.687	

Bed Conditions		
Char bed height	5.95	cm
Zone depth, cm	6.8	cm
Rate of zone rise	3.71	cm/h
Max. temperature		°C

Dry Gas Composition, %vol.		
H2	8.240	
CO	14.012	
CO2	9.629	
CH4	1.545	
balance N2	66.574	
Dry gas flow	3.639	Nm3/h
H2/CO	0.587	
CO/CO2	1.470	
Dry gas HHV	3.435	MJ/Nm3
Dry gas yield, DAF basis	3.523	Nm3/kg
Exit temp.°C	496	°C

Sampling Measurements	
Tar output	mg/Nm3
	% wt DAF
Solids output	mg/Nm3
	% wt DAF
Raw gas water content, %vol.	

Mass Balance

Input stream	kg/h
DAF wood	1.033
Ash	0.005
Water, wood	0.130
O2, air	0.807
N2, air	3.001
Water, air	0.031
TOTAL	5.008

Output stream, kg/h	
H2	0.027
CO	0.631
CO2	0.682
CH4	0.040
N2	3.001
Water	*0.413*
Tar	*0.023*
Ash	*0.005*
Char (R)	0.013
Char (gas)	*0.026*
TOTAL	4.860

Mass & Elemental Balance Closures, %

Mass	97.06
C	102.75
H	105.76
O	88.14

Figures in Italics are calculated from assumptions

Energy Balance		
Energy bal. (no heat loss)	90.74	[93.49]
Energy bal. + heat loss	107.91	[111.78]
Heat loss, % calculated	17.17	
Heat loss, % by difference	9.26	
[Figures in brackets, normalized for mass bal.]		
Conversion Efficiencies, %		
Cold gas	68.54	[63.51]
Hot gas (at exit temp.)	83.18	[77.08]
Raw (including tar + char)	91.09	[84.42]
[Figures in brackets are normalizedto closure]		

Temperature Profile, °C

External temperatures using contact thermocouple

cm above grate	External
40	20
28	76
20	404
14	729
12	492
8	384
4	241

Test:	11	Date:	23/2/93	Duration, mins:	62.68	
Objectives:	Agitated base case run Tar and water sampling after demister Char profile analysis Reaction temperature			**Specific Measurements:**	Tar Water Temperature Gas flow	After demister x3 Gas - assumed (b) Assumed average External & in bed Pitot tube

Feed		
Type	Wood blocks (batch 2)	
Size	6.35 - 12.7	mm
Moisture, % wet basis	10.35	%
Wet feed rate, kg/h	1.364	kg/h
Dry specific capacity	276.799	kg/m2h
Equivelence ratio	0.454	
Air/fuel ratio	2.962	

Bed Conditions		
Char bed height	4.88	cm
Zone depth, cm	11.26	cm
Rate of zone rise	1.91	cm/h
Max. temperature	1240	°C

Dry Gas Composition, %vol.		
H2	9.659	
CO	14.393	
CO2	12.808	
CH4	1.663	
balance N2	61.478	
Dry gas flow	3.723	Nm3/h
H2/CO	0.670	
CO/CO2	1.125	
Dry gas HHV	3.711	MJ/Nm3
Dry gas yield, DAF basis	3.059	Nm3/kg
Exit temp.°C	500	°C

Sampling Measurements			
Tar output	1	68.31	mg/Nm3
	2	139.68	mg/Nm3
	3	82.86	mg/Nm3
	average	96.95	mg/Nm3
	standard deviation	30.79	
Solids output	1	45.54	mg/Nm3
	2	163.10	mg/Nm3
	3	31.07	mg/Nm3
	average	79.90	mg/Nm3
	standard deviation	59.12	

Mass Balance

Input stream	kg/h
DAF wood	1.217
Ash	0.006
Water, wood	0.141
O2, air	0.764
N2, air	2.841
Water, air	0.024
TOTAL	4.994

Output stream, kg/h	
H2	0.032
CO	0.665
CO2	0.930
CH4	0.044
N2	2.841
Water	*0.413*
Tar	*0.023*
Ash	*0.006*
Char (R)	0.007
Char (gas)	*0.025*
TOTAL	4.987

Mass & Elemental Balance Closures, %

Mass	99.86
C	100.48
H	99.15
O	99.36

Figures in Italics are calculated from assumptions

Energy Balance		
Energy bal. (no heat loss)	84.09	[84.21]
Energy bal. + heat loss	104.01	[104.16]
Heat loss, % calculated	19.92	
Heat loss, % by difference	15.91	

[Figures in brackets, normalized for mass bal.]

Conversion Efficiencies, %		
Cold gas	64.28	[64.15]
Hot gas (at exit temp.)	77.32	[77.29]
Raw (including tar + char)	84.31	[83.96]

[Figures in brackets are normalized to closure]

Temperature Profile, °C

External temperatures using contact thermocouple

cm above grate	External
26	16
24	48
20	75
16	127
12	641
8	776
4	323
0	315

In bed thermocouples, temperature °C

cm from grate	8.5	16.8
Average °C	881	438
Standard deviation	266	257
min.	121	38
max.	1240	954

Test:	12	Date:	9/3/93	Duration, mins:	63.38

Objectives: Agitated base case run
Tar and water sampling after demister

Specific Measurements:

Tar	After demister x3
	Gas - assumed (b)
Water	Assumed (b)
Temperature	As test 11
Gas flow	Pitot tube

Feed

Type	Wood blocks (batch 2)	
Size	6.35 - 12.7	mm
Moisture, % wet basis	9.40	%
Wet feed rate, kg/h	1.619	kg/h
Dry specific capacity	332.037	kg/m2h
Equivelence ratio	0.447	
Air/fuel ratio	2.912	

Bed Conditions

Char bed height	3.51	cm
Zone depth, cm	11.67	cm
Rate of zone rise	0.47	cm/h
Max. temperature		°C

Dry Gas Composition, %vol.

H2	9.918	
CO	14.910	
CO2	12.928	
CH4	1.640	
balance N2	60.603	
Dry gas flow	4.453	Nm3/h
H2/CO	0.664	
CO/CO2	1.155	
Dry gas HHV	3.801	MJ/Nm3
Dry gas yield, DAF basis	3.050	Nm3/kg
Exit temp.°C	514	°C

Sampling Measurements

Tar output	1	63.74	mg/Nm3
	2	67.84	mg/Nm3
	3	43.87	mg/Nm3
	average	58.48	mg/Nm3
	standard deviation	10.47	
Solids output	1	84.64	mg/Nm3
	2	104.36	mg/Nm3
	3	90.49	mg/Nm3
	average	93.16	mg/Nm3
	standard deviation	8.27	

Mass Balance

Input stream	kg/h	Output stream, kg/h	
DAF wood	1.460	H2	0.039
Ash	0.007	CO	0.824
Water, wood	0.152	CO2	1.123
O2, air	0.901	CH4	0.052
N2, air	3.350	N2	3.351
Water, air	0.026	Water	*0.493*
TOTAL	5.897	Tar	*0.028*
		Ash	*0.007*
		Char (R)	0.007
		Char (gas)	*0.030*
		TOTAL	5.954

Mass & Elemental Balance Closures, %

Mass	100.98
C	102.08
H	101.59
O	102.39

Figures in Italics are calculated from assumptions

Energy Balance

Energy bal. (no heat loss)	85.73	[84.90]
Energy bal. + heat loss	102.34	[101.35]
Heat loss, % calculated	16.60	
Heat loss, % by difference	14.27	

[Figures in brackets, normalized for mass bal.]

Conversion Efficiencies, %

Cold gas	65.65	[64.15]
Hot gas (at exit temp.)	79.10	[77.29]
Raw (including tar + char)	85.92	[83.96]

[Figures in brackets are normalized to closure]

Temperature Profile, °C

Test:	13.1	Date:	17/3/93	Duration, mins:	30.53

Objectives:	Agitated insulated run Tar sampling Batch gas analysis	Specific Measurements:	Tar	Sampled via hand pump
			Water	Assumed (a)
			Temperature	External
			Gas flow	Pitot tube

Feed			**Bed Conditions**		
Type	Wood blocks (batch 2)				
Size	6.35 - 12.7	mm	Char bed height	4.28	cm
Moisture, % wet basis	10.20	%	Zone depth, cm	13.13	cm
Wet feed rate, kg/h	1.693	kg/h	Rate of zone rise	0	cm/h
Dry specific capacity	344.154	kg/m2h	Max. temperature		°C
Equivelence ratio	0.371				
Air/fuel ratio	2.417				

Dry Gas Composition, %vol.		**Sampling Measurements**		
H2	15.654	Tar output	629.09	mg/Nm3
CO	18.126		1.97	% wt DAF
CO2	12.251			
CH4	1.863	Solids output	591.30	mg/Nm3
balance N2	52.106		1.85	% wt DAF
		Raw gas water content, %vol.		
Dry gas flow	4.426	Nm3/h		
H2/CO	0.864			
CO/CO2	1.481			
Dry gas HHV	5.027	MJ/Nm3		
Dry gas yield, DAF basis	2.925	Nm3/kg		
Exit temp.°C	689	°C		

Mass Balance

Input stream	kg/h	Output stream, kg/h	
DAF wood	1.513	H2	0.062
Ash	0.007	CO	1.003
Water, wood	0.173	CO2	1.065
O2, air	0.775	CH4	0.059
N2, air	2.882	N2	2.883
Water, air	0.032	Water	*0.249*
TOTAL	5.383	Tar	*0.030*
		Ash	*0.007*
		Char (R)	0.000
		Char (gas)	*0.021*
		TOTAL	5.379

Mass & Elemental Balance Closures, %

Mass	99.92
C	105.86
H	93.38
O	97.45

Figures in Italics are calculated from assumptions

Energy Balance		
Energy bal. (no heat loss)	96.13	[96.21]
Energy bal. + heat loss	103.21	[103.29]
Heat loss, % calculated	7.07	
Heat loss, % by difference	3.87	
[Figures in brackets, normalized for mass bal.]		

Conversion Efficiencies, %		
Cold gas	73.85	[71.55]
Hot gas (at exit temp.)	91.09	[88.26]
Raw (including tar + char)	96.40	[93.40]
[Figures in brackets are normalized to closure]		

Temperature Profile, °C

cm above grate	External gla	Insulation
40	19	
20	657	
16	805	287
12		271
10	608	
8		231
4	512	28

Test:	13.2	Date:	17/3/93	Duration, mins:	31.53

Objectives: Agitated base case run
Tar sampling
Batch gas analysis

Specific Measurements:

Tar	Sampled via hand pump
Water	Assumed (b)
Temperature	External
Gas flow	Pitot tube

Feed

Type	Wood blocks (batch 2)	
Size	6.35 - 12.7	mm
Moisture, % wet basis	10.20	%
Wet feed rate, kg/h	1.707	kg/h
Dry specific capacity	346.872	kg/m2h
Equivelence ratio	0.440	
Air/fuel ratio	2.868	

Bed Conditions

Char bed height	9.86	cm
Zone depth, cm	9.58	cm
Rate of zone rise	0	cm/h
Max. temperature		°C

Dry Gas Composition, %vol.

	On-line Analyser	Batch sample
H2	11.363	9.73
CO	15.190	14.96
CO2	12.718	12.12
CH4	1.500	1.26
N2 (balance)	59.230	59.29
O2		2.99
C2-C4 gases		0.95
Total	100.000	101.29
Dry gas flow		4.691 Nm3/h
H2/CO		0.748
CO/CO2		1.194
Dry gas HHV		3.964 MJ/Nm3
Dry gas yield, DAF basis		3.075 Nm3/kg
Exit temp.°C		473 °C

Sampling Measurements

Tar output	823.05	mg/Nm3
	2.85	% wt DAF
Solids output	843.62	mg/Nm3
	2.93	% wt DAF

Raw gas water content, %vol.

Mass Balance

Input stream	kg/h
DAF wood	1.525
Ash	0.007
Water, wood	0.174
O2, air	0.927
N2, air	3.447
Water, air	0.038
TOTAL	6.119

Output stream, kg/h	
H2	0.048
CO	0.884
CO2	1.163
CH4	0.050
N2	3.448
Water	*0.522*
Tar	*0.044*
Ash	*0.007*
Char (gas)	*0.037*
TOTAL	6.202

Mass & Elemental Balance Closures, %

Mass	101.35
C	103.90
H	105.00
O	102.63

Figures in Italics are calculated from assumptions

Energy Balance

Energy bal. (no heat loss)	89.11	[87.92]
Energy bal. + heat loss	101.65	[100.30]
Heat loss, % calculated	12.55	
Heat loss, % by difference	10.89	

[Figures in brackets, normalized for mass bal.]

Conversion Efficiencies, %

Cold gas	69.03	[67.91]
Hot gas (at exit temp.)	81.18	[79.86]
Raw (including tar + char)	89.39	[87.94]

[Figures in brackets are normalizedto closure]

Temperature Profile, °C

cm above grate	External thermocouple
40	22
28	45
26	67
24	121
22	152
20	173
16	668
14	599
12	684
10	450
8	253
6	377
4	335
2	339
0	252

Test:	14.1	Date:	26/4/93	Duration, mins:	40.3

Objectives: Pyrolysis dominant run
Tar sampling

Specific Measurements:

Tar	Sampled
Water	Assumed (b)
Temperature	As test 13.2
Gas flow	Pitot tube

Feed

Type	Wood blocks (batch 2)	
Size	6.35 - 12.7	mm
Moisture, % wet basis	10.81	%
Wet feed rate, kg/h	1.026	kg/h
Dry specific capacity	207.161	kg/m2h
Equivelence ratio	0.411	
Air/fuel ratio	2.679	

Bed Conditions

Char bed height	9.61	cm, average
Zone depth, cm	6.99	cm
Rate of zone rise	28.05	cm/h
Max. temperature		°C

Dry Gas Composition, %vol.

H2	7.212
CO	12.310
CO2	13.696
CH4	1.547
N2 (balance)	65.236

Dry gas flow	2.376	Nm3/h
H2/CO	0.585	
CO/CO2	0.900	
Dry gas HHV	3.090	MJ/Nm3
Dry gas yield, DAF basis	2.608	Nm3/kg
Exit temp.°C	394	°C

Sampling Measurements

Tar output	493.04	mg/Nm3
	1.45	% wt DAF
Solids output	877.85	mg/Nm3
	2.58	% wt DAF

Raw gas water content, %vol.

Mass Balance

Input stream	*kg/h*
DAF wood	*0.911*
Ash	0.004
Water, wood	*0.111*
O2, air	0.517
N2, air	1.923
Water, air	0.022
TOTAL	3.489

Output stream,	kg/h
H2	*0.015*
CO	0.363
CO2	0.634
CH4	0.026
N2	1.923
Water	*0.265*
Tar	0.013
Ash	*0.004*
Char (R)	0.098
Char (gas)	0.019
TOTAL	3.361

Mass & Elemental Balance Closures, %

Mass	*96.35*
C	*96.69*
H	80.58
O	*90.45*

Figures in Italics are calculated from assumptions

Energy Balance

Energy bal. (no heat loss)	76.18	[79.07]
Energy bal. + heat loss	97.28	[100.97]
Heat loss, % calculated	21.10	
Heat loss, % by difference	23.82	

[Figures in brackets, normalized for mass bal.]

Conversion Efficiencies, %

Cold gas	45.63	[46.91]
Hot gas (at exit temp.)	54.06	[55.57]
Raw (including tar + char)	76.42	[78.55]

[Figures in brackets are normalized to closure]

Temperature Profile, °C

Test:	14.2	Date:	26/4/93	Duration, mins:	9.09
Objectives:	Gasification dominant run Tar sampling			**Specific Measurements:**	Tar: Sampled Water: Assumed (b) Temperature: As test 13.2 Gas flow: Pitot tube

Feed		**Bed Conditions**	
Type	Wood blocks (batch 2)		
Size	6.35 - 12.7 mm	Char bed height	9.57 cm, average
Moisture, % wet basis	10.81 %	Zone depth, cm	6.41 cm
Wet feed rate, kg/h	2.176 kg/h	Rate of zone rise	-146.25 cm/h
Dry specific capacity	*439.292 kg/m2h*	Max. temperature	°C
Equivelence ratio	0.448		
Air/fuel ratio	2.919		

Dry Gas Composition, %vol.				**Sampling Measurements**	
				Tar output	269.83 mg/Nm3
					0.95 % wt DAF
H2	10.846				
CO	16.454			Solids output	622.69 mg/Nm3
CO2	11.817				2.18 % wt DAF
CH4	1.267				
N2 (balance)	59.617			Raw gas water content, %vol.	
Dry gas flow		6.006	Nm3/h		
H2/CO		0.653			
CO/CO2		1.412			
Dry gas HHV		3.965	MJ/Nm3		
Dry gas yield, DAF basis		3.109	Nm3/kg		
Exit temp.°C		528	°C		

Mass Balance

Input stream	kg/h	Output stream, kg/h	
DAF wood	1.932	H2	0.058
Ash	0.009	CO	1.226
Water, wood	0.235	CO2	1.383
O2, air	1.195	CH4	0.054
N2, air	4.443	N2	4.444
Water, air	0.051	Water	*0.667*
TOTAL	7.865	Tar	0.018
		Ash	*0.009*
		Char (R)	0.000
		Char (gas)	0.033
		TOTAL	7.893

Mass & Elemental Balance Closures, %

Mass	100.36
C	101.42
H	99.14
O	100.68

Figures in Italics are calculated from assumptions

Energy Balance		
Energy bal. (no heat loss)	87.48	[87.17]
Energy bal. + heat loss	97.43	[97.09]
Heat loss, % calculated	9.95	
Heat loss, % by difference	12.52	
[Figures in brackets, normalized for mass bal.]		

Conversion Efficiencies, %		
Cold gas	69.81	[71.65]
Hot gas (at exit temp.)	83.85	[86.06]
Raw (including tar + char)	87.78	[90.09]
[Figures in brackets are normalized to closure]		

Temperature Profile, °C

Test:	**14.3**	Date:	26/4/93	Duration, mins:	32.55
Objectives:	Pyrolysis dominant run			**Specific Measurements:**	Tar: As test 14.1; Water: Assumed (b); Temperature: As test 13.2; Gas flow: Pitot tube

Feed		**Bed Conditions**	
Type	Wood blocks (batch 2)		
Size	6.35 - 12.7 mm	Char bed height	11.65 cm, average
Moisture, % wet basis	10.81 %	Zone depth, cm	5.52 cm
Wet feed rate, kg/h	1.168 kg/h	Rate of zone rise	29.09 cm/h
Dry specific capacity	*235.760 kg/m2h*	*Max. temperature*	°C
Equivelence ratio	0.442		
Air/fuel ratio	2.880		

Dry Gas Composition, %vol.		**Sampling Measurements**	
H2	7.003	Tar output	mg/Nm3
CO	12.501		% wt DAF
CO2	13.732	Solids output	mg/Nm3
CH4	1.606		% wt DAF
N2 (balance)	65.158	Raw gas water content, %vol.	
Dry gas flow	2.908 Nm3/h		
H2/CO	0.560		
CO/CO2	0.910		
Dry gas HHV	3.111 MJ/Nm3		
Dry gas yield, DAF basis	2.805 Nm3/kg		
Exit temp.°C	359 °C		

Mass Balance

Input stream	kg/h	*Output stream*, kg/h	
DAF wood	1.037	H2	*0.018*
Ash	0.005	CO	0.451
Water, wood	0.126	CO2	0.779
O2, air	0.633	CH4	0.033
N2, air	2.353	N2	2.353
Water, air	0.025	Water	*0.321*
TOTAL	4.179	Tar	*0.016*
		Ash	*0.005*
		Char (R)	0.101
		Char (gas)	*0.024*
		TOTAL	4.103

Mass & Elemental Balance Closures, %

Mass	*98.16*
C	102.48
H	85.05
O	93.63

Figures in Italics are calculated from assumptions

Energy Balance		
Energy bal. (no heat loss)	78.60	[80.07]
Energy bal. + heat loss	97.15	[98.97]
Heat loss, % calculated	18.55	
Heat loss, % by difference	21.40	

[Figures in brackets, normalized for mass bal.]

Conversion Efficiencies, %		
Cold gas	49.41	[50.86]
Hot gas (at exit temp.)	57.57	[59.26]
Raw (including tar + char)	78.84	[81.16]

[Figures in brackets are normalized to closure]

Temperature Profile, °C

Test:	14.4	Date:	26/4/93	Duration, mins:	13.92

Objectives: Gasification dominant run

Specific Measurements:

Tar	Sampled
Water	Assumed (b)
Temperature	As 13.2
Gas flow	Pitot tube

Feed

Type	Wood blocks (batch 2)	
Size	6.35 - 12.7	mm
Moisture, % wet basis	10.81	%
Wet feed rate, kg/h	1.778	kg/h
Dry specific capacity	358.813	kg/m2h
Equivelence ratio	0.448	
Air/fuel ratio	2.922	

Bed Conditions

Char bed height	12.1	cm, average
Zone depth, cm	7.64	cm
Rate of zone rise	-64.29	cm/h
Max. temperature		°C

Dry Gas Composition, %vol.

H2	10.893
CO	16.193
CO2	12.150
CH4	1.367
N2 (balance)	59.397

Dry gas flow	4.938	Nm3/h
H2/CO	0.669	
CO/CO2	1.343	
Dry gas HHV	3.978	MJ/Nm3
Dry gas yield, DAF basis	3.130	Nm3/kg
Exit temp.°C	424	°C

Sampling Measurements

Tar output	39.73	mg/Nm3
	0.14	% wt DAF
Solids output	238.41	mg/Nm3
	0.84	% wt DAF

Raw gas water content, %vol.

Mass Balance

Input stream	kg/h
DAF wood	1.578
Ash	0.008
Water, wood	0.192
O2, air	0.977
N2, air	3.633
Water, air	0.039
TOTAL	6.427

Output stream,	kg/h
H2	0.048
CO	0.990
CO2	1.167
CH4	0.048
N2	3.633
Water	*0.560*
Tar	*0.002*
Ash	*0.008*
Char (R)	0.000
Char (gas)	*0.006*
TOTAL	6.462

Mass & Elemental Balance Closures, %

Mass	100.56
C	99.31
H	100.46
O	102.17

Figures in Italics are calculated from assumptions

Energy Balance

Energy bal. (no heat loss)	81.86	[81.41]
Energy bal. + heat loss	94.04	[93.52]
Heat loss, % calculated	12.18	
Heat loss, % by difference	18.14	

[Figures in brackets, normalized for mass bal.]

Conversion Efficiencies, %

Cold gas	70.50	[74.96]
Hot gas (at exit temp.)	81.40	[86.55]
Raw (including tar + char)	82.12	[87.32]

[Figures in brackets are normalized to closure]

Temperature Profile, °C

Test:	T3	Date:	18/6/92	Duration, mins:	13.25

Objectives: Throated reactor
Tar and water sampling

Specific Measurements:

Tar	Sampled
Water	Sampled
Temperature	As test T4.2
Gas flow	Pitot tube

Feed

Type	Wood (batch 2)	
Size	6.35 - 12.7	mm
Moisture, % wet basis	9.19	%
Wet feed rate, kg/h	1.108	kg/h
Specific capacity by grate	261.380	kg/m2h
Specific capacity (throat)	800.476	kg/m2h
Equivelence ratio	0.523	
Air/fuel ratio	3.410	

Bed Conditions

Char bed height	6.36	cm
Zone depth, cm	6.79	cm
Height to void	8.57	cm

Dry Gas Composition, %vol.

H2	9.844
CO	16.456
CO2	9.435
CH4	1.679
balance N2	62.585

Dry gas flow	3.474	Nm3/h
H2/CO	0.598	
CO/CO2	1.769	
Dry gas HHV	4.001	MJ/Nm3
Dry gas yield, DAF basis	3.470	Nm3/kg
Exit temp.°C	606	°C

Sampling Measurements

Tar output	179.27	mg/Nm3
	0.674	% wt DAF
Solids output	667.75	mg/Nm3
	2.992	% wt DAF
Raw gas water content, %vol.	7.667	

Mass Balance

Input stream	kg/h
DAF wood	1.001
Ash	0.005
Water, wood	0.102
O2, air	0.724
N2, air	2.690
Water, air	0.037
TOTAL	4.559

Output stream,	kg/h
H2	0.030
CO	0.707
CO2	0.637
CH4	0.041
N2	2.691
Water	0.2735
Tar	0.007
Ash	*0.005*
Char (R)	0.000
Char (gas)	0.025
TOTAL	4.417

Mass & Elemental Balance Closures, %

Mass	96.90
C	105.92
H	94.92
O	86.98

Figures in Italics are calculated from assumptions

Energy Balance

Energy bal. (no heat loss)	97.19	[100.30]
Energy bal. + heat loss	104.81	[108.16]
Heat loss, % calculated	7.62	
Heat loss, % by difference	2.81	

[Figures in brackets, normalized for mass bal.}

Conversion Efficiencies, %

Cold gas	75.52	[72.06]
Hot gas (at exit temp.)	93.09	[88.12]
Raw (including tar + char)	97.65	[93.17]

[Figures in brackets are normalized to closure]

Temperature Profile, °C

Not determined

Test:	T4.1	Date:	14/7/92	Duration, mins:	50.17
Objectives:	Throated reactor Tar and water sampling			**Specific Measurements:**	Tar Sampled Water Sampled Temperature External Gas flow Pitot tube

Feed		**Bed Conditions**	
Type	Wood (batch 2)		
Size	6.35 - 12.7 mm	Char bed height	3.50 cm
Moisture, % wet basis	9.80 %	Zone depth, cm	9.44 cm
Wet feed rate, kg/h	1.729 kg/h	Height to void	8.06 cm
Specific capacity (grate)	405.178 kg/m2h		
Specific capacity (throat)	1240.856 kg/m2h		
Equivelence ratio	0.541		
Air/fuel ratio	3.525		

Dry Gas Composition, %vol.		**Sampling Measurements**	
H2	9.238	Tar output	368.89 mg/Nm3
CO	15.241		1.445 % wt DAF
CO2	10.466		
CH4	1.569	Solids output	841.07 mg/Nm3
balance N2	63.486		3.294 % wt DAF
Dry gas flow	5.498 Nm3/h		
H2/CO	0.605	Raw gas water content, %vol.	9.554
CO/CO2	1.472		
Dry gas HHV	3.727 MJ/Nm3		
Dry gas yield, DAF basis	3.542 Nm3/kg		
Exit temp.°C	650 °C		

Mass Balance

Input stream	kg/h	Output stream, kg/h	
DAF wood	1.552	H2	0.045
Ash	0.007	CO	1.035
Water, wood	0.169	CO2	1.116
O2, air	1.160	CH4	0.061
N2, air	4.311	N2	4.312
Water, air	0.059	Water	0.546
TOTAL	7.259	Tar	0.022
		Ash	0.006
		Char (R)	0.000
		Char (gas)	0.046
		TOTAL	7.188

Mass & Elemental Balance Closures, %

Mass	99.03
C	108.53
H	103.53
O	93.17

Figures in Italics are calculated from assumptions

Energy Balance		
Energy bal. (no heat loss)	99.47	[100.44]
Energy bal. + heat loss	105.97	[107.02]
Heat loss, % calculated	6.51	
Heat loss, % by difference	0.53	
[Figures in brackets, normalized for mass bal.]		

Conversion Efficiencies, %		
Cold gas	73.32	[69.19]
Hot gas (at exit temp.)	93.46	[88.19]
Raw (including tar + char)	99.95	[94.32]

[Figures in brackets are normalized to closure]

Temperature Profile, °C

External tempertures by contact thermocouple

cm above grate	°C
24	35
22	39
18	47
16	64
14	140
12	*237*
10	450
8	560
6	475
4	465
2	385
0	310

Test:	T4.2	Date:	14/7/92	Duration, mins:	21.15
Objectives:	Throated reactor Small feed size *[Pyrolysis dominant operation]*			**Specific Measurements:**	Tar: As test T4.1 Water: As test T4.1 Reactor tem: External Gas flow: Pitot tube

Feed		**Bed Conditions**	
Type	Wood (batch 2)		
Size	4.75 - 6.35 mm	Char bed height	8.67 cm
Moisture, % wet basis	9.08 %	Zone depth, cm	4.50 cm
Wet feed rate, kg/h	1.619 kg/h	Rate of zone rise	11.35 cm/h
Specific capacity (grate)	382.456 kg/m2h		
Specific capacity (throat)	1171.271 kg/m2h		
Equivelence ratio	0.471		
Air/fuel ratio	3.073		

Dry Gas Composition, %vol.		**Sampling Measurements**	
H2	11.331	Tar output	mg/Nm3
CO	16.647		% wt DAF
CO2	10.108		
CH4	1.736	Solids output	mg/Nm3
balance N2	60.177		% wt DAF
Dry gas flow	4.781 Nm3/h		
H2/CO	0.680	Raw gas water content, %vol.	
CO/CO2	1.611		
Dry gas HHV	4.239 MJ/Nm3		
Dry gas yield, DAF basis	3.263 Nm3/kg		
Exit temp.°C	541 °C		

Mass Balance

Input stream	kg/h	Output stream, kg/h	
DAF wood	1.465	H2	0.048
Ash	0.007	CO	0.981
Water, wood	0.147	CO2	0.936
O2, air	0.954	CH4	0.059
N2, air	3.547	N2	3.548
Water, air	0.049	Water	*0.482*
TOTAL	6.169	Tar	*0.019*
		Ash	0.007
		Char (R)	0.034
		Char (gas)	*0.037*
		TOTAL	6.118

Mass & Elemental Balance Closures, %

Mass	99.17
C	107.12
H	107.14
O	95.07

Figures in Italics are calculated from assumptions

Energy Balance		
Energy bal. (no heat loss)	100.40	[101.25]
Energy bal. + heat loss	105.59	[106.48]
Heat loss, % calculated	5.19	
Heat loss, % by difference	-0.40	
[Figures in brackets, normalized for mass bal.]		

Conversion Efficiencies, %		
Cold gas	76.81	[72.74]
Hot gas (at exit temp.)	91.39	[86.55]
Raw (including tar + char)	100.83	[95.49]

[Figures in brackets are normalized to closure]

Temperature Profile, °C

External tempertures by contact thermocouple

cm above grate	°C
40	25
22	39
20	41
18	53
16	75
14	142
12	390
10	425
8	390
6	365
4	365
2	350
0	330

Test:	T4.3	Date:	14/7/92	Duration, mins:	15.2	
Objectives:	Throated reactor Small feed size			**Specific Measurements:**	Tar Water Temperature Gas flow	As test T4.1 As test T4.1 As test T4.1 Gasmeter

Feed		**Bed Conditions**	
Type	Wood (batch 2)		
Size	4.75 - 6.35 mm	Char bed height	8.50 cm
Moisture, % wet basis	9.08 %	Zone depth, cm	4.38 cm
Wet feed rate, kg/h	1.716 kg/h		
Specific capacity (grate)	405.363 kg/m2h		
Specific capacity (throat)	1241.425 kg/m2h		
Equivelence ratio	0.453		
Air/fuel ratio	2.957		

Dry Gas Composition, %vol.		**Sampling Measurements**
H2	12.348	
CO	17.440	
CO2	9.438	
CH4	1.838	
balance N2	58.938	
Dry gas flow	4.979 Nm3/h	
H2/CO	0.709	
CO/CO2	1.867	
Dry gas HHV	4.509 MJ/Nm3	
Dry gas yield, DAF basis	3.206 Nm3/kg	
Exit temp.°C	628 °C	

Mass Balance

Input stream	kg/h	Output stream, kg/h	
DAF wood	1.553	H2	0.055
Ash	0.007	CO	1.070
Water, wood	0.156	CO2	0.910
O2, air	0.973	CH4	0.065
N2, air	3.617	N2	3.618
Water, air	0.050	Water	*0.502*
TOTAL	6.356	Tar	*0.020*
		Ash	*0.005*
		Char (R)	0.000
		Char (gas)	*0.041*
		TOTAL	6.286

Mass & Elemental Balance Closures, %

Mass	98.89
C	102.94
H	110.06
O	94.40

Figures in Italics are calculated from assumptions

Energy Balance		
Energy bal. (no heat loss)	102.96	[104.11]
Energy bal. + heat loss	109.47	[110.69]
Heat loss, % calculated	6.50	
Heat loss, % by difference	-2.96	
[Figures in brackets, normalized for mass bal.]		

Conversion Efficiencies, %		
Cold gas	80.28	[73.334]
Hot gas (at exit temp.)	97.52	[89.08]
Raw (including tar + char)	103.38	[94.44]
[Figures in brackets are normalized to closure]		

Temperature Profile, °C

Not determined

Test:	T5.1	Date:	24/8/92	Duration, mins:	18.68	
Objectives:	Throated reactor			**Specific Measurements:**	Tar	As test T4.1
					Water	As test T4.1
					Temperature	Bed thermocouple
						Heat loss as T4.1
						Exit temp. as T4.1
					Gas flow	Pitot

Feed		**Bed Conditions**	
Type	Wood (batch 2)		
Size	6.35 - 12.7 mm	Char bed height	3.75 cm
Moisture, % wet basis	10.35 %	Zone depth, cm	9.79 cm
Wet feed rate, kg/h	1.722 kg/h		
Specific capacity (grate)	401.085 kg/m2h	Max. temperature	1213 °C
Specific capacity (throat)	1228.323 kg/m2h		
Equivelence ratio	0.532		
Air/fuel ratio	3.467		

Dry Gas Composition, %vol.		**Sampling Measurements**
H2	9.898	
CO	17.486	
CO2	8.429	
CH4	1.133	
balance N2	63.055	
Dry gas flow	5.376 Nm3/h	
H2/CO	0.565	
CO/CO2	2.332	
Dry gas HHV	3.921 MJ/Nm3	
Dry gas yield, DAF basis	3.499 Nm3/kg	
Exit temp.°C	Not measured	

Mass Balance

Input stream	kg/h	Output stream, kg/h	
DAF wood	1.536	H2	0.047
Ash	0.007	CO	1.164
Water, wood	0.178	CO2	0.881
O2, air	1.129	CH4	0.043
N2, air	4.197	N2	4.197
Water, air	0.051	Water	*0.517*
TOTAL	7.098	Tar	*0.022*
		Ash	*0.007*
		Char (R)	0.000
		Char (gas)	*0.043*
		TOTAL	6.921

Mass & Elemental Balance Closures, %

Mass	97.51
C	106.42
H	99.66
O	88.74

Figures in Italics are calculated from assumptions

Energy Balance		
Energy bal. (no heat loss)	101.77	[104.37]
Energy bal. + heat loss	108.40	[111.17]
Heat loss, % calculated	6.63	
Heat loss, % by difference	-0.54	
[Figures in brackets, normalized for mass bal.]		

Conversion Efficiencies, %		
Cold gas	76.19	[70.28]
Hot gas (at exit temp.)	95.96	[88.52]
Raw (including tar + char)	102.20	[94.28]
[Figures in brackets are normalized to closure]		

Temperature Profile, °C	
Reaction temperture at 8 cm above grate, °C	
Average	1063
Standard deviation	94
Minimum	790
Maximum	1213

Test:	T5.3	Date:	24/8/92	Duration, mins:	19.85

Objectives: Throated reactor; High feed rate; Reaction temperature

Specific Measurements:

Tar	Sampled
Water	Sampled
Temperature	Bed thermocouple
	Exit temp. as T7.1
	External as T6.4
Gas flow	Pitot

Feed

Type	Wood (batch 2)
Size	6.35 - 12.7 mm
Moisture, % wet basis	10.35 %
Wet feed rate, kg/h	2.050 kg/h
Specific capacity (grate)	477.439 kg/m2h
Specific capacity (throat)	1462.158 kg/m2h
Equivelence ratio	0.564 -
Air/fuel ratio	3.676

Bed Conditions

Char bed height	5.37 cm
Zone depth, cm	8.17 cm
Max. temperature	1205 °C

Dry Gas Composition, %vol.

H2	9.935
CO	17.944
CO2	8.520
CH4	1.171
balance N2	62.430
Dry gas flow	6.841 Nm3/h
H2/CO	0.553
CO/CO2	2.181
Dry gas HHV	3.999 MJ/Nm3
Dry gas yield, DAF basis	3.741 Nm3/kg
Exit temp.°C	Not measured

Sampling Measurements

Tar output	426.58 mg/Nm3
	1.723 % wt DAF
Solids output	276.57 mg/Nm3
	1.117 % wt DAF
Raw gas water content, %vol.	7.39

Mass Balance

Input stream	kg/h
DAF wood	1.829
Ash	0.009
Water, wood	0.212
O2, air	1.425
N2, air	5.297
Water, air	0.064
TOTAL	8.836

Output stream, kg/h	
H2	0.061
CO	1.522
CO2	1.136
CH4	0.057
N2	5.298
Water	0.502
Tar	0.032
Ash	*0.009*
Char (R)	0.000
Char (gas)	0.012
TOTAL	8.627

Mass & Elemental Balance Closures, %

Mass	97.64
C	113.30
H	93.61
O	86.98

Figures in Italics are calculated from assumptions

Energy Balance

Energy bal. (no heat loss)	104.97	[107.52]
Energy bal. + heat loss	110.97	[113.66]
Heat loss, % calculated	6.00	
Heat loss, % by difference	-4.97	

[Figures in brackets, normalized for mass bal.]

Temperature Profile, °C

Reaction temperture at 8 cm above grate, °C

Average	834
Standard deviation	238
Minimum	402
Maximum	1205

Conversion Efficiencies, %

Cold gas	81.13	[73.11]
Hot gas (at exit temp.)	101.57	[91.53]
Raw (including tar + char)	105.44	[95.02]

[Figures in brackets are normalized to closure]

Test:	T6.1	Date: 12/10/92	Duration, mins:	29.93	
Objectives:	Throated reactor		**Specific**	Tar	Sampled
	Tar and water sampled		**Measurements:**	Water	Sampled
	Reaction temperature			Temperature	Bed thermocouple
					External as T4.2
					Exit temp. as T3
				Gas flow	Pitot

Feed		**Bed Conditions**		
Type	Wood (batch 2)			
Size	6.35 - 12.7 mm	Char bed height	7.67	cm
Moisture, % wet basis	11.33 %	Zone depth, cm	5.88	cm
Wet feed rate, kg/h	1.196 kg/h			
Specific capacity (grate)	275.613 kg/m2h	Max. temperature	1231	°C
Specific capacity (throat)	844.065 kg/m2h			
Equivelence ratio	0.571			
Air/fuel ratio	3.721			

Dry Gas Composition, %vol.		**Sampling Measurements**		
H2	10.800	Tar output	441.45	mg/Nm3
CO	18.069		1.863	% wt DAF
CO2	10.362	Solids output	1654.49	mg/Nm3
CH4	1.213		6.981	% wt DAF
N2 (balance	59.556	Raw gas water content, %vol.	5.986	
Dry gas flow	4.188 Nm3/h	Start-up sample		
H2/CO	0.598	Tar output	1594.0	mg/Nm3
CO/CO2	1.776			% wt DAF
Dry gas HHV	4.143 MJ/Nm3	Solids output	920.6	mg/Nm3
Dry gas yield, DAF basis	3.967 Nm3/kg			% wt DAF
Exit temp.°C	Not measured	Raw gas water content, %vol.	6.341	

Mass Balance

Input stream	kg/h	Output stream, kg/h	
DAF wood	1.056	H2	0.040
Ash	0.005	CO	0.939
Water, wood	0.136	CO2	0.846
O2, air	0.833	CH4	0.036
N2, air	3.096	N2	3.096
Water, air	0.033	Water	0.249
TOTAL	5.158	Tar	0.020
		Ash	*0.005*
		Char (R)	0.000
		Char (gas)	0.069
		TOTAL	5.301

Mass & Elemental Balance Closures, %

Mass	102.76
C	137.02
H	97.42
O	96.45

Figures in Italics are calculated from assumptions

Energy Balance			**Temperature Profile, °C**	
Energy bal. (no heat loss)	119.14	[115.94]	Reaction temperture at 8 cm above grate, °C	
Energy bal. + heat loss	126.48	[123.08]	Average	1071
Heat loss, % calculated	7.34		Standard deviation	67
Heat loss, % by difference	-19.14		Minimum	823
[Figures in brackets, normalized for mass bal.]			Maximum	1231

Conversion Efficiencies, %		
Cold gas	87.81	[69.42]
Hot gas (at exit temp.)	107.60	[85.08]
Raw (incuding tar + char)	119.62	[94.58]

[Figures in brackets are normalized to closure]

Test:	**T6.2**	Date: 12/10/92	Duration, mins:	29.73

Objectives: *Throated reactor*
Tar and water sampling
Reaction temperature

Specific Measurements: *Tar* *Sampled*
Water *Sampled*
Temperature *Bed thermocouple*
External as T4.2
Exit temp. as T4.2
Gas flow *Pitot*

Feed

Type	Wood (batch 2)	
Size	6.35 - 12.7	mm
Moisture, % wet basis	11.33	%
Wet feed rate, kg/h	1.445	kg/h
Specific capacity (grate)	332.822	kg/m2h
Specific capacity (throat)	1019.268	kg/m2h
Equivelence ratio	0.480	
Air/fuel ratio	3.130	

Bed Conditions

Char bed height	7.56	cm
Zone depth, cm	6.22	cm
Max. temperature	1225	°C

Dry Gas Composition, %vol.

H2	10.441	
CO	18.207	
CO2	10.575	
CH4	1.292	
balance N2	59.486	
Dry gas flow	4.265	Nm3/h
H2/CO	0.574	
CO/CO2	1.757	
Dry gas HHV	4.146	MJ/Nm3
Dry gas yield, DAF basis	3.345	Nm3/kg
Exit temp.°C	Not measured	

Sampling Measurements

Tar output	590.86	mg/Nm3
	2.088	% wt DAF
Solids output	470.87	mg/Nm3
	1.664	% wt DAF
Raw gas water content, %vol.	5.328	

Mass Balance

Input stream	kg/h
DAF wood	1.275
Ash	0.006
Water, wood	0.164
O2, air	0.846
N2, air	3.145
Water, air	0.034
TOTAL	5.469

Output stream,	kg/h
H2	0.040
CO	0.962
CO2	0.878
CH4	0.039
N2	3.145
Water	0.235
Tar	0.027
Ash	*0.006*
Char (R)	0.000
Char (gas)	0.015
TOTAL	5.347

Mass & Elemental Balance Closures, %

Mass	97.77
C	111.65
H	78.12
O	88.96

Figures in Italics are calculated from assumptions

Energy Balance

Energy bal. (no heat loss)	92.87	[94.99]
Energy bal. + heat loss	98.95	[101.20]
Heat loss, % calculated	6.08	
Heat loss, % by difference	7.13	

[Figures in brackets, normalized for mass bal.]

Temperature Profile, °C

Reaction temperture at 8 cm above grate, °C

Average	1046
Standard deviation	138
Minimum	422
Maximum	1225

Conversion Efficiencies, %

Cold gas	73.57	[74.35]
Hot gas (at exit temp.)	87.97	[88.91]
Raw (including tar + char)	93.18	[94.18]

[Figures in brackets are normalized to closure]

Test:	T6.4	Date: 12/10/92	Duration, mins:	30.8
Objectives:	Throated reactor Tar and water sampling Reaction temperature		**Specific Measurements:**	Tar Sampled Water Sampled Temperature Bed thermocouple Exit temp. as T7.1 Gas flow Pitot

Feed		**Bed Conditions**	
Type	Wood (batch 2)		
Size	6.35 - 12.7 mm	Char bed height	1.15 cm
Moisture, % wet basis	11.33 %	Zone depth, cm	11.95 cm
Wet feed rate, kg/h	2.016 kg/h		
Specific capacity (grate)	464.417 kg/m2h	Max. temperature	1114 °C
Specific capacity (throat)	1411.277 kg/m2h		
Equivelence ratio	0.588		
Air/fuel ratio	3.833		

Dry Gas Composition, %vol.		**Sampling Measurements**	
H2	6.469	Tar output	74.76 mg/Nm3
CO	*15.803*		0.294 % wt DAF
CO2	10.431		
CH4	1.086	Solids output	*112.14 mg/Nm3*
balance N2	66.211		0.441 % wt DAF
Dry gas flow	6.567 Nm3/h		
H2/CO	0.395	Raw gas water content, %vol.	6.113
CO/CO2	1.604		
Dry gas HHV	3.253 MJ/Nm3		
Dry gas yield, DAF basis	3.690 Nm3/kg		
Exit temp.°C	Not measured		

Mass Balance

Input stream	kg/h	Output stream, kg/h	
DAF wood	1.780	H2	0.038
Ash	0.008	CO	1.283
Water, wood	0.228	CO2	1.330
O2, air	1.446	CH4	0.050
N2, air	5.375	N2	5.376
Water, air	0.050	Water	0.433
TOTAL	8.887	Tar	0.005
		Ash	*0.008*
		Char (react	0.000
		Char (gas)	0.000
		TOTAL	8.524

Mass & Elemental Balance Closures, %

Mass	95.91
C	107.14
H	70.91
O	84.37

Figures in Italics are calculated from assumptions

Energy Balance		
Energy bal. (no heat loss)	84.68	[88.29]
Energy bal. + heat loss	90.88	[94.76]
Heat loss, % calculated	6.21	
Heat loss, % by difference	15.32	

[Figures in brackets, normalized for mass bal.]

Temperature Profile, °C

Conversion Efficiencies, %		
Cold gas	64.20	[70.64]
Hot gas (at exit temp.)	84.46	[92.93]
Raw (including tar + char)	84.98	[93.51]

[Figures in brackets are normalized to closure]

External temperatures by contact thermocouple, °C

cm above grate	°C	cm	°C
30	30	14	104
28	32	12	335
26	36	10	560
24	39	8	440
22	44	6	400
20	51	4	330
18	63	2	335
16	80	0	310

Test:	T7.1	Date: 17/12/92	Duration, mins:	21.9
Objectives:	Throated reactor Tar and water sampling Small feed size		**Specific Measurements:**	Tar Sampled Water Sampled Temperature External as T6.4 Gas flow Pitot

Feed		**Bed Conditions**	
Type	Wood (batch 2)		
Size	4.75 - 6.35 mm	Char bed height	6.71 cm
Moisture, % wet basis	9.57 %	Zone depth, cm	5.52 cm
Wet feed rate, kg/h	2.113 kg/h		
Specific capacity (grate)	496.517 kg/m2h		
Specific capacity (throat)	1520.585 kg/m2h		
Equivelence ratio	0.452		
Air/fuel ratio	2.946		

Dry Gas Composition, %vol.		**Sampling Measurements**	
H2	10.382	Tar output	255.01 mg/Nm3
CO	19.500		0.86 % wt DAF
CO2	9.060		
CH4	1.372	Solids output	337.81 mg/Nm3
balance N2	59.784		1.14 % wt DAF
Dry gas flow	5.970 Nm3/h		
H2/CO	0.532	Raw gas water content, %vol.	6.559
CO/CO2	2.211		
Dry gas HHV	4.333 MJ/Nm3		
Dry gas yield, DAF basis	3.139 Nm3/kg		
Exit temp.°C	646 °C		

Mass Balance

Input stream	kg/h	Output stream, kg/h	
DAF wood	1.902	H2	0.055
Ash	0.009	CO	1.440
Water, wood	0.202	CO2	1.051
O2, air	1.188	CH4	0.058
N2, air	4.415	N2	4.416
Water, air	0.027	Water	0.410
TOTAL	7.743	Tar	0.016
		Ash	*0.009*
		Char (R)	0.000
		Char (gas)	0.012
		TOTAL	7.468

Mass & Elemental Balance Closures, %

Mass	96.45
C	101.74
H	82.52
O	88.00

Figures in Italics are calculated from assumptions

Energy Balance		
Energy bal. (no heat loss)	92.61	[96.02]
Energy bal. + heat loss	98.55	[102.18]
Heat loss, % calculated	5.94	
Heat loss, % by difference	7.39	
[Figures in brackets, normalized for mass bal.]		

Conversion Efficiencies, %		
Cold gas	73.11	[74.18]
Hot gas (at exit temp.)	90.40	[91.73]
Raw (including tar + char)	92.78	[94.15]
[Figures in brackets are normalized to closure]		

Temperature Profile, °C

Not determined

Test:	T11	Date:	21/4/93	Duration, mins:	39.53

Objectives:	Stainless steel throat, insulated Tar and water sampling Reaction temperature

Specific Measurements:		
	Tar	Sampled
	Water	Sampled
	Temperature	External & 2 cm below throat
	Gas flow	Pitot

Feed

Type	Wood (batch 2)	
Size	6.35-12.7	mm
Moisture, % wet basis	10.63	%
Wet feed rate, kg/h	1.861	kg/h
Specific capacity (grate)	376.356	kg/m2h
Specific capacity (throat)	1323.128	kg/m2h
Equivelence ratio	0.324	
Air/fuel ratio	2.112	

Bed Conditions

Char bed height	Uncertain, dull red zone to grate.	
Zone depth, cm		
Max. temperature	1365	°C

Dry Gas Composition, %vol.

H2	16.793	
CO	19.707	
CO2	12.266	
CH4	1.958	
balance N2	49.277	
Dry gas flow	4.495	Nm3/h
H2/CO	0.853	
CO/CO2	1.607	
Dry gas HHV	5.410	MJ/Nm3
Dry gas yield, DAF basis	2.716	Nm3/kg
Exit temp.°C	669	°C

Sampling Measurements

Tar output	138.22	mg/Nm3
	0.40	% wt DAF
Solids output	250.52	mg/Nm3
	0.73	% wt DAF
Raw gas water content, %vol.	6.596	

Mass Balance

Input stream	kg/h
DAF wood	1.655
Ash	0.008
Water, wood	0.198
O2, air	0.741
N2, air	2.754
Water, air	0.030
TOTAL	5.385

Output stream, kg/h	
H2	0.068
CO	1.101
CO2	1.077
CH4	0.063
N2	2.754
Water	0.282
Tar	0.007
Ash	*0.008*
Char (R)	0.000
Char (gas)	0.004
TOTAL	5.364

Mass & Elemental Balance Closures, %

Mass	99.61
C	99.06
H	91.11
O	99.87

Figures in Italics are calculated from assumptions

Energy Balance

Energy bal. (no heat loss)	95.23	[95.61]
Energy bal. + heat loss	97.12	[97.51]
Heat loss, % calculated	1.89	
Heat loss, % by difference	4.77	

[Figures in brackets, normalized for mass bal.]

Temperature Profile, °C

Height above grate, cm

	Un-insulated	Insulated
30	35	23
10	713	59
0	328	

Reaction Temperature, °C

	2 cm below throat
Average	1107
Standard deviation	84
Minimum	932
Maximum	1365

Conversion Efficiencies, %

Cold gas	79.02	[81.36]
Hot gas (at exit temp.)	94.42	[97.21]
Raw (including tar + char)	95.45	[98.28]

[Figures in brackets are normalized to closure]

G 2 Energy Balance Summary

Table G2.1 Energy Balance Summary

Test	Total Inputs MJh^{-1}	Outputs, MJh^{-1}							Heat loss by difference
		Gas	Tar	Char (gas)	Char (reactor)	Sensible heat	Heat loss*	Total Outputs	
1.1	26.89	16.64	0.39	0.25	0.32	3.48	2.62	23.70	5.81
1.2	22.80	12.55	0.67	0.69	0.00	2.01	12.65	28.58	6.88
2.1	22.68	15.73	0.52	0.09	1.23	2.55	2.57	22.70	2.56
2.2	29.67	16.57	0.98	1.14	0.16	2.22	20.20	41.28	8.60
2.3	14.63	7.15	0.66	0.23	3.11	1.09	2.73	14.97	2.39
3	22.89	15.46	1.01	1.04	0.00	3.00	2.09	22.59	2.38
4	25.99	18.51	0.97	0.86	0.27	3.67	2.76	27.03	1.71
5	23.82	15.52	0.82	0.71	0.00	3.21	2.78	23.03	3.56
6	21.56	15.19	0.80	0.70	0.00	3.10	2.77	22.57	1.77
7	32.06	24.08	0.48	0.24	0.09	5.85	0.59	32.05	0.60
8	27.44	19.82	0.74	0.45	0.00	3.84	1.12	25.98	2.59
9	20.65	14.10	0.76	0.67	0.16	3.04	3.55	22.28	1.92
11	24.30	15.58	0.78	0.67	0.21	3.20	4.50	24.93	4.06
12	29.14	19.08	0.93	0.80	0.21	3.96	4.84	29.82	4.16
13.1	30.21	22.25	1.00	0.54	0.00	5.26	2.14	31.18	1.16
13.2	30.47	20.97	1.45	0.98	0.00	3.75	3.82	30.97	3.32
14.1	18.19	8.28	0.44	0.50	3.07	1.53	3.84	17.70	4.37
14.2	38.59	26.85	0.61	0.86	0.00	5.44	3.84	37.60	4.83
14.3	20.71	10.22	0.54	0.62	3.18	1.72	3.84	20.12	4.43
14.4	31.52	22.15	0.07	0.15	0.00	3.42	3.84	29.64	5.73
T3	20.03	15.06	0.23	0.66	0.00	3.52	1.53	20.99	0.56
T4.1	31.05	22.66	0.75	1.19	0.00	6.28	2.02	32.91	0.17
T4.2	29.29	22.40	0.65	0.98	1.08	4.29	1.52	30.93	-0.11
T4.3	31.04	24.82	0.68	1.08	0.00	5.38	2.02	33.98	-0.92
T5.1	30.72	23.31	0.73	1.12	0.00	6.11	2.04	33.30	-0.55
T5.3	36.58	29.54	1.05	0.32	0.00	7.49	2.20	40.59	-1.82
T6.1	21.11	18.46	0.66	1.80	0.00	3.70	1.55	25.20	-4.04
T6.2	25.57	18.67	0.89	0.40	0.00	3.70	1.55	25.20	1.81
T6.3	35.57	22.75	0.18	0.00	0.00	7.19	2.21	32.32	5.45
T7	37.94	27.68	0.54	0.33	0.00	6.58	2.25	37.39	2.81
T11	33.03	26.04	0.22	0.11	0.00	5.08	0.62	32.08	1.58

Note: * calculated (see Appendix F)

Table G2.2 Gasifier Output Energy Distribution (%)

Test	Gas	Tar	Char (gas)	Char (reactor)	Sensible heat	Heat loss (by difference)
Base Case - Stable						
1.2	55.04	2.94	3.03	0.00	8.82	30.18
2.2	55.85	3.30	3.84	0.54	7.48	28.99
3	67.54	4.41	4.54	0.00	13.11	10.40
4	71.22	3.73	3.31	1.04	14.12	6.58
5	65.16	3.44	2.98	0.00	13.48	14.95
6	70.45	3.71	3.25	0.00	14.38	8.21
Average	*64.21*	*3.59*	*3.49*	*0.26*	*11.90*	*16.55*
Pyrolysis Dominant						
2.3	48.87	4.51	1.57	21.26	7.45	16.34
14.1	45.52	2.42	2.75	16.88	8.41	24.02
14.3	49.35	2.61	2.99	15.35	8.31	21.39
Average	*47.91*	*3.18*	*2.44*	*17.83*	*8.06*	*20.58*
Gasification Dominant						
14.2	69.58	1.58	2.23	0.00	14.10	12.52
14.4	70.27	0.22	0.48	0.00	10.85	18.18
Average	*69.93*	*0.90*	*1.36*	*0.00*	*12.48*	*15.35*

APPENDIX H OPEN-CORE CHAR PROFILE DATA

H1 Size Distribution Graphs from Test 13

The size distribution of the layers taken from test 13 are shown in Figures H1.1-1.5. A vertical line drawn down from the point where the accumulative weight curve crosses the 50% line gives the weight average size for the layer (see Figure H1.1, the weight average size for layer 3 is shown).

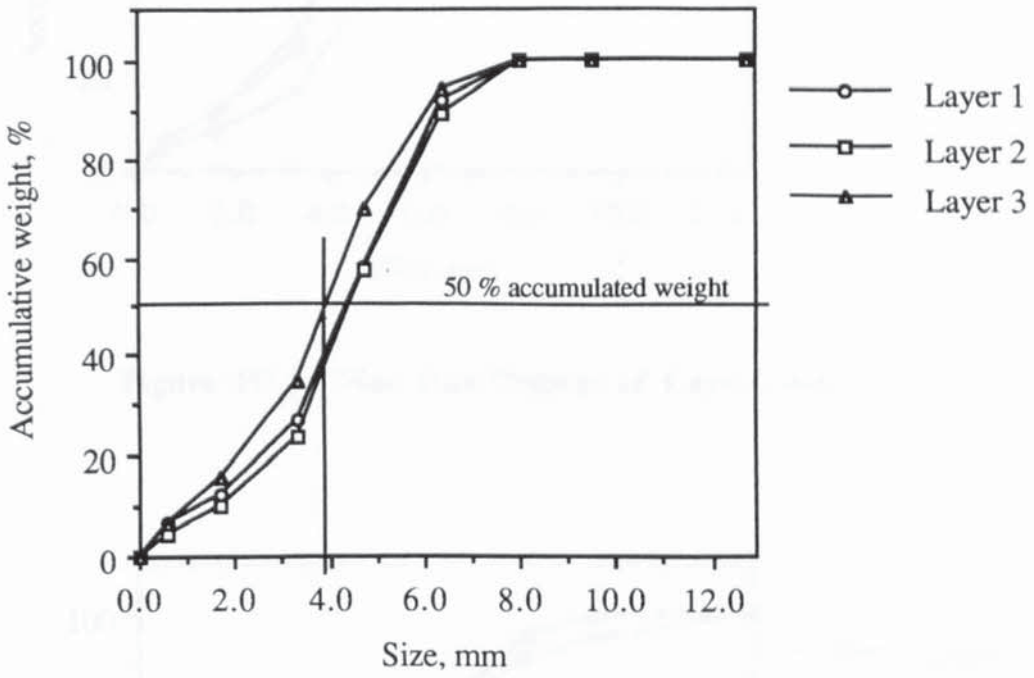

Figure H1.1 Size Distribution of Layers 1-3

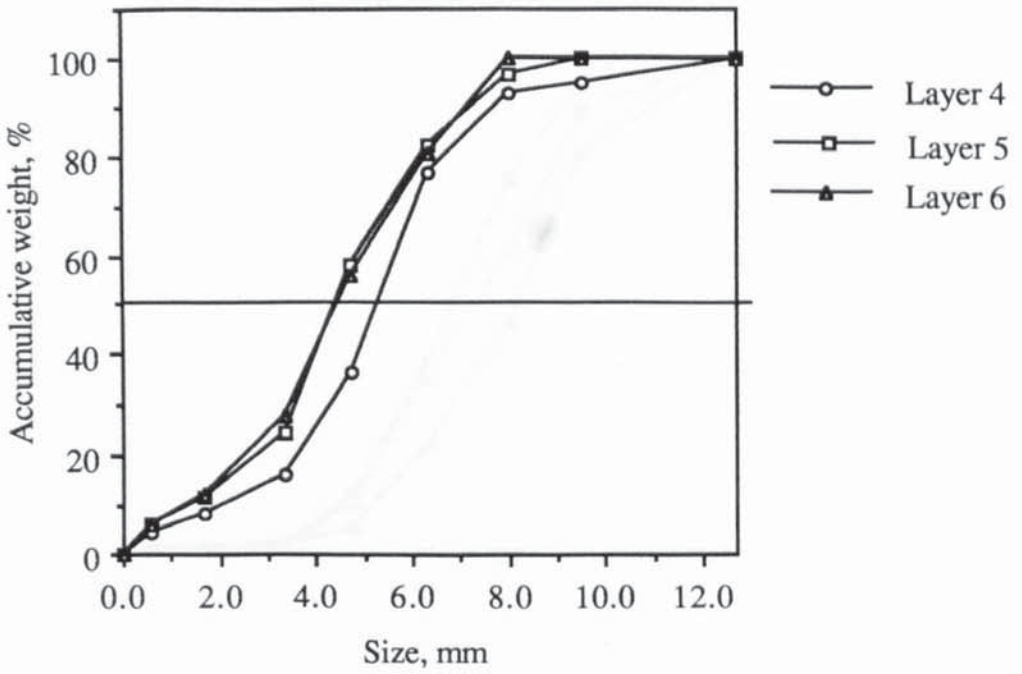

Figure H1.2 Size Distribution of Layers 4-6

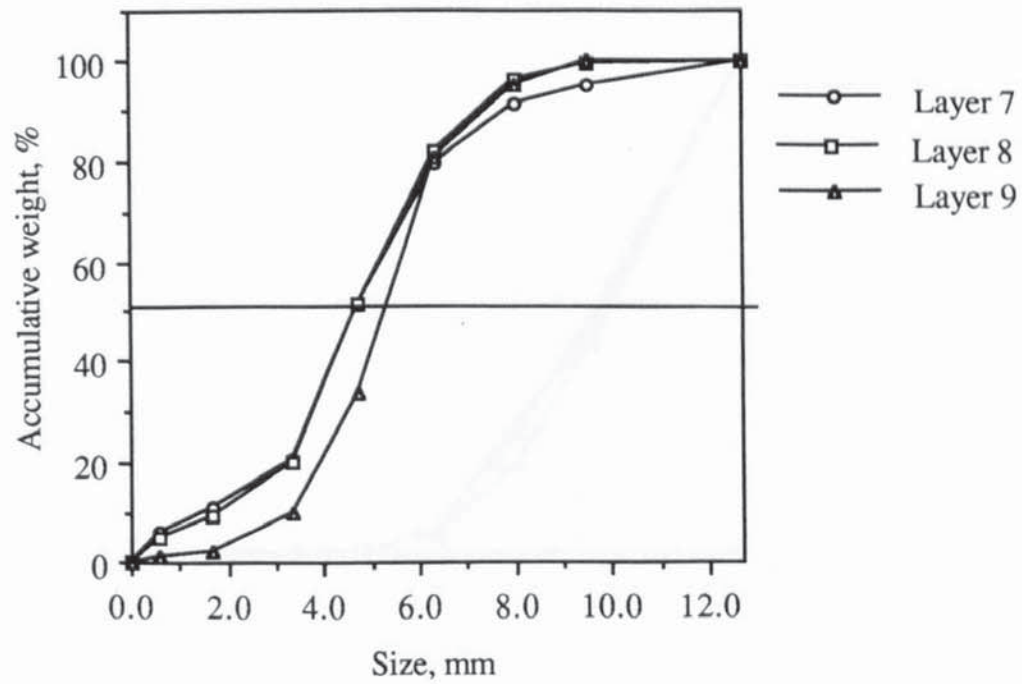

Figure H1.3 Size Distribution of Layers 7-9

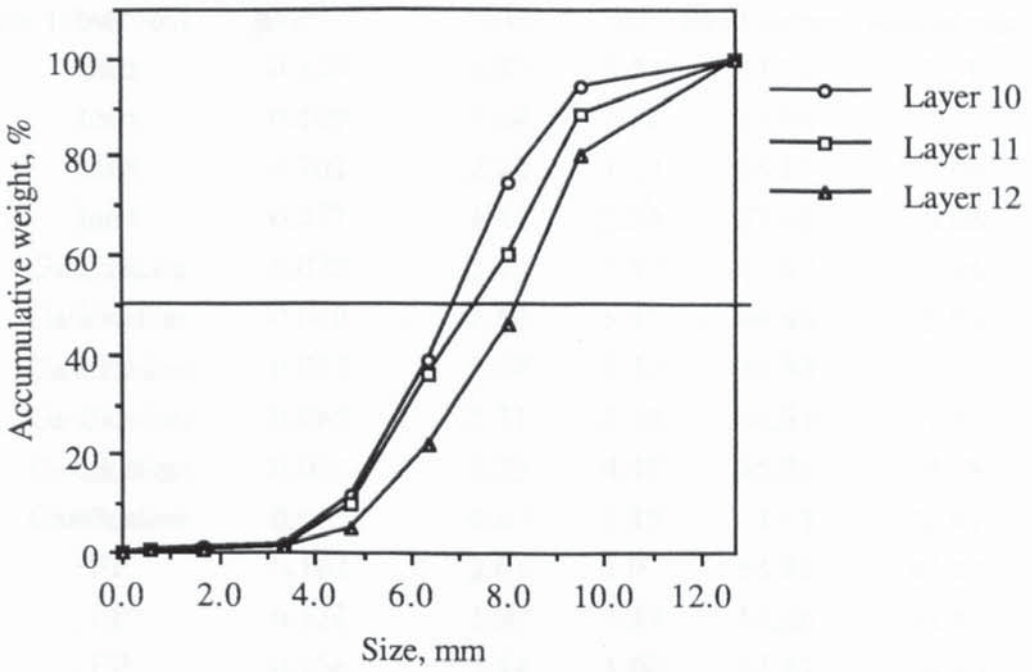

Figure H1.4 Size Distribution of Layers 10-12

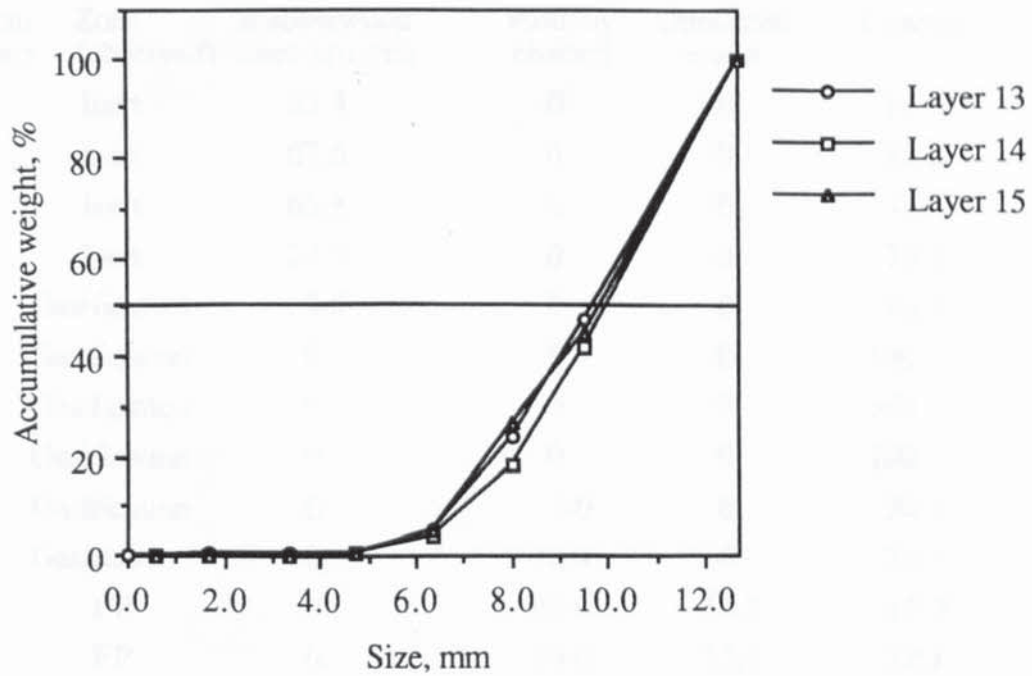

Figure H1.5 Size Distribution of Layers 13-15

Table H1.1 Char Analysis Profile

Layer, cm from grate	Zone (observed)	Bulk density, gcm^{-3}	Moisture %wb	Proximate analysis, % dry ash	fixed carbon	volatile matter
0-1	Inert	0.129	1.83	8.57	83.84	7.59
1-2	Inert	0.109	1.84	8.82	83.96	7.22
2-3	Inert	0.102	2.12	7.17	85.17	7.66
3-4	Inert	0.077	1.51	5.93	87.41	6.66
4-5	Gasification	0.073	2.42	7.97	85.67	6.36
5-6	Gasification	0.060	2.64	5.18	89.46	5.36
6-7	Gasification	0.055	1.57	5.24	88.38	6.38
7-8	Gasification	0.065	2.71	5.53	86.63	7.84
8-9	Gasification	0.062	1.75	4.47	85.95	9.58
9-10	Gasification	0.075	2.67	2.15	74.93	22.92
10-12	FP	0.107	2.01	1.92	54.81	43.27
12-15	FP	0.132	1.97	1.27	54.26	44.47
15-16	FP	0.156	3.14	1.00	44.17	54.83
16-19	Feed/FP	0.231	4.61	0.56	18.41	81.10
19-23	Feed	0.250	7.31	0.49	18.41	49.53
23-30	Feed	0.277	10.35	0.48	16.67	82.68

Table H1.2 Material Profile, % Weight

Layer, cm from grate	Zone (observed)	Rubberwood (start-up) char	Partially charred	Unreacted wood	Charred
0-1	Inert	83.4	0	0	16.6
1-2	Inert	67.5	0	0	32.5
2-3	Inert	65.8	0	0	34.2
3-4	Inert	24.3	0	0	75.7
4-5	Gasification	3.5	0	0	96.5
5-6	Gasification	0	0	0	100
6-7	Gasification	0	0	0	100
7-8	Gasification	0	0	0	100
8-9	Gasification	0	2.0	0	98.0
9-10	Gasification	0	26.9	0	73.1
10-12	FP	0	40.9	16.2	42.9
12-15	FP	0	55.6	17.4	27.1
15-16	FP	0	47.4	37.9	14.7
16-19	Feed/FP	0	17.4	77.3	5.3
19-23	Feed	0	4.2	95.3	0.6
23-30	Feed	0	0	100	0

APPENDIX I REACTION ZONE POSITIONS DURING TEST T3

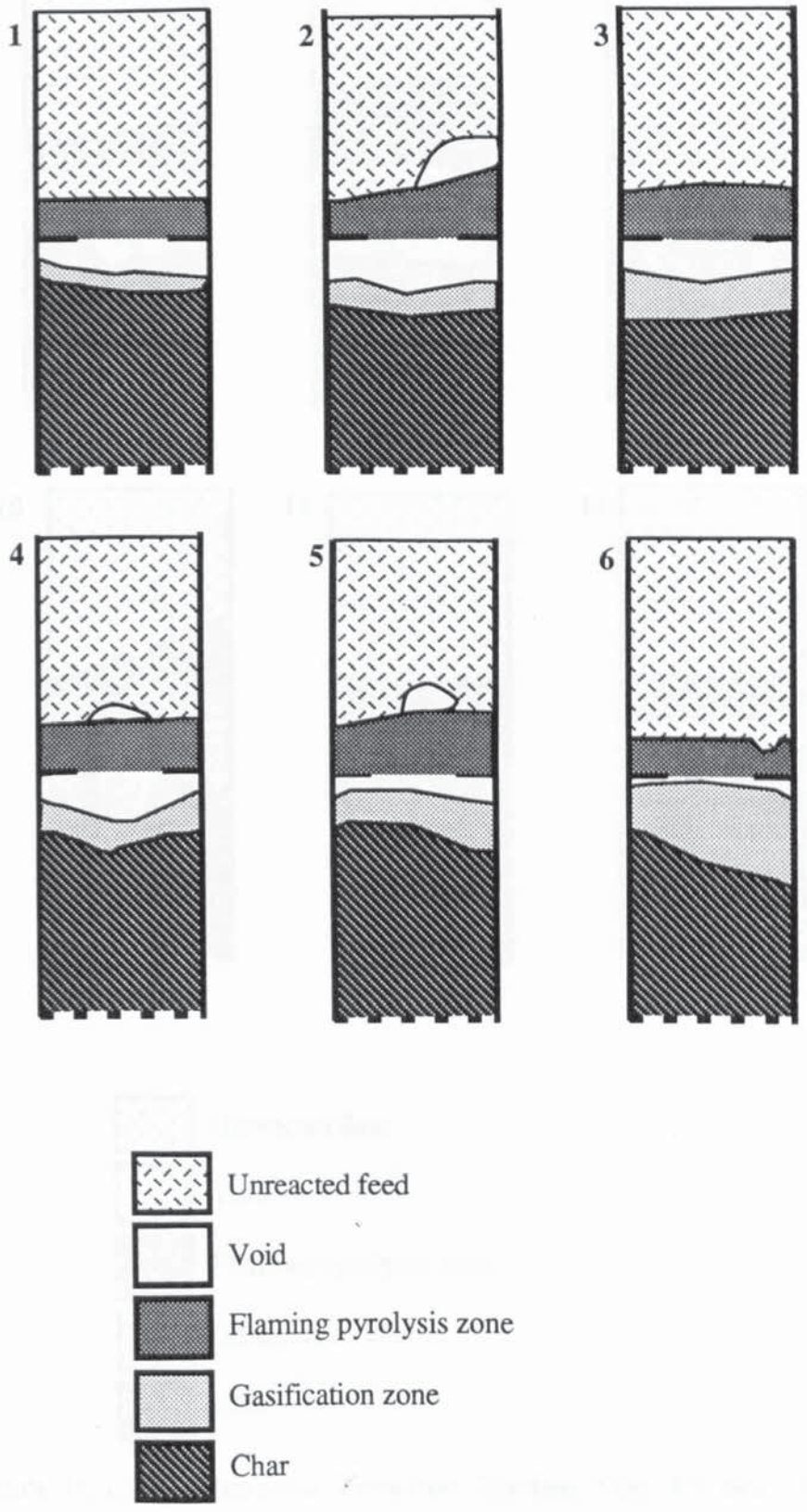

Figure I1.1 (a) Observed Zonation During Test T3, nos. 1-6

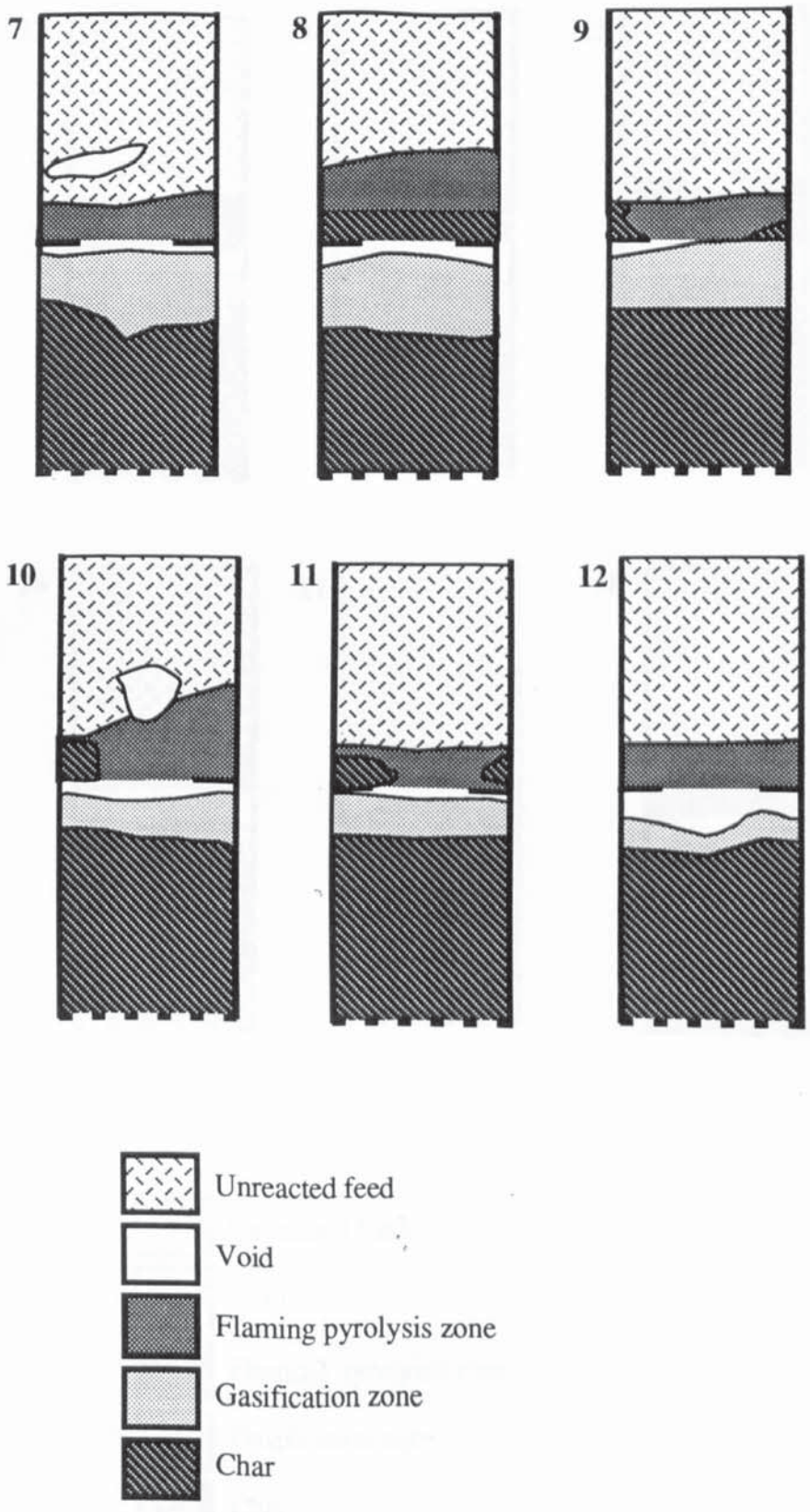

Figure I1.1(b) Observed Zonation During Test T3 nos. 7-12

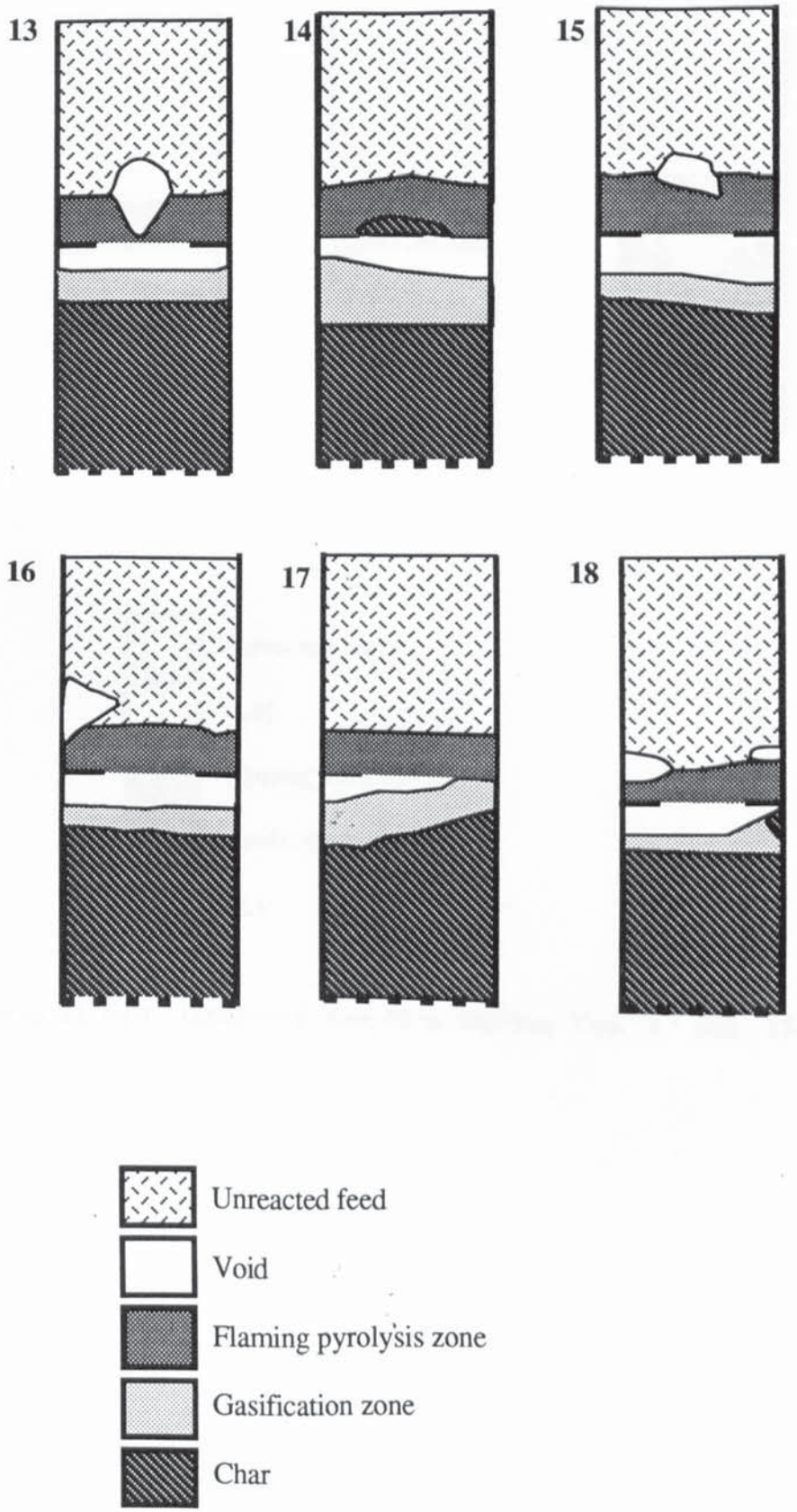

Figure I1.1(c) Observed Zonation During Test T3 nos. 13-18

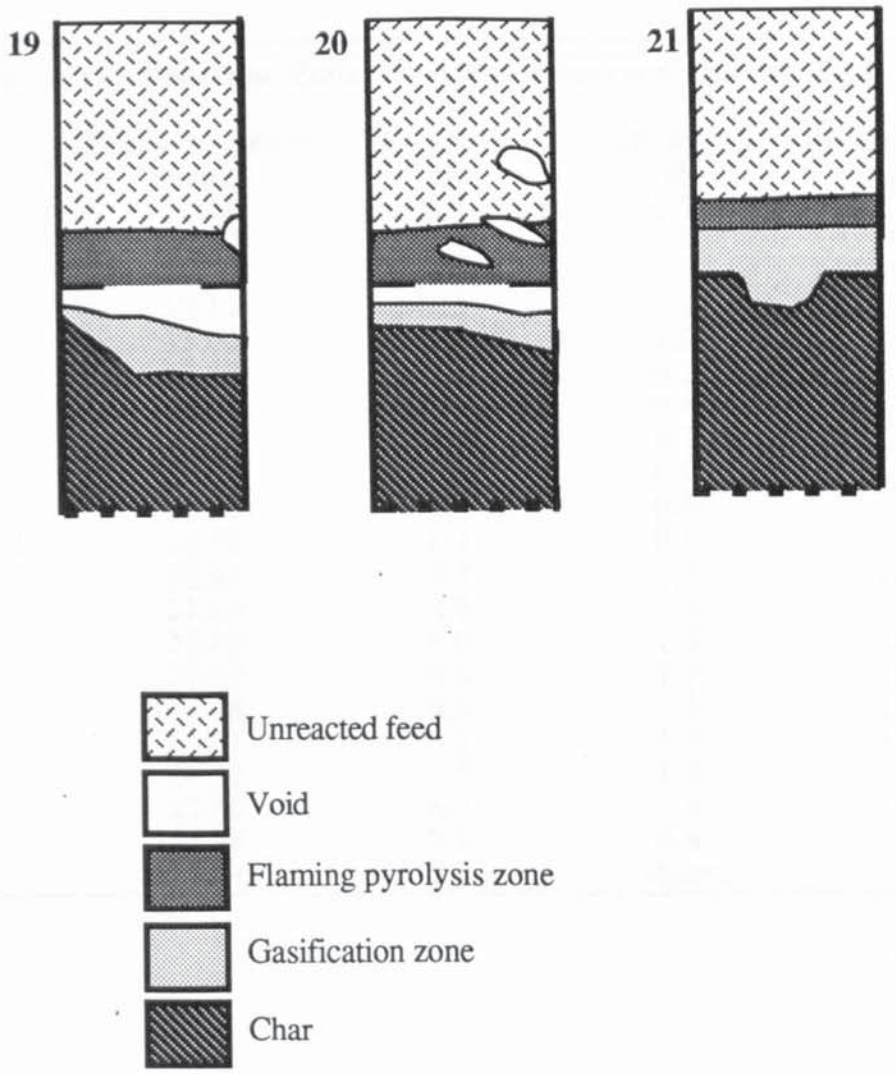

Figure I1.1(d) Observed Zonation During Test T3 nos. 19-21

Table I1.1 Reaction Zone Positions Observed During Test T3

Figure number	Time after start up minutes	Char bed cm	Throat gap cm	Pyrolysis front cm
1	9.75	6.5	1.7	11.8
2	11.50	6.5	2.0	14.8
3	11.67	6.5	1.5	12.4
4	12.17	7.3	1.4	12.2
5	13.00	7.6	1.0	12.8
6	13.50	6.4	0.2	11.7
7	14.50	7.0	0.4	11.8
8	15.34	6.1	0.7	13.7
9	15.38	6.9	0.2	11.8
10	16.57	7.7	0.6	13.2
11	16.58	8.3	0.3	11.8
12	18.93	7.2	1.3	12.0
13	21.60	5.9	1.3	12.2
14	22.43	6.0	1.4	12.4
15	22.87	6.8	1.9	12.8
16	23.18	6.8	1.5	12.3
17	23.61	6.7	1.9	12.0
18	24.33	7.5	1.5	11.8
19	25.00	6.7	1.4	12.2
20	27.38	7.9	0.8	12.6
21	27.87	9.2	absent	13.1

APPENDIX J MODELLING CALCULATIONS

J1 External and Internal Surface Area Calculation

The top and bottom surfaces at right angles to the pore length given in Figure 9.1 are mainly composed of empty space and are assumed not to contribute to the external surface of the particle. The external and internal areas of a cubic model particle with 20 μm pores are calculated in Equations J1.1 and J1.2.

$$\text{External area} = 4\,l^2 \qquad \text{(J1.1)}$$

$$\text{Internal area} = \frac{\pi}{D_{pore}}\, l^3 \qquad \text{(J1.2)}$$

Where l is the particle dimension, and D_{pore} is the pore diameter. The external surface area is expressed as a percentage of the total surface area The results for various particle sizes are presented in Table J1.1.

Table J1.1 Internal and External Surface Areas of Particles of Different Dimensions

Particle size mm	External area m^2	Internal area m^2	Total m^2	% External area
1	4.0×10^{-6}	1.6×10^{-4}	0.0002	2.48
2	1.6×10^{-5}	1.3×10^{-3}	0.0013	1.26
5.5	1.2×10^{-4}	2.6×10^{-2}	0.0197	0.46
10	4.0×10^{-4}	1.6×10^{-1}	0.1575	0.25
100	4.0×10^{-2}	$1.6 \times 10^{+2}$	157.5	0.03

J2 Temperature Response Curves

The temperature response curve given by Schneider (1963) for a plate with an insulated back face (case a) is described using curve fitting techniques by Equation J2.1.

$$Fo = 0.112 \times 10^{1.052T} \qquad \text{(J2.1)}$$

The temperature response curve given by Schneider (1963) for a semi-infinite solid (case b) is described by Equation J2.3.

$$\frac{L}{2\sqrt{Fo}} = 1.332 - (2.203T) + (0.94T^2) \qquad \text{(J2.2)}$$

where T is the dimensionless temperature parameter (see Section 9.4.2), Fo is the Fourier number and L is the distance from the heated surface.

J3 Product Gas Composition Calculations

J3.1 Water Gas Shift Equilibrium Constant

The equilibrium constant for the water gas shift reaction (Equation 2.6) is determined using the temperature dependency function;

$$36.72508 - \frac{3994.704}{T} + 4.462408 \times 10^{-3}T - 6.71814 \times 10^{-7}T^2 - 12.220277 \log T \quad \text{(J3.1)}$$

J4 Calculation of External Mass Transfer

The mass transfer coefficient is calculated according to Equation J4.1 (Section 9.6.1)

$$k_m = \frac{0.357\ N_{Re}^{-0.359}\ (\rho_m\ v)}{\varepsilon N_{Sc}^{2/3}} \quad \text{(J4.1)}$$

The superficial velocity v, is calculated as the gas volumetric flow rate divided by the reactor diameter. The Reynolds and Schmidt numbers are defined by Equations J4.2 and J4.3 respectively.

$$N_{Re} = \frac{d_p V \rho}{\mu} \quad \text{(J4.2)}$$

$$N_{Sc} = \frac{\mu}{\rho D} \quad \text{(J4.3)}$$

where:

dp = particle diameter
v = superficial velocity
ρ = gas mass density
μ = gas viscosity
D = gas diffusivity

The diffusivity is estimated using Equation J4.5 (Perry,1985).

$$D_{ab} = \frac{0.001T^{1.75}\ [(M_a + M_b) / M_aM_b]^{1/2}}{(P\ \upsilon_a^{1/3}\upsilon_b^{1/3})^2} \quad \text{(J4.4)}$$

where D_{ab} is the diffussivity of gas a in b, M is the molecular weight, P is the pressure in atmospheres and υ is the molar volume. In the calculation, the bulk gas was assumed to be nitrogen since this represents over 50% of the gas by volume in the gasifier.